A Multi-Tracer Study of the Role of Sea Ice in the Arctic Ocean Carbon Cycle

by

Kristina Anne Brown

B.Sc., The University of Victoria, 2006

A THESIS SUBMITTED IN PARTIAL FULFILLMENT OF

THE REQUIREMENTS FOR THE DEGREE OF

DOCTOR OF PHILOSOPHY

in

THE FACULTY OF GRADUATE AND POSTDOCTORAL STUDIES

(Oceanography)

THE UNIVERSITY OF BRITISH COLUMBIA

(Vancouver)

April 2014

Abstract

Recent Arctic warming and reduced summer sea ice extent have stimulated increased research into the role of sea ice in the high latitude carbon cycle. Using data collected on a number of field expeditions throughout the Arctic Ocean, I apply a multi-tracer approach to investigate the influence of the sea-ice life cycle on the biological and abiotic export of CO_2 into the sub-surface. The results of this study illuminate the role of sea ice in polar carbon cycling across the perennial sea ice region of the central Canada Basin and in the seasonal ice zone of the Canadian Arctic Archipelago. In the perennial sea ice region, lateral exchanges of shelf derived carbon were found to exert the most important control on carbon distribution in the central Canada Basin, both in the surface mixed layer and in the sub-surface halocline. Stable carbon isotope data suggest that surface water particulate organic carbon is derived, to a large extent, from external inputs from Eurasian rivers. Further, results from a suite of geochemical tracers show that sub-surface accumulation of dissolved inorganic carbon in the halocline reflects an organic matter remineralization signature derived from the shelves and transported into the halocline by dense Pacific winter waters. Within the seasonal ice zone, observations over the winter-spring transition illustrated a highly dynamic carbon cycle, and results from this study provide new insight into the biological, physical and chemical factors which contribute to C cycling in different depth horizons of the ice over this period. Physical constraints on inorganic carbon cycling dominated CO_2 distributions in the majority of the ice column early in the season. As the melt period advanced, sea ice melt dilution led to decreasing CO_2 partial pressures in brine, contributing to pCO_2 under-saturation and CO_2 uptake from the atmosphere as the melt period advanced. In contrast, the carbonate system in bottom ice layers was much more closely tied to

the flourishing algal community. Our inorganic carbon system measurements within natural sea ice brine samples further reveal the limitations of current thermodynamic constants used to compute carbonate system equilibrium in sea ice systems.

Preface

A version of Chapter 2 has been published: K. A. Brown, F. McLaughlin, P. D. Tortell, D. E. Varela, M. Yamamoto-Kawai, B. Hunt, and R. François. 2014. Determination of Particulate Organic Carbon Sources to the Surface Mixed Layer of the Canada Basin, Arctic Ocean. *Journal of Geophysical Research - Oceans* 119, doi:10.1002/2013JC009197. I conducted the field work, the laboratory analyses of inorganic carbon system components and stable isotopes of dissolved inorganic carbon, the geochemical data analyses, as well as the writing of this manuscript. Dr. F. McLaughlin, Dr. P. D. Tortell, and Dr. R. François provided invaluable feedback on data analyses and editorial feedback during many rounds of manuscript preparation and reviews. Dr. D.E. Varela and Dr. B. Hunt provided ancillary data and Dr. M. Yamamoto-Kawai provided guidance on field sampling and interpretation of geochemical data.

A version of Chapter 3 is in preparation for submission to a scientific journal. The co-authors are: K. A. Brown (first author), F. McLaughlin, R. François and P. D. Tortell. Title: Multi-Tracer study of Dissolved Inorganic Carbon sources to the Canada Basin (Arctic Ocean) Halocline. I conducted the field work, the laboratory analysis of carbon system components and stable carbon isotopes, the geochemical data analyses, as well as the writing of this manuscript. Dr. F. McLaughlin, Dr. R. François, and Dr. P. D. Tortell continue to provide extensive feedback on the interpretation of geochemical data and editorial feedback in preparation of the manuscript.

A version of Chapter 4 is in preparation for submission to a scientific journal. The co-authors are: K. A. Brown (first author), L.A. Miller, R. François, C.J. Mundy, G. Carnat, T.

Papakyriakou, M. Gosselin, K. Swystun and P. Tortell. Title: Inorganic carbon system dynamics in land-fast Arctic sea ice during the early-melt period. I conducted the field sampling and designed the time-series carbonate system study. I also conducted the laboratory analyses of inorganic carbon components and stable isotopes, the geochemical data analyses, as well as the writing of the manuscript. Dr. L. Miller, Dr. R. François, and Dr. P. D. Tortell, guided geochemical data analyses and interpretation. C.J. Mundy and M. Gosselin oversaw the field study and contributed ancillary data. T. Papakyriakou contributed instrumentation and expertise for the CO_2 flux chamber and peeper pCO_2 measurements, and K. Swystun contributed to sample collection, sampling program design, and flux chamber deployment. G. Carnat processed the CO_2 flux data.

A version of Chapter 5 has been accepted for publication: K. A. Brown, L. Miller, M. Davelaar, R. François, and P. D. Tortell. (*in press*) Over-determination of the carbonate system in natural sea ice brine and assessment of carbonic acid dissociation constants under low temperature, high salinity conditions. *Marine Chemistry*. I conducted the majority of the field work, laboratory and data analyses, as well as the writing of this manuscript. Dr. L. Miller, Dr. R. François, and Dr. P. D. Tortell, guided data analyses and were instrumental in preparing the manuscript for submission. M. Davelaar contributed to sample collection and analyses as part of one of the field campaigns.

Table of Contents

List of Tables

List of Figures

Acknowledgements

I am deeply indebted to my supervisory committee, Roger François, Philippe Tortell, Fiona McLaughlin, Lisa Miller, and Kristin Orians, for their mentorship and guidance throughout my thesis. Their insight, steadfast support, and willingness to take a chance on an enthusiastic neophyte made this project possible. I also greatly appreciate Michiyo Yamamoto-Kawai and Robie Macdonald for donating their time and expertise to helping me refine my understanding of Arctic Ocean system processes.

I would like to thank the following agencies for direct financial and logistical support during my PhD Thesis and fieldwork: the National Science and Engineering Research Council, Fisheries and Oceans Canada, the Northern Scientific Training Program, the Canadian Meteorological and Oceanography Society, and the Polar Continental Shelf Program.

I am grateful to Chief Scientists Sarah Zimmermann, David Barber, and CJ Mundy, as well as the captains and crews of the CCGS *Louis St. Laurent* and the CCGS *Amundsen,* and the PSCP Resolute Bay field personnel for contributing their expertise, resources, and often their comfort to facilitate fieldwork carried out in this thesis. Additionally, many thanks go to the numerous scientific personnel who participated in the 2008 and 2009 Joint Ocean Ice Study, the 2009 IPY-ArcticNet-GEOTRACES program, and the 2010 Arctic-ICE program for their tireless efforts in sample collection and enjoyable field-going company. Special thanks go to the many people who contributed to my Arctic-field education and who generously incorporated my sampling into their field programs. In particular, Rick Krishfield and the WHOI BGOS team, Jenny Hutchings, Alice Orlich, Nes Sutherland, Brian Hunt, David Griffith, Kyle Swystun and Virginie Galindo. My humble gratitude goes to Maureen Soon, Marty Davelaar, J.F. Hélie, Keith

Johnson, and Glenn Cooper for their invaluable contributions during field program preparation, deployment, and patient instruction during laboratory analyses.

I also want to thank my EOS grad student community for adding a lot of colour and fond memories to my time at UBC. Especially my long-time office mate Bart DeBaere and the past and present members of the Tornado and François Lab groups for many thoughtful discussions over the years.

Lastly, and most importantly, I would like to extend my most sincere gratitude to my family and friends; without their ceaseless love and support I would not have been able to devote so much of myself to realizing this goal. In particular, I want to thank Jeff, my mom, Rob, Grandma E, Aunt Brenda, Heather and Fred for their genuine interest and enthusiastic encouragement throughout this entire endeavour.

for jeff.

For whatever we lose (like a you or a me)

it's always ourselves we find in the sea

- e. e. cummings

Chapter 1: Introduction

The polar oceans play a pivotal role in the global carbon cycle as sites of significant deep water formation and atmospheric CO_2 sequestration. This CO_2 solubility-pump is not the only climate-sensitive process influencing polar CO_2 fluxes. In the frozen high latitudes, sea ice acts as a semi-permeable barrier between the surface ocean and the atmosphere (Gosink et al., 1976; Nomura et al., 2006) but can also be an active participant in CO_2 cycling as a direct source or sink of CO_2 to/from the atmosphere at different times of year (Miller et al., 2011a, 2011b; Nomura et al., 2010a; Papakyriakou and Miller, 2011; Semiletov et al., 2004). High-salinity brine contained within the sea ice matrix is also of particular interest in the polar carbon cycle. As a seasonal repository of inorganic carbon (Delille et al., 2007; Geilfus et al., 2012; Miller et al., 2011a, 2011b; Papadimitriou et al., 2012) and an important ecological province conducive to high primary productivity (Arrigo et al., 2010; Boetius et al., 2013; Kirst and Wiench, 1995; Niemi et al., 2011; Welch and Bergmann, 1989), sea ice brine is involved in the seasonal cycling of both dissolved and particulate forms of carbon. The export of high salinity brine into the underlying surface waters can transport dissolved inorganic carbon into the subsurface (Miller et al., 2011b; Omar et al., 2005; Rysgaard et al., 2011, 2009, 2007), potentially contributing to carbon sequestration. Furthermore, the accumulation of algal biomass within brine channels in bottom ice can contribute to particulate carbon export when this material sinks out of the surface mixed layer (e.g., Boetius et al., 2013; Gibson and Trull, 1999).

Recent reduced summer sea ice extent and polar warming have stimulated increased effort to understand the role of sea ice in the transfer of carbon between the atmosphere and the ocean

(Barber et al., 2012; Loose et al., 2011; Parmentier et al., 2013; Rysgaard et al., 2011). The goal of this thesis is to investigate the influence of the sea ice life cycle on the export and sequestration of CO_2, in both inorganic and organic forms, below the mixed layer in polar seas. Using a multi-tracer approach, data from four field investigations are combined to examine CO_2 cycling through biotic and abiotic pathways as sea ice forms, grows, and undergoes melt.

1.1 The Global Carbon Cycle and the Importance of the Arctic Ocean

High latitude oceans play a disproportionate role in regulating atmospheric CO_2 concentrations on timescales longer than a few hundred years. This is due to the direct connection of polar surface waters with the deep ocean, via deep water formation and isopycnal ventilation, and the increased capacity of cold polar seas to take up CO_2 (Sarmiento and Gruber, 2006). For instance, seasonal cooling in the North Atlantic Ocean makes this region a major sink for CO_2, delivering CO_2 to depth with the formation of North Atlantic Deep Water (NADW; e.g., Broecker and Peng, 1992; Keeling and Peng, 1995; Takahashi et al., 2009). The NADW CO_2 sink has been estimated to take up on the order of 0.11 ± 0.04 PgC yr^{-1} (Pg = 10^{15}; Mikaloff Fletcher et al., 2007) and is tightly regulated by the export of freshwater and carbon from the Arctic Ocean into the sites of deep water formation in the Greenland, Iceland, and Norwegian (GIN) seas (e.g., Aagaard and Carmack, 1994; Carmack et al., 2008).

North of the GIN seas, the Arctic Ocean itself also plays an important role in the global carbon cycle. Bates and Mathis (2009) estimated that the Arctic Ocean contributes to the uptake of 66 - 199 TgC yr^{-1} (Tg = 10^{12} g), or on the order of 5 - 14 % of the global balance of CO_2 sources and

sinks (mean global ocean CO_2 uptake ≈ 1400 TgC yr^{-1}; Takahashi et al., 2009). This is similar to the 200 ± 20 TgC yr^{-1} CO_2 uptake estimated by Ocean Global Climate Models (Mikaloff Fletcher et al., 2007). Limited access to winter data may underestimate the CO_2 out-gassing from shallow shelves and flaw leads/polynyas, as well as the CO_2 uptake contributions associated with sea ice brine export. These contributions have been estimated to range from - 38 to + 4 TgC yr^{-1} (where a positive sign represents a flux from the ocean to the atmosphere; Bates and Mathis, 2009; Rysgaard et al., 2011).

The Arctic Ocean is an enclosed basin that has limited exchanges with the North Atlantic and North Pacific, and is heavily influenced by terrestrial inputs of freshwater and carbon (Figure 1-1; summarized in Macdonald et al., 2010). Annual inorganic carbon fluxes into and out of the upper Arctic Ocean (inorganic carbon inventory ≈ 25 Pg) are dominated by seawater exchange with the Pacific and Atlantic, with ≈ 12 % of the inorganic carbon inventory exchanged via inflows through the Barents Sea and Bering Strait, and outflows through Fram Strait (Bates and Mathis, 2009). River inputs contribute on average ≈ 3300 km^3 of freshwater per year to the Arctic Ocean's vast continental shelves, carrying with them ≈ 12 TgC yr^{-1} of inorganic and organic carbon from terrestrial sources and coastal erosion (e.g., Macdonald et al., 2010 and references therein). The net air-ocean exchange balances these inputs (- 66 to - 199 TgC yr^{-1}) with the shelves and central basins generally acting as CO_2 sinks, and localized areas of sea ice melt and river input representing sources of CO_2 to the atmosphere (Bates and Mathis, 2009).

Sea ice at the surface of the Arctic Ocean further regulates freshwater and carbon fluxes throughout its life cycle. Primarily, sea ice acts as a means to redistribute freshwater around the

Arctic Ocean, either by removing it (≈ 2850 km^3 yr^{-1} exported into the North Atlantic via Fram Strait and ≈ 480 km^3 yr^{-1} via the Canadian Arctic Archipelago; Macdonald et al., 2010) or by concentrating and storing it on longer time-scales within the Beaufort Gyre (Carmack et al., 2008). In addition to freshwater storage, sea ice is intimately involved in the seasonal flux of CO_2 between the surface Arctic Ocean and the atmosphere. Recent work has shown sea ice can be a direct source or sink of CO_2 to/from the atmosphere at different times of year (e.g., Miller et al., 2011a, 2011b; Nomura et al., 2010a; Papakyriakou and Miller, 2011; Semiletov et al., 2004). Furthermore, the persistence of sea ice and its summertime extent are intrinsically tied to the CO_2 balance of many Arctic terrestrial and marine systems (Parmentier et al., 2013). Continued summertime sea ice losses are predicted to reduce the Arctic Ocean's ability to take up CO_2 over long time scales (e.g., Cai et al., 2010; Else et al., 2013; Steiner et al., 2013), amplifying the warming impact of increasing atmospheric CO_2 concentrations. Observed changes in the character of the Arctic Ocean sea ice landscape over the last three decades has motivated increased effort to better understand the role of sea ice in the transfer of carbon between the atmosphere and the ocean (e.g., Barber et al., 2012; Loose et al., 2011; Parmentier et al., 2013; Rysgaard et al., 2011) but has left many questions yet unanswered. In the sections below, I present background information on the present state of knowledge of the sea ice carbon cycle, and highlight the specific research questions investigated in this thesis.

1.1.1 The Marine Inorganic Carbon System

Unlike most other gases, CO_2 dissolves in seawater to form a weak acid that reacts with H_2O, donating protons to solution and forming its conjugate bases of bicarbonate (HCO_3^-) and carbonate (CO_3^{2-}):

$$CO_{2(aq)} + H_2O \leftrightarrow H_2CO_3^* \leftrightarrow H^+ + HCO_3^- \leftrightarrow 2H^+ + CO_3^{2-} \quad (1)$$

In this reaction, H_2CO_3* refers to the sum of CO_2(aq) + H_2CO_3, which are difficult to distinguish analytically and are thus typically considered together (Morel and Hering, 1993; Sarmiento and Gruber, 2006; Stumm and Morgan, 1996).

Equilibrium relationships between these species in solution are defined by thermodynamic equilibrium constants (equations 2-4), where { } refers to the activity of ions in solution, fCO_2 to the fugacity of CO_2 in units of atm, and K_o is the Henry's Law constant depicting CO_2 solubility in solution that is in thermodynamic equilibrium with CO_2 (g), with units of mol (kg soln)$^{-1}$ atm^{-1} (Zeebe and Wolf-Gladrow, 2001). Thermodynamic equilibrium constants can be related to stoichiometric equilibrium constants, and therefore concentrations of species in solution, by accounting for the effects of solution ionic strength and composition on ion activity (as a function of solution salinity), and for temperature and pressure effects on standard reaction free energies (which affect thermodynamic equilibrium constants). Conditional equilibrium constants[1] (K^*, with K_1^* and K_2^* in units of mol kg^{-1}) can thus be derived to describe inorganic carbon speciation with respect to solution properties (equations 5-7), and defined in terms of measurable quantities (equations 5-9), yielding an algebraic system of four equations (6-9), that

[1] Conditional equilibrium constants, conventionally denoted by * (e.g., K_1^* & K_2^*), are constants valid for a particular ionic strength and account for the activity coefficients of species in a multi-component solution; the solubility constant (or Henry's Law constant) K_o, however, is left without this designation. For simplicity we treat K_o as a thermodynamic constant (solution ionic strength approaching zero) and can therefore make the assumptions that (1) {H_2CO_3*} is equal to [H_2CO_3*] as the activity coefficient, γ_{H2CO3*}, for a neutral species can be considered ≈ 1 for dilute solutions (Morel and Hering, 1993); and (2) fugacity ≈ partial pressure (following the discussions of Weiss, 1974).

solve for six unknowns ([H_2CO_3*], [HCO_3^-], [CO_3^{2-}], K_1^*, K_2^*, [H^+]), using a combination of any two measurable parameters ([CO_2], pH, DIC, and Carbonate Alkalinity - CAlk; Zeebe and Wolf-Gladrow, 2001).

Extensive laboratory work has been done to determine conditional equilibrium constants as they relate to solution physical conditions, specifically temperature (T), salinity (S) and pressure (P) (e.g., Dickson and Millero, 1987; Goyet and Poisson, 1989; Hansson, 1973; Lee et al., 2000; Mehrbach et al., 1973; Millero, 1995; Roy et al., 1993; Stumm and Morgan, 1996; Weiss, 1974). However, the application of conditional constants outside of laboratory determined S, T, P ranges, or the determination of which two measurable parameters yields the most accurate calculated results, remains to be agreed upon (Johnson et al., 1999; Lee et al., 2000; Lueker et al., 2000; Wanninkhof et al., 1999; Zeebe and Wolf-Gladrow, 2001). Determination of the most accurate set of constants for use in high S, low T sea ice environments is a main contribution of this thesis (see below, section 1.4).

$$K_o = \{H_2CO_3^*\} / fCO_2 \qquad (2)$$

$$K_1 = \{H^+\}\{HCO_3^-\} / \{H_2CO_3^*\} \qquad (3)$$

$$K_2 = \{H^+\}\{CO_3^{2-}\} / \{HCO_3^-\} \qquad (4)$$

$$K_o = [H_2CO_3^*] / pCO_2 \qquad (5)$$

$$K_1^* = [H^+] [HCO_3^-] / [H_2CO_3^*] \quad (6)$$

$$K_2^* = [H^+] [CO_3^{2-}] / [HCO_3^-] \quad (7)$$

$$DIC = [H_2CO_3^*] + [HCO_3^-] + [CO_3^{2-}] \quad (8)$$

$$CAlk = [HCO_3^-] + 2[CO_3^{2-}] \quad (9)$$

As CAlk (Carbonate Alkalinity) is not measurable on its own, we use the determination of Total Alkalinity to derive the contribution of CAlk to the above system of equations. Total Alkalinity (TA) refers to the titratable excess of proton acceptors over proton donors (expressed in equivalents per kg of solution) and is defined precisely as $TA = [HCO_3\text{-}] + 2[CO_3^{2-}] + [B(OH)_4^-] + [OH^-] + [HPO_4^{2-}] + 2[PO_4^{3-}] + [H_3SiO_4^-] + [NH_3] + [HS^-] – [H^+]_F – [HSO_4^-] – [HF] – [H_3PO_4]$, where $[H^+]_F$ is the free concentration of hydrogen ions (DOE, 1994). CAlk accounts for roughly 96% of seawater TA.

1.2 The Seasonal Sea Ice Cycle

The Canada Basin interior experienced perennial sea ice cover until the late 1990's (e.g., Perovich et al., 2003), after which there has been a persistent decline in summer sea ice extent, a decreased proportion of multiyear sea ice cover, and a lengthening of the summer melt season (Kwok et al., 2009; McLaughlin et al., 2011; National Snow and Ice Data Center, 2010; Stroeve et al., 2008). The seasonal cycle of sea ice formation and growth in fall/winter, break up in late

spring, and open water conditions by mid-summer exert important controls on both the chemistry and biology of the surface ocean, potentially influencing the net export of both particulate and dissolved carbon below the mixed layer. The following discussion outlines the seasonal sea ice cycle at a typical station in the central Canada Basin, examining chemical and biological changes experienced by the surface ocean as sea ice forms, grows and begins to melt (as summarized in Figure 1-2).

1.2.1 Evolution of Inorganic Carbon Chemistry over Polar Freeze-Up

Consider a typical offshore, ice-free location within the central Canada Basin during transition from summer to fall surface water conditions (Table 1-1). As the atmospheric temperature drops, surface waters cool toward the freezing point (≈ -1.17 °C at S = 21.5).

The thermodynamic properties of equilibrium constants describing carbonate speciation (K_0, K_1^*, and K_2^*) cause them to be affected by the change in temperature experienced at our example station, dropping from 8° C to - 1.17 °C (Table 1-1). Here we consider a closed system, where DIC and TA are always in concentrations proportional to salinity, to assess the effects of lowering temperature (and later, increasing salinity) on carbonate speciation, and the measureable parameters pCO_2 and pH [2]. Here we assume that the carbonic acid dissociation constants (K_1^* and K_2^*) derived for seawater by Mehrbach et al. (1973; refit by Dickson and

[2] For simplicity, this example considers T and S effects on the carbonate system under a closed system only. In effect, both closed and open system scenarios can be encountered during the transition from open to sea ice covered waters. Surface waters dipping below freezing point would be considered an open system, where consideration of pCO_2 and other carbonate system parameters would need to take the effects of CO_2 off-gassing or invasion into account as surface waters equilibrate with the overlying atmosphere. Once sea ice begins to form, however, brines in the colder layers of the ice can become trapped by lowered porosity and can be cut off from exchange with the atmosphere or surface waters, representing a closed system.

Millero, 1987) and K_0 derived by Weiss (1974) are valid at these low temperatures and high salinities (discussed below and in section 1.4).

As seen in Figure 1-3(a) reducing the temperature of the surface water toward the freezing point results in a decrease in K_1* and K_2* and an increase in K_o (equations 5, 6, 7). From the equations above we can take this to infer that as K_o increases, the importance of the aqueous phase increases, resulting in increased CO_2 solubility in surface waters. For K_1* and K_2*, their drop in line with temperature indicates that [HCO_3^-] becomes slightly more important, shifting the equilibria toward the aqueous CO_2 phase. Indeed we see in Figure 1-3 (b) that under this temperature change pCO_2 decreases, driving surface waters toward higher levels of under-saturation with respect to the atmosphere (2009 Annual Mean Atmospheric CO_2 at Mauna Loa = 387.35 ppm; NOAA, 2010). This change is coupled with an increase in solution pH, which results in an increase in CO_2 solubility as temperatures decrease (Figure 1-3b).

Seawater freezing point is dependent on surface water salinity, as the presence of dissolved inorganic salts act to depress solid ice formation to below 0 °C (as summarized in Petrich and Eicken, 2010); under the surface conditions listed in Table 1-1 surface waters in our model system will begin freezing around - 1.17 °C. Since seawater freezing temperature approaches the temperature of maximum density, as surface waters approach the freezing point they will experience thermohaline convection until the entire upper mixed layer is at freezing point (Petrich and Eicken, 2010). Convection in the upper mixed layer brings deeper waters to the surface. If these waters are at or below saturation with respect to atmospheric CO_2, this combination of surface cooling and convective mixing will promote CO_2 uptake over the depth

of the mixed layer (Anderson et al., 2004; Gleitz et al., 1995; Glud et al., 2002; Rysgaard et al., 2007; Shcherbina, 2004). Once the mixed layer is at the freezing point, solid impurities in the seawater begin to act as nuclei for ice crystal formation (Petrich and Eicken, 2010). Ice crystals begin to form throughout the upper mixed layer until a surface layer of ice slush accumulates, reducing wind stress and thermohaline mixing, and allowing needle/spicule-like ice crystals, mm's in length, to aggregate into a frazil ice layer (Petrich and Eicken, 2010). Consolidation of a surface slush layer is followed by quiescent growth of congelation ice, with new layers of ice growth added to the bottom of the growing sheet (Petrich and Eicken, 2010). If conditions are more turbulent, granular frazil ice will form a surface layer on the order of days. Within a week of cooling, a transition zone of granular frazil ice and mixed columnar ice forms with sea ice grains and inter-granular pore spaces of various shapes and sizes. Quiescent growth conditions emerge once the surface layer is thick enough to reduce the wind/thermohaline mixing, and columnar ice, characterized by long prismatic grains of several cm's diameter and 10's of cm's long and highly connected pore/channel systems, begins to form (Petrich and Eicken, 2010).

If we consider sea ice forming under ideal conditions, water molecules tend to arrange themselves tetrahedrally, forming a crystal structure less dense than its liquid form; constraints on size and electrical charge restrict the incorporation of salts into the crystal lattice, as voids encased in the water molecules are much too small for almost all major ions in seawater (Petrich and Eicken, 2010). The consequence of this size limitation is that as sea ice forms, major ions in solution are continuously rejected at the advancing ice-water interface as the ice grows and are expelled into the water column below (Gawarkiewicz et al., 1998; Petrich and Eicken, 2010). However, about 30% of the salts (and some biological organisms) are retained in liquid

inclusions within the solid ice matrix. This concentration of salts forms a saline solution termed "brine", and drainage of this brine into the water column, via well connected channels forming in columnar ice, may have important consequences for CO_2 as sea ice forms. As the sea ice layer is continually cooled from the surface, its increased thickness and reduced porosity act to restrict direct interaction between the atmosphere and the ocean. This reduces surface mixing and impedes direct gas exchange. Open brine channels can, however, act as a conduit for indirect gas exchange between surface waters and the atmosphere (e.g., Semiletov et al., 2004), and brine drainage into the surface waters has also been shown to enhance the transfer of CO_2 into the surface mixed layer (e.g., Rysgaard et al., 2007).

As with decreased T, increasing S has significant effects on the activity and thermodynamic equilibria of the carbonate system components. Figure 1-4 (a) illustrates the effect of removing fresh water (or forming ice) from the surface seawater reported in Table 1-1. From this diagram we can see that as salinity increases (and assuming solution ionic composition and ionic strength remain in constant proportion to the initial surface seawater salinity) K_1* and K_2* are shown to increase, whereas K_o decreases. These changes in K*'s result in the decreased solubility of gaseous CO_2 and drive equilibria toward favouring [$H_2CO_3^*$] and [CO_3^{2-}] as carbonate species in solution. This results in an increase in solution pCO_2 and decrease in pH with increasing salinity (Figure 1-4b), which is associated with the redistribution of carbonate parameters, specifically an increase in the proportion of H_2CO_3* (Figure 1-4c). The direct and indirect effects of surface water cooling and salinization on the carbonate system during the fall period are summarized in Figure 1-2.

These results may not accurately depict the carbonate system response experienced under natural salinizing conditions, as the behaviour of K's, and other system components such as borate equilibria, are not well constrained at high salinity (discussed below); however, they should be applicable at salinities up to at least 43 (Dickson and Millero, 1987). The shift in K_2* also results in a change in the proportion of carbonate ions in solution with respect to bicarbonate (Figure 1-4c), driving the equilibrium in equation (1) towards the right. This is expected to contribute to the increase in carbonate alkalinity (CAlk), which works to enhance the carbon-carrying capacity of the solution by promoting the dissociation of carbonic acid (H_2CO_3) and the dissolution of CO_2 from the atmosphere into the surface waters, despite the decrease in solubility predicted by K_o (Miller and DiTullio, 2007).

1.2.2 Winter Cooling and Sea Ice Growth

As winter progresses, temperatures at the ice surface continue to decrease and brines retained in the sea ice matrix further concentrate, often approaching salinities on the order of 150 (Miller et al., 2011a). The continued increase in solution ionic strength results in the further depression of K_o (increasing pCO_2 as in Figure 1-4a and Figure 1-4b), with K_1* increasing to a maximum at S = 51 (K_1* = 0.8074) and K_2* increasing to a maximum at S = 78 (K_2* = 0.6491; not shown) followed by a decline. Increasing K_1* and K_2* result in an increase in the proportion of [CO_3^{2-}] in solution in the closed system considered here. The predictions of the behaviour of K_1* and K_2* at temperatures well below the freezing point are questionable, however, as the polynomial nature of the equations of state used to characterize K_1* and K_2* as a function of T and S were derived for general seawater conditions (S = 19 to 43; T = 2 to 35 °C; Mehrbach et al., 1973) and should be applied with caution outside of these experimental ranges.

As sea ice continues to thicken over the freezing season, temperatures in the upper portions of the ice will decrease and approach the decreasing air temperature, reducing the connectivity of the brine channel network and working to further concentrate salts (and ionic strength) in brine solution (Petrich and Eicken, 2010). Furthermore, an increased dissolved salt concentration corresponds to an increase in the concentration of Ca^{2+}, HCO_3^- and CO_3^{2-} ions in solution, which can then combine to form $CaCO_3$ according to equation (10) (Assur, 1958).

$$Ca^{2+} + 2HCO_3^- \leftrightarrow CaCO_3\,(s) + H_2O + CO_2\,(aq) \qquad (10)$$

As the concentration of seawater ions increase in solution, a sequential precipitation of minerals is predicted to occur as temperatures in brine fluids decrease, with $CaCO_3$ polymorphs predicted to precipitate first at a temperature of -1.9°C (e.g., Assur, 1958; Marion, 2001). The presence of the anhydrous polymorph ikaite ($CaCO_3 \cdot 6H_2O$) within the sea ice brine channel network has been reported in both the Arctic and Southern oceans (e.g., Dieckmann et al., 2010, 2008) and more recent discoveries suggest it may be a ubiquitous feature of sea ice systems (e.g., Fischer et al., 2013; Geilfus et al., 2013; Nomura et al., 2013a; Rysgaard et al., 2013).

The formation of $CaCO_3$ from seawater brines presents another opportunity for redistribution of parameters in the carbonate system, and potentially leads to an increased export of DIC (over TA) to the underling water column as the products of this precipitation reaction can become separated depending on where in the ice they form (Figure 1-2). For example, in the cold upper layers of ice, porosity is reduced and $CaCO_3$ salts forming in brines can become trapped until

melting occurs in the spring (Rysgaard et al., 2007). Although $CaCO_3$ migration is restricted, CO_2 derived from its formation (equation 10) is still able to diffuse down-gradient through open/connected brine channels into the underlying water. In the lower layers of ice, $CaCO_3$ can be removed from the highly porous ice matrix by gravity drainage of brine and solid precipitates. The combination of these processes in the upper and lower ice can lead to an increased accumulation of CO_2 over $CaCO_3$ in the waters below growing ice, and provide a mechanism to increase surface water pCO_2, as DIC is rejected from the ice preferentially over TA (Rysgaard et al., 2007). The potential exists for this mechanism to result in significant transport of CO_2 into the water column below forming/accumulating ice, but the importance of this sea ice derived CO_2 pump to net carbon sequestration will depend on the transport of these dense, high CO_2, surface waters below the mixed layer and their ability to convect and contribute to the formation of intermediate or deep waters in the Arctic Ocean (Anderson et al., 2004; Rysgaard et al., 2007; Shcherbina, 2004).

1.2.3 Spring Warming and Sea Ice Melt

The re-emergence of the sun above the horizon at the end of polar winter reintroduces heat and light to the polar landscape. As surface warming commences, sea ice porosity and permeability begin to increase, resulting in a new opportunity for winter trapped brines to resume migration through the ice (Figure 1-2). Vertical and lateral percolation of brines (and/or sea ice melt water) is a function of sea ice permeability, which increases dramatically as temperatures increase (Petrich and Eicken, 2010). Desalination processes are most efficient during the late spring/early summer melt seasons, when sea ice porosity and permeability are highest; likewise, zero/low salinity melt water, produced both at the surface and bottom of the ice floe, is capable of

displacing high salinity brines through melt water flushing and brine convection, respectively (as summarized in Petrich and Eicken, 2010). Tracking backwards through Figure 1-3 and Figure 1-4 brine freshening due to melt water flushing leads to a reduction in K_1* and K_2* and a slight increase in K_o, which drive the system back to lower pCO_2, and an increased proportion of HCO_3^- in measured DIC. Changes experienced throughout the winter in natural sea ice systems are not entirely reversible, however, as would be expected by considering this "closed system" example. In fact, the separation of the products of equation (10) would result in the loss of DIC from the original seawater composition (Table 1-1). Likewise, degassing of brine solution into the sea ice matrix under the extremely high pCO_2 conditions predicted by Figure 1-4(b) would also change the brine inorganic carbon inventory. These changes to the DIC/TA ratios of brines potentially permit further CO_2 uptake (e.g., CO_2 from the atmosphere or ice matrix, or the water column) when undersaturated brines are exposed to the atmosphere or mix with underlying surface waters (Rysgaard et al., 2011).

Another consideration as spring emerges is the increased influence of photosynthesis on DIC concentrations within brine and in the seawater under the ice. To interleave biotic factors into the discussion, biological populations residing in sea ice should be traced back to the initial fall cooling of surface seawater. When sea ice formation occurs in the beginning of autumn, a time when microbial populations in the surface waters can still be relatively high, frazil ice crystals nucleating in the surface mixed layer can scavenge particles (such as micro-algae, heterotrophic protists, and bacteria) as they form and float to the surface (as summarized in Arrigo et al., 2010 and Deming, 2010). These particles become concentrated by as much as 50 times surface water abundances in the newly forming sea ice. As the ice pack continues to grow from below and

progresses into the columnar growth stage, the highly porous lower margin of the columnar layer extends into the surface waters, allowing a tight coupling between the growing ice floe and the water below (Arrigo et al., 2010). Although internal algal/bacterial/microzoan communities can remain in the upper frazil layer as sea ice grows, their survival depends on a replenishment of nutrients through surface flooding (e.g., Kennedy et al., 2002). The tighter connectivity of the lower ice column to surface waters provides virtually uninterrupted access to nutrient replenishment, allowing the communities associated with the sea ice basal (skeletal) layer of the floe to flourish (Arrigo et al., 2010; Thomas et al., 2010). While it is expected that respiration by resident heterotrophic communities dominates throughout the dark period of winter (Deming, 2010), when the sun emerges in spring and light becomes available for photo-autotrophs, photosynthesis quickly dominates carbon and nutrient cycling within the nutrient replenished portions of the ice pack, resulting in large populations of sea ice algae overtaking the bottom 0.2 m of the ice sheet (Arrigo et al., 2010 and references therein).

Summer ice melt in the coastal regions culminates in ice-free waters, heavily stratified by surface freshening. In some regions, such as in the deep central basins, summer melt leaves highly porous, melt pond speckled ice pans which persist into the fall freezing season, becoming multiyear ice. Stratification due to melt water accumulation increases the amount of time the surface layer has to interact with the atmosphere, promoting air-sea CO_2 equilibration. On the other hand, while K_o decreases (pCO_2 increases) due to higher temperatures (Figure 1-3a,b), surface water pCO_2 can be reduced by algal primary production. This drives particulate organic carbon (POC) export out of the surface mixed layer and promotes increased atmospheric CO_2 uptake (e.g., Arrigo et al., 2010 and references therein; Gibson et al., 1999). Persistent ice cover

maintains a substrate for the continued growth of bottom ice associated algae, and melt pond communities develop in ponds which maintain connectivity to nutrient supplies from under ice waters either through freeboard flushing or by melting out and flooding with seawater from below (Gleitz et al., 1995; Kennedy et al., 2002; Papadimitriou et al., 2009; Thomas et al., 2010). These communities also contribute to DIC drawdown in surface waters and the production and export of POC to the water column. Throughout the summer, melt water flushing continues to reduce the salinity of the persisting ice pack, resulting in the extremely low bulk salinity, on the order of 2-3, which characterizes Arctic multiyear ice (Petrich and Eicken, 2010). This further contributes to the freshening of under ice waters, which are primed to refreeze once temperatures plummet again in the fall.

1.3 Stable Carbon Isotopes as Tracers of Carbon-Cycling

The life cycle of sea ice, as just described, is summarized in Figure 1-2. While it is clear that sea ice can represent a strong source or sink of CO_2 from the atmosphere depending on the season, the contribution of seasonal processes to the net sequestration of carbon over the yearly cycle remains elusive. Stable carbon isotopes may be a useful tool to aid in answering this question. Isotopic signatures of particulate organic and dissolved inorganic carbon (POC and DIC) have been applied as tracers of carbon cycling in various polar system studies (e.g., Forest et al., 2011; Gibson et al., 1999; Griffith et al., 2012; Henley et al., 2012; Kennedy et al., 2002; Naidu et al., 2000; Papadimitriou et al., 2009, 2007; Parsons et al., 1989), but few have used them to look at processes occurring over the life cycle of sea ice.

1.3.1 Definitions and Theory

Carbon occurs naturally in two stable isotopic forms, ^{12}C (12 atomic mass units) and ^{13}C (13.0034 atomic mass units), with natural abundances of 98.89 % and 1.11 % respectively. A particularly important property of isotopic substances is their slightly different physiochemical behaviour due to slightly different atomic masses. This results in fractionation effects between isotopic pools when participating in reactions pathways that do not go to completion (as summarized in Zeebe and Wolf-Gladrow, 2001). For example, consider a closed container of seawater in equilibrium with a headspace. A $CO_2(aq)$ molecule containing a ^{13}C atom, the heavier of the two stable isotopes, will experience a lower vibrational frequency than the same molecule with a ^{12}C atom. This is due to the constraints of increased mass on vibrational energy. The result is that the $^{13}CO_2(aq)$ molecule requires more energy input to enter the gaseous phase with respect to the $^{12}CO_2(aq)$ molecule, leading to the build-up of $^{13}CO_2(aq)$ in solution, and $^{12}CO_2(g)$ in the headspace above. This phenomenon of isotope partitioning between phases, or between the products and reactants of a reaction, is termed an isotope fractionation effect.

Isotope fractionation effects can occur under thermodynamic equilibrium (i.e., in reaction pathways where no "net" reaction takes place as forward and backward rates are equal; termed equilibrium isotope effects) or under non-equilibrium conditions (i.e., where incomplete or unidirectional processes take place; termed kinetic isotope effects). Both equilibrium and kinetic isotope effects can lead to fractionation of isotopes between product and reactant pools, as long as the transformation of reactant to product is not complete. If transformation of the reactant to the product does continue to completion, the product will exhibit the same isotope ratio as the reactant and no isotopic fractionation will occur.

For considerations in the following text, when referring to the different concentrations of natural isotopes and fractionation effects on these distributions, isotope abundance in a sample is reported in terms of the ratio of $^{13}C/^{12}C$ with respect to a standard (equation 11). Samples collected as a component of this thesis were analyzed for their isotopic composition using an isotope ratio mass spectrometer (Isoprime-Microgas Multiflow system for δ^{13}C-DIC and Finnigan Deltaplus mass spectrometer for δ^{13}C-POC) with ratios reported with respect to the standard Vienna PeeDee Belemnite (vPDB), in units of per mil (‰).

$$\delta^{13}C = \left[\frac{\left({}^{13}C/{}^{12}C \right)_{Sample} - \left({}^{13}C/{}^{12}C \right)_{vPDB}}{\left({}^{13}C/{}^{12}C \right)_{vPDB}} \right] \times 1000\ ‰ \qquad (11)$$

1.3.2 Application to Marine and Polar Systems

Stable carbon isotopes have been well established as a useful tool in global applications of marine geochemistry and marine biology (e.g., François et al., 1993; Rau et al., 1992, 1991), and sea ice systems have not been left out in this regard. For example, polar scientists have utilized stable carbon isotopes extensively to investigate food web interactions (e.g., Forest et al., 2011; Hobson et al., 2002; Parsons et al., 1989), sedimentary material origin (e.g., Drenzek et al., 2007), and determine water column POC contributions of sea ice associated and pelagic algal communities (e.g., Arrigo et al., 2003; Gibson et al., 1999; Gleitz et al., 1995; Kennedy et al., 2002; Tremblay et al., 2006); however, only a few studies have attempted to utilize stable carbon isotopes as a tracer of chemical or biological changes during the life cycle of sea ice and/or that

of its associated brines (e.g., Gleitz et al., 1995; Kennedy et al., 2002; Munro et al., 2010; Papadimitriou et al., 2009, 2007). As was highlighted in the previous discussion, isotope effects are exhibited when reaction pathways are not allowed to continue to completion. In satisfying these conditions, Figure 1-2 illustrates several instances during the sea ice life cycle where products or reactants participating in reorganization of the carbonate system can be separated, and thus can potentially exhibit a measureable isotope effect on the resultant DIC pool.

Recent work by Papadimitriou et al. (2007, 2004) demonstrates that changes to the carbonate system under increasing brine salinity can lead to isotope effects. These authors were able to distinguish the effects of CO_2 degassing from a high salinity brine solution from that of $CaCO_3$ precipitation based on the distinct isotope effects associated with each of these processes. For example, at isotopic equilibrium and 0 °C, degassed CO_2 will be depleted in ^{13}C relative to HCO_3^- remaining in solution, according to the relationship $\varepsilon_{(CO2(g)\text{-}HCO3\text{-})eq}$ = - 10.7 ‰ (Zhang et al., 1995). On the other hand, precipitated $CaCO_3$ will be ^{13}C enriched, on the order of $\varepsilon_{(Calcite\text{-}HCO3\text{-})eq}$ = + 1.2 ‰ to $\varepsilon_{(aragonite\text{-}HCO3\text{-})eq}$ = + 3.1 ‰ (Romanek et al., 1992; Figure 1-5). Under equilibrium conditions, degassing of CO_2 alone (degassing into the brine channel or spaces in the sea ice matrix), leaves brine solution isotopically heavier than the parent seawater, whereas precipitation of $CaCO_3$ leaves brines isotopically lighter. Even larger magnitude isotope effects would be expected under kinetic fractionation occurring at gas-liquid and solid-liquid interfaces (Turner, 1982). Physical conditions during brine formation and concentration will strongly regulate which combination of fractionation effects are experienced by a brine solution, and as such, the magnitude of isotope effect captured by the final exported brine could potentially be as spatially heterogeneous as the ice itself. It can be expected, however, that under the conditions of

brine formation, the separation of reactants and products (either through CO_2 degassing or $CaCO_3$ precipitation) will most likely lead to an exported brine with an isotopic value differing from that of its parent water mass, suggesting the potential to utilize stable carbon isotope ratios to trace the addition of brines into the water column.

Biological organisms residing in sea ice will also impart an isotopic effect as they utilize CO_2 for photosynthesis (algae), or change the isotopic composition of the solution as they turn over particulate carbon during remineralization (heterotrophic bacteria and grazers). Carbon uptake and fixation during photosynthesis results in the preferential utilization of ^{12}C, with the largest isotope effect occurring during the fixation of carbon by the enzyme Ribulose Bisphosphate Carboxylase (RuBisCO). C isotope fractionation by RuBisCO has been estimated to be on the order of Δ -27.7 ‰ (Wong and Sackett, 1978). Algal biomass derived from C fixation thus exhibits a lighter (^{12}C enriched) isotopic signature than the original DIC pool, which becomes progressively ^{13}C enriched as more biomass is created. Growth under well supplied CO_2 conditions (for example, under conditions where nutrients are actively replenished by water column mixing), leads to the production of ^{12}C enriched (light) POC, whereas growth under conditions of limited CO_2 supply, (such as a semi-closed system of a brine channel network or under high algal growth rates) leads to a reduced isotope effect with POC becoming progressively more ^{13}C enriched (heavy) as CO_2 supply dwindles (as summarized in Thomas et al., 2010). Other factors such as cell physiological state, mechanisms of inorganic C uptake and assimilation, and phytoplankton species composition can also affect the magnitude of isotope effect in the resulting POC, and subsequently DIC, pools (e.g., Burkhardt et al., 1999; François et al., 1993; Henley et al., 2012; Michener and Schell, 1994). Comparatively, the isotope effect

imparted by respiration is minimal; resulting in evolved CO_2 expressing a stable isotope ratio equivalent to the remineralized POC (as summarized in Thomas et al., 2010).

Although biological activity in sea ice brines will lead to isotope effects in essentially the opposite direction of those seen during $CaCO_3$ precipitation, it is anticipated that these two different processes will occur during different times in sea ice evolution, only slightly overlapping in influence (e.g., $CaCO_3$ precipitation from fall to early spring, and photosynthesis occurring from early spring to early fall). By distinguishing between the effects of these different processes (biological vs. chemical) on stable isotope signatures of brine DIC and POC, it may in fact be possible to distinguish between carbon contributed to the water column via sea ice formation, growth and melt, and that imparted through air-sea gas exchange or removed by biological processes.

1.4 Thesis Organization

Many fundamental questions remain unresolved regarding the role of sea ice in the high latitude carbon cycle. For example, ongoing hydrographic changes associated with the decline in sea ice extent have been shown to impact the delivery and production of organic carbon along the shallow Arctic Ocean shelves (e.g., Arrigo et al., 2008; Carmack and Chapman, 2003; Macdonald et al., 2004b; McLaughlin et al., 2011), but little is known about how these changes will influence carbon distributions and composition in the newly ice free interior basins. In addition, although sea ice has been shown to be a direct source of CO_2 in winter (e.g., Papakyriakou and Miller, 2011) and a sink in late spring (e.g., Geilfus et al., 2012; Nomura et al.,

2013b, 2010), the processes governing the switch between these two extremes over the winter-spring transition have been given limited attention. Likewise, export of high-salinity brine during sea ice formation has been suggested as a mechanism to transfer DIC to surface waters, while TA is retained in the ice (e.g., Miller et al., 2011b; Omar et al., 2005; Rysgaard et al., 2011, 2009, 2007), but the role of this process in sequestering CO_2 on longer time scales with export below the mixed layer remains to be elucidated (e.g., Loose et al., 2011; Miller et al., 2011b). Furthermore, despite a growing interest in the carbonate system in sea ice brine over the past decade, the sea ice community lacks a basic characterization of the thermodynamic equilibria governing the inorganic carbon system in sea ice. This is critical information needed to understand the role of sea ice in the polar ocean carbon cycle.

This thesis attempts to address these questions through the investigation of naturally occurring stable isotope and geochemical tracers. The thesis is organized into four data chapters, which discuss the results from four field campaigns throughout the Canadian Arctic from 2008 to 2011. After this introduction, the second and third chapters apply stable carbon isotopes to trace the contributions of sea ice derived carbon (DIC and POC) into the water column of the Canada Basin, Arctic Ocean. The fourth and fifth chapters look more closely at carbon cycling within sea ice itself, using the measurement of carbonate system parameters (DIC, TA, pH, pCO_2) and stable isotopes (δ^{13}C-DIC and δ^{18}O-H_2O) to illustrate inventory changes over the winter-spring transition and discuss the quantification of carbonate system changes in high salinity, low temperature systems.

The four core data chapters are:

Chapter 2: Determination of Particulate Organic Carbon Sources to the Surface Mixed Layer of the Canada Basin, Arctic Ocean

In this chapter, I used stable carbon isotopes to evaluate the regional sources of POC in the surface mixed layer of the central Canada Basin. I found a strong link between high productivity and carbon uptake rates along the shallow shelves and the isotopic enrichment of ^{13}C. In contrast, isotopically-depleted POC in the central Canada Basin appeared to be sourced externally, through advective transport of riverine organic matter, whereas multi-year sea ice contributed negligibly to POC distributions. Freshwater sources to the central basin suggested that Russian river inputs are the predominant source of ^{13}C depleted organic matter to the mixed layer of the central Canada Basin.

Chapter 3: Multi-Tracer Study of the Dissolved Inorganic Carbon Content of the Canada Basin (Arctic Ocean) Halocline

I applied stable carbon isotopes and nutrient tracers to investigate the conservative and non-conservative processes contributing DIC to the DIC maximum in the south-western Canada Basin halocline. Results from this study indicate that air-sea gas exchange and sea ice brine injection of CO_2 are not important processes contributing DIC to halocline source waters. Rather, remineralization of organic matter along the Bering and Chukchi Sea

shelves was the overwhelming contributor of dissolved inorganic carbon to the south-western Canada Basin halocline in 2008 and 2009.

Chapter 4: Inorganic Carbon System Dynamics in Land-Fast Arctic Sea Ice during the Early-Melt Period

This chapter summarizes the findings of a six-week time series of discrete carbonate system and stable carbon isotope measurements in the Canadian Arctic Archipelago collected during the winter-spring transition. Thermodynamic processes contributing to freshwater brine dilution led to decreasing CO_2 partial pressures observed over the time peroid, while CO_2 diffusion across the ice-atmosphere and ice-water interfaces was impeded. The impact of seawater brine dilution and $CaCO_3$ dissolution on CO_2 distribution throughout the sea ice column was also evaluated, illustrating a major role for $CaCO_3$ dissolution in CO_2 uptake with spring warming.

Chapter 5: Over-Determination of the Carbonate System in Natural Sea Ice Brine and Assessment of Carbonic Acid Dissociation Constants under Low Temperature, High Salinity Conditions

In my last data chapter, I measured a number of carbonate system parameters in natural sea ice brine samples in order to 'over-determine' the system and thus evaluate the accuracy of equilibrium constants extrapolated from lower salinity, higher temperature oceanic waters. Through this study, we confirmed that seawater derived carbonic acid dissociation

constants may not be readily extrapolated to sea ice brine systems. Furthermore, we quantified average offsets between calculated and measured carbonate system parameters ranging from 10 % to 43 %. Our results underscore the need for the specific determination of carbonate system equilibrium constants under appropriate sea ice temperature and salinity conditions.

1.5 Tables

Table 1-1. Summer surface water conditions in the central Canada Basin [72.65 N, 144.74 W]

Date	July 24, 2008	**DIC**	1744 μmol kg^{-1}
Depth	1.7 m	**TA**	1837 μmol kg^{-1}
Temp	8.1 °C	$\boldsymbol{pCO_2}$	343 μatm
Salinity	21.46	$\mathbf{pH_{sws}}$	8.06

1.6 Figures

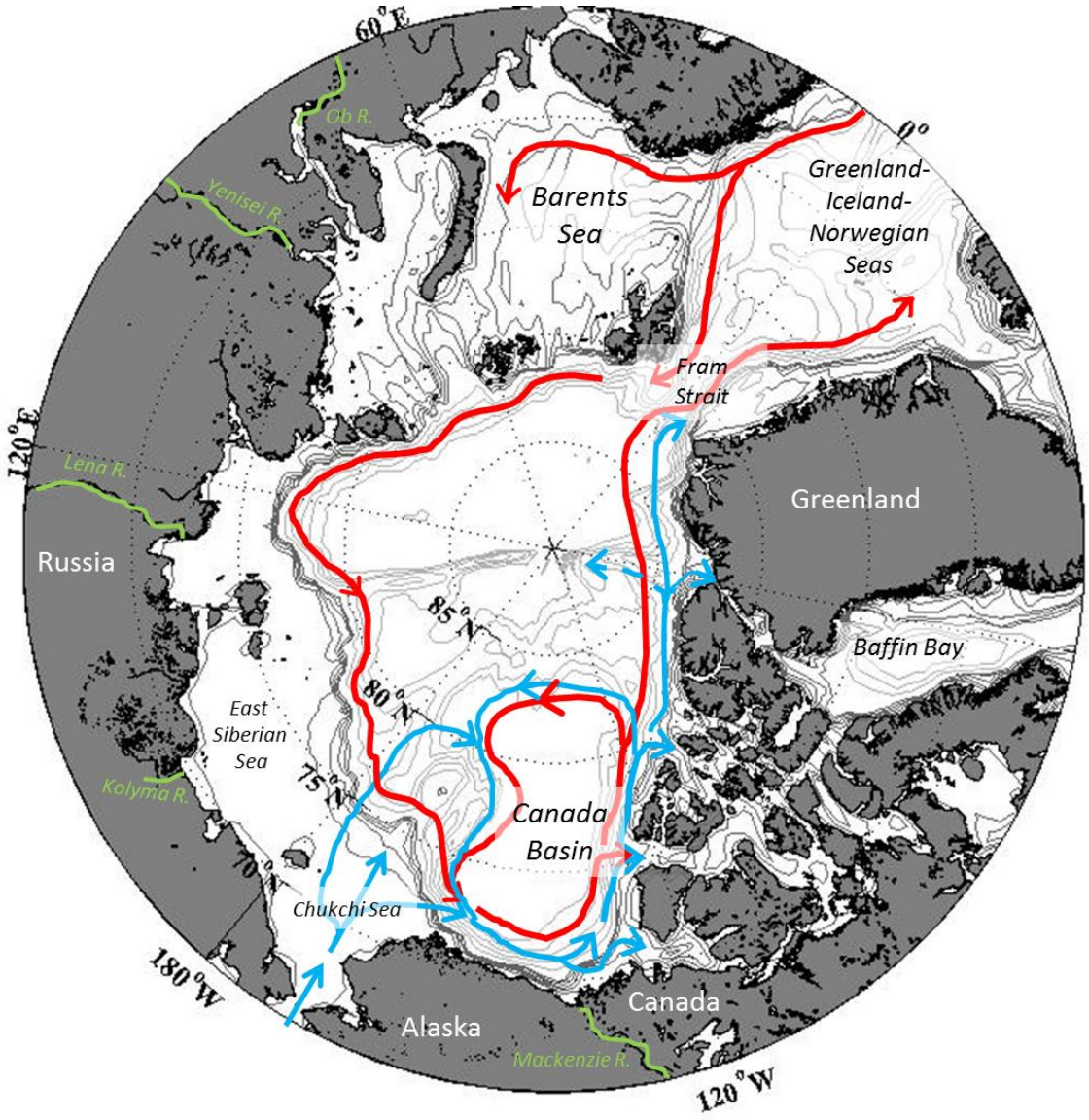

Figure 1-1. Map of the Arctic Ocean. Generalized circulation of major sub-surface Atlantic Ocean in-flows (> 200 m; red arrows) and surface Pacific Ocean flows (blue arrows), with emphasis placed on the Canada Basin (after McLaughlin et al., 1996; Macdonald et al., 2004b). Five of the major Arctic rivers are highlighted in green (a sixth would be the Yukon River which is transported into the Canada Basin via Alaskan Coastal Current flow through Bering Strait). Bathymetry indicated by light grey lines from 0 to 500 m (at 100 m intervals) and from 500 - 3000m (at 500 m intervals).

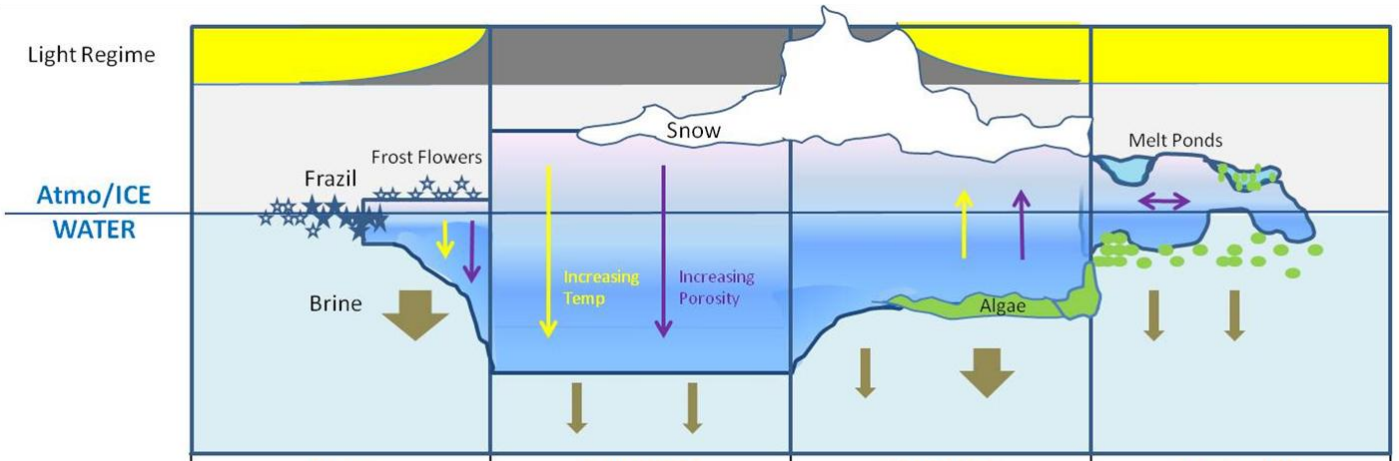

	FALL	WINTER	SPRING	SUMMER
Temperature	decreasing	decreasing	increasing	increasing
Salinity	increasing	increasing	decreasing	decreasing
T: K_o, K_1^*,K_2^*	$K_o\uparrow$ $K_1^*\downarrow$ $K_2^*\downarrow$	$K_o\uparrow$ $K_1^*\downarrow$ $K_2^*\downarrow$	$K_o\downarrow$ $K_1^*\uparrow$ $K_2^*\uparrow$	$K_o\downarrow$ $K_1^*\uparrow$ $K_2^*\uparrow$
S: K_o, K_1^*,K_2^*	$K_o\downarrow$ $K_1^*\uparrow$ $K_2^*\uparrow$	$K_o\downarrow$ $K_1^*\uparrow$ $K_2^*\uparrow$	$K_o\uparrow$ $K_1^*\downarrow$ $K_2^*\downarrow$	$K_o\uparrow$ $K_1^*\downarrow$ $K_2^*\downarrow$
$[CO_2](aq)$	lower temperatures increase CO_2 solubility	can migrate through connected brine channel network and into surface waters	reduced as $CaCO_3$ is resolubilized; increase in air-sea gas exchange through open brine channels	biological uptake reduces pCO_2, promoting undersaturation
$CaCO_3$	rising salinity increases $[CO_3^{2-}]$ proportion in DIC	trapped in brine channels	diluted and resolubilized	low salinity & high temp reduces proportion of $[CO_3^{2-}]$
Direct/Indirect Effects	well mixed surface layer leading up to ice formation; salts concentrated into brines; air-sea exchange reduced as ice layer forms	air-ocean exchange significantly reduced (upper pack porosity very low due to low temp); porosity remains slightly higher in warmer lower layers; $CaCO_3$ formation	emergence of light and revival of biological communities; increased porosity with warming; begin melt water flushing of brine channels	melting leads to surface stratification; algal communities in surface waters and associated with bottom ice draw down DIC

Figure 1-2. Summary of the sea ice annual cycle (see text for details).

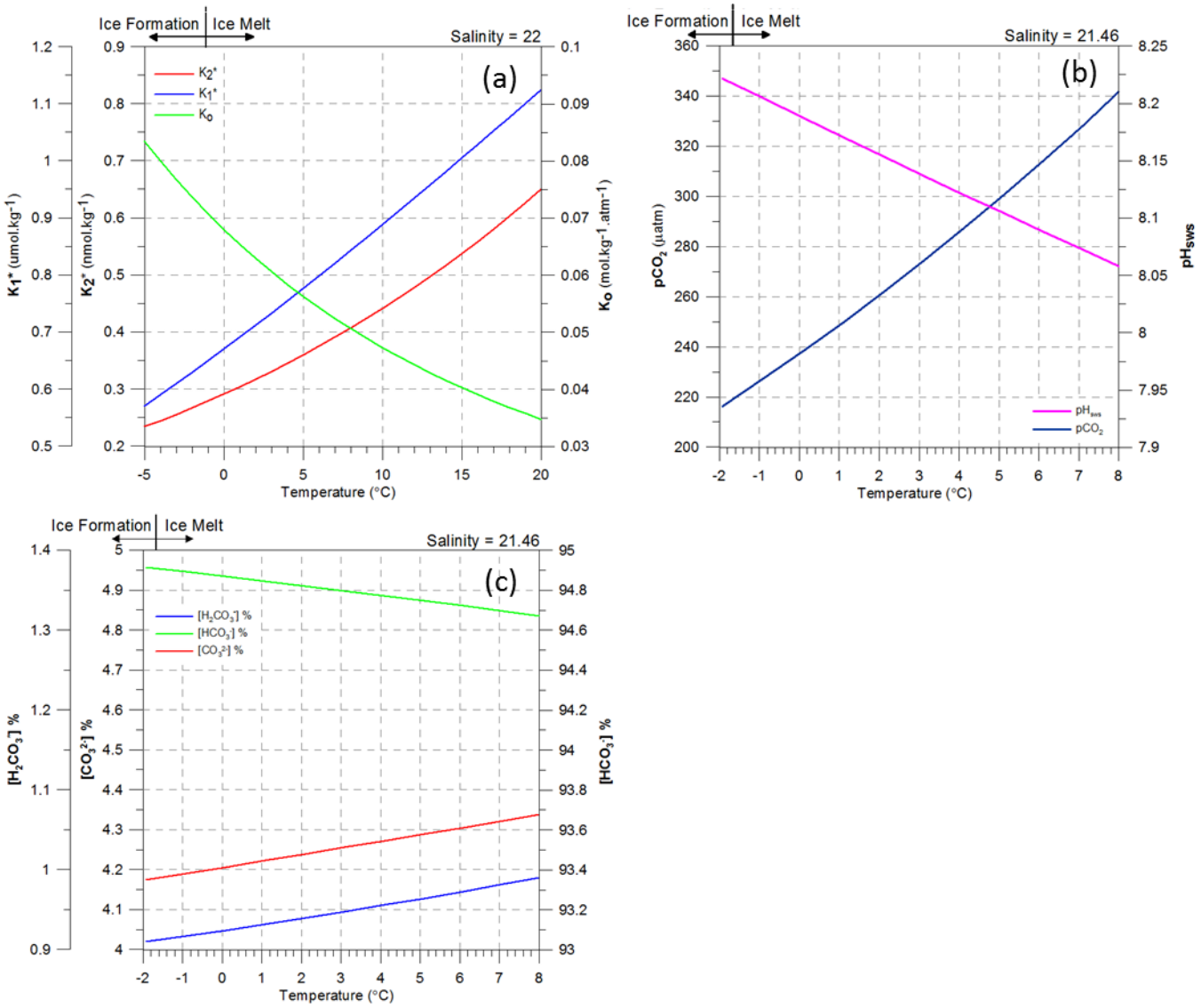

Figure 1-3. Cooling Seawater (a) Equilibrium constants K_o, K_1*, K_2*, as a function of temperature; (b) pCO_2 and pH_{SWS} as a function of temperature; (c) Solution composition of carbonate species as a % of DIC. *Equilibrium constant calculations* (a): K_1 and K_2 after Mehrbach et al. (1973) refit by Dickson and Millero (1987); K_o after Weiss (1974); KSO_4 after Dickson (1990). *Carbonate System Calculations* (b) and (c): CO2Sys (Pierrot et al., 2006) holding DIC, TA, and salinity constant according to Table 1-1. K_1 and K_2 as in (a).

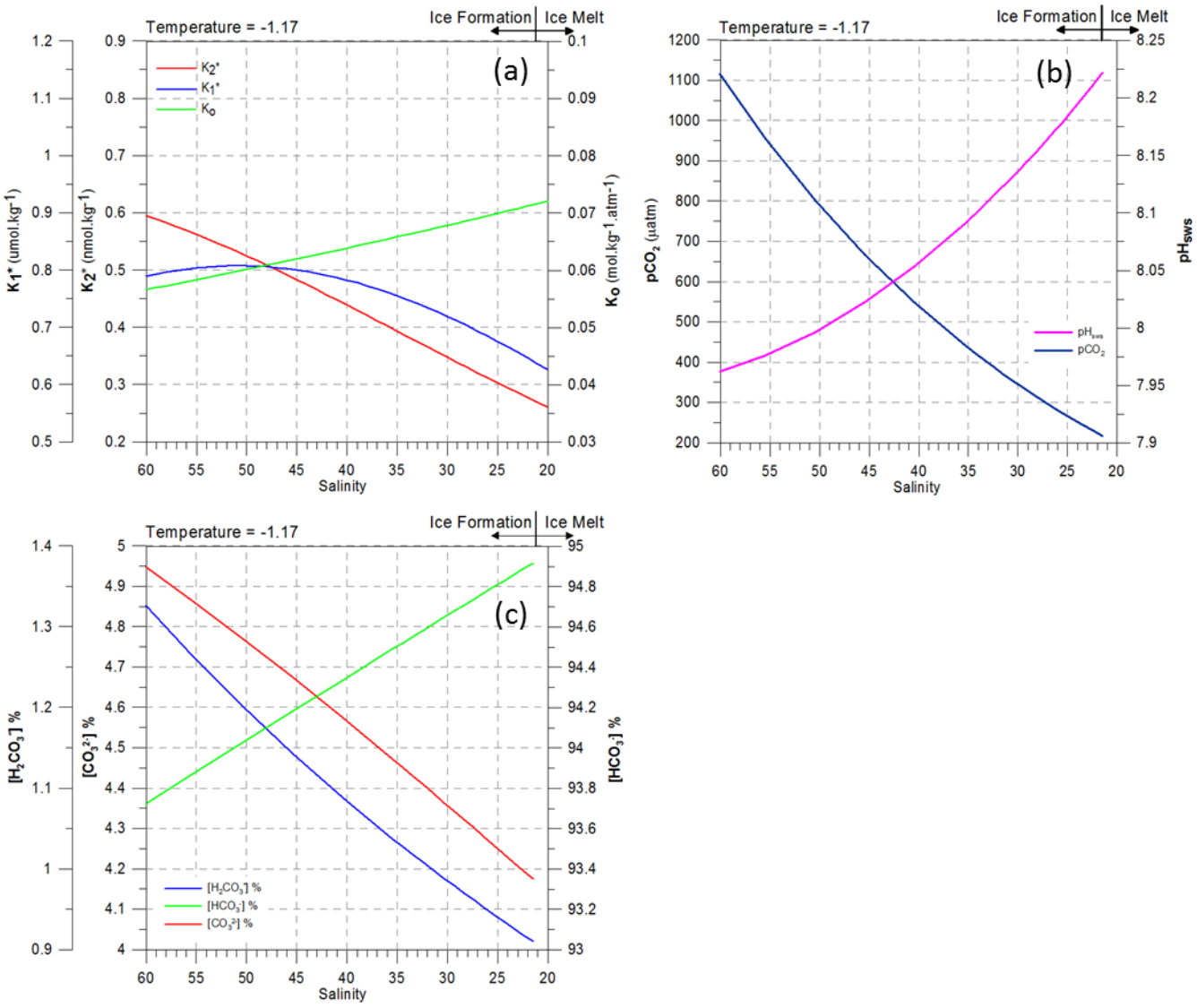

Figure 1-4. Removing Ice From Seawater (a) Equilibrium constants K_o, K_1*, K_2*, at constant temperature; (b) pCO_2 and pH_{SWS} as a function of salinity; (c) Solution composition of carbonate species as a % of DIC. Scales are the same as Figure 1-3. *Equilibrium constant calculations* (a): as in Figure 1-3(a); *Carbonate System Calculations* (b) and (c): CO2Sys (Pierrot et al., 2006) holding DIC and TA in constant proportion to salinity according to the initial conditions outlined in Table 1-1 and maintaining temperature at -1.17 °C. K_1 and K_2 as in Figure 1-3(a).

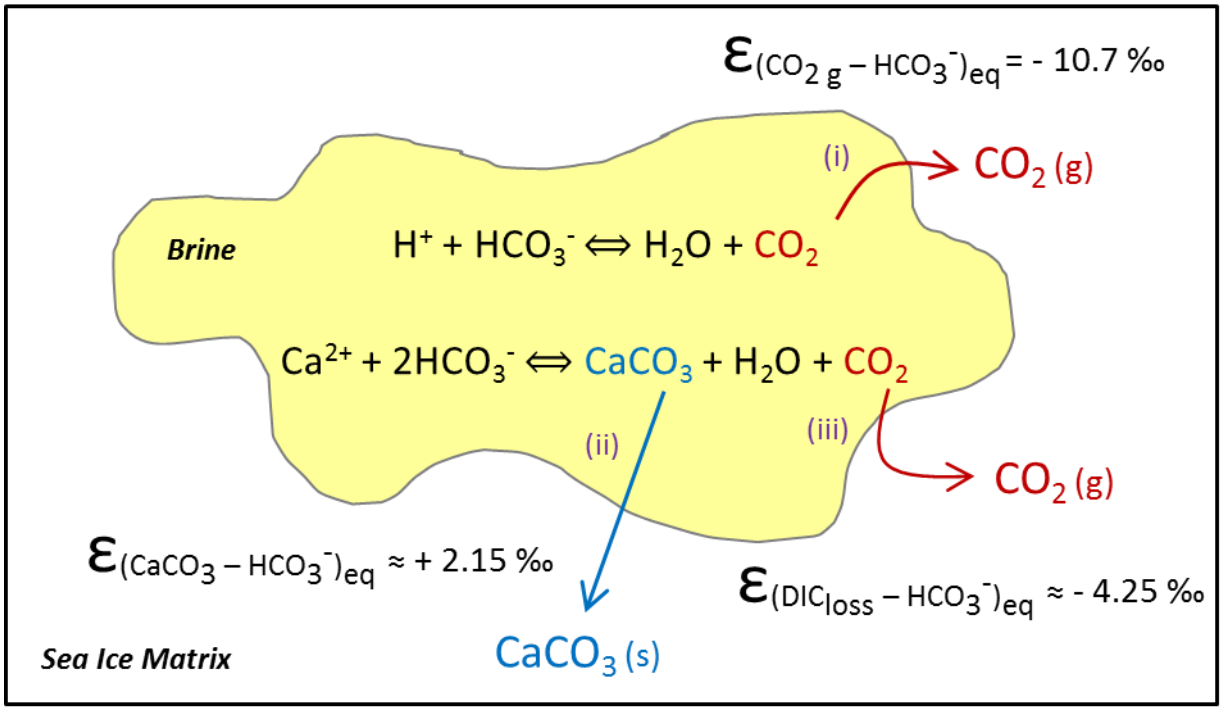

Figure 1-5. Equilibrium fractionation effects on the carbon stable isotope signatures of CO_2 and $CaCO_3$ during out-gassing and precipitation from brine solution. For example, (i) CO_2 out-gassing from solution will be isotopically depleted on the order of - 10.7 ‰ with respect to brine DIC, whereas (ii) $CaCO_3$ precipitated from solution will be isotopically enriched on the order of + 2.15 ‰ ($\varepsilon_{calcite}$ = + 1.2 ‰ and $\varepsilon_{aragonite}$ = + 3.1 ‰). If both $CaCO_3$ precipitation and CO_2 degassing remove DIC from brine simultaneously (50 % each), DIC lost from solution (DIC_{loss}) will be isotopically depleted on the order of - 4.25 ‰ with respect to brine solution ($\varepsilon_{loss\ calcite}$ = - 3.8 ‰ and $\varepsilon_{loss\ aragonite}$ = - 4.7 ‰), , after Papadimitriou et al. (2004).

Chapter 2: Determination of Particulate Organic Carbon Sources to the Surface Mixed Layer of the Canada Basin, Arctic Ocean

Stable isotope ratios of particulate organic carbon (POC), together with other tracers, were analyzed in samples from the Canada Basin surface mixed layer in 2008 and 2009. Sampling was conducted during the end of the 2008 melt season and at the beginning of the 2009 freeze up under a variety of surface conditions, including open water, newly formed seasonal ice, and multi-year ice. In both years, POC exhibited a wide isotopic range (δ^{13}C-POC -24.5 to -31.1 ‰), with the most isotopically-depleted material generally found in the central basin. Isotopically-enriched material was found on the shelves, consistent with higher biological production and strongly correlated with in situ carbon-uptake rates. In contrast, offshore in the central basin, there was no significant relationship between δ^{13}C-POC distributions and either chlorophyll *a* or aqueous CO_2 concentrations, suggesting that in situ biological production was not the dominant control. Analysis of freshwater sources suggested that the sea ice melt contribution of POC to surface waters in the central Canada Basin exerted a negligible influence on δ^{13}C-POC distributions, and instead isotopically-depleted POC in the surface waters of the central Canada Basin were sourced externally through advective transport of riverine organic matter. We show that alkalinity and meteoric water content can be used to distinguish POC inputs from North American and Russian rivers and our analysis suggests that Russian river inputs are the predominant source of ^{13}C-depleted organic matter to the mixed layer of the central Canada Basin.

2.1 Introduction

Dramatic hydrographic changes in surface waters of the Canada Basin have been observed since the early 2000's in conjunction with a persistent decline in summer sea ice extent and reduced multiyear sea ice presence throughout the Arctic Ocean (Kwok et al., 2009; McLaughlin et al., 2011; National Snow and Ice Data Center, 2010; Stroeve et al., 2008). Over this period, the Canada Basin surface mixed layer (SML) freshened (McLaughlin et al., 2011; Morison et al., 2012; Serreze et al., 2006; Yamamoto-Kawai et al., 2005, 2009), warmed (Jackson et al., 2010b), and shoaled, becoming increasingly stratified (McLaughlin and Carmack, 2010; Toole et al., 2010).

Changes in sea ice extent and melt season length are expected to impact particulate organic carbon (POC) delivery and production within the Canada Basin SML through enhanced pelagic primary productivity (Arrigo et al., 2008; Lee and Whitledge, 2005), changes in production from sea ice algae (Boetius et al., 2013; Lee et al., 2011), and changes to the pathways of sea ice and surface water transport (e.g., Morison et al., 2012). Effects due to increased Arctic river discharge and sediment erosion (Carmack et al., 2006; Lalande et al., 2009; Macdonald et al., 2004b) will also have impacts. Enhanced pelagic primary productivity has already been attributed to diminishing sea ice cover and enhanced upwelling along the shallow Arctic shelves (Arrigo et al., 2008; Tremblay et al., 2011), while in the perennially ice covered central basin stratification and downwelling have reduced nutrient availability (McLaughlin and Carmack, 2010; Yang, 2009) in a system where POC concentrations are already exceedingly low compared to the shallow shelves (Cai et al., 2010; Jackson et al., 2010a). It is thus likely that ongoing hydrographic changes in the Arctic Ocean will influence the distribution and cycling of POC

throughout the basin, and shift the relative magnitude of various POC sources. The extent to which such changes in POC cycling have already occurred is presently unknown.

Stable isotopic signatures of particulate organic carbon (δ^{13}C-POC) have been used as tracers of POC provenance in marine systems. In particular, studies in high latitude oceans have used δ^{13}C-POC to distinguish between pelagic and sea ice algal communities (Arrigo et al., 2003; Gibson et al., 1999; Henley et al., 2012; Kennedy et al., 2002; Schubert and Calvert, 2001; Tremblay et al., 2006; Zhang et al., 2012), and between marine and terrigenous inputs along the continental shelf (e.g., Griffith et al., 2012; Naidu et al., 2000; Parsons et al., 1989; Stein and Macdonald, 2004). As such, δ^{13}C-POC distributions in the SML may provide a sensitive indicator of the influence of changing sea ice conditions and climatic warming on POC delivery and production within the central Canada Basin once baseline observations are established.

In this study we employ δ^{13}C-POC to investigate POC sources to the SML of the Canada Basin. By sampling at different periods during the year under a variety of surface ocean conditions, from open water regions into the multi-year ice pack, we were able to examine spatial and temporal variability in δ^{13}C across various sea ice and hydrographic regimes. To aid this investigation, a suite of geochemical tracers were also used to characterize the SML, specifically: freshwater composition and sources (oxygen isotope ratios (δ^{18}O-H_2O), nutrients (NH_4, NO_3^- + NO_2^-), inorganic carbon system (dissolved inorganic carbon (DIC) and total alkalinity (TAlk)) and its isotopic signature (δ^{13}C-DIC), photosynthetic biomass (chlorophyll *a*), and carbon uptake rates.

2.2 Sample Collection and Analytical Methods

2.2.1 Sampling and Analyses of Geochemical Parameters

Hydrographic observations and geochemical samples were collected aboard the *CCGS Louis S St-Laurent* as part of the Canada-US Joint Ocean Ice System Study (JOIS) and the International Polar Year Canada's Three Oceans (IPY-C3O) program (Figure 2-1). Samples were collected primarily from the deep central (> 750 m bottom depth) Canada Basin in the summer of 2008 (July 17th to August 21st) and fall of 2009 (September 17th to October 15th). An additional transect consisting of four stations was sampled from the shallow Mackenzie Shelf (~60 m bottom depth) to the deep central Canada Basin (~3000 m bottom depth) in the late summer of 2009 (August 27th to September 12th) aboard the *CCGS Amundsen* as part of a joint IPY ArcticNet and GEOTRACES program (Figure 2-1, inset).

Samples for geochemical analyses during the JOIS-IPY-C3O cruises were collected either from 10 L Niskin bottles mounted on an ice-strengthened CTD rosette system or from the ship's underway intake located at a nominal depth of 9 m. Underway samples were collected while the ship was approaching station, with sampling (duration ~ 11 min.) beginning about 20 minutes prior to arrival on station (equivalent to ~ 4 km). Conductivity, temperature, and pressure were measured using a CTD mounted on the rosette (Seabird SBE911+ system). Seawater conductivity measurements were verified against discrete salinity (S) samples taken from each rosette cast. Salinity samples were analyzed using a Guildline Autosalinometer Model 8400B calibrated with IAPSO standard seawater. Further details on geochemical sampling and

shipboard measurements of S, as well as methods for chlorophyll *a*, and nutrients (NO_3^- + NO_2^-, NH_4^+) during the JOIS-IPY-C3O programs can be found in McLaughlin et al., (2012).

Analytical precision for each geochemical parameter measured in this study is listed in Table 2-1 and presented as the pooled standard deviation (*S*p). *S*p is calculated for a series of duplicate sample measurements (x_1 and x_2) carried out under similar conditions and is determined as $Sp=[\sum(xi_1-xi_2)^2/2k]^{1/2}$, where k is the number of duplicate pairs analyzed (IUPAC, 1997). It is assumed that measurements carried out under similar conditions are of the same precision, although their means may differ, and as such, *S*p is a better estimate of the underlying standard deviation of the analyses than individual calculated standard deviations of k measurements (IUPAC, 1997).

Geochemical methods and sampling details for the IPY-ArcticNet-GEOTRACES cruise are described in Else et al. (2013), whereas the determination of δ^{13}C-POC, δ^{13}C-DIC, and carbon uptake rates are described below.

2.2.2 Oxygen Isotopes

$\delta^{18}O$-H_2O samples were collected from Niskin bottles on the ship's CTD-Rosette in 2008 and from the surface seawater intake system in 2009 during the JOIS-IPY-C3O programs, following the methods outlined in Epstein and Mayeda (1953). $\delta^{18}O$-H_2O samples were analyzed at Oregon State University's COAS Stable Isotope Lab using a Thermo Finnigan DeltaPlus XL isotope ratio mass spectrometer. Oxygen isotopic values are reported in per mil (‰) with respect to Vienna Standard Mean Ocean Water (V-SMOW) (standard error ± 0.05 ‰).

2.2.3 Stable Isotope Composition of POC

δ^{13}C-POC samples were collected from the ship's seawater intake system during the JOIS-IPY-C3O cruises, and from 10 L Niskin bottles during the IPY-ArcticNet-GEOTRACES program. Between 2 and 8 L of surface seawater were collected into 2 L polycarbonate bottles and immediately filtered through 47 mm or 25 mm pre-combusted (4+ hrs at 450 °C) glass microfiber filters (Whatman GF/F, 0.7 μm). Filters were stored at - 80 °C and later oven dried at 50 °C for 24 hrs. To remove particulate inorganic carbon, filters were acid fumed over concentrated HCl for 2 days, then dried again at 50 °C for 24 hrs. δ^{13}C-POC was determined at UBC-PCIGR on a Finnigan Deltaplus mass spectrometer, calibrated against international standards NBS-19 and NBS-20, and reported with respect to Vienna Peedee Belemnite (VPDB) (standard error ± 0.2 ‰). δ^{13}C-POC values reported in this study are based on the analyses of duplicate filters and carbon concentration values have a relative standard deviation (% RSD) of 1-2 %.

2.2.4 Dissolved Inorganic Carbon, Total Alkalinity, and δ^{13}C-DIC

Samples for the determination of DIC, TAlk, and δ^{13}C-DIC were collected from Niskin bottles (2008 and 2009) and from the ship's seawater intake (2009) during the JOIS-IPY-C3O program. Carbonate system parameters (pH, TAlk, and δ^{13}C-DIC) collected during the IPY-ArcticNet-GEOTRACES program were likewise collected from Niskin bottles. In 2008, DIC and TAlk samples were drawn, bubble free, from each Niskin bottle using clean Tygon tubing into 250 mL borosilicate glass reagent bottles, allowed to overflow 1 full volume, and the headspace was adjusted to 1 % of sample volume with a stopper. Samples were preserved with 100 μL saturated

$HgCl_2$ before sealing with ground glass stoppers treated with silicon-free high vacuum grease and secured with electrical tape. Samples were stored at 4 °C until analysis. In 2009, 10 L surface samples from the underway system were collected as the ship approached station. After gently inverting the container three times to homogenize the sample, a spigot fitted with clean Tygon tubing was attached and subsamples for discrete geochemical parameters were collected in the same manner as from Niskin bottles. In both years, δ^{13}C-DIC samples were carefully drawn, free of bubbles, into 30 mL amber soda-lime glass bottles, allowed to fill twice the bottle volume, and sealed with no headspace. Samples were preserved with 30 μL saturated $HgCl_2$ and sealed with Poly-Seal*-lined caps, secured with Parafilm, and maintained at 4 °C until analysis.

Although underway intake systems on vessels can pose CO_2 contamination risk when not properly cleaned (e.g., Juranek et al., 2010), DIC samples collected from the ships underway intake matched very well (within 0.5 %; n = 29) with discrete station samples. We believe this small error to be within the error of spatial-temporal heterogeneity of the two sampling events (intake sampling while approaching station and on station rosette) and thus have not applied any correction for difference in sample collection methods.

DIC was measured coulometrically following Dickson et al. (2007) using either a VINDTA 3D (Marianda) or SOMMA-I (Brookhaven National Labs) system at the Institute of Ocean Sciences, Sidney, B.C.. TAlk was determined using an open-cell continuous titration with an automated Dosimat 665 titrator (Metrohm) and Red Rod pH combination electrode (Radiometer Analytical). Endpoint detection was determined using a modified version of Dickson et al.'s

(2007) LabView program. Both DIC and TAlk were calibrated against certified reference materials provided by Andrew Dickson (Batch 88, Scripps Institute of Oceanography).

δ^{13}C-DIC samples collected during both the JOIS-IPY-C3O and IPY-ArcticNet-GEOTRACES programs were analyzed at GEOTOP Stable Isotope Laboratory (Université du Québec à Montréal) using a Micromass Isoprime continuous flow isotope ratio mass spectrometer equipped with a MultiFlow (Isoprime) automated injection system. Carbon isotopic values are reported in per mil (‰) with respect to VPDB referenced to the NBS-19 and LSVEC scales (standard error ± 0.1 ‰). All δ^{13}C-DIC values reported in this study are based on duplicate analyses.

2.2.5 Surface Mixed Layer Carbon Uptake Rates (Photosynthetic Rate)

On-deck experiments for the measurement of in situ carbon (C) uptake rates were carried out at each station during the IPY-ArcticNet-GEOTRACES program. Triplicate water column samples were obtained at 50 % incident surface irradiance within the euphotic zone, corresponding roughly with 3 - 22 m water depth (where the surface mixed layer was between 10 - 23 m; Else et al., 2013). Samples used for the determination of total C-uptake were inoculated using $KH^{13}CO_3$ (99 % purity) isotope tracer stock (Cambridge Isotopes Laboratories) with the target ^{13}C enrichment of each sample being < 10 % of the total ambient DIC. Samples were covered with neutral density screening to simulate the 50 % irradiance level and incubated on-deck in acrylic tanks continuously replenished with surface seawater for approximately 24 hours. Samples were collected onto glass fiber filters (GF/F) and then dried at 60 °C. Isotopic composition and total particulate organic C and N were measured at the Stable Isotope Facility at

the University of California Davis with a PDZ Europa ANCA-GSL elemental analyzer and a PDZ Europa 20-20 isotope ratio mass spectrometer. Carbon uptake rates were calculated from ^{13}C-assimilation as described by Hama et al. (1983).

2.2.6 Sea Ice Core Samples

Full thickness sea ice cores from new, first-year, and multi-year ice were collected opportunistically at several locations during the 2009 JOIS-IPY-C3O program using a Kovacs Mark II 9cm diameter corer. Once removed, full core lengths (new ice) or sub-sections cut with a hand saw (multi-year ice) were melted at room temperature for physical (S) and geochemical ($\delta\ ^{13}C$-POC, $\delta\ ^{18}O$-H_2O) measurements. Sea ice melt S was determined using a handheld conductivity meter (YSI Model 30 SCT Handheld Conductivity Meter: precision ± 2 %; resolution 0.1) operating on a factory calibration, with periodic recalibration to a conductivity standard set of 1 mS cm^{-1}, 10 mS cm^{-1}, and 50 mS cm^{-1}. Sea ice cores used for $\delta\ ^{13}C$-POC and $\delta\ ^{18}O$-H_2O determination were melted in the dark at room temperature within gas tight Tedlar™ film bags. $\delta\ ^{13}C$-POC and $\delta\ ^{18}O$-H_2O samples from melted sea ice were processed in the same manner as seawater samples described above.

2.2.7 Sea Ice Concentration

Sea ice concentration along the cruise track was obtained at 3.125 km resolution from the University of Bremen, Germany (www.seaice.de). Daily concentrations were determined from the Advanced Microwave Scanning Radiometer sensor (89 GHz frequency) on NASA's Earth Observing System satellite (AMSR-E) using the ARTIST Sea Ice algorithm (Spreen et al., 2008).

The reported sea ice concentration at each station was determined by a nearest neighbour bi-linear interpolation between the four grid cells closest to the actual station location.

2.3 Calculations

2.3.1 Surface Mixed Layer Determination

The depth of the SML at each station was calculated using 1 m averaged downcast CTD data and defined as the point where potential density first exceeded the shallowest sampled density by 0.01 kg m^{-3} (relative to 0 dbar), following Toole et al. (2010). Since most of the 2008 sampling period was in late summer when surface waters were highly stratified (especially near the shelf), SML depths found to be within 3 m of the air-ocean interface (or, < 2 m from the shallowest sampled depth of 0.99 m, following Toole et al., 2010) were recalculated using a density-difference criterion of 0.1 kg m^{-3}. Mean SML S and T were then determined.

2.3.2 Freshwater Components

Freshwater components of the SML were quantified using measured $\delta\,^{18}O\text{-}H_2O$, S, and TAlk following Yamamoto-Kawai et al. (2009). Components of the SML in the Canada Basin include: Arctic meteoric water (MW, which includes both river inflow and precipitation); sea ice melt (SIM) or formation (-SIM); and Pacific water (PW) which is the saline end member and enters via the Bering Sea. Fractional contributions of the three end member components can be determined from the following equations (after Östlund and Hut, 1984):

$$f_{SIM} + f_{MW} + f_{PW} = 1$$

$$f_{SIM}S_{SIM} + f_{MW}S_{MW} + f_{PW}S_{PW} = S_{OBS}$$

$$f_{SIM}\delta^{18}O_{SIM} + f_{MW}\delta^{18}O_{MW} + f_{PW}\delta^{18}O_{PW} = \delta^{18}O_{OBS}$$

where f_{SIM} becomes negative when brine is added to surface waters during sea ice formation. Here we use end member values as selected for the Canada Basin by Yamamoto-Kawai et al. (2009), and listed in Table 2-2: the PW end member values are determined from mean near bottom (~ 50 m) water properties in the Bering Strait; SIM from sea ice sampled within the Canada Basin; and MW from Arctic river properties described by Cooper et al. (2008). We used a non-zero S_{SIM} end member (S_{SIM} = 4) to include salt that is retained as brine in the sea ice matrix and subsequently released to surface waters upon melt. For comparison we also calculated the freshwater fractions using S_{SIM} = 0 which, on average, underestimated the sea ice melt fraction (*f*SIM = - 0.0088) and overestimated the meteoric water faction (*f*MW = + 0.0005). As this difference negligibly impacted the derivation of other calculated parameters (< 1 % change in $pAlk_o$ and S_o, calculated as described below) we have chosen to maintain the use of S_{SIM} = 4 end member so that our calculated freshwater inventories can be compared to other studies conducted in the same region (e.g., Guay et al., 2009; McLaughlin et al., 2011; Yamamoto-Kawai et al., 2005, 2009).

Uncertainty in the calculation of freshwater fractions (f_{SIM} and f_{MW}) using our data set are ± 0.02, and are derived primarily from uncertainty in $\delta\,^{18}O\text{-}H_2O$ analyses (Table 2-1). Seasonal

variability in Bering Sea through-flow S (31.9 - 33) and $\delta^{18}O$ (- 1.2 to - 0.5 ‰) further influence f_{SIM} and f_{MW} calculations by ± 0.02 or less (as discussed in Yamamoto-Kawai et al., 2009). Freshwater components of the SML along the 2009 shelf-basin transect, presented in Else et al. (2013), were recalculated following Yamamoto-Kawai et al. (2009) for comparison with our central Canada Basin data, as well as data from Yamamoto-Kawai et al. (2009) and McLaughlin et al. (2011).

The origin of the MW runoff component can be further resolved using TAlk, a quasi-conservative property in the Arctic Ocean, as discussed in Yamamoto-Kawai et al. (2009). Since nutrient concentrations in the central Canada Basin SML are low, we have chosen to neglect the biological impacts on alkalinity (e.g., Brewer and Goldman, 1976) and treat TAlk as a conservative tracer of mixing. If nitrate and ammonium assimilation and organic matter remineralization were included in our consideration of TAlk, our values would change by as little as - 0.40 to + 0.20 μmol kg^{-1} (see Yamamoto-Kawai et al. (2009) for a discussion on the use of Potential Alkalinity). Normalizing TAlk (NAlk) to the reference S of incoming Pacific water highlights riverine additions of TAlk to the SML over additions of SIM (as TAlk additions due to SIM dilution are much smaller, Table 2-2) and removes any small influence of local precipitation, which dilutes TAlk and S equally (S ≈ 0, TAlk ≈ 0 μmol kg^{-1}):

$$NAlk = (\frac{TAlk}{S}) \times S_R$$

where S refers to measured S and S_R is the reference S of PW (S = 32.5). North American and Eurasian river inputs to the Canada Basin SML can be identified based on their alkalinity as they dilute incoming Pacific water. Herein we distinguish the Ob', Yenisey, Lena, and Kolyma rivers as representing the major "Eurasian" riverine sources to the Arctic Ocean (following Cooper et al., 2008) and more specifically "Russian" riverine sources as the subset contribution from the Lena and Kolyma rivers. Higher alkalinity values are found in North American than Eurasian rivers (TAlk ~ 1600 μmol kg^{-1} versus ~ 800 μmol kg^{-1} respectively, Cooper et al., 2008). River inputs will elevate NAlk above the PW end member (TAlk ~ 2200 μmol kg^{-1}), allowing the contributions of these two sources to be qualitatively distinguished when combined with the observed MW content (Yamamoto-Kawai et al., 2009). Our use of NAlk to distinguish fresh water sources in the SML is substantiated by barium measurements from the 2008 sampling program, with high barium concentrations, which provide a quantitative assessment of incoming North American rivers, being associated with regions of high NAlk and high MW content in 2008 (McLaughlin et al., 2011).

2.3.3 Inorganic Carbon System Components

CO_2(aq) concentration was calculated from measured DIC, TAlk, S, and T using the MS Excel version of CO2Sys (co2sys_xls_program, Pierrot et al., 2006), with equilibrium constants K_1 and K_2 defined by Mehrbach et al. (1973) and refit by Dickson and Millero (1987), and the dissociation constants for $KHSO_4$ determined by Dickson (1990). Similarly, DIC and CO_2(aq) reported for the IPY-ArcticNet-GEOTRACES program were calculated from measured values of TAlk and pH following the same methodology, as described in Else et al. (2013). $\delta\ ^{13}C$ -CO_2(aq) was calculated from measured $\delta\ ^{13}C$-DIC, DIC, TAlk, and T, using the equations of Mook (1986)

and Zhang et al. (1995) for carbon isotope fractionation factors derived in freshwater (as summarized in Zeebe and Wolf-Gladrow, 2001).

2.4 Results

Observations carried out in this study took place during three different field programs, spanning three seasonal periods, and different regions of the Canada Basin. With these differences in mind, results from the two basin-wide cruises carried out during the JOIS-IPY-C3O program in the summer of 2008 and the fall of 2009 are presented first, followed by those from the shelf-basin transect carried out during the IPY-ArcticNet-GEOTRACES program in the summer of 2009. As described below, these different regions showed strongly contrasting $\delta^{13}C$ distributions and controlling factors.

2.4.1 Observations of the Canada Basin Surface Mixed Layer: Summer 2008 vs. Fall 2009

2.4.1.1 Physical Characteristics of the Canada Basin Surface Mixed Layer

We observed significantly different SML characteristics in the Canada Basin during the 2008 and 2009 field campaigns. The 2008 field program was carried out while sea ice was still melting (National Snow and Ice Data Center, 2010) and, as such, the Canada Basin was characterized by large areas of open water (Figure 2-2a). Sea ice concentrations of 50 – 90 % were only found north of 80° in the west and north of 75° in the east. Ice free regions in the south were very fresh and warm, especially near the shelf, with more saline and near the freezing point waters found north of 75° and in the presence of ice (Figure 2-2b,c). In contrast, the fall 2009 field program

was carried out two months later in the annual cycle, after the onset of freeze up (National Snow and Ice Data Center, 2010). At that time, the central basin SML was characterized by much higher concentrations (> 90%) of sea ice (Figure 2-2g), lower T (Figure 2-2h), and a much reduced range of S (Figure 2-2i). In 2009 open water was found south of 72° across the entire Beaufort Shelf and also near 75°N in the west, north of Alaska (Figure 2-2g). In regions with significant sea ice concentration, T was close to the freezing point, whereas open ocean waters were slightly warmer (Figure 2-2h). Mean SML S exhibited a smaller range in 2009 (23.50 to 28.01) compared to 2008 (18.77 to 30.01), with fresher waters in the southwest and more saline waters in the northwest and east (Figure 2-2i).

The difference in SML depth between sampling years likely reflects the different seasonal periods that we sampled (Figure 2-2d,j). Shallower SML depths were observed in the summer of 2008 ($\bar{x}$ = 7.4 +/- 3.8 m) than in the fall of 2009 ($\bar{x}$ = 13.5 +/- 6.5 m). The deepest SML depths (up to 25 m) were observed offshore in the eastern region of the survey in 2009 (Figure 2-2j). The 2008 SML was observed to be more evenly distributed as a 5 – 10 m layer in the central basin (Figure 2-2d), with a pronounced maximum in the northwest, up to 19 m depth. In both years the shallowest depths were found along the Beaufort Shelf.

Generally, MW contributed more than SIM to surface freshening of the SML over most regions in both 2008 and 2009 (Figure 2-2e,f; k,l). In 2008, fractions of MW were highest (20 %) near the mouth of the Mackenzie River in the east and decreased northward (Figure 2-2f). Lower MW concentrations (≈ 12.5 % MW) and apparent sea ice formation (negative SIM) were seen in the northwest (Figure 2-2e). The region of apparent sea ice formation (negative SIM) was also

associated with higher S (Figure 2-2c) and a deeper mixed layer (Figure 2-2d), possibly indicating deep convective mixing associated with sea ice formation. In 2009, high SIM content was restricted to the south (Figure 2-2k), and decreased towards the northeast. MW was more evenly distributed over the entire basin in 2009 with no signal of Mackenzie River outflow (Figure 2-2l).

The spatial distribution of NAlk is used to assess MW sources across our survey region. In 2008 high NAlk was observed in the southeastern Beaufort Shelf (Figure 2-3a), with concentrations decreasing towards the north, similar to the MW distribution (Figure 2-2f). Low S in conjunction with high MW and NAlk values (Figure 2-2c,f; Figure 2-3a) indicate Mackenzie River inflow is the source of freshening in the south east (cf. McLaughlin et al., 2011, barium surface map). In contrast, lower NAlk concentrations observed in conjunction with high MW content north of 75° N indicate Eurasian rivers are the primary source of MW in the northwest (Figure 2-3a). In 2009, relatively high values of NAlk (~ 2400 μmol kg^{-1}) were found centered in the basin coincident with the highest MW concentrations, however these values were much lower than those observed in 2008 near the Mackenzie River outflow (~ 2600 μmol kg^{-1}; Figure 2-3a,e), which suggests that Eurasian rivers were the main source of surface freshening in 2009 (cf. McLaughlin et al., 2011).

2.4.1.2 Chlorophyll *a*, $\delta^{13}C$ -POC, and CO_2(aq) Distributions in the SML

Surface mixed layer chlorophyll *a* concentrations in both the summer of 2008 and fall of 2009 were extremely low in the central basin and almost always less than 0.1 μg L^{-1} (Figure 2-3b,f). These values are consistent with observations of low SML phytoplankton biomass (Taylor et al.,

2013; Yun et al., 2012), and a deep chlorophyll *a* maxima (average ~50 m in the central basin; Yun et al., 2012). In 2008 the highest concentrations of chlorophyll *a* were found near the mouth of the Mackenzie River (up to 0.47 μg L^{-1}) and along the southern Beaufort Shelf (Figure 2-3b). In 2009, chlorophyll *a* was more uniformly distributed and low everywhere, with a maximum value of 0.15 μg L^{-1} observed north of the Mackenzie River (Figure 2-3f).

δ ^{13}C -POC values ranged from - 24.5 to - 31.1 ‰ in 2008 (Figure 2-3c), with isotopically-enriched values found north of 75 °N and in the south along the Beaufort Shelf. Although δ ^{13}C-POC covered a similar range in 2009, from - 26.1 to - 30.7 ‰, the mean δ^{13}C -POC in the central basin was more isotopically-depleted than in 2008, and more enriched values were found only in the south (Figure 2-3g). Stable carbon isotopic signatures of DIC were similar in both years, with average δ ^{13}C -DIC values of + 1.51 ‰ (± 0.39) and + 1.47 ‰ (± 0.14) in 2008 and 2009 respectively (not shown). Similarly, δ ^{13}C -CO_2(aq) varied over a small range of - 10.3 ‰ (± 0.2) and - 10.5 ‰ (± 0.2) in 2008 and 2009 respectively (not shown). CO_2(aq) concentrations exhibited similar variability in both years (Figure 2-3d,h) with values ranging from 15.5 to 24.9 μmol kg^{-1}.

2.4.1.3 Sea Ice δ ^{13}C-POC

Bulk sea ice samples were collected opportunistically to characterize potential δ ^{13}C-POC SML sources from melting ice. Table 2-3 reports S, δ ^{13}C-POC, and POC measurements from full depth or partial ice cores collected in new ice (a newly-frozen lead between two large multi-year ice floes), young ice (snow covered and formed between multi-year floes in a consolidated pack), and multi-year ice during the fall 2009 field season. SML δ ^{13}C-POC measured from the

underway system at each of the ice sampling stations was, on average, isotopically-depleted with respect to the ice core samples ($\bar{x}$ = - 29.1 ± 0.3 ‰, n = 3 stations). These SML values were found to be significantly different from overlying young and new ice ($p << 0.05$), but not different from multi-year ice ($p = 0.52$) (*students T test*).

2.4.2 Mackenzie Shelf to Central Canada Basin Transect: Late Summer 2009

In addition to our multi-year investigation of SML properties in the central Canada Basin, we also collected a limited set of observations of SML δ^{13}C-POC and biogeochemical properties at four stations along a transect from the mouth of the Mackenzie River (~60 m bottom depth) into the deep central basin around 74.5 °N (~3000 m bottom depth) during the 2009 late summer season.

2.4.3 Physical Characteristics of the SML along the Shelf-Basin Transect

Water column physical properties at the four stations are summarized in Table 2-4. The shelf-basin transect, conducted in late summer 2009, was characterized by ice-free waters along the shelf and full ice cover in the central basin (Table 2-4). In conjunction with increasing ice concentration, SML T decreased as SML S and mixed layer depth increased with distance from the shelf. Our recalculated freshwater fractions differ slightly from those reported in Else et al. (2013) due to different choices of end member values. Despite a small absolute discrepancy, our calculations and those of Else et al. (2013) illustrate SIM and MW contributions to the SML decrease with distance from the shallowest Mackenzie Shelf station (S1) into the basin, following trends in sea ice concentration, T, and S. High NAlk values coincident with high MW content at the shallow shelf stations illustrate the influence of Mackenzie River waters, and

values decrease moving northward off the shelf. These late summer observations corroborate those made during the fall 2009 (section 2.4.1.1) indicating Mackenzie River input (not sampled in fall 2009) was restricted to the shallow shelf and that Eurasian rivers were the main source of surface freshening in the central basin in 2009 (cf. McLaughlin et al., 2011).

2.4.3.1 SML δ^{13}C -POC and Photosynthetic Rate along the Shelf-Basin Transect

δ^{13}C-POC values along the shelf-basin transect ranged from - 25.3 to - 29.1 ‰, comparable to measurements from similar stations collected in the summer of 2008 (- 24.5 to - 28.0 ‰, Figure 2-3c). In both years, δ^{13}C values became more isotopically depleted with distance from the shallowest shelf station (Table 2-4). As such, δ^{13}C-POC values along the 2009 shelf-basin transect were highly correlated with MW content ($r^2 > 0.99$, not shown). Photosynthetic C-uptake rates measured in the SML (at 50 % light level) ranged from 0.237 to 2.246 mgC m^{-3} d^{-1} and were highest at the shallow Mackenzie Shelf station, with rates decreasing towards the central basin. When compared with C-uptake rates determined during the fall 2009 cruise (Yun et al., 2012), we observed a significant relationship between C-uptake rates and δ^{13}C-POC in both summer and fall of 2009, with higher C-uptake rates associated with isotopic enrichment in ^{13}C (Figure 2-4). This correlation was stronger for the late summer 2009 shelf-basin samples ($r^2 = 0.99$, not shown) than the fall 2009 central Canada Basin ($r^2 = 0.56$, not shown), but since both trend lines had virtually identical slopes, they were combined ($r^2 = 0.89$).

2.5 Discussion

Isotopic signatures of POC within the surface mixed layer (SML) of the Canada Basin were found to cover a broad isotopic range from -24.5 to -31.1 ‰ (Figure 2-3c,g). The following discussion endeavours to explain this variability in the context of measured biological and hydrographic parameters. We first contrast δ^{13}C-POC between shallow shelf and deep central basin (> 750 m bottom depth) sites, which illustrates the dominant control of in situ POC production on the shelf. Subsequently, we address the wide range of δ^{13}C-POC variability within the central basin, which appears to be mostly explained by external POC inputs.

2.5.1 Factors controlling δ^{13}C-POC variability from Shallow Shelf to Deep Central Basin

The strong positive relationship observed between the isotopic signatures of POC and photosynthetic rates along the shelf-basin transect in the late summer of 2009 indicated that in regions of enhanced primary production, marine derived POC dominated the POC pool. Isotopically this translated into a typical "marine" carbon isotopic signature in the shallow Mackenzie Shelf (~ - 24 ‰; Macdonald et al., 2004a; Naidu et al., 2000), where photosynthetic rates in the SML were the highest. Mackenzie River waters are well documented as contributing nutrients to shelf waters for phytoplankton growth (e.g., Carmack et al., 2006; Macdonald et al., 2004a) and likely explain high photosynthetic rates measured in 2009 (Figure 2-4), and high chlorophyll *a* biomass measured in 2008 (Figure 2-3b) within the shallow shelf waters of this region.

Zhang et al. (2012) observed a similar relationship between enhanced phytoplankton productivity (associated with ice free, warm, nutrient enriched waters) and isotopic depletion of δ^{13}C-POC entering the deep central Canada Basin from the shallow Chukchi Shelf. The authors suggested higher marine productivity on the Chukchi Shelf contributed to the observed enrichment of δ^{13}C-POC values ($\approx$ - 21 ‰ on the shelf compared to $\approx$ -28 ‰ in the central basin). Furthermore, they associate a strong correlation between δ^{13}C-POC and [CO_2(aq)] as evidence of a photosynthetic control on δ^{13}C-POC, as observed in previous studies (e.g., François et al., 1993; Rau et al., 1989, 1991, 1992). Our shallow shelf (higher productivity) observations corroborate those of Zhang et al. (2012), indicating the potential for biological control of C isotope fractionation. In contrast to high productivity shelf waters, central basin waters are expected to show more ^{13}C-depleted POC, reflecting lower production rates due to enhanced sea ice, lower T, and low nutrient concentrations. Indeed, δ^{13}C-POC in the deep central basin SML was generally found to be isotopically-depleted compared to the shallow shelves.

2.5.2 Factors Controlling δ^{13}C-POC Variability within the Central Canada Basin SML

Although δ^{13}C-POC values in the central basin SML were generally low, they exhibited a wide range (-24.5 to -31.1 ‰; Figure 2-3c,g) which requires an explanation. Sources of POC to the central Canada Basin SML include in situ production (pelagic, as described above, or ice-associated production) and advective processes (surface water or sea ice circulation) which transport material from the shelves into the central basin. Each of these sources has the potential to deliver POC with a somewhat distinctive range of isotopic signatures, allowing them to be qualitatively distinguished, if not definitively characterized. For instance, it is generally considered that phytoplankton in open ocean conditions produce more ^{13}C-depleted POC (- 18 to

-25 ‰, Macdonald et al., 2004a; Parsons et al., 1989) than sea ice associated algal communities, growing under semi-closed system conditions in bottom ice (as enriched as - 9 ‰, Tremblay et al., 2006). More recent studies, however, have suggested that pelagic and sea ice derived δ^{13}C-POC within polar systems can cover ranges of -20 to -34.7 ‰ and -9 to - 29 ‰, respectively (Pineault et al., 2013; Sallon et al., 2011), indicating that quantitative deconvolution of these two distinct sources from the SML using δ^{13}C-POC alone is challenging. Ice rafting of sediments from the Mackenzie and Beaufort shelves (- 19.4 to - 25.3 ‰, Naidu et al., 2000), and riverine transported terrestrial POC derived from land plants and their detritus (- 23 to -28 ‰, Parsons et al., 1989) may also contribute to SML δ^{13}C -POC distributions in the central basin if POC remains suspended within the SML as it is transported into the basin. The following discussion will explore each of these POC sources and the likelihood of their contributions to stable isotope signatures found in the interior Canada Basin SML in 2008 and 2009.

2.5.2.1 In situ Pelagic Production as a Source of POC

The relationship observed between δ^{13}C-POC and photosynthetic rate along the shelf-basin transect is consistent with previous observations by Yun et al. (2012) in the central Canada Basin during fall 2009. These authors observed a C-uptake rate range of ~ 0.05 to 0.3 mg C m^{-3} d^{-1} which corresponded with our δ^{13}C-POC samples, measured in parallel, that ranged from ~ - 30 to - 28 ‰. These central basin data fall within the 'oceanic end-member' of our shelf-basin transect observations (stations L1 and L2), and suggest that low primary productivity waters are indeed characterized by low δ^{13}C values.

As photosynthetic rate measurements were not available for the majority of SML samples collected during the 2008 and 2009 sampling programs at stations in the central basin (~ 12 %, n = 10), we rely on other geochemical tracers to gain a perspective on the full data set. If in situ pelagic primary production were the main driver of SML POC distributions in the central basin during 2008/9, δ^{13}C-POC would be expected to follow [CO_2(aq)], the inorganic carbon substrate for POC production. This relationship reflects changes in cellular carbon demand over supply ratios, which ultimately influence the relative degree of isotope fractionation by the principal carbon fixing enzyme, RuBisCO. A number of field studies have observed a strong negative correlation between [CO_2(aq)] and δ^{13}C-POC in surface ocean waters throughout the global ocean (e.g., François et al., 1993; Rau et al., 1989, 1991, 1992), including productive regions of the Arctic (Zhang et al., 2012), and gap layers within Antarctic sea ice (Papadimitriou et al., 2009). However, δ^{13}C-POC values observed in this study showed no statistically-significant dependence on [CO_2(aq)] (Figure 2-5). Pineault et al. (2013) attributed the presence of isotopically light pelagic POC (as low as -34.7 ‰) as indicative of slow growth at low temperature, low light, and high DIC within the south-eastern Beaufort Sea. Furthermore, they observed an enrichment in pelagic δ^{13}C-POC as chlorophyll *a* and the proportion of ice associated algae increased within the surface waters. However, there was no correlation between δ^{13}C-POC and chlorophyll *a* concentration (r^2 = 0.07, not shown) observed during our study. These results, combined with the lack of a photosynthetic rate-dependence of δ^{13}C-POC, suggest that C supply / demand ratios do not impart a first order control on δ^{13}C-POC distributions in the central Canada Basin SML. Taxon specific effects and phytoplankton community composition have also been shown to exert a significant influence on C isotope fractionation (e.g., Burkhardt et al., 1999; Henley et al., 2012) and the isotopic signature of POC imparted to surface waters

from sea ice (e.g., Pineault et al., 2013), but the influence of these factors cannot be examined with our data from 2008 and 2009. Nonetheless, our results indicate that SML δ^{13}C-POC in the low productivity central Canada Basin is decoupled from [CO_2(aq)] and chlorophyll *a*.

2.5.2.2 Sea Ice as a Source of POC

Regardless of sea ice POC provenance (suspended shelf sediments or ice-associated algal communities) a simple mass balance can be used to estimate POC delivery to the SML by sea ice melt in the central basin. Assuming sea ice melt was the only source of measured δ^{13}C-POC found in the central basin SML, the following relationship can be derived:

$$\begin{aligned} POC_{Mix}(\mu mol\,C\,L^{-1}) \times V_{Mix}(L) \times \delta^{13}C\,POC_{Mix}(‰) \\ = POC_{SIM}(\mu mol\,C\,L^{-1}) \times V_{SIM}(L) \times \delta^{13}C\,POC_{SIM}(‰) \\ + POC_{SML}(\mu mol\,C\,L^{-1}) \times V_{SML}(L) \times \delta^{13}C\,POC_{SML}(‰) \end{aligned} \quad (1)$$

where the subscripts Mix, SIM, and SML refer to contributions from the SIM + SML mixture, SIM, and SML (pre-sea ice melt) respectively. We calculated the average SIM contribution to the SML at the three sea ice stations, and obtained an average f_{SIM} of 0.02. This value would result from 200 L of sea ice melt water being added to a 10 m thick SML (or a 10 m x 1 m x 1 m mixed layer volume), roughly equivalent to melting 0.22 m of sea ice ($\rho \approx 920$ kg m^{-3}) over this area. In this calculation we assumed that the sea ice described in Table 2-3 was representative of melted ice at each site and that the POC (μmol C) content of the SML layer is determined from POC_{Mix} - POC_{SIM}. As Table 2-3 indicates, even the addition of sea ice melt with the highest measured POC concentration (18.67 μmol C L^{-1} x 0.02) would result in a small POC

contribution to the SML (0.37 μmol C L^{-1}). Using the range of δ^{13}C-POC and POC values listed in Table 2-3, we rearranged equation (1) to calculate that POC contributed to the SML via sea ice melting within the central basin could result in a $\Delta\delta^{13}C\text{-}POC_{(SML - MIX)}$ of -1.14 to + 0.37 ‰. In other words, melting sea ice within the central basin could enrich SML δ^{13}C-POC by as much as 1.14 ‰, or deplete its δ^{13}C-POC signature by as much as 0.37 ‰. Although these values suggest that δ^{13}C-POC from sea ice melt could serve to enrich the SML δ^{13}C-POC pool in ^{13}C, we conclude that the melting of multi-year sea ice in the central basin does not contribute enough POC to the SML to exert a strong influence on SML δ^{13}C-POC.

2.5.2.3 River Supplied Terrestrial Organic Material as a Source of POC

Terrestrial sources also supply POC to the Arctic Ocean. Enhanced coastal erosion and sediment export into coastal seas are expected to accompany increased Arctic river discharge with climactic warming; augmenting the supply of terrestrial POC to the Arctic shelves (e.g., Carmack et al., 2006; Lalande et al., 2009; Macdonald et al., 2004b). The Mackenzie River is the most proximal source for riverine input into the Canada Basin (Figure 2-1), and represents the dominant source of terrestrial TOC to the Beaufort Sea and Mackenzie shelves (Naidu et al., 2000; Rachold et al., 2004). The POC inputs from the Mackenzie River have a wide range of δ^{13}C-POC values, from -22 to -34 ‰ (Macdonald et al., 2004a; McClelland et al., 2008; Naidu et al., 2000). However, once transported into the Mackenzie Delta, approximately half of the river-derived material becomes trapped within the delta and another ≈ 40 % settles on the shelf (Macdonald et al., 1998), leaving little material to be transported into the basin interior.

The NAlk and MW content distributions indicated that Mackenzie River outflow was restricted to the shelf region in 2008 and was not detectable in 2009, limiting its ability to transport POC into the central basin during these years. Mackenzie River inflow into the central Canada Basin is variable, and surface currents were shown to entrain Mackenzie River water eastward along the coast towards the Canadian Arctic Archipelago from the early 2000's through 2006 (Yamamoto-Kawai et al., 2009). This mechanism may have contributed to reduced Mackenzie River transport into the central basin in 2009 (McLaughlin et al., 2011). Indeed, NAlk data suggested that Eurasian river inputs dominated the SML MW content in both 2008 and 2009, and were likely the major source of riverine POC in the central basin. Eurasian river input was found to contribute up to 75-100 % of MW in the Canada Basin in the two years preceding this study (McLaughlin et al., 2011), and was the dominant freshwater source to Canada Basin surface waters over the 2000's (Guay et al., 2009; McLaughlin et al., 2011; Yamamoto-Kawai et al., 2005, 2009).

Riverine contributions to the SML can be further resolved by removing the contribution of SIM to TAlk and S at each station, deriving $TAlk_o$ and S_o respectively, using previously derived freshwater fractions (after Yamamoto-Kawai et al., 2009):

$$S_O = \frac{(S - S_{SIM} f_{SIM})}{(1 - f_{SIM})} \quad (2)$$

$$TAlk_O = \frac{(TAlk - TAlk_{SIM} f_{SIM})}{(1 - f_{SIM})} \quad (3)$$

Freshening of the PW end member (S = 32.5, TAlk ~ 2200 μmol kg^{-1}; Figure 2-6) exclusively by river input results in a dilution of S_o and a proportional decrease in $TAlk_o$ depending on the source river. The most proximal major river sources to the Canada Basin include North American (Mackenzie and Yukon) and Russian (Lena and Kolyma) rivers, which can be distinguished based on their average flow-weighted alkalinity values as described in Table 2-2. We have determined the fraction of North American versus Russian river contribution to SML freshening at each station by calculating $TAlk_o$ as a function of S_o (Figure 2-6). If either riverine source contributed 100 % of the MW, it would dilute S_o and $TAlk_o$ according to the following equations:

$$TAlk_O = f_P TAlk_P + f_R TAlk_R \quad (4)$$

$$S_O = f_P S_P + f_R S_R \quad (5)$$

where subscripts R and P refer to river water and Pacific water end member, respectively (Table 2-2), and $f_P + f_R = 1$. This allows the derivation of $TAlk_o$ as a linear function of S_o according to:

$$TAlk_o = \frac{TAlk_P - TAlk_R}{S_P - S_R} \times S_o + \frac{TAlk_R \cdot S_P - TAlk_P \cdot S_R}{S_P - S_R} \quad (6)$$

as depicted in Figure 2-6. $TAlk_o$ calculated for each station using equation (4) falls between the two linear functions obtained from equation (6), indicating that the meteoric water in each of

these samples can be described as a mixture of different proportions of North American and Russian rivers (Figure 2-6). We can thus estimate the proportion of each meteoric water source according to the equation:

$$f_{RR} = \frac{(TAlk_O Measured - TAlk_O NAR_{100})}{(TAlk_O RR_{100} - TAlk_O NAR_{100})} \quad (7)$$

$$f_{NAR} = 1 - f_{RR} \quad (8)$$

where $TAlk_o$ RR_{100} and $TAlk_o$ NAR_{100} refer to $TAlk_o$ expected with 100 % contributions of Russian and North American rivers respectively (equation 6), with average river alkalinity values reported in Table 2-2. Figure 2-6 further reinforces the conclusion that Russian rivers were the dominant freshwater source in the Canada Basin SML during our study as the majority of our sample points fall close to the Russian river (Lena + Kolyma) dilution line (cf. *Yamamoto-Kawai et al.*, (2009), their figure 6). Likewise, the map showing the distribution of f_{RR} (Figure 2-7) clearly shows the dominance of Russian rivers as the source of meteoric water in Canada Basin both in 2008 and 2009.

If the distribution of SML δ^{13}C-POC in the central basin is controlled by mixing between one marine and one riverine source of POC, δ^{13}C-POC should, in turn, be a linear function of S_o. Yet, plotting all δ^{13}C-POC vs S_o does not yield a clear trend (Figure 2-8). However, when we distinguish between samples dominated by Russian rivers (> 60%) and North American rivers

(> 50%) contributions to their meteoric water content, two distinct linear correlations emerge (Figure 2-8).

For the samples dominated by Russian river inputs, we find a trend toward more isotopically-depleted δ^{13}C-POC associated with increased MW contribution to SML freshening (decreased S_o), suggesting that for these samples, δ^{13}C-POC is predominantly controlled by mixing between terrestrial POC delivered by Russian rivers and marine POC produced in the interior of the Arctic Ocean. Reported values for the marine end member δ^{13}C-POC in Canada Basin is ≈ - 24 ‰ (Macdonald et al., 2004a; Naidu et al., 2000), which corresponds to a $S_o \approx 30$ (Figure 2-8), and suggests a marine production end member from the central basin, far from the direct influence of river input. The δ^{13}C-POC measured in the Kolyma and Lena rivers ranges from ≈ - 25 to -36 ‰ (McClelland et al., 2008), while δ^{13}C-POC within the Lena Basin has values in the range of ≈ -25 to -32 ‰ (Rachold et al., 2004; Sánchez-García et al., 2011). The mixing line shown in Figure 2-8 is consistent with a riverine end member δ^{13}C-POC ranging between ≈ -30 to -36 ‰. Russian rivers are therefore plausible sources of both δ^{13}C-POC and low NAlk observed in our study.

Waters from the Siberian shelf, influenced by input from the Lena and Kolyma rivers ($S_o < 27$) could enter the central Canada Basin from the northwest and transport refractory terrestrial POC into the basin interior. Although transport times are long, diversion of Eurasian runoff into the Canada Basin under a high Arctic-Oscillation index is cited as a major freshening mechanism in the Canada Basin from 2005-2008 (Morison et al., 2012). Advection of these low S coastal waters into the Canada Basin has the potential to contribute low NAlk and isotopically-depleted

δ^{13}C-POC. It has been postulated that climate change may promote Eurasian river inflow eastward along the Russian shelves, as observed in 2003 and 2004 by Guay et al. (2009), diverting DOC (and part of the POC) from the Eurasian Basin into the Canada Basin (Macdonald et al., 2004b). Although historical δ^{13}C-POC data from the central Canada Basin are limited, our present data set indicates such transport occurred in 2008 and 2009.

For samples receiving meteoric water predominantly from North American rivers, we also observed a linear trend when plotting δ^{13}C-POC vs S_o, but with a slope nearly orthogonal to the trend obtained with Russian rivers (Figure 2-8). Here, the lowest δ^{13}C- POC values coincide with the highest S_o, suggesting that the source of low δ^{13}C-POC was not associated with North American river input. Instead, the samples with low S_o (i.e., the highest fraction of Mackenzie River water) were associated with isotopically-enriched δ^{13}C-POC, reflecting high productivity on the Beaufort shelf, as discussed in section 2.5.1.

Although Russian river waters may carry terrestrially derived POC into the low productivity waters of the central Canada Basin SML, evidence from studies examining vertical POC export in the Canada Basin suggest this refractory, isotopically-depleted material would not contribute significantly to the vertical flux of carbon, as export of surface POC in these regions is minimal (Cai et al., 2010; Griffith et al., 2012). Instead POC at depth appears to be associated with lateral advection from the shelves into the basin interior and marine-derived production that occurs at the deep chlorophyll *a* maximum ~45-60 m (e.g., Griffith et al., 2012; Honjo et al., 2010).

2.6 Conclusions

This study presents the first assessment of particulate organic carbon stable isotope distributions across the Canada Basin SML, from the seasonally ice-free shelf to the deep, perennially ice-covered central basin. Our observations illustrate a strong biological imprint on $\delta^{13}C$ in the near shore waters of the Mackenzie Delta, which is absent in the low production waters of the deep Canada Basin where $\delta^{13}C$-POC and metrics of in situ C-fixation are decoupled. Advective transport of isotopically-depleted refractory terrestrial material from Russian rivers instead appears to dominate SML isotopic distributions in the central basin where primary productivity and POC concentrations are low.

Predictions of a seasonally ice-free Arctic Ocean within the next few decades (Stroeve et al., 2012; Wang and Overland, 2009) are expected to reinforce the hydrographic changes that have occurred in the central Canada Basin SML over the past decade, including increased freshening (e.g., Morison et al., 2012) and stratification (e.g., McLaughlin and Carmack, 2010). Along-shelf upwelling will favour nutrient replenishment to the near-shore SML, and an increased marine contribution to POC in these regions via enhanced marine primary productivity (McLaughlin and Carmack, 2010; Nishino et al., 2011). Increased sea ice melt and freshwater diversion from Eurasian shelves into the central Canada Basin (Guay et al., 2009; Morison et al., 2012) will strengthen stratification within the Beaufort Gyre and act to decrease POC production (Cai et al., 2010; McLaughlin and Carmack, 2010; Nishino et al., 2011). This dichotomy in the influence of sea ice retreat and surface freshening on POC production is expected to further reinforce the POC versus S_o relationships observed in this study, where POC transported with Eurasian river waters dominated $\delta^{13}C$-POC distributions in the central basin, and marine primary productivity

dominated δ^{13}C-POC along the shelves. This study demonstrates the utility of applying δ^{13}C-POC along with other tracers to investigate POC sources, and as such, it represents a valuable tool to monitor future changes to the Arctic Ocean carbon cycle associated with climate change.

2.7 Tables

Table 2-1. Pooled standard deviation (Sp) of duplicate geochemical analyses

		2008		2009	
Parameter	**Units**	***Sp***	**k**	***Sp***	**k**
S		0.002	156	0.007	134
Chlorophyll *a*	µg L^{-1}	0.031	37	0.012	3
$NO_3^- + NO_2^-$	mmol m^{-3}	0.08	247	0.07	191
NH_4^+	mmol m^{-3}	0.04	163	0.02	120
$\delta^{18}O\text{-}H_2O$	‰ V-SMOW	0.04	13	0.03	20
DIC	µmol kg^{-1}	3.36	10	0.75	10
TAlk	µmol kg^{-1}	18.83	11	1.52	10
$\delta^{13}C$-DIC	‰ VPDB	0.01[a]	217[a]	0.01[a]	217[a]

[a)] 2008 & 2009 analyzed as a single set

Table 2-2. End member values used to determine freshwater composition in the surface mixed layer (after Yamamoto-Kawai et al., 2009)

	Pacific Water (PW)	**Sea Ice Melt (SIM)**	**Meteoric Water (MW)**	
S	32.5	4	0	
$\delta^{18}O$ (‰ V-SMOW)	-0.8	-2	-20	
TAlk (µmol kg^{-1})	2200	263	1620[a]	620[b]

[a)] Flow weighted average Alkalinity from Mackenzie & Yukon Rivers (Cooper et al., 2008)
[b)] Flow weighted average Alkalinity from Lena & Kolyma Rivers (Cooper et al., 2008)

Table 2-3. Sea ice cores and underlying sea water collected for δ ^{13}C-POC determination in the central Canada Basin, Fall 2009

Sea Ice Description	Ice Thickness (cm)	Sampled Thickness (cm)	S	δ ^{13}C-POC (‰ VPDB)	POC (µmol L^{-1})	n
New Ice (Re-Frozen Lead)	6.5 - 8	6.5 - 8	12.1 - 13.0	-27.29 to -26.64	5.88 - 18.67	6
Young Ice (between Multi-year floes)	80 - 88	80 - 88	3.7	-27.73 to -26.87	10.29 - 15.48	2
Multi-year Floe	294	74 - 113	2.3 - 2.9	-29.81 to -26.42	4.84 - 12.91	6
Underlying SML	--	--	26.37 - 28.01	-29.59 to -28.80	1.17 - 2.84	3

Table 2-4. Surface mixed layer properties along the Mackenzie Shelf to central Canada Basin transect, Summer 2009

STATION	Lat (°N)	Lon (°W)	Sea Ice (%)	SML T (°C)	SML S	SIM (%)	MW (%)	DIC (µmol kg^{-1})[a]	TAlk (µmol kg^{-1})	NAlk (µmol kg^{-1})	[CO_2(aq)] (µmol kg^{-1})[a]	δ^{13}C-POC (‰, VPDB)
S1	69.501	-138.00	0	3.097	21.889	16.0	18.6	1744.40	1814.88	2694.68	20.4	-25.30
S2	70.001	-138.51	0	0.922	23.326	14.6	15.4	1700.90	1761.35	2454.09	22.0	-27.31
L1	71.106	-139.03	18	-1.054	25.660	9.6	12.7	1824.60	1899.59	2405.95	21.8	-29.10
L2	74.594	-137.12	99	-1.405	26.720	5.0	13.4	1875.90	1965.32	2390.46	20.4	-28.65

[a] calculated from measured values of TAlk and pH

2.8 Figures

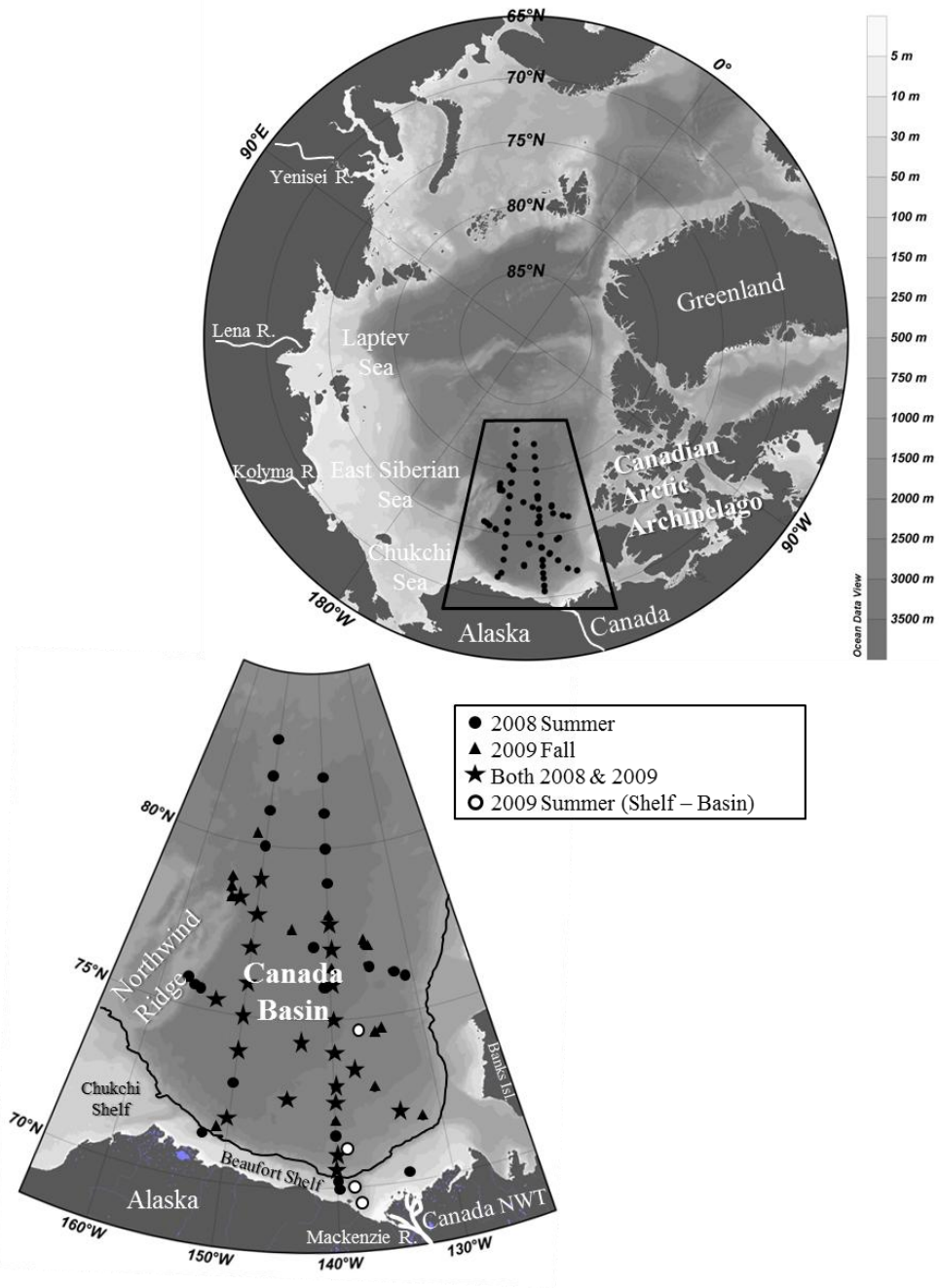

Figure 2-1. Bathymetric map of the Arctic Ocean with the Canada Basin study area outlined in black. Grey scale indicates bottom depth in meters. Inset plot: detail of Canada Basin study area with sampling locations visited during the JOIS-IPY-C3O cruises in the summer of 2008 (circles), fall 2009 (triangles), or both (stars), indicated by black filled symbols; sampling locations visited during the IPY-ArcticNet-GEOTRACES program shelf-basin transect in the summer of 2009 indicated by white filled circles. The black line indicates the 500 m isobath.

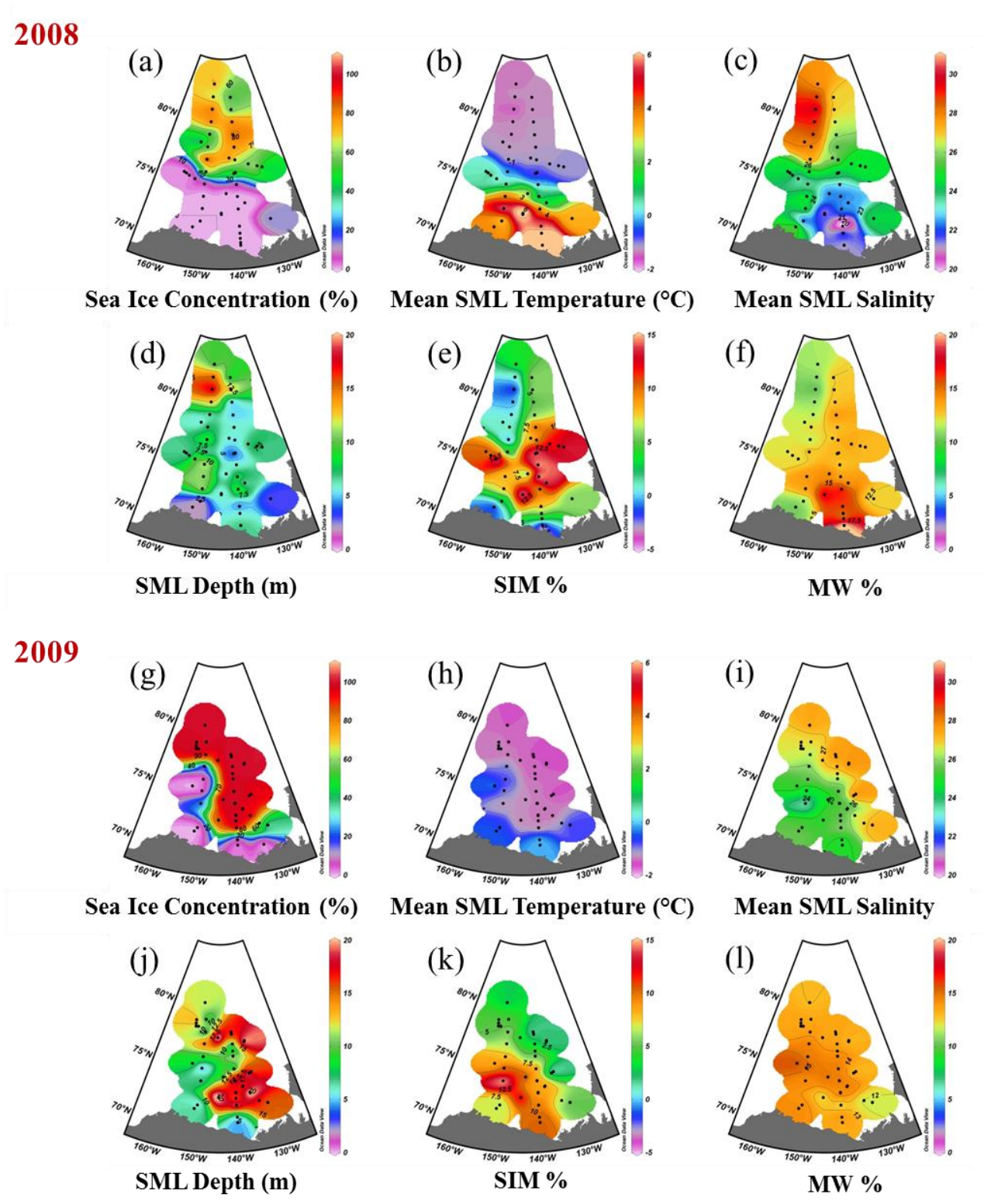

Figure 2-2. Underway observations in the Canada Basin surface mixed layer during summer 2008 (a-f) and fall 2009 (g-l): (a,g) Sea Ice Concentration [%], (b,h) Mean Temperature [°C],

(c,i) Mean Salinity, (d,j) Mixed Layer Depth [m], (e,k) Sea Ice Melt Content [%], (f,l) Meteoric Water Content [%]. Value ranges are indicated by the colour bar scales on the right and sampling locations by black filled circles (as in Figure 2-1).

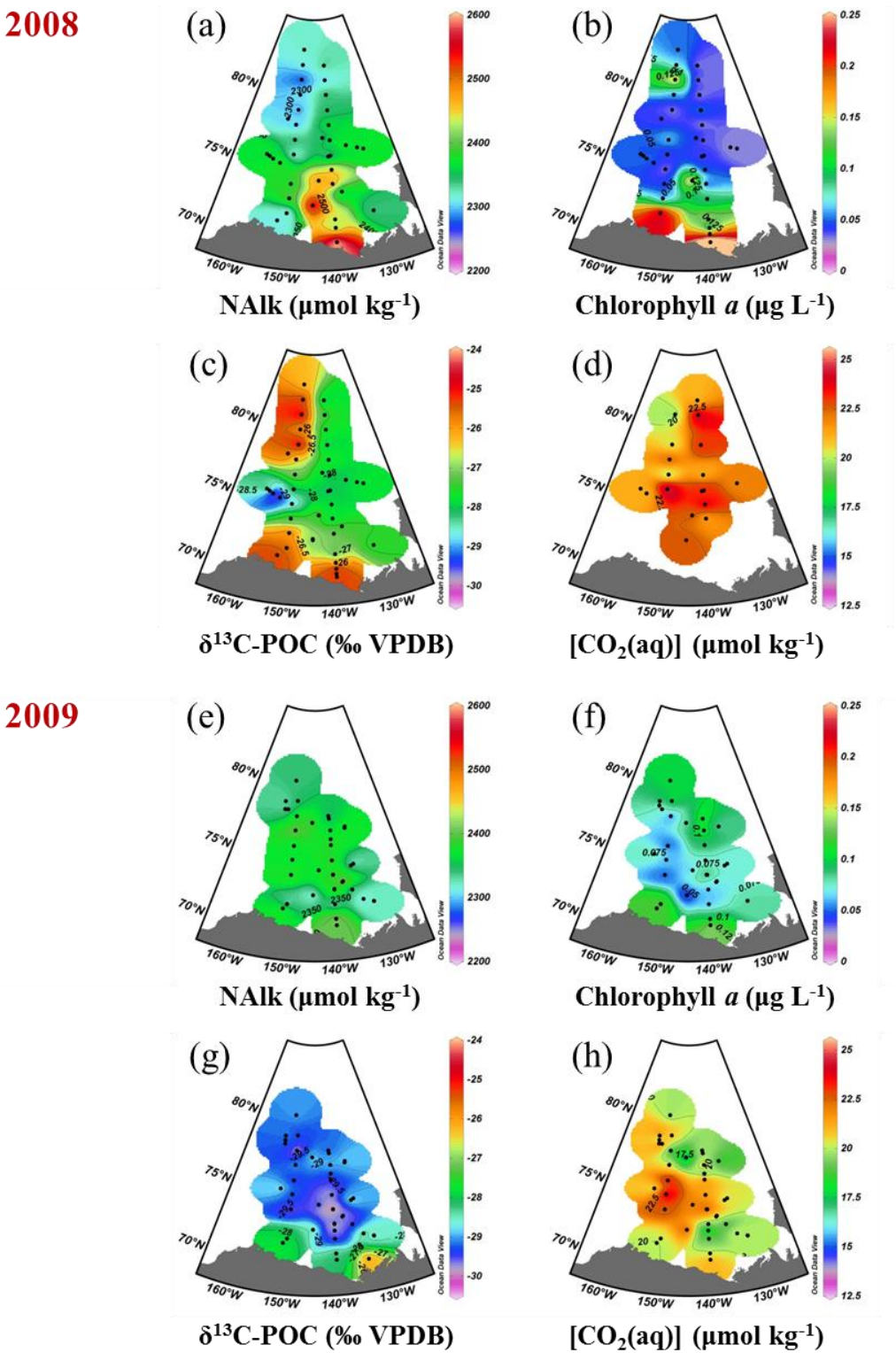

Figure 2-3. Underway observations in the Canada Basin surface mixed layer during summer 2008 (a-d) and fall 2009 (e-h): (a,e) NAlk [µmol kg^{-1}], (b,f) Chlorophyll *a* [µg L^{-1}], (c,g)

δ ^{13}C-POC [‰ VPDB], (d,h) [CO_2(aq)] [µmol kg^{-1}]. Value ranges are indicated by colour bar scales on the right and sampling locations by black filled circles (as in Figure 2-1).

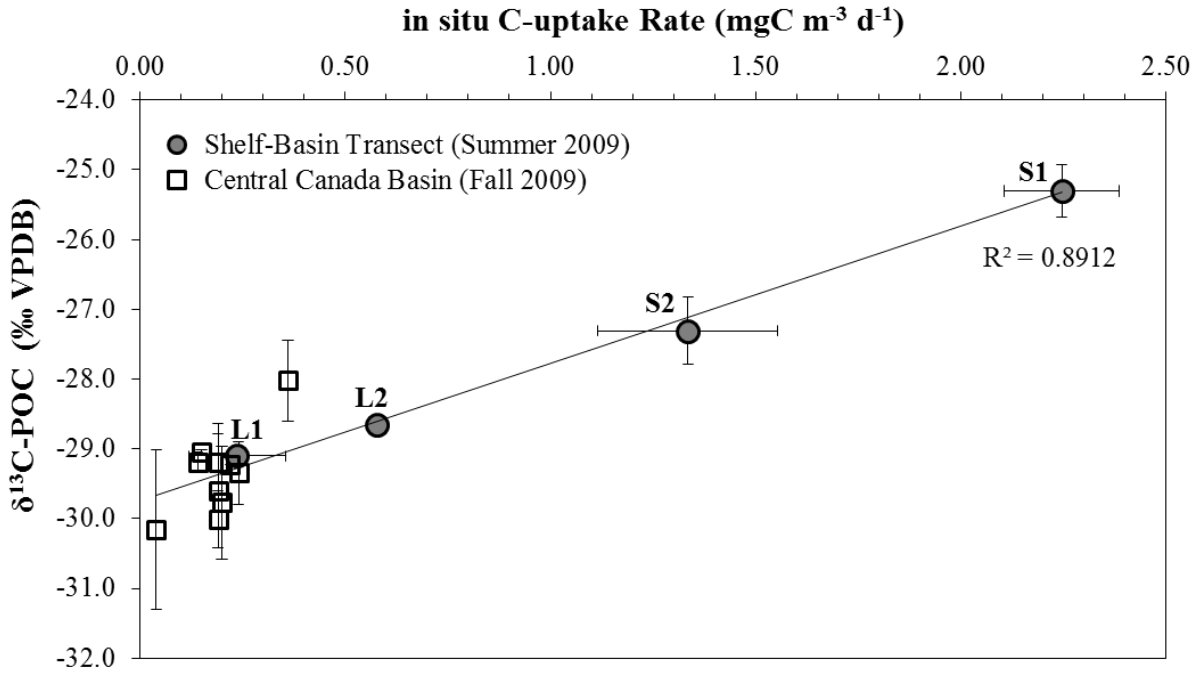

Figure 2-4. Surface mixed layer δ ^{13}C-POC [‰ VPDB] plotted against in situ C-uptake rates [mgC m^{-3} d^{-1}] measured along the shelf-basin transect in the summer of 2009 (filled circles - 50% light level; this study) and the central Canada Basin in the fall of 2009 (open squares - 50% light level; from Yun et al., 2012). δ ^{13}C-POC error bars represent the standard deviation (±) of duplicate analyses, the absence of error bars indicates only 1 filter measurement was available. C-uptake rate error bars represent Standard Error of triplicate analyses; SE for station L2 was smaller than the symbol. Daily C-uptake rates for fall 2009 were estimated from the hourly rates reported in Table 2-2 in Yun et al. (2012), using a 10-h photoperiod. Station names along the shelf-basin transect are indicated (refer to Table 2-4).

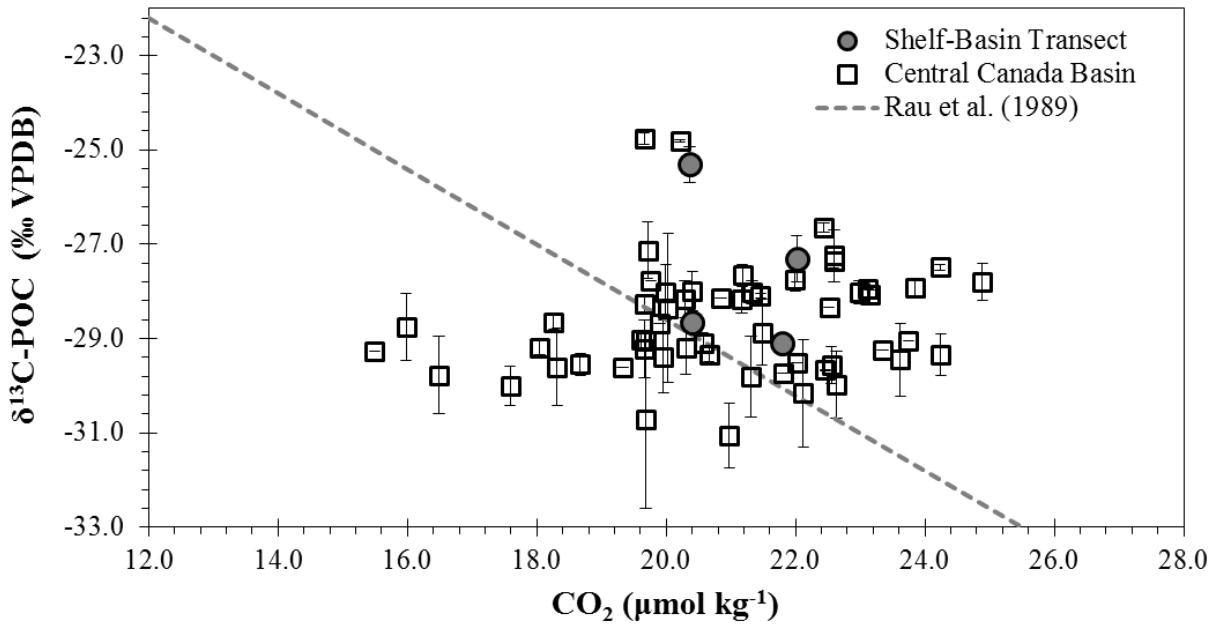

Figure 2-5. Surface mixed layer δ ^{13}C-POC [‰ VPDB] plotted against [CO_2(aq)] [µmol kg^{-1}] for samples collected in the central Canada Basin (summer 2008 and fall 2009, open squares) and along the shelf-basin transect (summer 2009, filled circles). δ ^{13}C-POC error bars as in Figure 2-4. Grey dashed line represents the relationship between Southern Ocean δ ^{13}C-POC and [CO_2(aq)] presented by Rau et al. (1989) (δ ^{13}C-POC = -0.8 [CO_2(aq)] – 12.6).

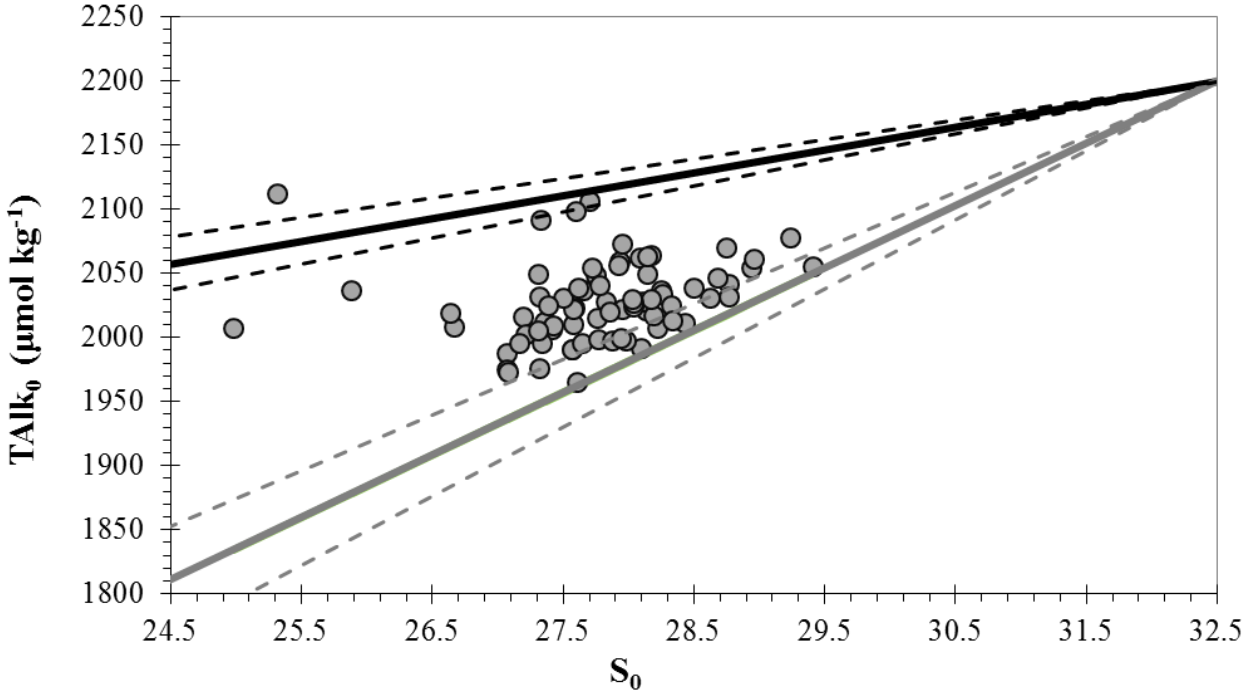

Figure 2-6. Surface mixed layer Total Alkalinity ($TAlk_o$, [µmol kg^{-1}]) plotted against Salinity (S_o), both of which have been corrected for the influence of sea ice melt. Data include central Canada Basin (summer 2008 and fall 2009) and the shelf-basin transect (summer 2009) samples. Lines represent the expected relationship where 100 % of meteoric water is contributed from North American (black) or Russian (grey) rivers (Table 2-2; equation 6). Dashed lines indicate potential contributions of individual rivers: Mackenzie (black dashed lower limit), Yukon (black dashed upper limit), Kolyma (grey dashed lower limit), and Lena (grey dashed upper limit), after Cooper et al. (2008).

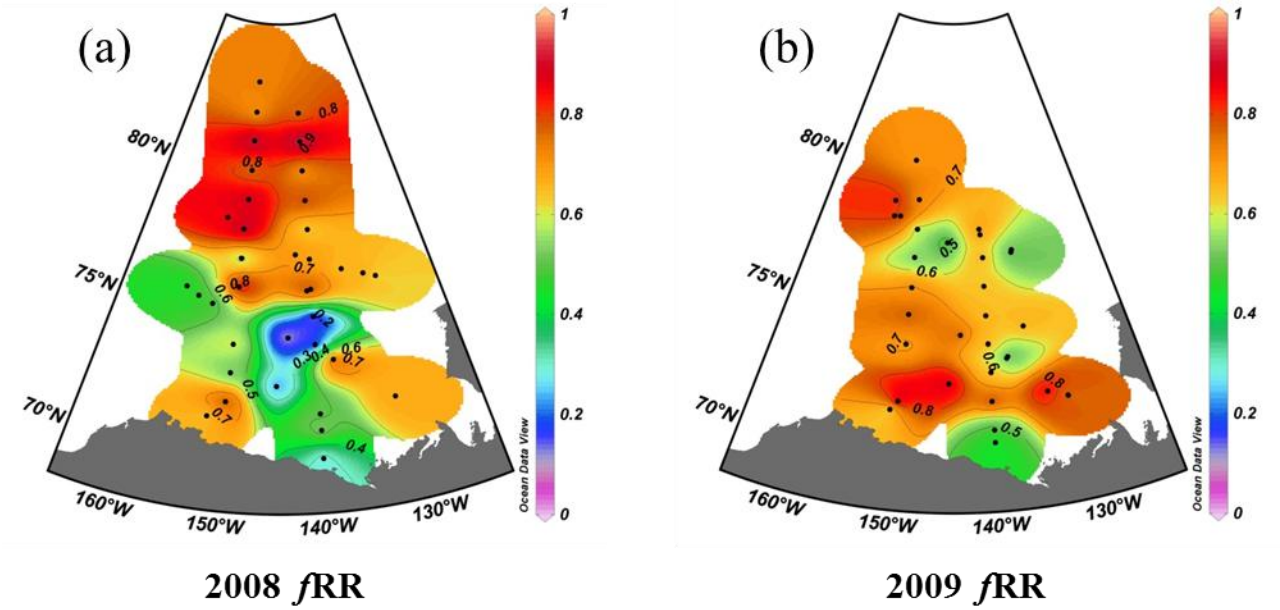

2008 *f*RR **2009 *f*RR**

Figure 2-7. Fraction of Russian river water in the central Canada Basin surface mixed layer during the summer of 2008 (a) and the fall of 2009 (b). The fraction of Russian river water was determined using equation (7), and is described in detail in the text.

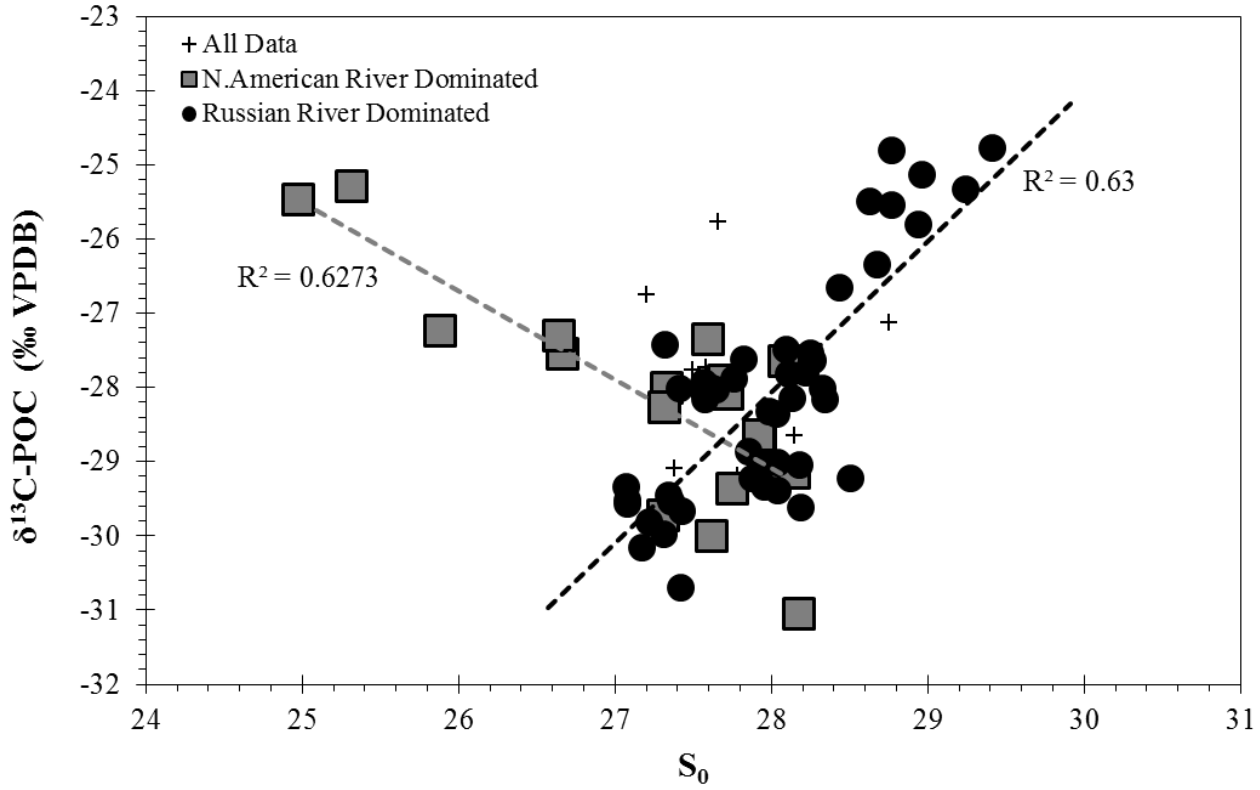

Figure 2-8. Surface mixed layer δ ^{13}C-POC [‰ VPDB] plotted against S_o for all data presented (2008 and 2009). Samples dominated by North American derived river inputs (> 50%) are denoted by filled squares, whereas filled circles indicate samples dominated by Russian (Lena + Kolyma) derived river inputs (> 60 %). Samples with insufficient data to determine *f*RR are indicated by crosses.

Chapter 3: Multi-Tracer Study of Dissolved Inorganic Carbon Sources to the Canada Basin (Arctic Ocean) Halocline

The goal of this study was to examine the dissolved inorganic carbon maximum in the Canada Basin halocline using a suite of geochemical tracers, including stable carbon isotopes, to gain insight into the factors driving the persistence of this feature. Here we present hydrographic and geochemical observations in the upper 500 m of the south-western Canada Basin water column from the summer of 2008 and fall of 2009. We use these observations to distinguish conservative and non-conservative processes contributing dissolved inorganic carbon to halocline source waters, including shelf sediment organic matter remineralization, air-sea gas exchange, and sea ice brine export. Our results indicate that remineralization of organic matter along the Bering and Chukchi Sea shelves is the overwhelming contributor of dissolved inorganic carbon to Pacific Winter Waters forming the south-western Canada Basin middle halocline. Although mixing between the middle and lower halocline serves to spread the dissolved inorganic carbon maximum over a broader salinity range than that of the nutrient maximum, once this mixing is accounted for organic matter remineralization can explain all the variability in both dissolved inorganic carbon and phosphate within the Canada Basin halocline.

3.1 Introduction

The Arctic Ocean is a hydrographically complex enclosed sea, with large-scale freshwater inputs from rivers and North Pacific inflows balanced by oceanic heat and salt contributions from the North Atlantic. As well as being the entry point for relatively fresh, nutrient-rich inputs from the

Pacific Ocean, the Canada Basin is the final sub-basin to receive inflowing warm, saline Atlantic water in the general Arctic Ocean circulation (Figure 3-1a; as summarized in McLaughlin et al., 2011). In contrast to the other Arctic Ocean sub-basins, the upper waters of the Canada Basin are composed of a stacked, multi-halocline complex maintained by waters from a variety of source regions. While surface water distributions are controlled by the dominant atmospheric circulation (e.g., McLaughlin et al., 2011; Proshutinsky, 2002), lateral advection of shelf modified dense waters is the major process contributing to the sub-surface halocline (e.g., Aagaard and Carmack, 1994; Aagaard et al., 1981; McLaughlin et al., 2004; Melling and Lewis, 1982). The combination of high riverine input, the seasonal cycle of sea ice formation and melt, and the inflow of Pacific water maintain the strong stratification and high nutrient content of the Canada Basin halocline (e.g., Aagaard and Carmack, 1989; McLaughlin et al., 2011, 2004).

Inflowing water from the Pacific, via the Bering and Chukchi Sea shelves, dominates the upper and middle halocline of the Canada Basin (McLaughlin et al., 2004; Shimada, 2005; Yamamoto-Kawai et al., 2008). These high nutrient Pacific waters are modified by seasonal shelf processes during transit, including sea ice formation/melting, biological productivity, sediment interaction (McLaughlin et al., 2004; Shimada, 2005; Shimada et al., 2001; Yamamoto-Kawai et al., 2008), and intermittent mixing with inflowing East Siberian Sea water (e.g., Anderson et al., 2010). Summertime modified shelf water, called Pacific Summer Water (PSW), is the main contributor to the upper halocline and is characterized by a local temperature maximum between salinity (S) = 31 and S = 32, as well as low nutrient and high oxygen concentrations associated with summer production throughout the Chukchi Sea (McLaughlin et al., 2004). Winter modified Bering-Chukchi Shelf waters (called Pacific Winter Water; PWW) comprise the middle

halocline and are characterized by near freezing-point temperature and S ≈ 33.1 (Cooper et al., 1997; McLaughlin et al., 2004; Melling and Moore, 1995; Shimada, 2005). The predominant features of PWW are the persistent and laterally extensive maxima in nutrients and dissolved inorganic carbon (DIC; e.g., Anderson et al., 2010; Cai et al., *in press*; Jones and Anderson, 1986; Mathis et al., 2007; McLaughlin et al., 2004; Moore et al., 1983). The strong stable stratification of the halocline complex works to isolate deeper layers from the surface, effectively sequestering this high carbon, high nutrient reservoir from the upper water column where it could otherwise contribute to increased primary production (e.g., McLaughlin and Carmack, 2010) and CO_2 efflux to the atmosphere (e.g., Cai et al., 2010). While the nutrient and DIC maxima are thought to be at least partially derived from sedimentary organic matter remineralization as PWW flows over the highly productive Bering and Chukchi Sea shelves (e.g., Aagaard et al., 1981; Anderson et al., 2010; Cooper et al., 1997; Jones and Anderson, 1986; Melling and Lewis, 1982; Shimada, 2005), the contributions of other processes that alter DIC concentrations in halocline source waters have not been sufficiently investigated.

Although remineralization of organic material within the surface sediments is the major contributor of nutrients and DIC to PWW, other conservative (dilution/concentration) and non-conservative (air-sea gas exchange and sea ice brine rejection) processes can also contribute DIC to these waters as they flow across the shallow shelves. For example, photosynthetic draw-down of DIC in the highly productive Bering and Chukchi shelves leaves shelf waters undersaturated with respect to CO_2 at the end of the growing season (Bates et al., 2005; Cai et al., *in press*; Kaltin and Anderson, 2005; Murata and Takizawa, 2003). These northward flowing Pacific waters experience cooling as autumn commences, increasing CO_2 solubility and enhancing their

capacity to take up CO_2 from the atmosphere. This scenario of cooling CO_2 undersaturated waters promotes the direct uptake of CO_2 via air-sea gas exchange as Pacific waters transit the shelf in winter, increasing their DIC content without a proportional change in nutrient concentrations.

Recent studies in the polar coastal seas have suggested sea ice formation may also promote the transport of DIC into dense waters formed on the shelves in winter. During sea ice formation, concentration of high salinity brine results in the inorganic precipitation of $CaCO_3$ within the sea ice, leaving the remaining brine with an excess of DIC over Total Alkalinity (TAlk) (e.g., Rysgaard et al., 2007). The contribution of this high salinity, high DIC brine to dense water formation in the shallow shelf seas would result in the export of excess DIC (relative to TAlk) into the halocline (Anderson et al., 2004; Loose et al., 2011; Rysgaard et al., 2007). Several studies have demonstrated a direct contribution of DIC to the water column associated with brine export during sea ice formation (e.g., Miller et al., 2011b; Omar et al., 2005; Rysgaard et al., 2007), and have estimated that this sea ice 'CO_2 pump' could be a significant source of DIC to the surface mixed layer in regions of intense sea ice formation (Rysgaard et al., 2011). If indeed the sea ice CO_2 pump is important, the sequestration of DIC within the Canada Basin halocline may be sensitive to changes in seasonal sea ice formation. At present, few data sets exist to quantitatively examine the contribution of the sea ice CO_2 pump to subsurface waters.

Stable carbon isotopes of DIC (δ^{13}C-DIC) may provide a way to distinguish the contributions of sediment remineralization, air-sea gas exchange, and sea ice associated carbon export to the DIC maximum in the Canada Basin halocline. Carbon isotope and nutrient tracers have been applied

to distinguish air-sea gas exchange from biological DIC uptake/remineralization in several global ocean studies (e.g., Broecker and Maier-Reimer, 1992; Lynch-Stieglitz et al., 1995), but these tracers have yet to be applied in the Arctic Ocean. Stable carbon isotope data could also potentially be useful in tracing sea ice derived DIC, if the inorganic carbon added to surface waters via brine export carries a distinct isotopic signature compared to the seawater below (e.g., Papadimitriou et al., 2004; this thesis, Chapter 4). As illustrated in this thesis (Chapter 4), $CaCO_3$ re-dissolution in spring sea ice has been linked to isotopic enrichment of in situ brines by as much as + 2.25 ‰ compared to underlying seawater. These data suggest that $CaCO_3$ precipitation as sea ice forms in the fall/winter may have an opposite effect, isotopically depleting brines as $CaCO_3$ is removed. Either of these isotopic excursions (enrichment or depletion) would produce brine with an isotopic signature different from that of the parent seawater, potentially allowing them to be distinguished after mixing.

The goal of this study was to examine the DIC maximum in the Canada Basin halocline using a suite of geochemical tracers, including stable carbon isotopes, to gain insight into the factors driving the persistence of this feature. We present nutrient, oxygen, DIC, and stable isotope ($\delta^{18}O$-H_2O and $\delta^{13}C$-DIC) profiles from the upper 500 m of the south-western Canada Basin water column collected in the summer of 2008 and fall of 2009. We use these observations to distinguish the contributions of shelf sediment remineralization products, air-sea gas exchange, and sea ice brine export to the PWW DIC maximum.

3.2 Sample Collection and Analytical Methods

3.2.1 Sampling and Analyses of Geochemical Parameters

Hydrographic observations and geochemical samples presented in this study were collected aboard the *CCGS Louis S St-Laurent* as part of the Canada-US Joint Ocean Ice System Study (JOIS) and the International Polar Year Canada's Three Oceans (IPY-C3O) program. Samples were collected along transects from the shallow shelf near Barrow Alaska towards the north-east into the deep central Canada Basin (> 750 m bottom depth; Figure 3-1b), in the summer of 2008 (July 17th to August 21st) and fall of 2009 (September 17th to October 15th). Historical hydrographic and geochemical data (1997 - 2007) from summer cruises throughout the Canada Basin were made available through the Canadian Data Report of Hydrography and Ocean Sciences series and Woods Hole Oceanographic Institution Beaufort Gyre Observational System (http://www.whoi.edu/page.do?pid=66521).

Samples for geochemical analyses were collected from 10 L Niskin bottles mounted on an ice-strengthened CTD rosette system as described in Brown et al., (2014; this thesis, Chapter 2), following the methods outlined in McLaughlin et al. (2012). Analytical precision for each geochemical parameter measured in this study is listed in Table 3-1 and presented as the pooled standard deviation of all replicate measurements (*S*p). *S*p is calculated for a series of duplicate sample measurements (x_1 and x_2) carried out under similar conditions and is determined as $Sp = [\sum (xi_1 - xi_2)^2 / 2k]^{1/2}$, where k is the number of duplicate pairs analyzed (IUPAC, 1997). It is assumed that measurements carried out under similar conditions are of the same precision, although their means may differ, and as such, *S*p is a better estimate of the underlying standard

deviation of the analyses than individual calculated standard deviations of k measurements (IUPAC, 1997).

3.2.2 Oxygen Isotopes

$\delta^{18}O$-H_2O samples were collected following McLaughlin et al. (2012) and analyzed following Epstein and Mayeda (1953). Sample analyses were carried out at Oregon State University's COAS Stable Isotope Lab using a Thermo Finnigan DeltaPlus XL isotope ratio mass spectrometer. Oxygen isotopic values are reported in per mil (‰) with respect to Vienna Standard Mean Ocean Water (V-SMOW) (standard error ± 0.05 ‰).

3.2.3 Dissolved Inorganic Carbon, Total Alkalinity, and δ^{13}C-DIC

Samples for the determination of Dissolved Inorganic Carbon (DIC) and Total Alkalinity (TAlk) were drawn, bubble free, from each Niskin bottle using clean Tygon tubing into 250 mL borosilicate glass reagent bottles, allowed to overflow 1 full volume, and the headspace was adjusted to 1 % of sample volume with a stopper. Samples were preserved with 100 µL saturated $HgCl_2$ before sealing with ground glass stoppers treated with silicon-free high vacuum grease and secured with electrical tape. Samples were stored at 4 °C until analysis. Similarly, δ^{13}C-DIC samples were carefully drawn, free of bubbles, into 30 mL amber soda-lime glass bottles, allowed to overfill twice the bottle volume, and sealed with no headspace. Samples were preserved with 30 µL saturated $HgCl_2$ and sealed with Poly-Seal*-lined caps, secured with Parafilm, and maintained at 4 °C until analysis.

DIC was measured coulometrically following Dickson et al. (2007) using either a VINDTA 3D (Marianda) or SOMMA-I (Brookhaven National Labs) system at Fisheries and Oceans Canada's Institute of Ocean Sciences, Sidney, B.C., Canada. TAlk was determined using an open-cell continuous titration with an automated Dosimat 665 titrator (Metrohm) and Red Rod pH combination electrode (Radiometer Analytical). Endpoint detection was determined using a modified version of Dickson et al.'s (2007) LabView computer program. Both DIC and TAlk were calibrated against certified reference materials provided by Andrew Dickson (Batch 88, Scripps Institute of Oceanography).

$\delta\ ^{13}$C-DIC samples were analyzed at GEOTOP Stable Isotope Laboratory (University du Quebec à Montréal) using a Micromass Isoprime continuous flow isotope ratio mass spectrometer equipped with a MultiFlow (Isoprime) automated injection system. Carbon isotopic values are reported in per mil (‰) with respect to VPDB referenced to the NBS-19 and LSVEC scales (standard error ± 0.1 ‰). All $\delta\ ^{13}$C-DIC values reported in this study are based on duplicate analyses.

3.2.4 Oxygen and Nutrients

Samples for the determination of oxygen, nitrate + nitrite ($NO_3^- + NO_2^-$), orthophosphate (PO_4^{3-}), and ammonium (NH_4^+) were collected and analyzed on board the *CCGS Louis S St-Laurent* in both years as described in McLaughlin et al. (2012). Dissolved inorganic nitrogen (DIN) was determined from measured nutrient values ($DIN = NO_3^- + NO_2^- + NH_4^+$) and has an associated error of 0.09 and 0.07 mmol m^{-3} for 2008 and 2009 respectively. Error terms on calculated DIN

values are derived by combining the analytical precision for NO_3^- + NO_2^- and NH_4^+ analyses (Table 3-1).

3.3 Calculations

3.3.1 Freshwater Components

Freshwater components of the water column were quantified from measured $\delta^{18}O$-H_2O, S, and nutrients (DIN and $[PO_4^{3-}]$) following Yamamoto-Kawai et al. (2008) using the following mass balance (equations 1 - 3). We characterized Canada Basin waters sampled in this study as a mixture of Arctic meteoric water (MW, which includes both river inflow and precipitation); sea ice melt (SIM) or formation (-SIM); and a saline end-member (SE) (after Östlund and Hut, 1984):

$$f_{SIM} + f_{MW} + f_{SE} = 1 \quad (1)$$

$$f_{SIM}S_{SIM} + f_{MW}S_{MW} + f_{SE}S_{SE} = S_{OBS} \quad (2)$$

$$f_{SIM}\delta^{18}O_{SIM} + f_{MW}\delta^{18}O_{MW} + f_{SE}\delta^{18}O_{SE} = \delta^{18}O_{OBS} \quad (3)$$

where subscripts SIM, MW, and SE refer to end member composition as outlined in Table 3-2, *f* refers to the fractional contribution of each component, and the subscript OBS refers to measured quantities. Following Östlund and Hut (1984), f_{SIM} becomes negative when brine is added to

surface waters during sea ice formation. Following Yamamoto-Kawai et al. (2008) and Jones et al. (1998) the saline end-member (SE) contributing to the mixing model for waters with $S \leq 33$ is Pacific water (PW) entering the basin through Bering Strait, with salinity (S_{SE}) and oxygen-isotope composition (δ_{SE}) as described in Table 3-2. For Canada Basin waters with $S > 33$, SE is a mixture of both Atlantic (ATW) and Pacific (PW) waters, the proportions of which are determined using their nutrient composition, following Yamamoto-Kawai et al. (2008). Briefly, the following N:P relationships have been derived for either Atlantic and Pacific waters entering the Canada Basin:

$$DIN^{ATW} = 17.499 \times {PO_4}^{ATW} - 3.072 \quad \textit{(for S > 33 waters, after Jones et al., 1998)} \qquad (4)$$

$$DIN^{PW} = 13.957 \times {PO_4}^{PW} - 11.306 \quad \textit{(for } S \leq \textit{33 waters, after Yamamoto-Kawai et al., 2008)} \quad (5)$$

here we use DIN to account for the effects of nitrification on the N:P relationship of Pacific waters inflowing into the Canada Basin (see Yamamoto-Kawai et al., 2008, for discussion). As there is no ammonium present in Atlantic waters by the time they reach the Canada Basin, DIN ≈ NO_3 in equation 4.

For each measured DIN value in our data set, two expected phosphate values are computed, one based on the Pacific Water line (P_{PW}; equation 5), and one based on the Atlantic Water line (P_{ATW}; equation 4). The ratio of PW to ATW (R_{PW}) in each $S > 33$ sample is then determined

from the observed phosphate concentration (P_{OBS}) and the calculated phosphate (P_{PW}, P_{ATW}) according to the ratio R_{PW} (equation 6; following Yamamoto-Kawai et al., 2008):

$$R_{PW} = \frac{(P_{OBS} - P_{ATW})}{(P_{PW} - P_{ATW})} \quad (6)$$

Therefore, for S > 33 waters in the Canada Basin, S_{SE} and δ_{SE} from equations 1-3 are determined as follows:

$$S_{SE} = S_{PW} \times R_{PW} + S_{ATW} \times (1 - R_{PW}) \quad (7)$$

$$\delta_{SE} = \delta_{PW} \times R_{PW} + \delta_{ATW} \times (1 - R_{PW}) \quad (8)$$

Here we use end member values as selected for the Canada Basin by Yamamoto-Kawai et al. (2008), as in Table 3-2. The PW end member values are determined from mean near bottom (~ 50 m) water properties in Bering Strait. SIM is derived from sea ice sampled within the Canada Basin and MW is obtained from Arctic river properties described by Cooper et al. (2008). The overall uncertainty in the calculation of freshwater fractions (f_{SIM} and f_{MW}) using our data set is ± 0.02, and is derived primarily from uncertainty in $\delta^{18}O$-H_2O analyses (Table 3-1). Seasonal variability in Bering Sea through-flow S (31.9 - 33) and $\delta^{18}O$ (- 1.2 to - 0.5 ‰) further influence f_{SIM} and f_{MW} calculations by ± 0.02 or less (as discussed in Yamamoto-Kawai et al. (2009). The potential error in the calculation of R_{PW} was determined to be < 0.14 when

phosphate concentrations were constrained between 1.5 - 2.3 μmol kg^{-1} and 0.6 - 1.1 μmol kg^{-1} for Pacific and Atlantic waters respectively (see discussion in Yamamoto-Kawai et al., 2008). For any samples with S > 33 but no accompanying nutrient data (31 % of 2008 samples), R_{PW} was determined based on a regression of R_{PW} against salinity, R_{PW} = -0.524 * Salinity + 18.283 (r^2 = 0.979), using the remaining 2008 + 2009 S > 33 data set (n = 71). Values of R_{pw} calculated with this regression have an estimated additional uncertainty of ± 0.06.

3.3.2 DIC Disequilibrium in Pacific Winter Water

Following Yamamoto-Kawai et al. (2011; equation 9), the DIC disequilibrium (DIC_{diseq}) within PWW (S ≈ 33.1) was determined as the observed DIC concentration of the sample (DIC_{obs}) minus the expected DIC concentration of the sample in equilibrium with the atmosphere at in situ conditions ($DIC_{eq,}$ @ S,T,P, TAlk).

$$DIC_{diseq} = DIC_{obs} - DIC_{eq} \quad (9)$$

Measured TAlk, atmospheric pCO_2, S, and T were used to calculate DIC_{eq} using the MS Excel version of CO2Sys (co2sys_xls_program, Pierrot et al., 2006), with equilibrium constants K_1 and K_2 defined by Mehrbach et al. (1973) and refit by Dickson and Millero (1987), and the dissociation constants for $KHSO_4$ determined by Dickson (1990). To determine atmospheric pCO_2 when PWW was at the surface, we use the mean age of 12 ± 5 yrs for S ≈ 33.1 waters as determined by Anderson et al. (2010). Here we use annual average atmospheric pCO_2 values from Barrow Alaska provided by CDIAC (http://cdiac.ornl.gov/ftp/trends/co2/barrsio.co2) for

the years 1996 and 1997, to derive an average pCO_2 value of 365 ppmv. This value is identical to the annual average over the period 1991 - 2002 (1996 minus 5 yrs to 1997 plus 5 yrs).

3.3.3 DIC and PO_4 Normalized to S = 35

To correct for the influences of freshwater fluxes and sea ice brine concentration that change DIC and PO_4 proportionally with salinity, we normalized measured DIC and PO_4 values to a salinity of 35 (as illustrated with DIC in equation 10). As riverine and sea ice melt freshwater sources contribute to the non-conservative addition of DIC to the Arctic Ocean we corrected for this DIC input following Friis et al. (2003) as employed by Shadwick et al. (2011) (equation 11):

$$DIC_{norm} = \frac{DIC_{obs}}{S_{obs}} \times S_{35} \tag{10}$$

$$DIC_{norm} = \frac{(DIC_{obs} - DIC_{S=0})}{S_{obs}} \times S_{35} + DIC_{S=0} \tag{11}$$

here, DIC_{obs} refers to the observed DIC value and $DIC_{s=0}$ to the riverine and sea ice melt DIC contribution. We chose a salinity of 35 to remove the influence of mixing between source water saline end members (Pacific versus Atlantic waters) and used the intercept of the plot of DIC versus salinity over the interval of S = 25 to 33.1 to determine the $DIC_{S = 0}$ value of 1013 μmol kg^{-1}. This value is consistent with previous estimates of average freshwater DIC contributions from the Yukon River, which range from ≈ 690 to 1629 μmol L^{-1} (Guo et al., 2012; Kaltin and Anderson, 2005; PARTNERS data http://www.arcticgreatrivers.org/data.html) and is

major source of terrestrial DIC to the Chukchi and Bering seas (Cai et al., *in press*). The correction for riverine DIC contribution (equation 11) was applied only to samples with *f*MW > 0.01 (section 3.3.1). We chose not to correct for riverine contributions of PO_4 to Canada Basin waters as a negative intercept is found in a plot of PO_4 versus salinity. It is likely that the majority of river derived nutrients delivered to coastal estuaries are quickly depleted due to high rates of primary production during the spring/summer when riverine inputs are highest.

3.3.4 AOU in Pacific Winter Water

We determined Apparent Oxygen Utilization (AOU) in PWW following Omar et al. (2005), using the determination by Najjar and Keeling (1997), as in equation 12:

$$AOU = (O_{2\,meas} - O_{2\,sat}) + \left(1 - \frac{p}{1013.25}\right) \times O_{2\,sat} \qquad (12)$$

where $O_{2\,meas}$ and $O_{2\,sat}$ are the measured and calculated saturation concentrations, respectively. O_2 saturation values were calculated using the T and S-dependent solubility function of Weiss (1970) and were normalized to 1 atmosphere as a function of atmospheric pressure (*p*) (Najjar and Keeling, 1997). We use annual average atmospheric pressure values from Barrow Alaska, provided by CDIAC (http://cdiac.ornl.gov/ftp/trends/co2/barrsio.co2), for the years 1996 and 1997 to derive an average *p* value of 1015.03 hPa. The AOU value derived by equation 12 results in a negative value of oxygen utilization in halocline PWW, and for clarity in our discussion we have multiplied AOU values determined above by (-1) to emphasize the maximum consumption of oxygen with a positive value.

3.3.5 Nitrate Deficit, N*

The effects of denitrification on the nitrate:phosphate ratio of the products of organic matter remineralization can be illustrated by the determination of N* (equation 13; Gruber and Sarmiento, 1997), as applied by Newton et al. (2013):

$$N^* = 0.87 \times \left(NO_3 - 16 \times PO_4 + 2.9 \right) \; mmol\, m^3 \qquad (13)$$

here, 16 refers to the Redfield stoichiometric ratio of N:P in marine organic matter (16:1) and 2.9 mmol m^{-3} is a factor added to bring the mean ocean N* value to approximately zero. The 0.87 multiplier is determined from the N:P ratio of denitrification (-104), based on surface ocean phytoplankton, divided by the difference in N:P between denitrification and nitrification (-104 - 16) (Gruber and Sarmiento, 1997). This derivation makes N* a conservative tracer whose distribution in the oceans is only impacted by denitrification, nitrification of organic-rich organic matter, and water mass transport (Gruber and Sarmiento, 1997).

3.4 Results

This study was carried out over two years, during different seasonal periods. In 2008, water column profiles were collected during the late summer season (July/August), whereas in 2009 samples were collected during the early fall, after the onset of freeze-up (September/October; NISDC, 2010). Although these seasonal differences translated into widely variable hydrographic

and biogeochemical properties in the surface mixed layer (this thesis, Chapter 2), we treat the geochemical features of PWW in the halocline as seasonally independent and as representative of "averaged" properties, with small scale gradients mixed away as PWW flow off-shelf and contribute to the deep basin halocline (e.g., Newton et al., 2013). As detailed below (section 3.4.3), the magnitude of the DIC maximum, and the salinity distribution over which it was found, was consistent between all years of data compared 1997 - 2009, corroborating the negligible impact of seasonal differences on PWW between our two sampling years.

3.4.1 General Hydrographic Profiles in the South-Western Canada Basin 2008 & 2009

Figure 3-1(c-f) depicts the general hydrography in the upper 500 m of the water column at two example stations occupied in 2008 and 2009 along the slope (BL4 ≈ 900 m, red square; BL8 ≈ 3000m, green square; Figure 3-1b) and two in the deep basin (CB4 ≈ 3000 m, blue square; CB9 ≈ 3000 m, purple square; Figure 3-1b). The hydrographic and geochemical parameters from all seven stations sampled in 2008 and 2009 are considered below.

The seasonal mixed layer in the Canada Basin makes up the upper 30-50 m of the water column (McLaughlin et al., 2004) and is highly variable between the two years (and/or seasons) (Figure 3-1,c-f). Below this seasonal feature, lies PSW in the upper halocline at an averaged depth of 90 m. This water mass is associated with a maximum in sub-surface temperature (light grey horizontal lines, Figure 3-1c-f) and a salinity of ≈ 31 to 32 (McLaughlin et al., 2004). Next PWW is found in the middle halocline, observed at a depth of 120 - 220 m and associated with a minimum in sub-surface temperature (blue horizontal lines, Figure 3-1c-f) and a salinity of ≈ 33.1 (McLaughlin et al., 2004). As illustrated in Figure 3-1(c-f; blue horizontal lines), the

PWW layer deepens from the slope into the basin due to Ekman convergence and the accumulation of freshwater within the Beaufort Gyre (e.g., McLaughlin and Carmack, 2010; Proshutinsky, 2002). Below the middle halocline both temperature and salinity increase in the transition to Atlantic waters (AW), characterized by a temperature maximum observed at a depth of ≈ 440 m (green horizontal lines, Figure 3-1c-f; McLaughlin et al., 2004).

3.4.2 Nutrient Distribution

Averaged nutrient concentrations (illustrated using PO_4, Figure 3-2a) were low in the low salinity surface waters to S = 31 (0.63 ± 0.11 mmol m^{-3}), and then began to increase in PSW, reaching a maximum in the PWW. The nutrient maximum at each station is clearly associated with the salinity of the PWW middle halocline layer in both years (S = 33.00 ± 0.15, Table 3-3).

3.4.3 The Dissolved Inorganic Carbon Maximum

The dissolved inorganic carbon (DIC) maximum at each station was determined from a profile of DIC concentration with depth (Table 3-4). DIC data collected in 2008 and 2009 were grouped into salinity bins across all stations and pooled into a single plot (± standard deviation; Figure 3-2b). Basin-wide averages (± standard deviation) observed during JOIS cruises from 1995 to 2007 were also compared (region enveloped by 2 black lines). When computed with respect to salinity, the historical average DIC value of 2224 ± 6 μmol kg^{-1} associated with the DIC maximum (over the interval of S = 33.25 to 33.5) was virtually indistinguishable from average maxima in 2008 and 2009 (Table 3-4), indicating that the Canada Basin DIC maximum feature was consistent between years. At all stations sampled in 2008 and 2009, the range of salinity over which the DIC maximum was spread differed from that of the PWW nutrient maximum

(S ≈ 33.0; Table 3-3; Figure 3-3); moreover, the depth of the DIC maximum at each station was 34 ± 14 m and 19 ± 16 m deeper than that of the nutrient maximum in 2008 and 2009, respectively (cf. Table 3-3 and Table 3-4).

3.4.4 Stable Carbon Isotope Distributions

The stable isotopic composition of DIC (δ^{13}C-DIC) covered a wide range from - 0.59 to + 2.19 ‰ and + 0.03 to + 1.73 ‰ in 2008 and 2009 respectively (Figure 3-2c). The distribution of δ^{13}C-DIC was observed to mirror that of DIC and orthophosphate (PO_4; Figure 3-2a,b,c), with isotopically heavy values in the low-salinity, low nutrient surface waters, minimum values within the nutrient-rich halocline from S ≈ 32.59 to 34.04, and increasingly heavier values towards the Atlantic layer (S ≈ 34.5; Figure 3-2c). The salinity range of the minimum δ^{13}C-DIC value at each station was broader than that seen for the DIC maximum (cf. Figure 3-2b and Figure 3-2c).

3.4.5 Sea Ice Brine and Meteoric Water Fraction

A signal of sea ice brine rejection (negative sea ice melt fraction, -*f*SIM) was observed from S ≈ 28 to S = 33.42, where it reached a maximum (i.e., minimum in -*f*SIM; Figure 3-2d). The presence of sea ice brine decreased slightly through the PSW layer (31 < S < 32), likely from mixing along the shallow shelves, then continued to increase through PWW layer (S = 33.1) to S = 33.4 and subsequently decreased with increasing S because of mixing with fSIM ≈ 0 in the Atlantic layer. The presence of sea ice melt water (+ *f*SIM) was observed only above a salinity of 28. Meteoric water fraction (*f*MW) decreased from a high of 0.17 in the low salinity surface waters to a minimum of 0.03 associated with PWW (S = 33.0), then increased again to 0.05 at S = 33.42 corresponding to the minimum in *f*SIM (Figure 3-2d).

3.4.6 Geochemical Tracers of DIC Provenance in the Canada Basin Halocline (30 < S < 34.8)

3.4.6.1 Freshwater Dilution and Concentration of DIC with Respect to Salinity

Conservative changes of DIC with respect to changing salinity can be evaluated by normalizing measured DIC concentrations to a reference salinity (Figure 3-4a). Here, dilution of riverine and sea ice melt inputs and conservative concentration of DIC in sea ice brine are accounted for, allowing the mixing between water masses to be emphasized. The maximum values of DIC_{norm} at each station were confined to a similar salinity range as the non-normalized values (S = 33.0 to 33.5 versus S = 33.15 to 33.58, for salinity normalized and non-normalized DIC values respectively), indicating that conservative concentration of DIC cannot account for the DIC increase between PSW and PWW. We define the Atlantic layer by the deep temperature maximum in each depth profile (after McLaughlin et al., 2004), and found this feature to be associated with S = 34.81 ± 0.02 in our study region. Mixing between these three water masses, PSW (S ≈ 31.5), PWW (S = 33.0 to 33.5), and Atlantic T-maximum (S = 34.81), determine the properties of the halocline (Figure 3-5). As such, mixing with either PSW or Atlantic water serves to diminish DIC within PWW.

3.4.6.2 Organic Matter Remineralization Contribution

Apparent Oxygen Utilization (AOU; calculated as per section 3.3.4) can be used as a tracer to estimate the removal of oxygen from ocean waters by remineralization of organic material (Sarmiento and Gruber, 2006). Figure 3-4b illustrates a maximum in oxygen utilization

associated with the nutrient maximum (Table 3-3), but like DIC, this feature is spread over a broader salinity range than the nutrient maximum (Table 3-4).

Similarly, the denitrification component of organic material remineralization (N*) was found to be the largest (i.e., most negative) associated with the PWW nutrient maximum (Table 3-3; Figure 3-4c), with values in this layer as low as - 13.9 mmol m^{-3}. Denitrification was also evident in the PSW layer, with negative values as low as - 11.5 mmol m^{-3} (Figure 3-4c).

Only at the shallowest shelf station (BL2, ≈ 150 m depth) was the N* minimum associated with a salinity other than that of the nutrient maximum. At this station, the minimum N* reached the lowest levels in our study area (-16.5 mmol m^{-3}) and occurred at S ≈ 32.6 (green highlighted points, Figure 3-4c). These values are consistent with high rates of sediment denitrification found along the shallow Chukchi Shelf (Chang and Devol, 2009).

3.4.6.3 Air-Sea Exchange Contribution

We can approximate the DIC change related to sea air-sea flux associated with CO_2 uptake or degassing, as Pacific waters seasonally transit north across the Chukchi Shelf. Figure 3-4d illustrates that waters in the south western Canada Basin have an excess DIC of up to ≈ 90 μmol kg^{-1} in the PWW (S ≈ 33.1), whereas PSW with S ≈ 30 to 32 show a deficit in DIC. This implies PWW is significantly oversaturated with respect to atmospheric CO_2 and would represent a source of CO_2 to the atmosphere while at the surface.

3.5 Discussion

Samples collected from the south-western Canada Basin in 2008 and 2009, and throughout the basin in 1995 to 2007, illustrate the persistence of a DIC maximum associated with the middle halocline (PWW), a feature also observed in other studies (e.g., Anderson et al., 1988; Anderson et al., 2010; Bates et al., 2005; Cai et al., *in press*; Jones and Anderson, 1986; Shadwick et al., 2011). The averaged maximum DIC concentration at each station was found to be similar between years (2008 and 2009) and between seasons sampled (summer and fall), exhibiting a relatively narrow range of 2226.8 ± 7.2 μmol kg^{-1}(Figure 3-2b). Unlike the nutrient maximum, which was confined to PWW (S ≈ 33.0; Figure 3-2a), the DIC maximum spread from the middle (PWW) into the lower halocline (S = 33.15 to 33.58). Previous studies (Anderson et al., 1990; Cai et al.,*in press*; McLaughlin et al., 2004; Woodgate et al., 2005) also showed the DIC maximum was spread over a broader salinity range than the nutrient maximum (S > 33.1), into the layer where nutrient (PO_4) concentrations decrease (Table 3-5). Bates et al. (2005) and Mathis et al. (2009) observed the DIC maximum along the Chukchi Sea shelf (west of our study area) to be associated with the nutrient maximum, suggesting our 2008 and 2009 data to the north-east may have been more affected by mixing that occurs along the slope. Diapycnal mixing of PWW and Atlantic waters along the Chukchi borderland (along the western side of the Canada Basin) has been cited as an important contributor to the ventilation of the lower halocline in the Canada Basin (Woodgate et al., 2005).

The mismatch between the nutrient maximum (S = 33.0) and the DIC maximum (S = 33.15 to 33.58; Figure 3-3) suggests there may be different biogeochemical controls on DIC and nutrient sources to the halocline. The following discussion will consider both data sets (2008 and 2009)

together, and focus on describing potential sources of DIC to the south-western Canada Basin halocline. In addition to DIC and nutrient data, our field observations provide new information on the distribution of δ^{13}C-DIC signatures across the halocline. We found that although the stable isotopic composition of DIC had reached a minimum value in the PWW, the minimum occurred over a wide salinity range that included PSW, PWW, and Atlantic layers (S = 32.59 - 34.04). The utility of δ^{13}C-DIC as a DIC source tracer is discussed below.

3.5.1 Contributors of DIC to the Canada Basin Halocline

Winter shelf waters can have their DIC content altered by both conservative and non-conservative processes. Conservative processes influencing DIC include water mass mixing and freshwater (river water + sea ice melt) dilution, whereas air-sea exchange and the formation/decay of organic material can introduce non-conservative DIC changes. Of these processes, only air-sea gas exchange will result in a change in DIC independently of other parameters such as nutrients. The formation of sea ice along the shelves in winter introduces another set of processes that can alter DIC content in winter surface waters. During sea ice formation, concentration of salts into brine solution results in the conservative concentration of DIC and nutrients with respect to salinity, contributing DIC and nutrients to the water column when brines drain into surface waters. Additionally, rejection of DIC-rich brine has been reported to contribute DIC, in excess of TAlk, to surface waters under newly forming ice (e.g., Anderson et al., 2004; Rysgaard et al., 2007), suggesting that sea ice formation may also constitute a non-conservative addition of DIC to the water column.

The persistence of a maximum feature in the plot of DIC_{norm} verses S (Figure 3-4a), suggests that conservative processes are not the main sources of DIC to the DIC maximum, as salinity-normalization should remove any dependence of DIC on salinity. Of the non-conservative sources of DIC, air-sea gas exchange and brine injection of excess DIC (relative to TAlk), can be distinguished from the formation and decay of organic material by their effect on DIC, δ^{13}C-DIC and other tracers. For instance, gas exchange and sea ice brine injection of excess DIC will alter DIC concentrations and δ^{13}C-DIC independently of other nutrients, whereas organic matter decay will contribute DIC, δ^{13}C-DIC and nutrients in stoichiometric ratios associated with marine organic material. The remaining discussion will focus on these non-conservative processes that contribute DIC to the Canada Basin halocline by distinguishing their influence on DIC, δ^{13}C-DIC and nutrient concentrations.

3.5.2 Processes that Change both DIC and Nutrient Inventories

Nutrient regeneration within the Arctic Ocean, either along the shallow shelf seas or within the water column, has been cited as a major contributor to the high nutrient and DIC concentrations within the Canada Basin middle halocline (e.g., Anderson et al., 2010; Jones and Anderson, 1986). As dense PWW transits the shallow Bering and Chukchi Sea shelves, these waters interact with organic rich sediments and carry nutrients and DIC derived from organic matter remineralization off-shelf (e.g., Anderson et al., 2010; Cooper et al., 1997; Nishino et al., 2005; Yamamoto-Kawai et al., 2006). If the nutrient and DIC maxima are both derived from remineralization of organic material, their concentrations in PWW should reflect the stoichiometry of marine organic material and the isotopic composition of DIC should reflect a biological signature.

Calculated values of AOU and DIC_{diseq} (Figure 3-4b,d) show strong correspondence over the halocline (S = 31 to 33.58). Further, these two tracers are linearly correlated between PSW and PWW (S = 31 to 33; AOU vs. DIC_{diseq}, $r^2 = 0.77$). Both DIC and AOU increase with PO_4 over the PSW to PWW salinity range (Figure 3-6) suggesting increased concentrations of both are related to PO_4 remineralization. However, neither the DIC nor AOU increase follow expected marine organic matter stoichiometries (106:1 for DIC:PO_4 and 150:1 for AOU:PO_4; Sarmiento and Gruber, 2006). Rather, the DIC increase follows a 160:1 slope as PO_4 increases, resulting in a significant excess of DIC in the high salinity PWW (Figure 3-6a). In contrast, calculated AOU values fall below the expected AOU:PO_4 = 150:1, suggesting either mixing or air-sea gas exchange may have increased oxygen concentrations (and thus decreased the apparent O_2 deficit) in these waters (Figure 3-6b). Although the positive relationship between both DIC and AOU to increasing PO_4 concentrations suggests organic matter remineralization is a major contributor of nutrients and DIC to PWW, it is unclear why these ratios would diverge so dramatically from the stoichiometry expected of marine organic matter remineralization along the shallow shelves (e.g., 160:1 vs. 106:1 for DIC:PO_4).

Other processes beyond organic matter decay in shelf sediments could contribute to the increased nutrient concentrations in PWW. In particular, winter transport of high nutrient Bering Sea water would also have sufficient nutrient and DIC concentrations to contribute to the Canada Basin halocline maxima, without the addition of nutrients from the Chukchi Shelf (Cooper et al., 1997). Cooper et al. (1997) determined that typical "Arctic Ocean Upper Halocline" water (N ≈ 20 μM; Si ≈ 45 μM; δ18O ≈ -1.1 ‰; as defined by Macdonald et al., 1989) could be found

along the Bering Sea slope at depths less than 100m. Following Cooper et al. (1997), we can approximate the composition of Pacific waters flowing through the Bering Strait in winter by looking at high nutrient waters along the southern Bering Sea slope (Table 3-6; Figure 3-7). Using data collected by the *RV Mirai* in September 2000 (http://www.godac.jamstec.go.jp/darwin/cruise/mirai/mr00-k06/e;jsessionid=F832B1C7C87E0B64DF2A1019490A153D) we can estimate the geochemical composition of Bering Sea "winter" waters based on these properties (Table 3-6) and similarly, use samples collected in the Bering Strait to approximate summer shelf waters (Table 3-6; Figure 3-7).

Our estimated Bering Strait summer water (open squares, Figure 3-6) has a composition quite similar to PSW in the south-western Canada Basin. Furthermore, the DIC/PO_4 ratio in estimated Bering Sea winter water (open triangle, Figure 3-6a) falls along the expected 106:1 stoichiometry line of marine organic material. In contrast, estimated Bering Sea winter water AOU (open triangle, Figure 3-6b) lies within our measured values in south-western Canada Basin PWW. These observations indicate that nutrient and AOU concentrations in PWW can be explained both by transport of nutrient rich North Pacific waters upwelled from the Bering Sea slope and sediment organic matter remineralization along the shallow Bering and Chukchi seas. However, the much higher DIC in Canada Basin PWW, with respect to PO_4, must have another explanation.

Stable carbon isotope data can be used to provide additional constraints on the sources of DIC to PWW. Modern δ^{13}C-DIC distributions in the interior ocean are dominated by biological

fractionation (Schmittner et al., 2013), resulting in an inverse relationship between deep water δ^{13}C-DIC and nutrient accumulation from organic matter remineralization (Broecker and Maier-Reimer, 1992; Kroopnick, 1985). Measured δ^{13}C-DIC in the northern North Pacific and Bering Sea has been shown to be largely controlled by biological activity and upwelling/deep water mixing (Tanaka et al., 2003), suggesting that δ^{13}C-DIC values in PSW and PWW would be tightly coupled with nutrients if organic matter remineralization were the main contributor of DIC. Using our δ^{13}C-DIC data, we examined the relationship between nutrient concentrations and stable C isotopes in the Canada Basin halocline (Figure 3-8). As observed for DIC distributions, we found a close correspondence between δ^{13}C-DIC depletion and PO_4 enrichment between PSW and PWW.

Broecker and Maier-Reimer (1992) derived an approximation for the dependence of δ^{13}C-DIC on PO_4, based on mean ocean nutrient and organic matter composition (equation 14, as modified by Lynch-Stieglitz et al., 1995):

$$\delta^{13}C \cdot DIC = 2.7 - 1.1 \times PO_4 \qquad (14)$$

This mean ocean relationship matches well with our observations from the south-western Canada Basin (solid line Figure 3-8, circles); however, our values are consistently isotopically lighter for the same PO_4 concentration. Similarly, Charles and Fairbanks (1990) used a stoichiometric relationship of $[\delta^{13}C{:}PO_4org]{:}DIC \approx 0.93$ ‰ / μmol kg^{-1} (Broecker and Peng, 1982) and postulated that normalizing δ^{13}C-DIC to PO_4 should produce constant values if remineralization of organic material were the only control on δ^{13}C-DIC distributions (equation 15):

$$\delta^{13}C \cdot DIC_{Norm} = \delta^{13}C \cdot DIC + (0.93 \times PO_4) \quad (15)$$

Indeed, our observations show that normalizing δ^{13}C-DIC values from PSW and PWW removes any dependence on PO_4 concentration (Figure 3-8, triangles). This further indicates that the isotopic offset observed between our data and the mean ocean relationship defined by Broecker and Maier-Reimer (1992) is likely due to regional differences between Arctic Ocean samples and the mean global ocean (Figure 3-8, circles). The correlation between δ^{13}C-DIC and PO_4, and the constant value of PO_4-normalized δ^{13}C-DIC, provides strong evidence that organic matter remineralization is the dominant contributor of both DIC and PO_4 to PWW, despite the miss-match between the depths of nutrient and DIC maxima (Figure 3-3).

Figure 3-6 and Figure 3-8 suggest that either imported North Pacific nutrients or nutrients regenerated in the Bering and Chukchi shelf sediments could contribute to both the nutrient and DIC maxima associated with PWW. Furthermore, both of these sources would contribute nutrients and DIC in the same stoichiometric proportions resulting in similar changes in AOU, DIC, and δ^{13}C-DIC. As a result, these geochemical tracers cannot effectively resolve the contribution of North Pacific deep water from shelf sediment processes as DIC sources to PWW.

Unlike PO_4, N* distributions can provide information on the relative contribution of shelf-derived nutrients. This is due to the presence of denitrification (i.e., NO_3^- reduction to N_2) under anaerobic shelf sediment conditions, a well documented feature of the Bering and Chukchi

shelves (e.g., Devol et al., 1997; Nishino et al., 2005; Yamamoto-Kawai et al., 2008, 2006). Strong nitrate depletion (negative N*; Figure 3-4c) is a signature of denitrification on the N:P ratio in the south-western Canada Basin PWW. Average N* values associated with the nutrient maximum, -10.57 and -10.04 mmol m^{-3} in 2008 and 2009, respectively (Table 3-3), are significantly different from the -2 to -4 mmol m^{-3} values found along the Bering Sea shelf break (200m depth; Granger et al., 2013), where North Pacific waters begin their transit. Similarly, the N* values observed in PWW in the Canada Basin are significantly lower than the our estimated Bering Sea winter water found further north up the slope (-5.9 mmol m^{-3}; Table 3-6). The 6 to 8 mmol m^{-3} depletion in N* indicates nutrient concentrations in PWW are strongly impacted by sediment organic matter remineralization. Granger et al. (2013) calculated that between 20 - 100 % of the nitrate associated with winter waters on the inner Bering Sea shelf (south of the Bering Strait) derived from organic matter remineralization directly on the shelf, as opposed to entrainment of high nutrient waters found deeper on the slope. These authors observed a dramatic decrease in N* (≈ - 6 to - 13 μmol L^{-1}) in bottom waters moving northward from the slope. Furthermore, an increased proportion of NO_3^- nitrified in situ (as determined by ^{18}O-NO_3) was strongly correlated with further depletion of N* (Granger et al., 2013). In our data, values of N* were less strongly depleted in the DIC maximum (Table 3-4), but they still departed markedly from the incoming Bering Sea shelf water. This provides strong evidence that the PWW DIC maximum is associated with DIC derived from the remineralization of organic material in the sediments of the Bering and Chukchi Sea shelves, with the remineralization products entrained by North Pacific waters as they transit the shelf in winter.

3.5.3 Processes that Change DIC, Without Altering Nutrient Inventories

In addition to the DIC derived from organic matter remineralization in the Chukchi and Bering Shelf sediments, other non-conservative processes, such as air-sea gas exchange and sea ice brine rejection, may also be important contributors of DIC to PWW.

3.5.3.1 Air-Sea Gas Exchange

Exchange of CO_2 between the surface ocean and the atmosphere is a process that can strongly decouple δ^{13}C-DIC from its biological relationship with nutrient concentrations (Charles and Fairbanks, 1990). Atmosphere-ocean δ^{13}C equilibration is temperature dependant, and given sufficient time, results in an isotopic enrichment of polar surface waters (Mook et al., 1974; Zhang et al., 1995). However, isotopic equilibration between CO_2 in the atmosphere and the oceanic pool of DIC is slow (≈ 10 years for a 50 m mixed layer) and equilibrium is never actually achieved (Lynch-Stieglitz et al., 1995). Incomplete equilibration between the ocean and the atmosphere results in a depletion of surface δ^{13}C-DIC in the subpolar regions, where cooling increases CO_2 solubility and permits atmospheric CO_2 uptake (Broecker and Maier-Reimer, 1992; Lynch-Stieglitz et al., 1995; Schmittner et al., 2013). In contrast, outgassing of CO_2 works to enrich surface water δ^{13}C-DIC until equilibrium is achieved (due to preferential loss of the lighter isotopic species; Lynch-Stieglitz et al., 1995).

PWW halocline waters showed CO_2 to be supersaturated over atmospheric equilibrium (strong positive DIC_{diseq}, Figure 3-4d), indicating these waters would lose CO_2 to the atmosphere during transit and become more isotopically enriched as a result. Annual mean transit times between Bering Strait and the head of Barrow Canyon suggest the residence time of Pacific Water in the

Chukchi Sea is on the order of 3 to 6 months (Cai et al., *in press*; Woodgate and Aagaard, 2005; Woodgate et al., 2005). As such, Pacific waters transiting the shallow Chukchi and Bering Sea shelves in winter would be limited in their ability to lose CO_2 to the atmosphere during this relatively short transit time, especially under the intermittent cover of ice. Although Figure 3-6b suggests oxygen uptake from the atmosphere may have contributed to diminishing AOU in PWW, air-sea exchange of oxygen in waters transiting the Bering and Chukchi seas has been observed to be of relatively minor importance compared to remineralization/recycling of organic matter and dilution by sea ice melt (Cooper et al., 1999). This suggests the impact of air-sea exchange on DIC would be even more limited, as air-sea equilibration of CO_2 takes ≈ 20 times longer than oxygen due to the solution chemistry of DIC (as summarized in Sarmiento and Gruber, 2006). The strong over-saturation of PWW, coupled with a δ^{13}C-DIC signature lighter than that of PSW ($31 < S < 32$, Figure 3-2c) indicates that air-sea gas exchange is not an important contributor to the DIC maximum in the south-western Canada Basin halocline.

3.5.3.2 Sea Ice Formation and Brine Rejection

The injection of high salinity brine into the water column during sea ice formation (negative *f*SIM) is a distinctive feature of the Canada Basin halocline, observed in both PSW and PWW layers, and extending to a salinity of 33.42 (Figure 3-2d; McLaughlin et al., 2011; Yamamoto-Kawai et al., 2008). While the conservative concentration of DIC with increasing salinity in forming brines will be accounted for in the normalization of DIC to S = 35 (Figure 3-4a), non-conservative DIC additions to the water column may also accompany sea ice formation. High pCO_2 found in waters below forming sea ice in the Canadian Arctic and north-east of Greenland has been attributed to the increased efficiency of DIC export, over TAlk, due to the separation of

the products of $CaCO_3$ precipitation in the highly saline brine liquids (equation 16; Rysgaard et al., 2007).

$$Ca^{2+} + 2HCO_3^- = CaCO_3 + CO_2 + H_2O \quad (16)$$

For instance, CO_2 can readily diffuse through the porous network of brine channels and accumulate in the surface waters below the growing sea ice, whereas solid $CaCO_3$ can become trapped (Rysgaard et al., 2007). Through this mechanism, sea ice formation and growth may result in the transport of "excess" CO_2 into below-ice surface waters (i.e., excess DIC over TAlk), above that imparted by conservative concentration of salts.

The $CaCO_3$ formation following equation 16 will also result in the fractionation of ^{13}C into isotopically heavy $Ca^{13}CO_3$ and isotopically light $^{13}CO_2$ (Papadimitriou et al., 2004; Romanek et al., 1992), resulting in a different composition of brine $\delta^{13}C$-DIC compared to parent seawater. Thus, brine injected into the water column during sea ice formation could contribute isotopically light $\delta^{13}C$-DIC and an increased ratio of DIC/TAlk to surface waters if isotopically heavy $CaCO_3$ were to stay within the forming sea ice (as observed in this thesis, Chapter 4).

If brine export alone was responsible for the ≈ 150 μmol kg^{-1} increase in DIC within PWW, over that of PSW (Figure 3-4d), we can apply a simple mass balance to determine the brine isotopic signature required to deplete average PSW isotopic values (+ 1.32 ‰) toward the measured average in the DIC maximum (+ 0.41 ‰) following equation 17:

$$sDIC_{PWW}\,(\mu mol\,L^{-1}) \times V_{PWW}(L) \times \delta^{13}C\,DIC_{PWW}(‰)$$
$$= sDIC_{PSW}\,(\mu mol\,L^{-1}) \times V_{PSW}(L) \times \delta^{13}C\,DIC_{PSW}\,(‰)$$
$$+ sDIC_{Brine}(\mu mol\,L^{-1}) \times V_{Brine}(L) \times \delta^{13}C\,DIC_{Brine}(‰) \quad (17)$$

here *PWW* refers to values measured in the PWW DIC maximum, *PSW* refers to Pacific Summer Water transiting the Chukchi Shelf at the end of season before freeze-up, and *Brine* refers to the DIC added surface waters with brine export as sea ice is formed. To account for the conservative concentration of DIC with respect to salinity as sea ice forms, DIC values have been normalized to a constant salinity of 35, denoted with an "s" prefix (sDIC = DIC/S * 35). Water volume is approximated over a 20 m mixed layer (1 m x 1 m x 20 m), where the amount of brine added is calculated from the average *f*SIM associated with the DIC maximum (*f*SIM = - 0.060, Table 3-4) and the volume of PSW receiving brine input is calculated from the difference. PWW DIC, S, and δ^{13}C-DIC are taken as average values from Table 3-4; PSW DIC, S and δ^{13}C-DIC are taken as the average measured values between 31 < S < 32 (2075 μmol kg^{-1}, 31.5, and +1.32 ‰, respectively; Figure 3-2). Brine DIC was determined from the mixing volume equation, $sDIC_H = 0.94*sDIC_{PSW} + 0.06*sDIC_{Brine}$. For the purposes of this calculation, sDIC values in μmol kg^{-1} were assumed equivalent to μmol L^{-1}.

Considering conservative concentration of DIC alone, a salinity increase of 2 (31.5 to 33.5) would account for ≈ 130 μmol kg^{-1} of the ≈ 150 μmol kg^{-1} increase in DIC between PSW and PWW (Figure 3-4d). As sDIC will account for this conservative DIC contribution, the "excess" DIC contribution to PWW associated with brine rejection could be ≈ 20 μmol kg^{-1}. We assume

this excess DIC has an identical isotopic signature as the rest of the brine, and that this isotopic composition is derived from the mobile reaction products (CO_2) of equation 16.

From this calculation we estimate the $sDIC_{Brine}$ concentration required to increase water column $sDIC_{PSW}$ by 20 μmol kg^{-1} and deplete $\delta^{13}C\text{-}DIC_{PSW}$ by 0.91 ‰ over a 20 m mixed layer depth is on the order of ≈ 2722 μmol kg^{-1} with $\delta^{13}C$-DIC = -11.7 ‰. This value is clearly higher than any reasonable sDIC contribution from brine formation. As well, such a light isotopic signature is difficult to rationalize. Although the fractionation factor between HCO_3^- and $CaCO_3$ in ikaite has yet to be determined, temperature independent fractionation factors for aragonite and calcite ($\varepsilon_{CaCO3\text{-}HCO3\text{-}}$) are as much as + 2.7 ‰ and + 1.0 ‰, respectively (Romanek et al., 1992). It seems unlikely that $CaCO_3$ precipitation within the ice (following equation 16) would lead to a brine solution ≈ 13 ‰ lighter than its parent seawater DIC (Note: as HCO_3^- makes up > 90% of DIC at seawater pH, its isotopic signature essentially identical to $\delta^{13}C$-DIC). Furthermore, this calculation assumes that equation 16 does not lead to CO_2 degassing from brine solution, which would serve to enrich the remaining brine solution. Laboratory studies have illustrated, however, that CO_2 degassing could be quantitatively as important as $CaCO_3$ precipitation during sea ice formation (Papadimitriou et al., 2004). As well, such degassing would act to reduce any "excess" CO_2 accumulated in the brine from $CaCO_3$ precipitation, effectively counteracting the accumulation of an isotopically light DIC signature in exported brine.

The calculations described above assume that the entire sDIC enrichment of PWW is due to brine rejection (≈ 130 μmol kg^{-1} due to conservative concentration and ≈ 20 μmol kg^{-1} due to $CaCO_3$ formation). This assumption is incompatible with several lines of evidence (Figure 3-6

and Figure 3-8) showing that organic matter remineralization in the sediments is clearly a major contributor to DIC accumulation in the halocline (section 3.5.2). Without a better idea of the fractionation factors associated with ikaite precipitation from solution or the physical controls on CO_2 degassing from brine as sea ice forms, a quantitative determination of the potential for sea ice brine to contribute "excess" DIC (over TAlk) to the water column cannot be further investigated using stable carbon isotopes at this time. Although δ^{13}C-DIC may have the potential as a natural tracer of sea ice-derived DIC additions to the water column, our evaluation suggests that non-conservative sea ice brine injection of CO_2 is not an important process contributing DIC to PWW in this region. Rather, our results suggest that addition of CO_2 to PWW by the remineralization of sediment organic material is the predominant non-conservative source of DIC to the south-western Canada Basin halocline.

3.5.4 The Nutrient and DIC Maxima Mismatch

While our analyses have allowed us to identify the dominant remineralization sources of DIC to PWW, the mismatch between the salinity signature of the nutrient maximum and the DIC maximum (Figure 3-3) requires further explanation. As discussed below, our observations suggest that physical mixing between end member water masses in the halocline can be invoked to explain the differential salinity ranges of the nutrient and DIC maxima.

Figure 3-9(a) illustrates DIC and PO_4 concentrations within the upper (PSW) and middle (PWW) halocline (filled triangles) and the lower halocline to the depth of the temperature maximum of the Atlantic layer (ATL, open triangles). Mixing lines can be drawn between average DIC and PO_4 values in PSW (purple square), PWW (orange square), ATL (green square) and are

illustrated with purple and green lines respectively (Figure 3-9a). The difference in slope seen between the PSW-PWW line (purple line) and the PWW-ATL line (green line) illustrates that DIC concentrations in the Atlantic layer are almost as high as PWW. The smaller DIC and PO_4 gradient between PWW and ATL waters indicates that mixing between PWW and ATL will have less of an impact on DIC than on PO_4. In the transition between Pacific and Atlantic halocline waters (along the PWW to ATL line) this translates into a larger salinity range for the DIC maximum (S = 33.0 - 33.58), relative to the PO_4 maximum (S ≈ 33.0). This, in turn, explains the mismatch between the salinity of the maximum PO_4 and DIC values shown in Figure 3-3 and Figure 3-4a. Once mixing and conservative contributions of PO_4 and DIC are accounted for (salinity-normalized values depicted as circles, Figure 3-9b) marine organic matter remineralization (characterized by a 106:1 DIC:PO_4 stoichiometry) can be invoked to explain the variability in DIC and PO_4 within the upper (PSW to PWW) and lower (PWW to ATL) halocline.

3.6 Conclusions

Using stable carbon isotopes, AOU and nutrient tracers, we investigated the contribution of various processes to the formation of the DIC maximum in the south-western Canada Basin halocline. This investigation has illustrated that once conservative contributions are accounted for, the nutrient and DIC maxima in PWW are dominantly sourced from the products of organic material remineralization within Bering and Chukchi Sea sediments entrained in northward flowing Pacific water during winter and delivered to the deep basin. Mixing between PWW and

the Atlantic water in the lower halocline explains the mismatch between the salinity fingerprint of maximum DIC (S = 33.0 - 33.58) and the PO_4 ($S \approx 33.0$) concentrations.

Our analysis indicates that air-sea gas exchange and non-conservative brine export of "excess" DIC (over TAlk) are not important contributors to the Canada Basin DIC maximum. Despite the negligible impacts of these surface processes on the DIC content of PWW, the "continental shelf CO_2-pump" associated with sea ice formation is still the main driver for the delivery of CO_2 to the halocline (e.g., Anderson et al., 2010) and may be sensitive to a warming Arctic climate. This pump acts to maintain the CO_2 under-saturation of shelf waters in contact with the atmosphere that persists throughout the ice-covered winter months (Anderson et al., 2010). If changing climatic conditions along the Arctic shelves leads to increased sea ice production in winter (to fill the larger open-water areas formed by intensified summer melt), this could result in an increase in the frequency of events that act to ventilate the halocline at depth (e.g., Shimada, 2005; Weingartner et al., 1998; Winsor and Chapman, 2002), potentially increasing the delivery of DIC to the Canada Basin halocline. On the other hand, increased freshwater flux to the Arctic could serve to increase stratification and decrease shelf water salinity (e.g., Winsor and Chapman, 2002), stifling the formation of waters dense enough to ventilate the halocline; this would reduce the "continental shelf CO_2 pump", promoting CO_2 efflux along the shelves (e.g., Anderson et al., 2010). Furthermore, ice edge retreat beyond the shelf break in summer may promote the upwelling of high DIC waters onto the shallow shelves, potentially contributing to further CO_2 efflux under high wind mixing conditions (Carmack and Chapman, 2003).

3.7 Tables

Table 3-1. Pooled standard deviation (Sp) of duplicate geochemical analyses

Parameter	Units	2008		2009	
		Sp	**k**	**Sp**	**k**
S		0.002	156	0.007	134
$NO_3^- + NO_2^-$	mmol m^{-3}	0.08	247	0.07	191
NH_4^+	mmol m^{-3}	0.04	163	0.02	120
H_3PO_4	mmol m^{-3}	0.01	242	0.01	206
Oxygen	mmol m^{-3}	1.340[b]	181	0.313[b]	195
$\delta^{18}O$-H_2O	‰ V-SMOW	0.04	13	0.03	20
DIC	µmol kg^{-1}	3.65	35	3.65	35
TAlk	µmol kg^{-1}	3.49	11	3.49	11
$\delta^{13}C$-DIC	‰ V-PDB	0.01[a]	217[a]	0.01[a]	217[a]

[a] 2008 & 2009 analyzed as a single set

[b] Oxygen Sp was determined as mL/L and converted to mmol m^{-3} by multiplying by 44.661

Table 3-2. Salinity and $\delta^{18}O$ end member values used to determine water mass composition (after Yamamoto-Kawai et al., 2009)

	Atlantic Water (ATW)	**Pacific Water (PW)**	**Sea Ice Melt (SIM)**	**Meteoric Water (MW)**
S	34.87 ± 0.03	32.5 ± 0.02	4 ± 1	0
$\delta^{18}O$ (‰ V-SMOW)	0.24 ± 0.05	-0.8 ± 0.1	-2 ± 1.0	-20 ± 2

Table 3-3. Hydrographic and geochemical properties of the nutrient maximum at each station (2008 & 2009)

Year	Station	Latitude [°N]	CTD Pres [dbar]	CTD Temp [ITS-90 C]	CTD Salinity [PSS-78]	DIN [mmol m^{-3}]	H_3PO_4[a] [mmol m^{-3}]	DIC [µmol kg^{-1}]	δ^{13}C-DIC [‰ VPDB]	*f*MW	*f*SIM	AOU [mmol m^{-3}]	DICdiseq [µmol kg^{-1}]	N* [mmol m^{-3}]
2008	BL-2	71.396	126.9	-1.53	33.05	14.8	1.89	*n.d.*	0.60	0.045	-0.072	81.35	*n.d.*	-11.27
2008	CB-4	74.993	183.4	-1.55	32.89	14.4	1.82	*n.d.*	*n.d.*	*n.d.*	*n.d.*	81.46	*n.d.*	-10.26
2008	CB-9	78.003	192.8	-1.50	33.19	15.3	1.88	2227.47	*n.d.*	0.043	-0.071	97.81	62.35	-10.37
2008	Stn-A	72.601	181.2	-1.53	32.90	14.8	1.85	2206.89	0.60	0.044	-0.065	87.43	52.22	-10.35
2008 Average			**171.1**	**-1.53**	**33.01**	**14.8**	**1.86**	**2217.18**	**0.60**	**0.044**	**-0.069**	**87.01**	**57.29**	**-10.57**
2009	BL-2	71.396	103.5	-1.36	33.13	15.2	1.84	2210.78	*n.d.*	0.040	-0.058	95.21	56.78	-9.86
2009	BL-4	71.493	119.6	-1.37	32.68	14.4	1.82	2198.73	0.03	0.043	-0.057	87.53	51.23	-10.32
2009	BL-6	71.658	159.3	-1.47	32.96	15.1	1.84	2217.68	0.36	0.036	-0.059	91.99	45.59	-9.95
2009	BL-8	71.953	165.2	-1.50	32.95	15.7	1.87	2212.75	0.19	0.034	-0.056	94.74	47.16	-10.64
2009	CB-4	75.001	217.8	-1.53	33.06	15.0	1.82	2220.23	0.40	0.045	-0.065	84.81	57.57	-9.69
2009	CB-9	78.019	188.2	-1.50	33.16	15.7	1.86	2220.91	*n.d.*	0.042	-0.063	92.02	57.86	-9.76
2009 Average			**158.9**	**-1.45**	**32.99**	**15.2**	**1.84**	**2213.51**	**0.25**	**0.040**	**-0.060**	**91.05**	**52.70**	**-10.04**

[a] Maximum H_3PO_4 concentration measured in the profile at each station.

Table 3-4. Hydrographic and geochemical properties of the DIC maximum at each station (2008 & 2009)

Year	Station	Latitude [°N]	CTD Pres [dbar]	CTD Temp [ITS-90 C]	CTD Salinity [PSS-78]	DIN [mmol m^{-3}]	H_3PO_4 [mmol m^{-3}]	DIC[a] [µmol kg^{-1}]	δ^{13}C-DIC [‰ VPDB]	*f*MW	*f*SIM	AOU [mmol m^{-3}]	DICdiseq [µmol kg^{-1}]	N* [mmol m^{-3}]
2008	CB-4	75.021	227.0	-1.39	33.52	*n.d.*	*n.d.*	2239.38	*n.d.*	0.043	-0.061	88.25	64.36	*n.d.*
2008	CB-9	78.003	210.8	-1.29	33.58	14.7	1.70	2232.46	*n.d.*	*n.d.*	*n.d.*	96.10	58.95	-8.38
2008	Stn-A	72.601	222.8	-1.37	33.54	15.0	1.69	2222.97	0.54	0.034	-0.057	97.98	60.92	-7.94
2008 Average			**220.2**	**-1.35**	**33.55**	**14.9**	**1.70**	**2231.60**	**0.54**	**0.039**	**-0.059**	**94.11**	**61.41**	**-8.16**
2009	BL-2	71.396	140.9	-0.98	33.89	14.2	1.45	2212.34	0.60	0.025	-0.040	91.92	42.42	-5.42
2009	BL-4	71.493	158.2	-1.33	33.55	15.0	1.67	2221.49	0.29	0.038	-0.058	100.62	49.11	-7.68
2009	BL-6	71.658	172.1	-1.45	33.20	15.3	1.81	2227.84	0.44	0.044	-0.065	93.27	25.74	-9.33
2009	BL-8	71.953	179.6	-1.35	33.20	15.7	1.82	2215.76	0.30	0.038	-0.057	92.53	40.72	-9.59
2009	CB-4	75.001	248.3	-1.47	33.48	14.6	1.68	2228.22	*n.d.*	0.044	-0.067	85.50	52.96	-8.13
2009	CB-9	78.013	186.6	-1.50	33.15	15.3	1.83	2226.26	0.31	*n.d.*	*n.d.*	90.35	51.97	-9.69
2009 Average			**181.0**	**-1.35**	**33.41**	**15.0**	**1.71**	**2221.99**	**0.39**	**0.038**	**-0.057**	**92.36**	**43.82**	**-8.31**

[a] Maximum DIC concentration measured in the profile at each station.

Table 3-5. Western Arctic Ocean halocline as summarized by Cai et al., (*in press*)

	Source Water	Depth Range (m)	Salinity	[DIC] ($\mu mol\ kg^{-1}$)	[PO_4] ($\mu mol\ L^{-1}$)	Residence Time (yrs)
Upper and Middle Halocline	Pacific Water *with River Runoff*	~ 40 - 120	33.1	2160 - 2190	1.8	10
Lower Halocline	Atlantic Water *with Pacific Shelf Plumes*	~ 150 - 220	34.3	2170 - 2190	0.8	15

Table 3-6. Geochemical properties of water collected in Bering Strait and at intermediate depth along Bering Shelf slope from September 6-9th, 2000 aboard the *RV Mirai* (49MR00K06). Station locations illustrated in Figure 3-7.

	Max Depth (m)	Sample Depth (m)	Salinity	DIN ($mmol\ m^{-3}$)	H_3PO_4 ($mmol\ m^{-3}$)	DIC ($\mu mol\ kg^{-1}$)	AOU ($mmol\ m^{-3}$)	N* ($mmol\ m^{-3}$)
Bering Sea "Winter"[a] Water	114	60-75 m	32.75	18.5	1.84	2111.1	82.79	-5.9
Bering Strait Summer Water[b]	50	0 - 50 m	31.06	0.95	0.77	2000.6	15.17	-8.2

[a] Following the description of Cooper et al. (1997), water with geochemical properties associated with "Arctic Ocean Upper Halocline" water [N ≈20 μM; Si ≈ 45 μM; δ18O ≈ -1.1 ‰] could be found along the Bering Sea slope at depths less than 100m. They determined this water could contribute to the winter flow of Pacific waters along the shelves. Using the Mirai 2000 data set (Figure 3-7), waters sampled at 60 - 75m depth along the southern Bering Sea slope would satisfy the Cooper et al. (1997) description.

[b] Average water properties found in Bering Strait (averaged over the 50 m depth) in September 2009.

3.8 Figures

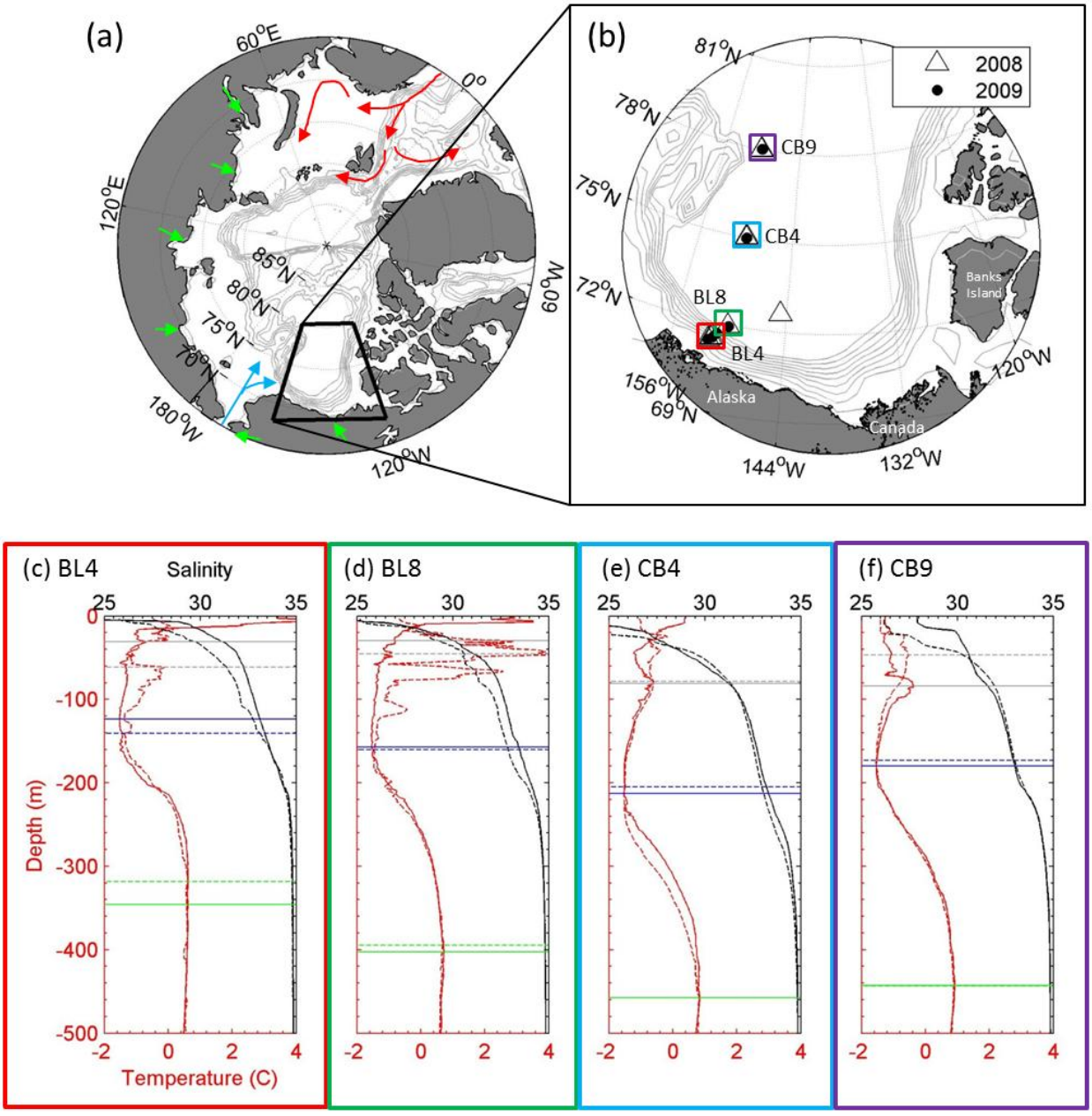

Figure 3-1. (a) The Arctic Ocean from the vantage point of the North American continent. Major oceanic in-flows, Pacific (blue arrows) and Atlantic (red arrows), and riverine sources (green arrows) are highlighted (after Macdonald et al., 2004b). Grey lines show bathymetry from 0 – 3000 m (500 m interval) and the black polygon indicates the location of our stations in the

Canada Basin (inset plot); (b) Inset plot of the Canada Basin, grey lines show bathymetry from 0 to 2000 m depth (interval 250m), with station locations illustrated as triangles (2008) and circles (2009). Coloured squares highlight example station profiles in subplots (c-f) below; (c-f) Temperature (red) and Salinity (black) profiles in the upper 500 m of the water column during the 2008 (solid lines) and 2009 (dashed lines) cruises for two example slope stations [(c) BL4 and (d) BL8] and two example deep basin stations [(e) CB4 and (f) CB9]. Grey, blue, and green horizontal lines refer to the depths of the subsurface temperature maximum (PSW), subsurface temperature minimum (PWW), and Atlantic layer T-maximum, in 2008 (solid lines) and 2009 (dashed lines) respectively.

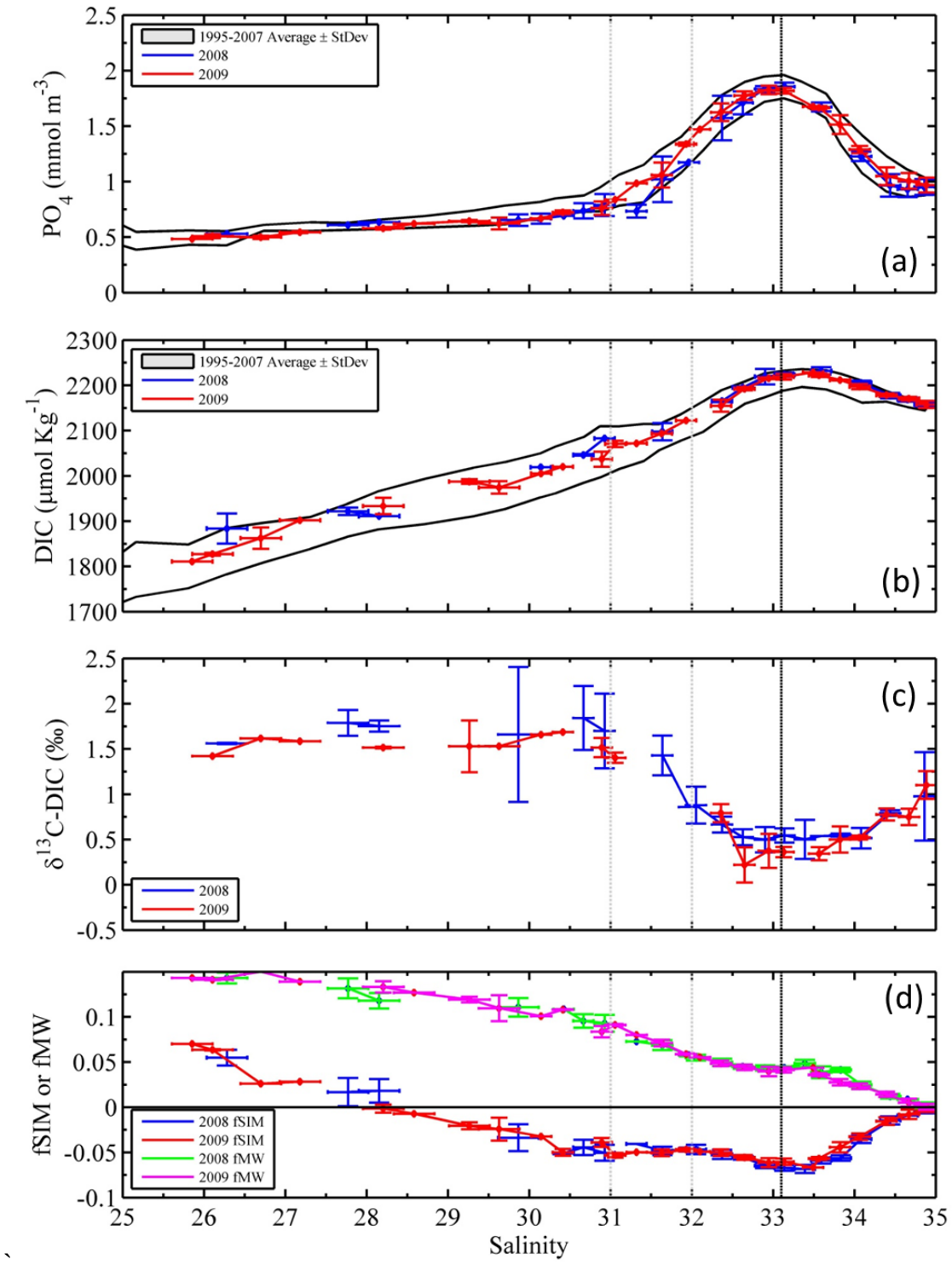

Figure 3-2. Tracer concentrations from the south-western Canada Basin, collected in 2008 (blue) and 2009 (red) respectively, plotted verses salinity. (a) Orthophosphate (PO_4; mmol m^{-3}); (b) DIC (µmol kg^{-1}); (c) δ^{13}C-DIC (‰);and (d) calculated fractions of sea ice melt (*f*SIM), brine

rejection (-*f*SIM), and meteoric water (*f*MW) content. Light grey vertical lines indicate Pacific Summer Waters (PSW, S = 31 to 32), whereas the black vertical line indicates the Pacific Winter Waters (PWW, S = 33.1). Historical data ranges determined from samples collected throughout the Canada Basin (1995-2007) are illustrated as 2 black lines enveloping data points in (a) and (b).

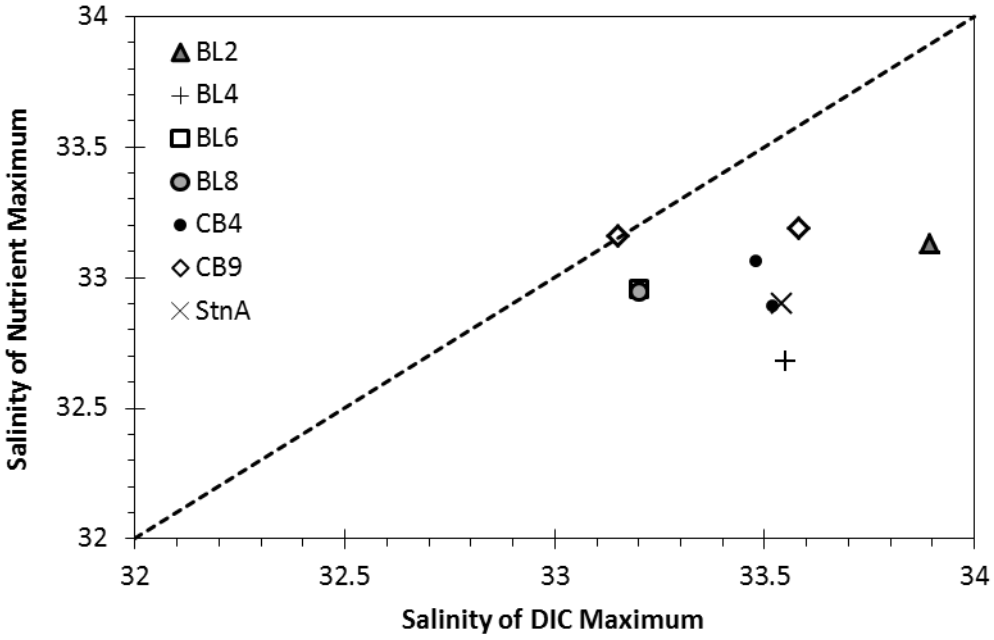

Figure 3-3. Measured salinity associated with the maximum DIC concentration at each station (2008 and 2009; Table 3-4) plotted against the measured salinity associated with the maximum nutrient concentration at the same station (Table 3-3). The dashed line is a 1:1 line, values falling on this line indicate the salinity of both maxima are identical.

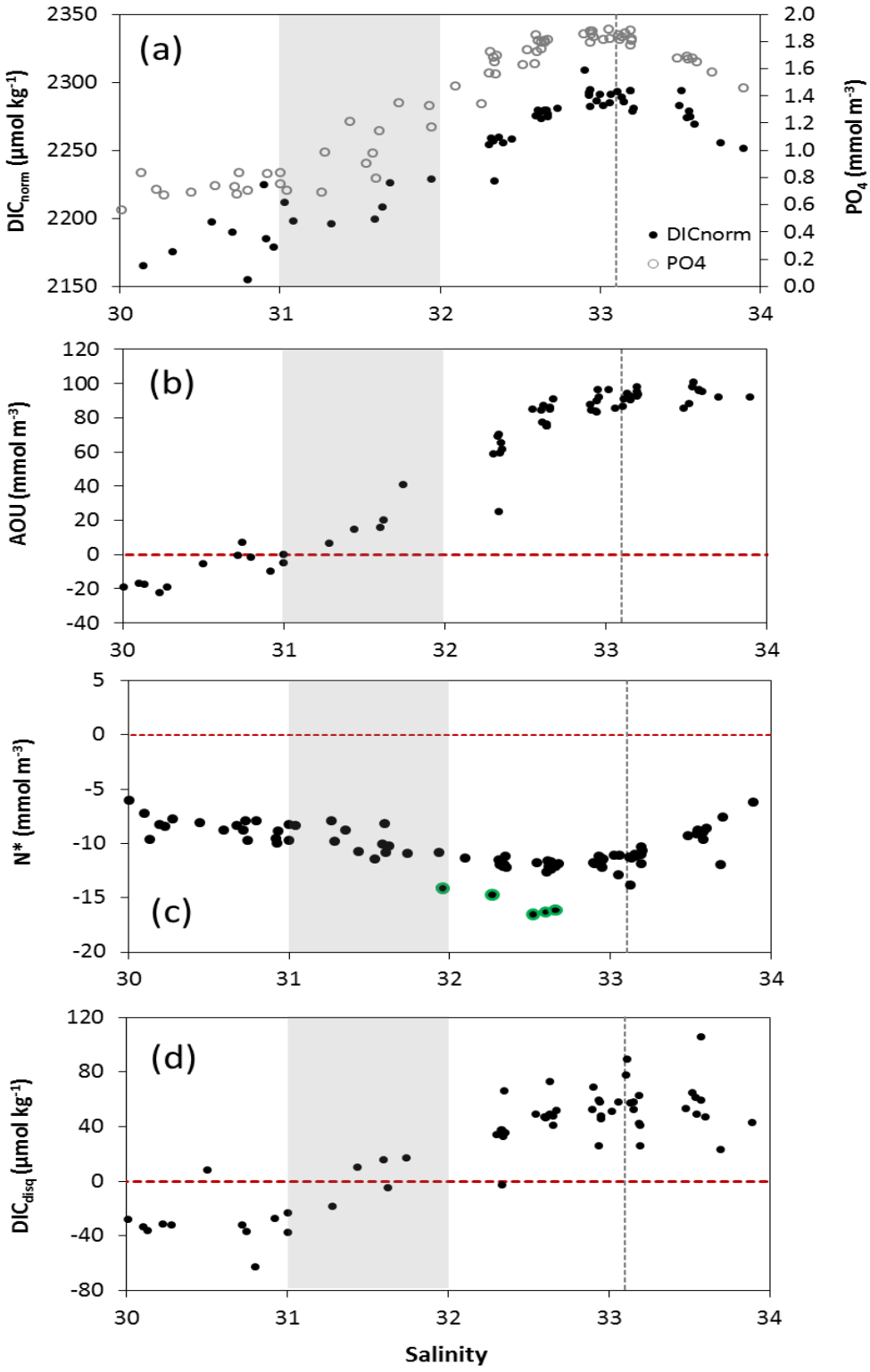

Figure 3-4. Tracer concentrations from the south-western Canada Basin halocline from both years (2008 & 2009) plotted verses salinity. (a)Salinity normalized DIC (DIC_{norm}, µmol kg^{-1};

filled circles) and orthophosphate (PO_4, mmol m^{-3}; open circles); (b) Apparent Oxygen Utilization (AOU; mmol m^{-3}); (c) N* (mmol m^{-3}); and (d) DIC_{diseq} (μmol kg^{-1}). The grey dashed vertical line indicates PWW (S = 33.1), grey shading indicates PSW (31 < S < 32), and red horizontal lines on (b),(c), and (d) indicate zero. Green circles in (c) single out data collected along the shallow shelf station BL2 (≈ 150 m depth).

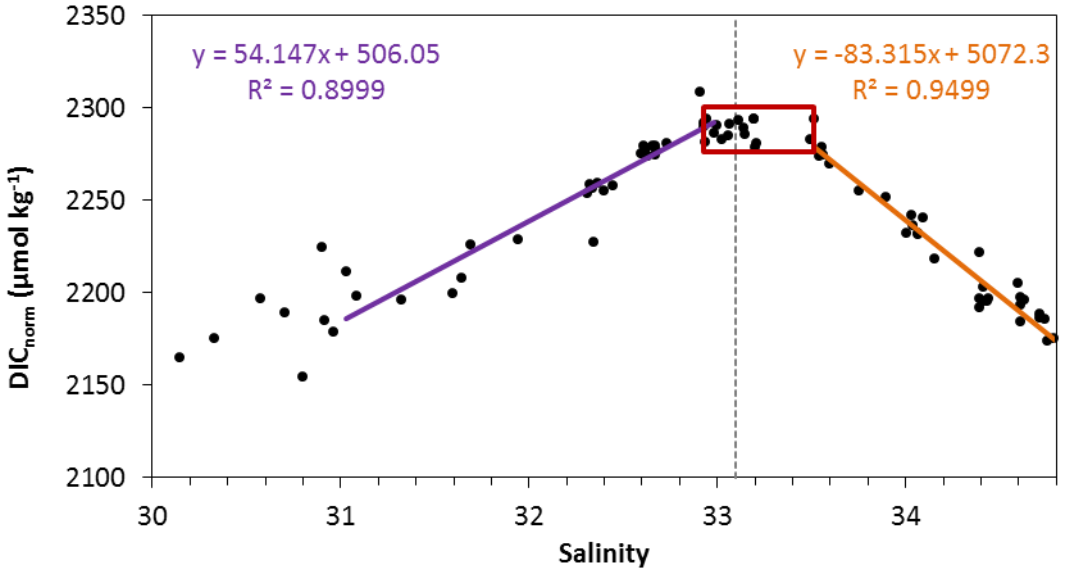

Figure 3-5. Measured DIC values normalized to S = 35 (DIC_{norm}), plotted versus salinity within the halocline (S = 31 to 34.8). Linear regression lines are illustrated through the upper halocline [PSW (S = 31 to 32) to PWW (S = 33.0 to 33.5); purple], and the lower halocline [PWW to Atlantic layer T-Maximum (S = 34.8); orange]. The red box demotes the salinity spread of the DIC maximum.

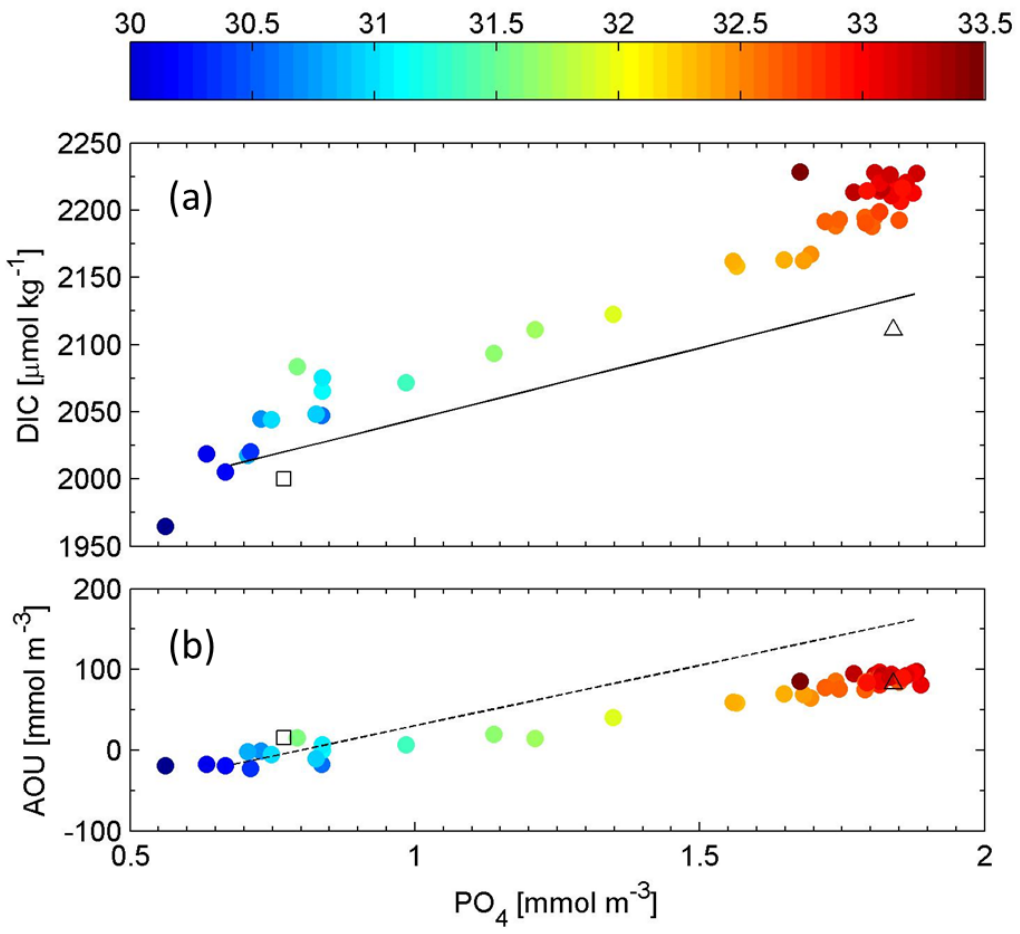

Figure 3-6. DIC (a) and AOU (b) plotted versus PO_4 between the PSW layer (S = 31 to 32) and PWW layer (S = 33.1 to 33.5). The symbol colour represents sample salinity matching the colour scale on top of panel (a). Lines represent the marine organic matter relationships of 106:1 for DIC:PO_4 (solid line) and 150:1 for AOU:PO_4 (dashed line) following Sarmiento and Gruber (2006): $106CO_2 + 16NO_3^- + H_3PO_4^{2-} + 78H_2O + 18H^+ = C_{106}H_{175}O_{42}N_{16}P + 150O_2$. Open square and triangle symbols represent Bering Strait Summer water and Bering Sea "Winter" water, respectively; see text and Table 3-6 for details.

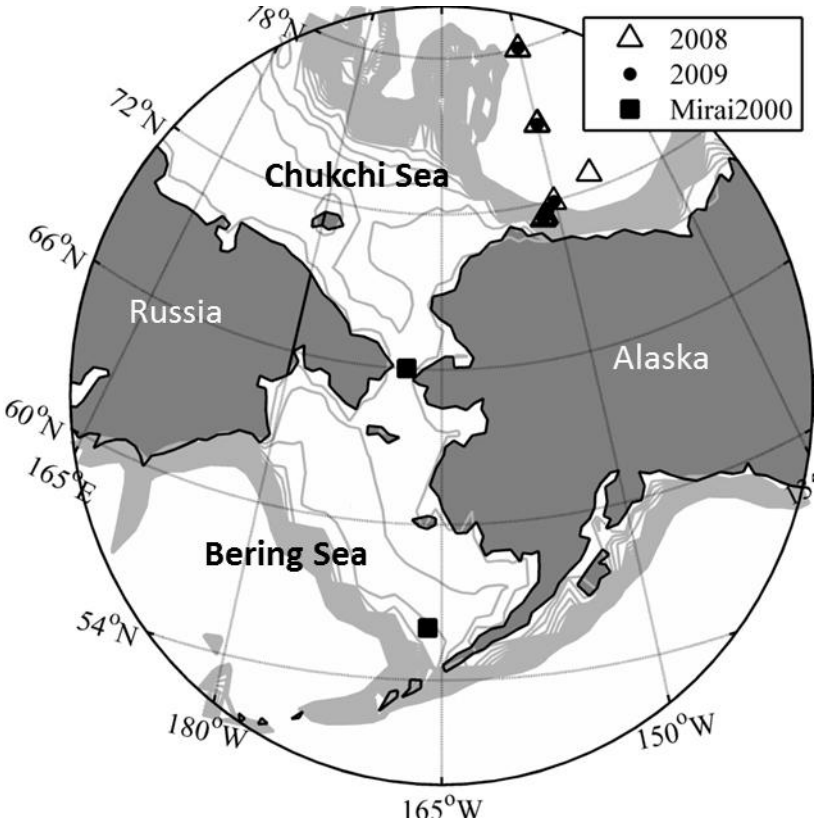

Figure 3-7. Map of the Bering and Chukchi Seas. Black squares indicate the locations of sampling stations occupied by the *RV Mirai* in September 2000: the Bering Sea slope station (56 N, - 166 W) at a depth of ≈ 110 m and the Bering Strait station (66 N, -168.5 W) at a depth of ≈ 50 m. Stations occupied in 2008 and 2009 during this cruise as in Figure 3-1b. Grey lines represent 50 m depth contours, from 0 to 500 m depth.

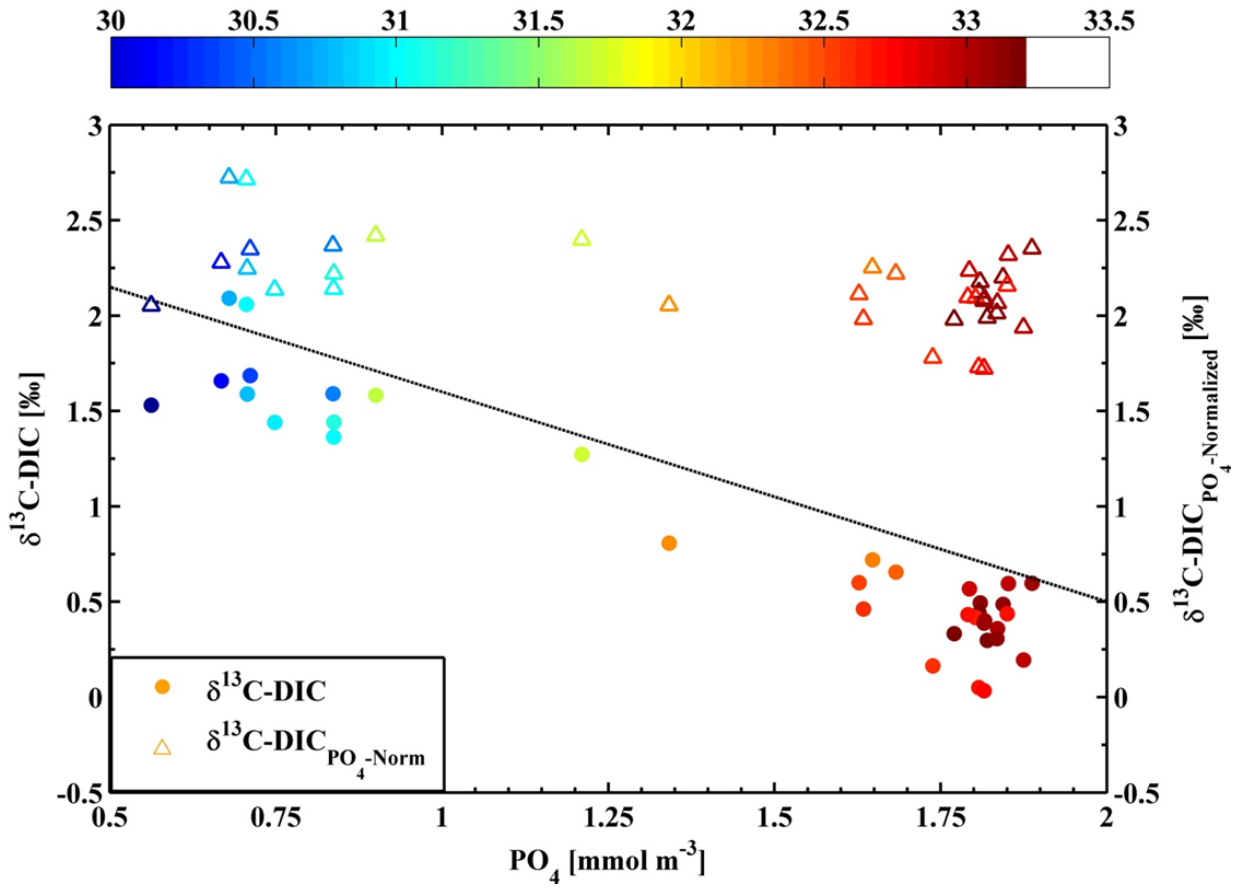

Figure 3-8. Stable carbon isotope composition of DIC plotted versus PO_4 between the PSW layer (S = 31 to 32) and PWW layer (S = 33.1 to 33.5). The symbol colour represents sample salinity matching the colour scale on top of the plot. Filled circles denote measured values whereas open triangles indicate δ^{13}C-DIC has been normalized to PO_4 ($\delta^{13}C\text{-}DIC_{PO4Normalized}$) following Charles and Fairbanks (1990), equation 15. The solid line represents the δ^{13}C-DIC vs. PO_4 relationship determined by Broecker and Maier-Reimer (1992): $\delta^{13}C\text{-}DIC = 2.7 - 1.1 * PO_4$

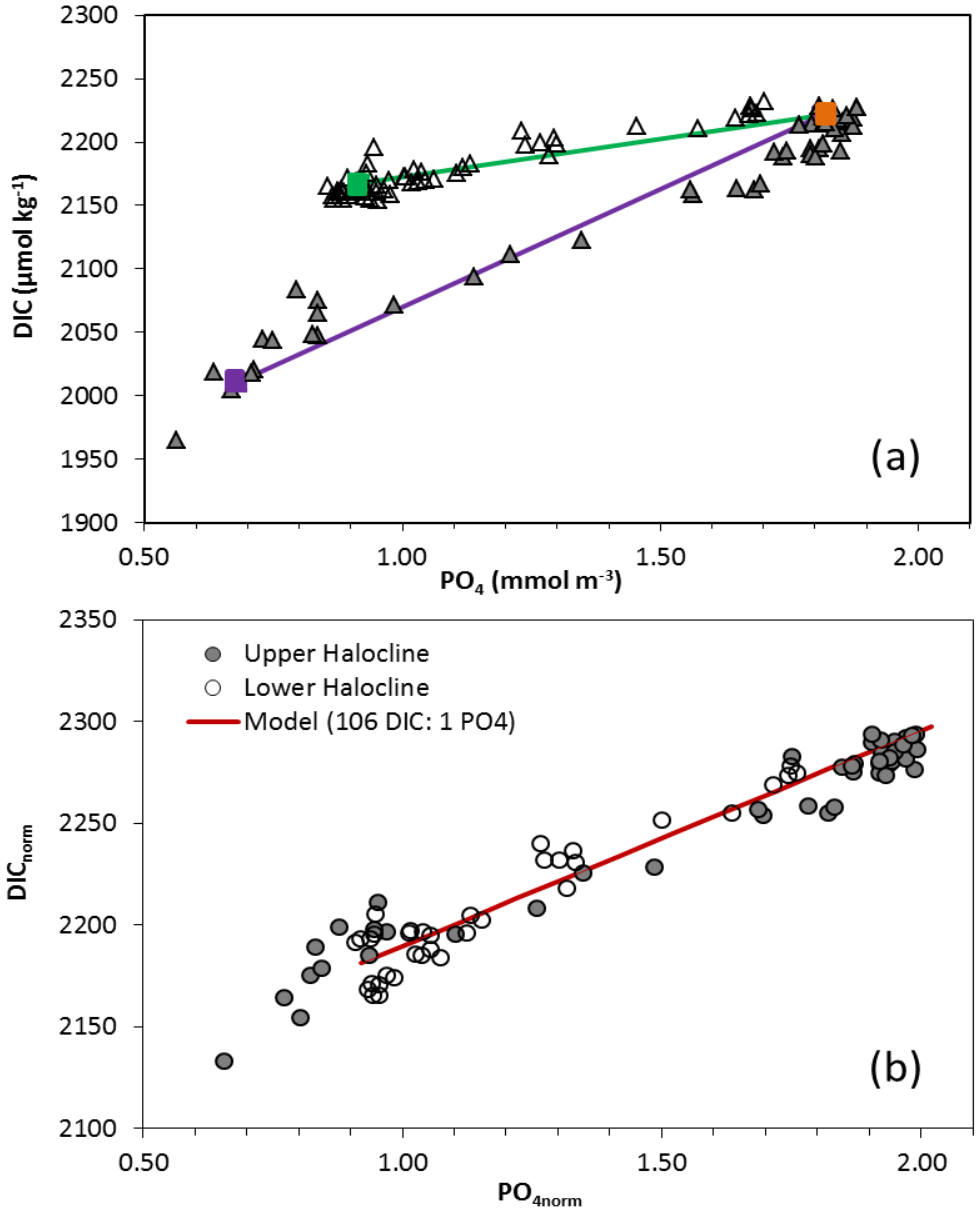

Figure 3-9. Plot of DIC versus PO_4 within the Canada Basin halocline (S = 31 to 34.8). (a) Measured values (triangles) from the upper halocline [PSW (S = 31 to 32) to PWW (S = 33.1 to 33.5)] are illustrated with filled symbols, whereas values from the PWW layer to Atlantic Layer T-Maximum (S = 34.8) are illustrated with open symbols. Mixing lines between average measured values in PSW and PWW (purple line) and PWW and Atlantic T-maximum (green line) can be drawn to illustrate the three mixing end members in the halocline. (b) Once mixing is accounted for (salinity-normalized values) marine organic matter remineralization can be invoked to explain all the variability in DIC and PO_4 within the halocline characterized by an ≈ 106:1 DIC:PO_4 stoichiometry. The red model line illustrates the addition of DIC and PO_4 to PSW in a 106:1 ratio.

Chapter 4: Inorganic Carbon System Dynamics in Land-Fast Arctic Sea Ice During the Early-Melt Period

We carried out a six-week time series of carbonate system and stable isotope measurements to investigate the effects of sea-ice on air-sea CO_2 exchange during the early melt period in the Canadian Arctic Archipelago. We observed significant changes in bulk sea ice and sackhole brine carbonate system parameters associated with increasing temperatures and the build up of chlorophyll *a* concentrations in bottom ice. The warming sea ice column could be separated into distinct geochemical zones where biotic and abiotic processes exerted different influences on inorganic carbon and pCO_2 distributions. In the bottom ice, biological carbon-uptake maintained undersaturated pCO_2 conditions throughout the time series, whereas pCO_2 was supersaturated in the upper parts of the ice. Low CO_2 permeability in the sea ice matrix and snow cover at the air-sea ice interface effectively impeded CO_2 efflux from the upper ice surface to the atmosphere, despite the strong pCO_2 gradient. Throughout the middle ice column, brine pCO_2 decreased significantly with time and was tightly controlled by sea ice temperature and in-situ melt dilution. Once the influence of melt dilution was accounted for, however, both $CaCO_3$ dissolution and seawater mixing were found to contribute alkalinity and inorganic carbon to brines, with the $CaCO_3$ contribution driving brine pCO_2 to values lower than predicted from melt-water dilution alone. This field study reveals a dynamic carbon system within the rapidly warming sea ice, prior to snow melt. We suggest that the early spring period preconditions the ice column towards pCO_2 under saturation, contributing to a weak CO_2 sink as the melt period advances.

4.1 Introduction

Sea ice plays an important role in polar marine biogeochemical cycles, particularly with respect to the transport and storage of climatologically active gases such as CO_2. As a semi-permeable interface, the presence of sea ice acts to impede gas transfer between the surface ocean and the atmosphere. However a number of studies have documented direct sources or sinks of CO_2 across sea ice-atmosphere interface at different times of year (e.g., Delille, 2006; Miller et al., 2011a, 2011b; Nomura et al., 2010a; Papakyriakou and Miller, 2011; Semiletov et al., 2004), suggesting its role is more complicated than that of a passive barrier. Seasonal redistribution of inorganic carbon across the atmosphere-ice-ocean interfaces is coupled with the yearly cycle of freezing and melt, and driven by both biological and abiotic processes. These processes include microbial activity (photosynthesis and respiration), brine concentration-dilution, calcium carbonate precipitate formation-dissolution, and inorganic carbon release to surface waters (e.g., Arrigo et al., 2010; Chierici et al., 2011; Miller et al., 2011b; Rysgaard et al., 2009; Thomas et al., 2010). The combination of such dynamic seasonal processes and heavy bias towards warm-period sampling has complicated derivation of a general statement of the net impact of the seasonal sea ice cycle on the polar carbon budget. Particularly lacking are data during the late winter to early spring transition.

The transition from late winter into early spring marks a period of rapid change in the sea ice physical and biogeochemical system. During this period, both abiotic and biotic processes throughout the ice column can contribute to inorganic carbon redistribution. Throughout the dark

and cold polar winter, biological activity is minimal and sea ice permeability is significantly decreased (e.g., Arrigo et al., 2010; Deming, 2010; Petrich and Eicken, 2010). This contributes to the build-up of CO_2 within sea ice brine channels, as brine salinity increases and carbonate minerals precipitate (e.g., Miller et al., 2011b). As a result, sea ice can become a source of CO_2 to the atmosphere with the advance of spring, when surface temperatures and sea ice permeability increase (Nomura et al., 2010a; Papakyriakou and Miller, 2011). CO_2 fluxes across the atmosphere-ice boundary are highly heterogeneous during this period of rapid temperature change, this results from strong variability in surface ice conditions (chemical and physical) and in the state of the overlying snow pack (e.g., Delille, 2006; Geilfus et al., 2012; Nomura et al., 2010b; Papakyriakou and Miller, 2011; Zemmelink et al., 2006). As spring warming advances further, CO_2 fluxes have been observed to switch direction, with the melting ice surface contributing to extensive CO_2 uptake from the atmosphere as a result of brine dilution within the warming, melting ice (e.g., Delille, 2006; Geilfus et al., 2012; Nomura et al., 2010a). This CO_2 drawdown over late spring-early summer is potentially enhanced by the dissolution of the calcium carbonate within the melting sea ice matrix (e.g., Dieckmann et al., 2010, 2008; Loose et al., 2011; Rysgaard et al., 2011; Thomas et al., 2010). In the lower ice column, increased porosity associated with warming of the ice column enhances the gravity-driven drainage of brines into under-ice waters, transferring salts and inorganic carbon into the surface mixed layer (Jones and Coote, 1981; Rysgaard et al., 2007) and enhancing seawater flushing (Zhou et al., 2013). Furthermore, biological processes within the bottom ice can also drive carbonate system variability as solar radiation and temperature increase. Over this period, autotrophic communities in the bottom ice experience dense growth as nutrients are replenished from seawater under

increasing light levels (e.g., Arrigo et al., 2010; Gleitz et al., 1995; Munro et al., 2010; Papadimitriou et al., 2012).

Changes occurring within the sea ice carbonate system at this critical time of year have received only sparse attention. Furthermore, few studies combine measurements at the atmosphere-ice and ice-seawater interfaces with adequate assessment of the remaining ice column. The goal of this study was to fill this data gap by documenting changes in inorganic carbon speciation, stable carbon isotopes, and CO_2 fluxes over the winter-spring transition in a land-fast ice system near Resolute Passage, Nunavut. Here we present carbonate system parameters (Total Alkalinity, Total Inorganic Carbon, pCO_2), stable isotopes ($\delta^{18}O$-H_2O, $\delta^{13}C$-TIC), chlorophyll *a*, and CO_2 flux measurements over a six-week times series to characterize the carbon cycle throughout the entire ice column, from the atmosphere-ice interface to the ice-seawater interface. Further, we test the application of stable carbon isotopes to distinguish between the impacts of abiotic and biotic systems on the inorganic carbon cycle (e.g., Munro et al., 2010; Papadimitriou et al., 2009, 2007, 2004). For example, as melt-water dilutes brine in warming ice, dissolution of $CaCO_3$ can lead to isotopic enrichment (i.e., increased ^{13}C / ^{12}C ratio) of trapped brine, coupled with an increase in brine dissolved inorganic carbon (DIC). Compared to the original seawater, however, there needs to be a concomitant out-gassing of CO_2 with $CaCO_3$ formation (without CO_2 out-gassing the brine will go back to its original seawater value). Photosynthetic uptake of DIC in the bottom ice would likewise enrich brine in ^{13}C, as algae discriminate against ^{13}C-bearing CO_2 in C-fixation via RubisCO, but would reduce brine DIC. Several studies have utilized stable carbon isotopes to trace inorganic and organic carbon cycling in the Antarctic seasonal sea ice (e.g., Kennedy et al., 2002; Munro et al., 2010; Papadimitriou et al., 2009, 2007); this will be the first

attempt to carry out similar studies of the inorganic carbon system in the Arctic. Through a combination of the above-mentioned geochemical tracers, this study characterizes inorganic carbon distributions within land-fast sea ice and discusses the processes driving inorganic carbon cycling over the winter-spring transition.

4.2 Methods

4.2.1 Field Site Description: Resolute Passage

The 2010 *Arctic - Ice Covered Ecosystem* (Arctic-ICE) study took place in Resolute Passage, Nunavut, Canada (Figure 4-1a). The sea ice camp was situated on smooth, land-fast, first-year sea ice, above a water column approximately 140 m deep in the Canadian Arctic Archipelago (CAA; Figure 4-1b). This region is typically characterized by sea ice cover for at least 10 months of the year, with first-year fast ice persisting for at least half of that time (Melling et al., 2008) and reaching its maximum thickness by mid-April (Shirasawa and Ingram, 1997). We collected time series samples from May 7th to June 19th 2010 (Julian Days, JD, 127-170; Table 4-1) on a three day rotation schedule.

4.2.2 Discrete Snow, Bulk Ice, Brine, and Under-Ice Surface Water Sampling

Discrete samples of snow, sea ice, brine, and under-ice surface water were collected at a new undisturbed site each sampling day (Figure 4-1c). Daily sample location selection was based on snow depth distribution at each new site, and carbon system sampling was carried out at sites that exhibited an average snow depth, which varied little over the course of the time series (13 ± 2 cm). Snow pits were first excavated with a flat metal shovel or spatula. Profiles of snow

temperature were recorded at 2 cm vertical intervals using a temperature probe (Traceable$^{(R)}$ Digital Thermometer, Model 4000, Control Company). A vertical profile of snow samples, using a 2 cm density cutter, was then collected into plastic bags (Nasco Whirl-PakR) and melted at room temperature in the Polar Continental Shelf Project (PCSP) laboratory for salinity determination. On several occasions, additional snow samples were collected for oxygen isotope ratio ($\delta\ ^{18}O$-H_2O) measurements.

Duplicate full depth sea-ice cores were cut by hand using a Kovacs Mark II 9 cm diameter corer, immediately sub-sectioned into 20 cm (2 x 10 cm) lengths, and sealed into gas tight Tedlar^{TM} film bags. The headspace was immediately removed using a hand pump, with careful attention not to apply vacuum to the sample. Bagged ice core sections were kept in coolers until transport back to the PCSP laboratory, where they were melted at room temperature in the dark. Once melted, Tygon tubing was fitted to the Tedlar^{TM} bag spigot, and any excess air (released as the ice sample melted) was removed. Assuming that the air removed from the bag was in equilibrium with the melt, we used the calculated melt pCO_2 to determine that no more than 0.3 % (often much less than 0.1 %) of the total carbon in the sample would have been lost from the system when removing the excess air. We further expect this loss to negligibly influence the stable isotope signatures of the melt. Once the excess air was carefully removed, samples were gently mixed to homogenize the melt and subsamples for geochemical parameters were removed through the Tygon tubing.

Sackholes were drilled with a 10” auger to depths of 130, 90, and 60 cm within the ice adjacent to the ice core drilling location (within 2 - 3 m). Immediately after drilling, sackholes were

sealed at the ice/snow interface with plastic-covered, high density foam plugs to limit gas exchange. Brine was allowed to accumulate in the sackholes over the course of the coring day (~ 5-6 hrs) then collected into 10-L cubitainers (Fisher Scientific) using an aquarium pump (QuietOne 800, Lifeguard Aquatics) to sample deep within the sackhole. Cubitainers were filled slowly to reduce bubble entrainment, with any bubbles or headspace removed by overfilling before sealing. The filled containers were then covered in black plastic bags to limit light exposure.

At the same sampling location, seawater from the ice-water interface was collected through an open core hole using an aquarium pump and 10 L cubitainer. As with sackhole brine samples, cubitainers were filled almost entirely with seawater, compacted and capped without headspace and placed in a black plastic bag to shield them from light. Collected brine and under-ice seawater was then transported to the heated sampling tent and inverted gently several times to homogenize before sub-samples for geochemical parameters were collected through tygon tubing on the cubitainer spigot.

Subsamples for total inorganic carbon (TIC) and total alkalinity (TA) were collected into 250 mL borosilicate glass reagent bottles (Pyrex), allowed to overflow 1 full volume, and stoppered after the headspace was adjusted to 1 % of the sample volume. Samples were preserved with 200 μL saturated $HgCl_2$ solution before sealing and securing the stoppers with silicon-free high vacuum grease (Apizon-M) and vinyl electrical tape (3M). Stable carbon isotope samples (δ^{13}C-TIC) were collected into 30 mL amber soda-lime glass bottles (Wheaton), allowed to overflow 1 bottle volume, preserved with 30 μL saturated $HgCl_2$, and sealed with no headspace using Poly-Seal*-

lined caps (Wheaton) secured with Parafilm-M (Sigma-Aldrich). Subsamples for the determination of $\delta\ ^{18}O\text{-}H_2O$ were collected into rinsed 20 mL clear borosilicate glass vials, and sealed using polypropylene caps with fluoropolymer resin/silicone septa (VWR) after McLaughlin et al. (2012). All samples were stored at room temperature in the PCSP laboratory until shipping south for analysis.

4.2.3 Continuous and In Situ Observations

4.2.3.1 In situ Peepers and Atmospheric pCO_2

The mixing ratio of CO_2 (xCO_2, ppmv) within the sea ice was monitored using in situ peeper gas samplers (Miller et al., 2011a; their figure 2). The peepers deployed during the Arctic-ICE 2010 field program consisted of 10-cm lengths of gas-permeable silicone tubing (3.5 cm ID, 0.16 cm wall; Allness Silicone Inc.) fitted around an aluminum spring coil (Raymond Springs) for support. Each end was sealed with a 3.5 cm diameter Teflon-foil lined rubber stopper (Cole-Parmer). Ports for sampling the ≈ 100 mL air space contained in the silicone chambers were created using two pieces of 0.31 cm OD stainless steel tubing (Supelco) inserted through the top rubber stopper of the peeper. To secure the peepers in the ice, holes were drilled through the sea ice to the underlying water using a 2" auger with a power head. Drilling all the way through to the underlying water allows the holes to fill with seawater to the freeboard line and freeze the peepers in place. Peeper arrays were deployed at 2 locations within 200 m of an eddy covariance CO_2 flux tower and about 100 m apart (Figure 4-1c). Peeper set 1 was set at depths of 10, 50, 70, and 90 cm (total ice thickness = 142 cm) and Peeper set 2 at depths of 60, 100, 145, and 152 cm below the top of the ice (total ice thickness = 145 cm, so the 152 cm peeper was in the underlying water). After allowing the peepers to freeze in place (3-5 days), each array was

sampled at 72 hr intervals by circulating the air within the system through a Continuous Automated CO_2 Sampler (CACS) system equipped with a LI-820 NDIR gas analyzer (Li-COR Environmental). With the CACS connected to the in/out ports on the peepers, air within the system was circulated past the detector in a closed loop using a peristaltic pump with a flow rate of 1 mL/min. The CACS system was calibrated on-site against CO_2 gas standards (1968 ppm and 958 ppm; PRAXAIR) at the start and end of the sampling program. Local atmospheric xCO_2 was recorded ~1.5 m off the snow surface using the CACS during each sampling event. The xCO_2 (ppmv) values measured with the CACS were converted to pCO_2 (µatm) using internal cell pressure and the average saturation vapour pressure of water (Weiss and Price, 1980) determined for in situ brine T and S conditions during our study.

4.2.3.2 Thermistors

In addition to discrete T core samples, sea ice and snow T was continuously monitored using a thermistor array (designed by Tim Papakyriakou, University of Manitoba) secured within a 2 m long PVC tube, and frozen into the ice at the start of the field program. Temperature measurements were taken every 3 seconds by a data logger (Campbell Scientific Model CR3000) and recorded in 1 minute averages over 23 depths from + 0.21 m above the ice surface (upper 21 cm of snow) to - 2.20 m below the ice surface (through the 140 cm thick ice column and into the upper surface waters).

4.2.3.3 Flux Chambers

Fluxes of CO_2 at the surface of the ice were measured using a LI-8100 automated soil CO_2 flux system (LiCOR Biosciences). To create an enclosed headspace for chamber measurements, a

PVC collar (10 or 5 cm high) was pressed into the snow pack, or cut into the ice surface using a custom-made metal toothed collar. The flux chamber was then placed on the collar, and snow was packed around the ensemble to ensure a tight seal. Once the flux chamber was in place, the domed-lid was closed and ambient CO_2 within the enclosed chamber was measured over time. The net change in pCO_2 over a 10 - 15 min interval was used to calculate the flux. At each sampling location, chamber CO_2 flux was measured at the snow surface (on snow) and the ice surface (immediately under the snow) at 3 sites within a 1 m x 1 m area of uniform snow character.

4.2.4 Geochemical Analyses

The salinity (S) of under-ice surface seawater, snow melt, bulk ice, and brine samples were measured with a hand-held conductivity meter (WTW Cond 330i) calibrated to a 0.01 mol L^{-1} KCl standard solution. Brine samples with S values greater than the instrument measurement range (S = 0 to 70) were diluted with equal parts distilled water before measurement. Reported accuracy for the hand-held conductivity meter is ± 0.1 over a salinity range of 0 to 42. For under-ice seawater samples, hand-held probe measurements were corrected by comparing S measured in seawater samples (collected from a 1 m x 1 m covered hole in a heated tent, using a Niskin bottle) with the hand-held conductivity meter and those measured by a CTD deployed through the same hole (SBE19plusCTD, Seabird Electronics; n = 40). Salinity (S) is reported on the Practical Salinity Scale 1978 (PSS78) without units.

Total inorganic carbon (TIC) was measured coulometrically following Dickson et al. (2007) using either a VINDTA 3D (Marianda) or SOMMA system at the Institute of Ocean Sciences,

Sidney, B.C., Canada. Following TIC analysis, total alkalinity (TA) was analyzed in a second sub-sample from the same bottle using the open-cell continuous titrant addition method with an automated Dosimat 665 titrator (Metrohm) and Red Rod pH combination electrode (Radiometer Analytical). The titration endpoints were determined by non-linear least squares fit (Dickson et al., 2007). Both TIC and TA were calibrated against certified reference materials (CRM 88 and 101) provided by Andrew Dickson (Scripps Institute of Oceanography).

The δ^{13}C-TIC samples were analyzed at the GEOTOP Stable Isotope Laboratory (Université du Québec à Montréal) using a Micromass Isoprime continuous flow isotope ratio mass spectrometer equipped with a MultiFlow (Isoprime) automated injection system. Carbon isotopic values are reported in per mil (‰) with respect to Vienna Peedee Belemnite (vpdb) referenced to the NBS-19 and LSVEC scale (standard error ± 0.1 ‰). The δ^{18}O-H_2O samples were analyzed at COAS Stable Isotope Laboratory (Oregon State University) using a Thermo Finnigan DeltaPlus XL isotope ratio mass spectrometer. Oxygen isotopic values are reported in per mil (‰) with respect to Vienna Standard Mean Ocean Water (V-SMOW) (standard error ± 0.05 ‰).

Analytical precision for each geochemical parameter measured in this study is listed in Table 4-2, where Sp refers to the pooled standard deviation (IUPAC, 1997) of k pairs of measurements.

4.3 Calculations

4.3.1 Bulk Ice Brine Salinity, Sackhole Brine Temperature, and Brine Volume

The salinity of brine contained in the original bulk ice samples, S_b, was approximated from the phase relationship between brine salinity and in-situ temperature, as described in Petrich and

Eicken (2010) for brine T > -23 °C (equation 1). This same phase relationship was rearranged and applied to approximate in situ brine temperature, T_{Sb}, of collected sackhole brine samples from measured salinity (Petrich and Eicken, 2010), as in equation 2.

$$S_b = \left(1 - \frac{54.11}{T}\right)^{-1} x\,1000 \qquad (1)$$

$$T_{Sb} = \left(\frac{54.11}{1 - \frac{1000}{S}}\right) \qquad (2)$$

We determine brine volume fraction (V_b/V) as a function of sea ice temperature and salinity after Cox and Weeks (1983), as summarized in Petrich and Eicken (2010), following equation 3.

$$\frac{Vb}{V} = \left(1 - \frac{Va}{V}\right) \frac{(\rho_i / 1000) S_{si}}{F_1(T) - (\rho_i / 1000) S_{si} F_2(T)} \qquad (3)$$

where Va/V refers to the air volume fraction, ρ_i is the density of pure ice in kg m^{-3} (ρ_i = 917 - 0.1403T), S_{si} is the bulk salinity of melted sea ice, and F_1(T) and F_2(T) are empirical functions based on phase relationships, as described by Cox and Weeks (1983) and Leppäranta and Manninen (1988). As bulk ice density was not measured in our samples, we assume the absence of air (i.e., $V_a/V = 0$) for simplicity in our calculations.

4.3.2 Partial Pressure of CO_2 in Sackhole Brine, Bulk Ice, and Under-Ice Surface Seawater

Partial pressure of CO_2 (pCO_2) in sackhole brine and under-ice surface seawater samples was calculated from measured TIC, TA, S (or S_b), and T (or T_{Sb}) using CO2Sys (Pierrot et al., 2006). Following Delille et al., 2007 we used carbonic acid dissociation constants, K_1 and K_2, determined by Mehrbach et al. (1973), refit by Dickson and Millero (1987) and dissociation constants for $KHSO_4$ determined by Dickson (1990). Brine pCO_2 values determined from bulk ice samples were calculated from measured bulk ice TA and TIC corrected to brine salinity (S_b). Here we have assumed that the carbonic acid dissociation constants in seawater are valid at these low temperatures and high salinities (see discussions in Delille et al., 2007; Miller et al., 2011a; and in this thesis, chapter 5).

4.4 Results

4.4.1 Snow Cover Characteristics

Across our sampling sites, the snow exhibited relatively isothermal depth profiles, with average temperatures (T) that followed air T fluctuations (Figure 4-2a), progressing from coldest values (-7.5°C) on day 130 (May 10) towards a fully melting (T > 0°C) snow pack by day 161 (June 10). Snow salinity (S) (Figure 4-2b) diminished with distance from the ice surface, with the highest S at the snow base (up to 12.3 at the start of the sampling day 130) decreasing towards S = 0 in the upper snow. Snow $\delta^{18}O$-H_2O became more isotopically depleted away from the saline snow base, with values of -11.01 ± 0.03 ‰ (n = 2) at the snow base and -20.72 ± 1.17 ‰ (n = 4) in the upper snow (S = 0).

Snow base S started to decrease more rapidly on day 151-152 (Figure 4-2b), when the whole snow pack T exceeded -2°C (transition from green to red contours on Figure 4-2a). Ice lenses, were found in the upper 5 - 9 cm of snow from day 159 onwards, signifying surface snow melt percolation and refreezing. Indeed, we observed a hard refrozen crust on the snow surface on day 161. Melt ponds began to form on day 165 (Mundy et al., 2014).

4.4.2 Land-Fast Sea Ice

4.4.2.1 Physical Properties

Sea ice thickness (142 ± 2 cm) and freeboard (10 ± 1 cm) remained relatively constant at sampling sites over the duration of this study. Temperatures in bulk ice and brine increased as surface air T warmed from an average of -12 °C in early May (not shown) to around 0 °C in early June (Figure 4-2c and Figure 4-2e; Table 4-3). Bulk ice T was at a minimum of around -7 °C at the ice surface at the beginning of the program, corresponding to high bulk ice S of 6.3 to 9.6 (Figure 4-2c,d). Bulk ice S was generally lower underneath the surface (10 - 30 cm), and became progressively less saline with time (Figure 4-2d). Likewise, S in the bottom 20 cm of ice generally decreased over the course of the sampling period (Figure 4-2d, Table 4-3). Brine volume (calculated using equation 3) mirrored the sea ice T distribution, with lowest values found in the cold upper ice (0.033) increasing with depth towards the warmer bottom ice (0.111) at the start of the sampling program (Figure 4-2g). High brine volume fraction (0.090 - 0.148) was observed throughout the ice column as it approached an isothermal T distribution at the end of the sampling period.

The bulk ice $\delta^{18}O$-H_2O data illustrate well-defined gradients in the lower two-thirds of the ice column (50 - 140 cm) that persisted relatively unchanged over the sampling period (Figure 4-3). In these layers, bulk ice $\delta^{18}O$-H_2O was enriched with respect to the under-ice surface water (-1.83 ± 0.06 ‰) and upper ice (10 - 30 cm; $\bar{x}$ = - 0.47 ± 0.06 ‰). Bottom ice $\delta^{18}O$-H_2O appeared to increase over the first half of the sampling program and remained at + 0.07 ± 0.03 ‰ after JD 140.

Sackhole brine S decreased dramatically over the time series, at all depths sampled (Table 4-4). Calculated brine T tracked the patterns in bulk ice, but with lower absolute values (cf. Figure 4-2c and Figure 4-2e). The correspondence between brine T and bulk ice T suggests that the sackhole samples successfully integrated the physical and chemical constituents of the ice pack above the sackhole depths.

Sackhole brine S decreased as the bulk ice warmed (depicted as change with sampling day in Table 4-4), and as increased permeability in the ice pack permitted in situ melt, brine drainage, and mixing with under-ice surface water.

4.4.2.2 Sea Ice Carbonate System

Observations of salinity-normalized TIC (sTIC), TA (sTA), and stable carbon isotopes ($\delta^{13}C$-TIC) are shown in Figure 4-4. Bulk ice and sackhole brine TIC and TA have been normalized to the average S of under-ice surface seawater (S = 32.5) to remove the influence of dilution by freshwater from melt.

At the beginning of the sampling program, bulk ice sTIC throughout the majority of the upper ice column (average for 10 -110 cm, 2224.5 ± 53.7 μmol kg^{-1}) was higher than under-ice surface seawater values (2132.1 ± 5.0 μmol kg^{-1}). Over the course of the season, sTIC values in the upper ice column decreased to within water column values (Figure 4-4a; Table 4-3). Bottom ice sTIC was always lower than water column values, decreasing to an average value of ≈ 1220 μmol kg^{-1} by the end of the sampling period. As with sTIC, bulk ice sTA at the beginning of the sampling period was initially much higher than water column values (sTA = 2333.9 ± 51.7 μmol kg^{-1} versus 2226.9 ± 3.7 μmol kg^{-1} for seawater) through the majority of the ice column (10 - 110 cm). In contrast to sTIC, however, sTA did not change significantly over the course of our sampling season (Figure 4-4b; slope = 0.03, $r^2 \approx 0$, Table 4-3). In the bottom ice layer, sTA was closer to water column values throughout the sampling period (bottom ice = 2278 ± 113 μmol kg^{-1}), with a measureable decrease at the end of the sampling season.

Sackhole brine sTIC and sTA values from the upper to middle parts of the ice (60 and 90 cm) were always lower than the under-ice surface seawater average (Figure 4-4d and Figure 4-4e). In general, the salinity-normalized values increased in the upper and middle parts of the ice column and decreased in sackholes that extended to the bottom of the ice (Table 4-4).

The TA/TIC ratio measured within the bulk ice increased throughout the ice column over the time series (Figure 4-5a). Early in the sampling season bulk ice TA/TIC was similar to the underlying surface seawater (1.045 ± 0.001), then increased as the season progressed following the sTIC decrease and brine volume increase (Figure 4-4a and Figure 4-2g, respectively). Sackhole brine TA/TIC was higher than bulk ice and surface seawater values in the early season,

and showed marginal increase over the sampling period (Figure 4-5b). The discrepancy between bulk ice and sackhole brine TA/TIC values likely reflects the contribution of $CaCO_3$ dissolution, as precipitated salts would be retained in bulk ice samples, but not in draining brine (e.g., this thesis, Chapter 5, section 5.3.1).

4.4.2.3 Stable Carbon Isotope Ratios

The δ^{13}C-TIC values we measured in bulk ice samples were quite variable (-0.52 to +3.38 ‰ vpdb) and generally became more enriched with time as the ice pack warmed (Figure 4-4c; Table 4-3). Unlike TIC and TA, δ^{13}C-TIC values showed no relationship with S ($r^2 < 0.03$). Isotopic values throughout the majority of the ice column (10-110 cm) became enriched in ^{13}C over the course of the 6 week time series, whereas bottom ice samples followed no such trend (Table 4-3). We observed a strong negative relationship between δ^{13}C-TIC and sTIC within the 90-110 cm section of the ice column (slope = -0.007, $r^2 = 0.71$; Table 4-3), but not at any other depths. The δ^{13}C-TIC values in bottom ice samples showed virtually no correlation with any of the other variables sampled.

Sackhole brine δ^{13}C-TIC values ranged from + 0.97 to + 2.96 ‰ vpdb and were generally isotopically heavier than those measured in bulk ice, and always isotopically heavier than the under-ice surface seawater (+ 0.69 ± 0.08 ‰). In contrast to bulk ice samples, sackhole brine in the mid-ice column (60 cm and 90 cm depth) became more isotopically enriched over the course of the sampling program (Figure 4-4f), as S decreased with increasing ice T (Table 4-4). Isotopic enrichment within the 60 and 90 cm sackholes was more strongly correlated with S and sTA,

than with sTIC (last three columns in Table 4-4). Brine isotopic values in the deepest sackhole samples (130 cm) were only weakly correlated with other measured parameters (Table 4-4).

4.4.2.4 Brine pCO_2

Brine pCO_2 diminished dramatically with depth in the ice column and with time. This was observed in calculated bulk ice (3326 to 2 μatm; Figure 4-4g) and sackhole brine (1128 to 200 μatm; Figure 4-4h) samples, and for in situ peeper measurements (1280 to 230 μatm; Figure 4-4i). At each time point, the highest pCO_2 values within the ice column were measured in the upper ice and diminished to the lowest values at the bottom ice. As well, brine pCO_2 throughout the entire ice column diminished over the course of the time series. Under-ice surface water pCO_2 values (383 ± 7 μatm) were close to equilibrium with respect to the atmosphere (384 ± 4 μatm) for the duration of the sampling program, and showed little temporal change. Brine pCO_2 in the upper ice (10 - 30 cm) remained above saturation with respect to the atmosphere until JD157 (Figure 4-6a), whereas bottom ice was always undersaturated with respect to the under-ice surface seawater after JD131 (Figure 4-4g). Brine pCO_2 calculated from bulk ice and sackhole brine samples (Figure 4-4g,h) and measured in situ with the peepers (Figure 4-4i) was closely related to brine volume (a function of T and S; Figure 4-7).

4.4.3 Ice-Atmosphere CO_2 Flux

Results from CO_2 flux chamber measurements from all surfaces (sea ice, snow, hoar layer, slush, and surface melt ponds) are depicted in Figure 4-6b and Figure 4-6c. In general, fluxes from all surfaces were small and ranged from + 0.058 to - 0.051 μmol m^{-2} s^{-1} (negative fluxes imply CO_2 uptake into the ice). We observed a general transition from positive fluxes from the ice (into the

atmosphere) during the first 8 days of observations towards a negative flux (into the ice) after JD 153. Fluxes from the snow were generally positive (towards the atmosphere) or neutral ($Flux_{CO2}$ = 0) during the whole sampling period, while the highest negative fluxes occurred over slush and melt ponds, or directly into the ice. The transition from positive to negative fluxes shown in Figure 4-6b,c corresponds with gradual warming of the snow and ice surfaces, with an apparent threshold T of the ice surface between - 3.5 to - 2.7 °C (Figure 4-2). A hoar frost layer measurement in the middle of the time series showed zero net flux (Figure 4-6c), while late-season measurements in the slush and melt-ponds showed negative (into ice) CO_2 fluxes (Figure 4-6b). Over this period, pCO_2 within the upper ice column (10 - 30 cm) was up to an order of magnitude higher than atmospheric pCO_2, and remained higher than atmospheric values until at least JD154-156 (Figure 4-6a).

4.5 Discussion

Our observations over the winter-spring transition illustrate the influence of sea ice on the seasonal air-sea CO_2 exchange during this dynamic season. High brine pCO_2 at the beginning of the sampling program in early spring appeared to be associated with relatively small CO_2 efflux from the ice. As warming progressed, the gradual decrease in brine pCO_2 over the sampling period culminated with uptake of CO_2 into the melting ice, when brine was undersaturated with respect to the atmosphere (Figure 4-4 and Figure 4-6). The decrease in pCO_2 throughout the sea ice column must be associated with processes that influence TA and/or TIC in the brine, or processes which act directly on CO_2 itself (Figure 4-8a). These processes include biological production of organic C, CO_2 degassing, brine dilution, and calcium carbonate ($CaCO_3$)

precipitation. In the discussion below, we examine the relative importance of these various processes, by assessing the changes in carbonate system parameters and other biogeochemical tracers.

Based on our observations of TIC and TA, the sea ice column can be divided into three distinct biogeochemical "zones", where different processes appeared to affect the carbonate system over the time series. The bottom ice (120 - 140 cm) and the ice-water interface make up the first biogeochemical zone. While the dilution of brine TA and TIC with freshwater ice melt is apparent in bulk ice samples from the majority of the ice column (10 - 110 cm; Figure 4-8b), bottom ice samples deviate from this general dilution trend. Bottom ice samples fall along a line with a much reduced slope (m = 0.62; Figure 4-8b) compared to the remaining bulk ice samples (m = 1.099; Figure 4-8b). They also deviate from the dilution line of average seawater (m = 1.04), and have a corresponding non-zero intercept (b = 199.9 ± 20.1 μmol kg^{-1}; r^2 = 0.96). The deviation of bottom ice samples from the freshwater dilution line is further highlighted when bulk ice TA and TIC values are normalized to average seawater, S = 32.5 (black x's, Figure 4-8c); suggesting that inorganic carbon in the bottom ice is influenced by different processes, in addition to melt dilution.

The middle ice column (50 - 110 cm) makes up the second biogeochemical zone. Here, dilution of TA and TIC was more or less conservative as sea ice T increased and S decreased (Figure 4-8b and Figure 4-8d). Linear regression lines drawn through brine and bulk sea ice data points approach the origin (intercepts of -7.9 ± 10.7 μmol kg^{-1} and 116.2 ± 61.0 μmol kg^{-1} for bulk ice and sackhole brine, respectively, Figure 4-8b,d), indicating the dominant influence of freshwater

dilution. Lastly, the upper ice (10 - 30 cm) and ice-atmosphere interface make up the third biogeochemical zone. Stable oxygen isotope values in this layer suggest either faster sea ice growth (isotopic fractionation between seawater and forming ice is reduced at higher sea ice growth rates; Toyota et al., 2013) or the influence of snow meltwater penetration (e.g., Nomura et al., 2010a), distinguishing it from the ice column below (Figure 4-3; upper ice is isotopically light). Therefore, in the following discussion, we subdivide sea ice between the ice-atmosphere interface and upper ice (10 - 30 cm), the mid-ice column (50 -110 cm), and bottom ice (120 - 140 cm) to distinguish the different processes that affect the carbonate system in these three zones.

4.5.1 Bottom Ice and Ice-Water Interface

Samples collected from the bottom 20 cm of the sea ice were characterized by low pCO_2 values (Figure 4-4g), that were under-saturated with respect to the atmosphere and the seawater on all sampling days after the first measurements on 8 May (JD128; Figure 4-9). These data suggest that $CaCO_3$ dissolution and/or organic matter formation dominantly influenced pCO_2 in this layer (Figure 4-8a). Neither CO_2 degassing nor mixing with seawater could have accounted for these low values since seawater pCO_2 was higher than that in the bottom ice. Degassing would require the opposite gradient for diffusion toward the seawater, and mixing with seawater would have increased pCO_2 in the ice. Low pCO_2 in the bottom 20 cm of the ice corresponds well with low sTIC and high chlorophyll *a* until June 2nd (JD = 153; Figure 4-9), when bottom ice algae appeared to slough off into water column (Mundy et al., 2014). Photosynthetic activity was limited to the bottom 10 cm of the ice (Virginie Galindo, *personal communication*), likely due in part to high measured brine salinity in the mid-ice column (> 50 in all 60 and 90 cm sackholes; Arrigo and Sullivan, 1992), and reduced access to nutrient replenishment (e.g., Kennedy et al.,

2002). Even though surface water pCO_2 was generally in equilibrium with atmospheric values, bottom ice pCO_2 dropped precipitously as chl *a* increased at the beginning of our study (Figure 4-9). This evidence suggests the bottom ice algal community significantly drew down TIC within the bottom ice, but not enough to measurably deplete the underlying water column. We thus conclude that biological activity plays a dominant role in driving bottom ice pCO_2 distributions, as observed in previous studies (e.g., Delille et al., 2007; Geilfus et al., 2012; Gleitz et al., 1995; Munro et al., 2010; Papadimitriou et al., 2012).

4.5.2 Middle Ice Column (50 - 110 cm)

The distinct biological signal of non-conservative CO_2 drawdown was effectively restricted to the bottom ice (bottom 20 cm). Similarly, the potential influence of snow melt dilution or faster sea ice formation rate was restricted to within, at most, the upper 30 - 50 cm of the ice column. In between these two boundaries, the middle ice column (50 - 110 cm) experienced a dramatic decrease in pCO_2 as the ice warmed and melted (Figure 4-4g,h,i). The following section is devoted to understanding the change in pCO_2 within the middle ice column over the time series.

4.5.2.1 TA and TIC in the Middle Ice Column

4.5.2.1.1 Effect of Freshwater Dilution on Sackhole Brine TA and TIC

Sackhole brine TA and TIC measured in samples from the middle ice column indicate that freshwater dilution can explain a large portion of the decrease in these two parameters as the ice warmed (Figure 4-8d). Normalizing TA and TIC to constant salinity removes the freshwater dilution influence, but the normalized brine values still follow a quasi-linear trend (circles, Figure 4-8c). This remaining covariation in the salinity-normalized values indicates that other

processes have contributed to a change in both sTA and sTIC over the time series. In-situ processes, such as $CaCO_3$ dissolution and seawater mixing, would contribute sTA and sTIC to brine in a predictable manner. $CaCO_3$ dissolution would add TA:TIC to the brine in a 2:1 ratio (equation 4), whereas mixing with under-ice surface seawater (S = 32.5) would dilute brine along a mixing line with a slope of 0.78 (using a brine end member defined by the S = 95 sample; Figure 4-10a).

$$CaCO_3 + CO_2 + H_2O = Ca^{2+} + 2HCO_3^- \quad (4)$$

The slope of the brine sTA vs. sTIC relationship in Figure 4-8c (dashed line) is 1.03, only slightly lower than under ice surface seawater sTA:sTIC of 1.045; this suggests a combination of $CaCO_3$ dissolution and seawater mixing may have contributed to increasing brine sTA and sTIC, even as ice melt diluted TA and TIC more-or-less conservatively.

Geilfus et al. (2012) likewise observed a strong correlation between brine sTA and sDIC ($r^2 > 0.999$), but with a slope much lower than the underlying seawater (0.89 versus 1.049). They attributed this deviation to a combination of $CaCO_3$ precipitation and CO_2 degassing removing both TA and DIC from brine solution. An sTA:sDIC slope of 1:1 would indicate that CO_2 was lost from brine (taken up into brine) in mol:mol ratios as $CaCO_3$ precipitated from (dissolved into) solution. Geilfus et al.'s (2010) observations of a slope < 1 suggest that further CO_2 degassing occurred in addition to CO_2 loss associated with $CaCO_3$ formation. The brine sTA:sTIC slope between 1 and 2 observed in this study suggests that $CaCO_3$ dissolution + CO_2

uptake (equation 4) was instead combined in variable proportions with mixing of under-ice surface seawater.

4.5.2.1.2 Effect of Seawater Mixing and $CaCO_3$ Dissolution on Sackhole Brine sTA and sTIC

To clarify the following discussion, we use the term "seawater mixing" to generalize the process of seawater flushing of sea ice and concomitant brine drainage. As sea ice warms, permeability increases, permitting increased flushing of the more permeable ice with seawater from below (Zhou et al., 2013). Brine drainage and seawater flushing are considered coordinated processes in the warming sea ice, as brine draining from more permeable ice results in a return-flow of seawater into the ice, contributing to brine dilution (Vancoppenolle et al., 2010; Zhou et al., 2013).

If seawater mixing were solely responsible for quasi-linear trend of sackhole brine samples in Figure 4-8c, we would expect brine sTIC and sTA to approach seawater values along a mixing line between two end members: early-season saline brine and seawater. We can use the most saline sackhole brine sample (S = 95, JD134, 60cm) and average seawater (S = 32.5) as end members to define such a mixing line (Figure 4-10a, slope = 0.781). In contrast, $CaCO_3$ dissolution would produce a 2:1 slope in the sTIC vs. sTA relationship, according to equation 4 (Figure 4-8a). The combination of these two processes in variable proportions, however, would produce a slope between 0.781 and 2, as observed in our data set (Figure 4-8c). We use this section to attempt to establish the relative importance of seawater mixing and $CaCO_3$ dissolution to sTA and sTIC in sackhole brine samples.

To consider the variable impact of (1) seawater mixing and (2) $CaCO_3$ dissolution on sTIC and sTA measured in each brine sample we first determine the equation of a line with a 2:1 slope that connects each data point with the seawater mixing line (Figure 4-10a) using equation (5):

$$m_1 x + b_1 = m_2 x + b_2 \qquad (5)$$

here the subscript (1) refers to the slope and intercept for the seawater mixing line (0.781 and 563, respectively), and (2) refers to the slope and intercept of the 2:1 line for $CaCO_3$ dissolution. For the latter, the slope is 2 and the intercept is dictated by the sample. The difference in sTA and sTIC between the brine end member value and the intersection point of each sample on the seawater line represents the increase in sTA and sTIC resulting from seawater mixing (Figure 4-10a). The difference between the intersection point on the seawater line for each sample and the measured sample value represents the increase in sTA and sTIC due to carbonate dissolution (grey dashed line, Figure 4-10a). The results of this calculation are presented in Figure 4-10b and Figure 4-10c.

These calculations indicate that seawater mixing and $CaCO_3$ dissolution add roughly equal amounts of sTA to sackhole brines as salinity is diluted over our time series (Figure 4-10b). In contrast, seawater mixing contributes more sTIC than $CaCO_3$ dissolution (Figure 4-10c). The sTA and sTIC contributions associated with $CaCO_3$ dissolution become quantitatively more important with the dilution of brine salinity (as salinity is diluted, contributions of sTA and sTIC increase).

Our analyses suggest that $CaCO_3$ dissolution within melting sea ice could have contributed as much as 250 μmol kg^{-1} TA to early spring brines (Figure 4-10b). To put this value in context with other studies, Rysgaard et al. (2013) found average concentrations of 100 - 900 μmol kg^{-1} of $CaCO_3$ (as ikaite) in winter sea ice in Greenland, with $CaCO_3$ concentrations highest in the upper ice column. Their study illustrated that $CaCO_3$ in the upper ice accounted for the majority of bulk ice TA, whereas this proportion decreased towards the ice-water interface where more TA was found in solution. In contrast, an early spring study by Nomura et al. (2013) found $CaCO_3$ precipitates in only ≈ 30% of their sea ice, snow, and slush samples, amounting for between 27 to 54 μmol L^{-1} of the bulk melt. As the dissolution of 1 μmol kg^{-1} $CaCO_3$ would contribute 2 μmol kg^{-1} of TA to solution, our calculated ΔTA from $CaCO_3$ dissolution falls between these two studies (Figure 4-10b).

4.5.2.1.3 Effect of Seawater Mixing and $CaCO_3$ Dissolution on Sackhole Brine pCO_2

Even though seawater mixing and $CaCO_3$ dissolution were found to contribute a similar amount of sTA to brine solution (Figure 4-10b,c), the difference in the TA:TIC ratio of the inorganic carbon these two processes add will result in a differential impact on sackhole brine pCO_2. By adding the ΔsTA (and ΔsTIC) values determined in Figure 4-10b (and Figure 4-10c) to TA (and TIC) predicted from freshwater dilution of brine alone, we can estimate the change in sackhole brine pCO_2 associated with these two processes. Figure 4-10d illustrates the change in pCO_2 from the initial sackhole brine end member (S = 95) associated with freshwater dilution (black dashed line), seawater mixing + freshwater dilution (dashed-dotted line), or $CaCO_3$ dissolution + freshwater dilution (grey dotted line). From these calculations, sackhole brine pCO_2 can be

almost entirely attributed to freshwater dilution alone, as seawater mixing and $CaCO_3$ dissolution effectively cancel each other out at S < 80 (Figure 4-10d).

From this analysis we conclude that the influences of seawater mixing and $CaCO_3$ dissolution on sackhole brine sTA and sTIC are negated when their impact on pCO_2 is considered, and as such, freshwater dilution is the primary factor controlling pCO_2 in our sackhole brine samples. Sackhole brine pCO_2 was always lower than that measured in the peepers and bulk ice over the time series (Figure 4-4g,h,i), however, and may not adequately represent pCO_2 within the majority of the sea ice column. Although sackhole brine collection methods and sample handling practices attempted to limit exposure of samples to the atmosphere, off-gassing of such high pCO_2 brines as they were being collected potentially explains some of the discrepancy between peeper and sackhole measurements (Figure 4-4h,i).

On the other hand, all three methods of pCO_2 determination within the ice are associated with their own uncertainly, adding caveats to any direct comparison. For instance, sackhole samples are composed of brine collected over an unknown volume of sea ice, and represent at best an averaged value for the ice column, and at worst a value heavily biased toward the most permeable (warmest) layers of the ice, with a major influence from underlying seawater. Although discrete sea ice core samples can be tied with more certainty to a specific region of the ice column, analytical error associated with the measurement of TIC and TA in melt samples, combined with sample handling unknowns (e.g., CO_2 loss with air space before melts are sub-sampled, section 4.2.2), are compounded when TIC and TA values are scaled to brine S, which can be as much as 6 to 25 times that of measured bulk melt. In addition, $CaCO_3$ dissolution

during ice melt will add TA and TIC to solution in a 2:1 ratio, underestimating calculated pCO_2 at brine S. Direct in situ measurement of brine pCO_2 with the peepers ameliorates many of these issues; however, the process of installing the peepers by rapidly freezing them into an intact ice column also adds uncertainty that pCO_2 values are truly representative of the remaining pack. In spite of these caveats, all three observational methods illustrated a significant decrease in pCO_2 within the sea ice over the course of the sampling program (Figure 4-4g,h,i). The remainder of this section will use pCO_2 observations from in situ peeper samplers to determine if, like sackhole brines, freshwater dilution was the dominant process driving the dramatic pCO_2 decrease in peeper measurements in the middle ice column over our time series.

4.5.2.2 pCO_2 in the Middle Ice Column

4.5.2.2.1 Effect of Freshwater Dilution

Holding T constant, a decrease in brine S by freshwater dilution will increase CO_2 solubility by reducing the concentration of ions in solution and by shifting the carbonate equilibrium towards bicarbonate [HCO_3^-] and carbonate [CO_3^{2-}] ions, thus reducing pCO_2 (Zeebe and Wolf-Gladrow, 2001). As observed for sackhole brine samples (section 4.5.2.1.3), this process alone should explain the drop in pCO_2 measured by the in situ peepers as sea ice temperatures increased over the course of the sampling season (Figure 4-4i). Peeper observations were well correlated with T, which controls CO_2 solubility and ice permeability (Petrich and Eicken, 2010; Figure 4-11). Below the seawater freezing point (≈ -1.8 °C) CO_2 solubility in brine decreases as T drops and S increases. This occurs because the salting-out effect overrides the solubility increase with decreasing T, facilitating rapid CO_2 super-saturation within sea-ice brine (Papadimitriou et al., 2004). Delille (2006) observed a similar inverse correlation between brine pCO_2 and T in spring

Antarctic sea ice, suggesting that large decreases in brine pCO_2 in spring are driven by dilution of brine as ice melts.

We calculated the theoretical brine pCO_2 that would result from direct dilution of brine inorganic carbon with warming/freshening in a closed system (Figure 4-11). To determine a starting point for brine pCO_2 (red diamond, Figure 4-11) we chose a representative early season peeper measurement (pCO_2 = 1207 μatm, T = -4.45 °C, depth = 60 cm, JD = 139) and corresponding sackhole brine sample (S = 82, T = -4.83 °C, depth = 60cm, JD = 137) over a similar depth interval and ice temperature. We used equation 1 to calculate the S_b of the peeper sample and corrected the sackhole brine S_b and TA to this value. Even though we expect sackhole brine samples may have lost some CO_2 to the atmosphere during collection and handling (section 4.5.2.1.3), sackhole brine TA will not be affected by off-gassing and should therefore be representative of brine TA within the ice column. A brine TIC value was then calculated using peeper pCO_2 and sackhole brine TA using CO2sys (section 4.3.2). Calculated TIC and measured sackhole TA define our starting brine pCO_2 value, at peeper S and T (red diamond, Figure 4-11). The freshwater dilution line (dashed line, Figure 4-11) was then determined by diluting S, TA, and TIC conservatively to the new S_b value associated with T (equation 1).

This start value selection is nontrivial and the slope of the derived freshwater dilution line is extremely sensitive to this value. Great care was taken to derive a starting value most representative of observations from the early sampling period to model the evolution of pCO_2 with warming. Choosing a start value based on bulk ice TIC and TA measurements would have biased the model as solid $CaCO_3$ contained in the ice sample would dissolve during melt and

contribute to artificially reducing calculated pCO_2 compared to in situ conditions. Similarly, the use of the corresponding brine TIC value would have underestimated the pCO_2 change with dilution if CO_2 loss had occurred during sample collection. Calculated pCO_2 values are both sensitive to physical conditions (T,S) and directly dependant on inorganic carbon concentrations in solution, meaning that the early season peeper pCO_2 value, on its own, could not be used to determine the model. Therefore it was determined that this combination of sackhole brine measured TA and in situ peeper pCO_2 produced a start value that most closely represented early season observations and could then be used to model the impact of freshwater dilution with warming.

A similar comparison was carried out by Geilfus et al. (2012) modeling the impact of freshwater dilution on the relationship between equilibrator measured pCO_2 and T within sackhole brine. Instead of choosing an early season start value, their freshwater dilution curve was based on the average brine sTA and sTIC taken from all samples with S < 80. Geilfus et al. (2012) observed much greater variability in measured brine pCO_2 values (for example, from 750 - 1800 μatm at ≈ - 10 °C; their figure 9), likely due to carrying out measurements directly within sackholes after brine had accumulated (see caveats as noted above). This large spread in brine pCO_2 even at low ice T complicates the determination of the start value for the freshwater dilution line, making the choice of an average brine value most appropriate. In our study, choosing an average brine value would have heavily biased the dilution model towards later season samples and to processes such as seawater mixing that become much more important as ice permeability increases with warming (note: this is also likely an issue for Geilfus et al., as 36 % of their brine samples are at T > freezing point, suggesting a direct influence of seawater). Bearing this in mind, we feel that

the start value for our freshwater dilution model is the most appropriate characterization of observations from this study. However, we openly acknowledge that this model is highly sensitive to this start value, and that the conclusions drawn from it may change if different start values were used.

Our calculations suggest that melt dilution of brine alone would reduce brine pCO_2 following a predictable trajectory over the melt season (dashed line, Figure 4-11). However, this theoretical line predicts higher pCO_2 than we observed in most of our samples. As with sackhole brine samples (section 4.5.2.1.3), we can investigate the impact of seawater mixing and $CaCO_3$ dissolution on brine pCO_2 measured by the peepers.

4.5.2.2.2 Effect of $CaCO_3$ Dissolution and Seawater Mixing

As observed with sackhole brine pCO_2, mixing the brine end member (red diamond, Figure 4-11) with seawater serves to increase pCO_2 above the expected freshwater dilution line (grey solid line vs. dashed line). Thus we conclude that seawater mixing is not an important process contributing to the pCO_2 drop within the middle-ice column (50 - 100cm), but that it contributes to increase pCO_2 in the warmest, most permeable parts of the ice. On the other hand, $CaCO_3$ dissolution can be invoked on its own to explain the entire depression of pCO_2 values below the freshwater dilution line in Figure 4-11. For example, the 273 μatm pCO_2 offset between the freshwater dilution line and peeper measurements at the same temperature (green squares, Figure 4-11) can be accounted for by an addition of 521.5 μmol kg^{-1} TA (and 250.75 μmol kg^{-1} TIC) to brine solution associated with the in situ dissolution of $CaCO_3$. Not only does this indicate that $CaCO_3$ dissolution exerts a measureable influence on brine pCO_2 within the middle ice column,

but that this influence increases as temperature increases (or as salinity drops; e.g., measured values drop further away from freshwater dilution line in Figure 4-11). A similar relationship was observed within sackhole brine samples, where an increase in the contribution of sTIC from $CaCO_3$ dissolution was associated with decreasing brine salinity (Figure 4-10c). We thus conclude that a combination of freshwater brine dilution and $CaCO_3$ re-dissolution can largely explain the T-dependent changes in pCO_2 observed in the middle ice column.

4.5.2.3 Impacts of $CaCO_3$ Dissolution and Seawater Mixing on δ^{13}C-TIC

We conclude this section with a short discussion on the relationship between the dominant controls on sea ice pCO_2 and their impact on the observed increase in δ^{13}C-TIC within the middle ice column over the time series (Figure 4-4f). Stable isotope data from bulk ice and sackhole brine samples in the interior ice column corroborate the conclusions reached above. Brine samples from 60 and 90 cm showed ^{13}C enrichment over the course of the sampling program (Figure 4-4f), as sTA and sTIC increased (Figure 4-4d,e), and S decreased with warming ice T. This is consistent with $CaCO_3$ carbonate dissolution, which would enrich brine solution as isotopically heavy $CaCO_3$ is re-dissolved. On the other hand, bulk ice melt samples showed a weaker trend in ^{13}C enrichment (Figure 4-4c) and smaller increase in sTA, but a decrease in sTIC (Figure 4-4a). Bulk ice δ^{13}C-TIC samples reflect TIC within trapped brine and any carbonate salts within the ice, whereas sackhole brine δ^{13}C-TIC measurements should reflect dissolved inorganic carbon in the brine only. Since all carbonate present in the sample dissolves during the melting of ice for bulk ice measurements, the increase in bulk ice δ^{13}C cannot be due to higher carbonate dissolution, as in the sackhole brine. One possible explanation of this sTIC loss from bulk ice and smaller increase in δ^{13}C is brine drainage of isotopically light brine from

the mid-ice near the end of the sampling period when the sea ice was more porous. Degassing of isotopically light CO_2 would also show a similar trend, but this mechanism is not supported by our flux data (see below).

In a completely closed system, isotope effects associated with CO_2 degassing and $CaCO_3$ precipitation are negated once the backward reaction takes place upon re-dissolution. If the products of precipitation are separated after formation, as may be the case in open or semi-closed natural systems, the backward reaction of $CaCO_3$ dissolution will lead to brine solutions with isotopically heavy TIC. Direct CO_2 out-gassing, on the other hand, would remove isotopically light-CO_2 from brine solution without a change in sTA. The coupled increase in brine sTIC and isotopic ^{13}C-enrichment with warming and dilution (Figure 4-4d,f), precludes a major influence from biological assemblages in the mid-ice column. Photosynthetic DIC uptake would result in sTIC decrease and isotopic ^{13}C-enrichment, whereas heterotrophic remineralization of organic C would produce isotopically light DIC, reflecting the remineralization of isotopically light POC or DOC. The positive correlation between isotopic enrichment and the increase in sTIC and sTA with warming (Table 4-4) implies that $CaCO_3$ dissolution into brine solution was a significant contributor to the brine isotopic signature as previously observed by other studies (Papadimitriou et al., 2004).

4.5.3 Upper Ice

As with the mid-ice column (50 - 110 cm), freshwater dilution was the most important process controlling TIC and TA concentrations in the upper ice (10 - 30 cm; Figure 4-8b). Brine pCO_2 in the upper ice was significantly higher than atmospheric values until at least JD 153 (2 June;

Figure 4-6a). Over this same period, we measured a small CO_2 efflux from both the snow and ice surfaces (Figure 4-6b and Figure 4-6c). In contrast, we observed CO_2 uptake into the ice later in the season, at a time when we measured no flux across the snow surface. This implies that upward diffusivity of CO_2 in ice was low, and that processes in the snow impeded the transport and exchange of CO_2. High brine volume fractions (almost always > 5 %; Figure 4-7), warm ice temperatures (> - 5 °C after JD 136; Figure 4-2c), and high sackhole brine volume recovery (holes filled quickly with high salinity liquid) indicate that the sea ice was highly permeable throughout our study. This further suggests that the sea ice should have been a source of CO_2 to the atmosphere over this entire period, as brine pCO_2 was persistently oversaturated with respect to the atmosphere (Figure 4-4g,h,i).

In a highly permeable ice pack, the pCO_2 difference between sea ice brine and the overlying air has been cited as the main driver of air-sea ice CO_2 flux (Delille, 2006; Geilfus et al., 2012; Nomura et al., 2006). We measured a small positive CO_2 flux from the sea ice towards the atmosphere at the beginning of our time series (Figure 4-6c), which may be explained by the strong pCO_2 gradient between brine in the upper 30 cm of ice and the atmosphere (Table 4-5). Using calculated brine volume, the ideal gas law, and the brine-atmosphere pCO_2 gradient (Table 4-5), we can calculate the number of moles of CO_2 that would need to be lost from brine in the upper ice (0.3 m^3) to reach equilibrium with the atmosphere. On JD144, for example, 0.9 mmol of CO_2 would be lost to the atmosphere if the pCO_2 gradient between brine in the upper ice and the atmosphere were diminished to zero (i.e., brine pCO_2 = atmospheric pCO_2). The CO_2 flux measured between the ice and the atmosphere on JD144 (0.026 μmol m^{-2} s^{-1}) can be used to estimate the time required for the brine to equilibrate with the atmosphere. For these calculations,

the brine volume was determined by multiplying Vb/V by the 100 cm x 100 cm x 30 cm volume of ice (Table 4-5). We approximate a loss of 2.2 mmol CO_2 per m^2 per day from the upper ice, indicating that the ice-atmosphere pCO_2 gradient would be completely eroded in less than half a day (9.5 hrs), if not otherwise impeded.

Bulk ice samples collected from the upper 10 - 30 cm three and six days later (JD147 and 150) yielded average supersaturated brine pCO_2 values of 810 μatm and 1215 μatm, respectively (Figure 4-6a). This high super-saturation suggests either efflux from the ice to the atmosphere was restricted or that significant CO_2 production occurred in situ. Measured flux from the overlying snow on JD144 was likewise positive and accounted for almost 70 % of the flux from the upper ice (0.016 μmol m^{-2} s^{-1}; Figure 4-6b). To account for this efflux, while brine pCO_2 remained high, requires that CO_2 be produced at a similar rate.

Other early melt season studies have suggested that the snow pack itself can act as both as source of CO_2 and a barrier to CO_2 flux (Delille, 2006; Nomura et al., 2010b; Papakyriakou and Miller, 2011). Papakyriakou and Miller (2011) suggested that increased CO_2 uptake during periods of atmospheric warming could be caused by rapid heating of the brine-wetted snow base, dissolving $CaCO_3$ and taking up CO_2. Warming-cooling (promoting $CaCO_3$ dissolution and precipitation at the brine wetted snow base) and snow ventilation cycles (promoting CO_2 flux) could have contributed to the highly variable snow CO_2 flux measurements measured during the early part of our study (Figure 4-6b). This may also explain how CO_2 efflux could be measured from the snow surface while the flux from the ice surface was impeded (brine pCO_2 remains high).

Production of CO_2 within the upper ice during this period of warming is unlikely, especially as $CaCO_3$ dissolution would have contributed to CO_2 drawdown, not release (section 4.5.2).

Another possible explanation for the highly variable CO_2 flux at the snow surface may be the accuracy of the measurements themselves, as the flux chamber system may be unable to adequately resolve such small changes in CO_2. Although we do not have an appropriate determination of the error associated with the flux determination, over the 10 - 20 minute interval of each chamber measurement the instrument routinely recorded ΔpCO_2 of < 1 µatm. For example, a measurement of flux at the snow surface had an initial pCO_2 measurement of 393.4 µatm (to start flux evaluation at T_0) and a final measurement, 15 minutes later, of 394.3 µatm. At 1.5 % analytical error, this yields a $\Delta pCO_2 \approx 1 \pm 8$ µatm. As well, the ΔpCO_2 measured at the snow surface was routinely ≈ 25 % of that measured over the ice surface. This suggests that the flux chamber system may not be able to adequately measure the fluxes associated with the snow surface.

As air T increased, brine volume (and permeability) increased in the upper ice, meaning bulk CO_2 diffusion would have to have been completely blocked on JD 150 to account for the absence of an observable flux, despite the strong pCO_2 gradient (Table 4-5). Although we removed the snow before measuring the ice-air fluxes, refreezing of snow melt water within the surface ice may have blocked gas exchange. Likewise, refreezing of melt water and the formation of ice lenses within the snow pack can impede exchange between the snow and the atmosphere (Nomura et al., 2010b; Zemmelink et al., 2006). Ice lenses within the snow pack were not

observed at our field site until after JD 158, around the date when the snow surface began showing a consistently negligible CO_2 flux (Figure 4-6b).

After JD 150, the CO_2 sink into the snow-free sea ice surface strengthened (Figure 4-6c), whereas fluxes at the snow surface averaged around zero (Figure 4-6b). On our final time point in Table 4-5 (JD160), CO_2 uptake was measured at the ice surface (Figure 4-6c, Table 4-5), as pCO_2 in the upper ice became undersaturated with respect to the atmosphere (Figure 4-6a). This marked the transition from early season efflux to CO_2 uptake by the melting ice surface as warming advanced. Other studies have observed a similar transition between efflux and uptake over the spring season. Similarly, they attributed increased CO_2 absorption to snow melt dilution of the ice surface and the associated reduction in ice pCO_2 associated with internal ice melt (Delille, 2006; Geilfus et al., 2012; Nomura et al., 2010a; Zemmelink et al., 2006).

As snow and internal ice melt began to dilute the ice surface with warming (Figure 4-2d), CO_2 uptake increased (Figure 4-6c). The transition to a completely isothermal ice column after JD155 (Figure 4-2c) was accompanied by undersaturation of pCO_2 within the reminder of the ice column (Figure 4-4g,h,i). This transition toward pCO_2 under-saturation over the entire ice column would contribute to a weak CO_2 sink as melt advances, marking the end of the early melt period.

4.6 Conclusions

Observations over a six week time series of land-fast sea ice in Resolute Passage captured an important early melt period during the winter-spring transition. We observed a spatial and temporal segregation between the dominant processes controlling CO_2 within the ice over this period, distinguishing the bottom ice, middle ice column, and the ice-atmosphere interface into separate biogeochemical zones. Our time series illustrated that pCO_2 within the ice was strongly controlled by physical processes associated with warming. Sea ice melt dilution exerted a strong influence on pCO_2 within the majority of the ice column, except in the bottom ice, where biological DIC uptake maintained undersaturated pCO_2 conditions throughout the time series. Once the influence of melt dilution was accounted for, both $CaCO_3$ dissolution and seawater mixing were found to contribute sTA and sTIC to sackhole collected brines within the middle ice column. The effects of these sTA and sTIC contributions were canceled out, however, when sackhole brine pCO_2 was considered, indicating that freshwater dilution was the main factor determining pCO_2 within sackhole collected brines. In situ peeper observations likewise indicated that pCO_2 within the middle ice column was dominantly controlled by freshwater dilution. In contrast to sackhole brine samples, however, in situ pCO_2 measurements indicated that $CaCO_3$ dissolution contributed to a measurable reduction in brine pCO_2 over the early spring period. Gas fluxes at the ice surface in the early season suggest ice could act as a source for CO_2 to the atmosphere when brine pCO_2 is above atmospheric saturation. However, CO_2 diffusion appeared to be effectively impeded, enabling the persistence of a strong gradient favouring efflux. These observations suggest that the majority of the large pCO_2 reservoir retained in sea ice over winter is merely stored until freshwater dilution occurs again in spring. Aside from CO_2 drawdown by photosynthetic algae in the bottom 2 - 10 cm of ice, brine pCO_2 in the majority of

the ice column is controlled by solubility. This leaves the only net change in inorganic carbon inventory over the winter-spring transition associated with a small uptake of CO_2 due to $CaCO_3$ dissolution, likely balancing CO_2 loss during $CaCO_3$ formation in early winter.

Observations during this field study reveal a surprisingly dynamic carbon system within the sea ice, even before the snow had melted from the ice surface. Spatial segregation of abiotic and biotic processes during the early melt period create a heterogeneous, transitional environment in which the lower portion of the ice column can become sufficiently permeable and illuminated to support rapidly growing autotrophic communities, while the upper portion of the ice remains dominated by the physical constraints characterizing the late winter sea-ice system. Reduction of snow cover and the transition to a completely isothermal ice column mark the end of the early melt period and leave the ice column preconditioned towards pCO_2 under-saturation, contributing to a weak CO_2 sink as melt advances.

4.7 Tables

Table 4-1. Arctic-ICE 2010 sampling program

Sample Collection	Sampling Period
Ice Cores, Sackhole Brine, and Under-Ice Surface Seawater	May 7 - June 9 (JD 127 - 160)
Snow Properties	May 11 - June 10 (JD 131 - 161)
Peeper in situ pCO_2	May 11 - June 16 (JD 131 - 167)
Chamber CO_2-Fluxes	May 24 - June 19 (JD 144 - 170)

Table 4-2. Pooled standard deviation, Sp[a], of duplicate analyses for geochemical parameters

Parameter	Units	Under-Ice Surface Water		Bulk Ice		Sackhole Brine	
		Sp	**k**	***Sp***	**k**	***Sp***	**k**
S (probe)		0.2[b]	40	-[c]	-	-[c]	-
TIC	μmol kg^{-1}	4.42	10	0.26	3	18.19	25
TA	μmol kg^{-1}	3.72	9	4.81	32	4.56	23
δ^{13}C-TIC	‰ vpdb	0.14[d]	51	-[e]	-	0.10	44
$\delta^{18}O$-H_2O	‰ vsmow	0.03	3	0.03	4	-[f]	-

[a] IUPAC (1997); where k is the number of measurement pairs.
[b] maximum error on corrected probe salinity was observed to be ± 0.2; 92 % of corrected values fell within ± 0.1
[c] Salinity in bulk ice and sackhole brine samples was measured in single samples only, so Sp could not be determined.
[d] Sp for water δ^{13}C-TIC samples taken from a larger pooled data set including the 11 under-ice surface water samples from this study.
[e] Limitations on sample volume meant there were no true duplicate bulk ice δ^{13}C-TIC samples, we expect a similar analytical precision as for seawater and brine.
[f] Measurements of $\delta^{18}O$-H_2O are not reported for brine.

Table 4-3. Time series and property/property changes in bulk ice geochemical parameters. Correlations in columns 3 to 8 represent the change in each measured parameter per day within each interval of the ice column. The final table column (9) presents the bulk ice stable isotope composition change per μmol kg^{-1} change in sTIC.

Bulk Ice		T (°C / day)	S[a] (/ day)	Brine Vol. ([Vb/V] / day)	sTIC (μmol kg^{-1} / day)	sTA (μmol kg^{-1} / day)	δ^{13}C-TIC (‰ / day)	δ^{13}C-TIC (‰ / sTIC)
10 - 30 cm	Slope	0.119	-0.04	0.0012	-4.60	-2.65	0.04	-0.003
	r^2	0.93	0.33	0.59	0.18	0.07	0.55	0.24
50 - 70 cm	Slope	0.075	-0.02	0.0014	-2.06	1.75	0.03	-0.004
	r^2	0.95	0.05	0.55	0.08	0.11	0.43	0.35
90 - 110 cm	Slope	0.043	-0.02	0.0012	-6.42	-0.03	0.06	-0.007
	r^2	0.79	0.08	0.33	0.48	0.00	0.54	0.71
Bottom 20 cm	Slope	0.010	-0.05	-0.0008	-15.65	-4.38	0.01	-0.001
	r^2	0.16	0.43	0.08	0.39	0.14	0.00	0.09

[a] Bulk Ice S is reported on the Practical Salinity Scale 1978 (PSS78) without units.

Table 4-4. Time series and property/property changes in sackhole brine geochemical parameters. Correlations in columns 3 to 6 represent the change in each measured parameter per day. The final three table columns (7, 8, and 9) present brine stable isotope composition change per change in brine S, per μmol kg^{-1} change in sTIC, and per μmol kg^{-1} change in sTA.

BRINE		S[a] (/ day)	sTIC (μmol kg^{-1} / day)	sTA (μmol kg^{-1} / day)	δ^{13}C-TIC (‰ / day)	δ^{13}C-TIC (‰ / S)	δ^{13}C-TIC (‰ / sTIC)	δ^{13}C-TIC (‰ / sTA)
60 cm	Slope	-1.90	14.01	16.23	0.03	-0.02	0.001	0.002
	r^2	0.72	0.26	0.31	0.86	0.76	0.21	0.38
90 cm	Slope	-1.16	5.43	7.88	0.04	-0.03	0.003	0.004
	r^2	0.99	0.62	0.85	0.84	0.81	0.30	0.56
130 cm	Slope	-1.14	-3.28	-1.57	0.02	0.01	-0.005	-0.002
	r^2	0.56	0.22	0.06	0.09	0.09	0.40	0.05

[a] Brine S is reported on the Practical Salinity Scale 1978 (PSS78) without units.

Table 4-5. Estimate of the equilibration time between brine *p*CO2 in the upper ice (10 - 30 cm) and the atmosphere given the measured flux at the ice surface.

JD	T (°C)	S	Atmo pCO_2 (μatm)	Brine pCO_2 (μatm)[a]	Average V_b/V	Brine Volume[b] (L)	Δ CO_2 [Ice - Air][c] (μmol)	Measured CO_2 Flux [Ice - Air] [d] (μmol m^{-2} s^{-1})	Hours to Equilibrate pCO_2[e]
144	-4.1	70.8	385.4	1571	0.055	16.4	882	0.026	9.5
150	-3.9	67	384.2	1215.3	0.057	17.0	630	0.000	-
160	-2.2	38.6	380	303.5	0.089	26.8	-91	-0.031	0.8

[a] Brine pCO_2 calculated from Bulk Ice melt TIC and TA

[b] Calculated brine volume in 0.3 m vertical x 1m x 1m horizontal plane

[c] Number of moles of CO_2 lost/gained by brine volume upon equilibration with the atmosphere (i.e., brine pCO_2 = atmospheric pCO_2)

[d] Measured flux from the ice to the atmosphere

[e] Hours to reach equilibration between brine pCO_2 and atmospheric pCO_2 over 0.3 m x 1 m x 1m ice

4.8 Figures

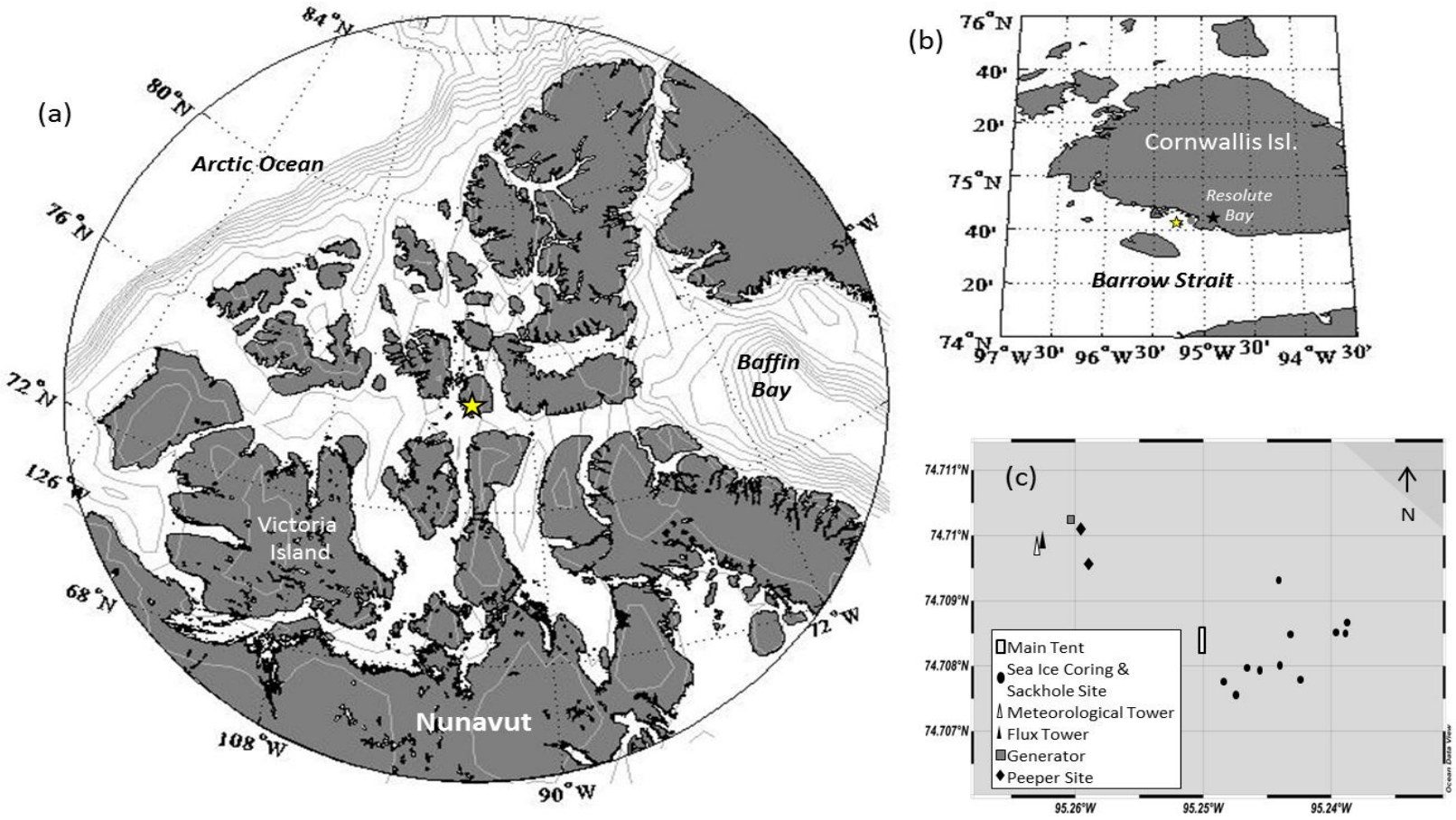

Figure 4-1. Map of Field Study location. Clockwise from left: (a) Canadian Arctic Archipelago, yellow star indicates location of Resolute Passage ice camp site (74.708°N 95.250°W); (b inset) zoom in of Cornwallis Island, study site (yellow star) and town of Resolute Bay, NU (black star); (c) Field camp layout.

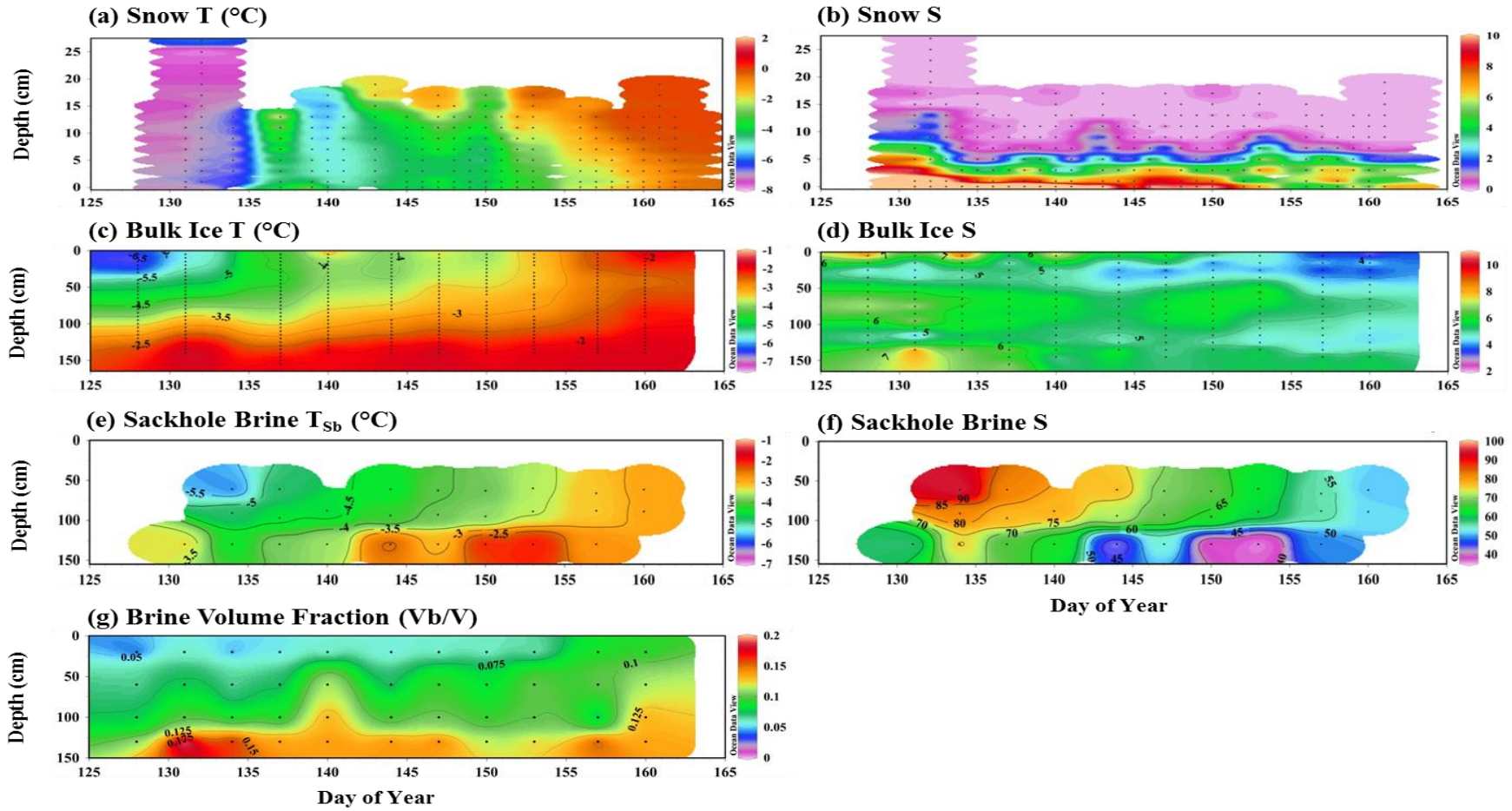

Figure 4-2. Six-week time series of physical conditions in the snow and sea ice. (a) Snow Temperature (°C); (b) Snow Salinity; (c) Bulk Ice Temperature (°C); (d) Bulk Ice Salinity; (e) Sackhole Brine Temperature (°C); (f) Sackhole Brine Salinity; (g) Brine Volume Fraction (Vb/V). Note differences in color scales for different sample types. White space on panels represents no data coverage.

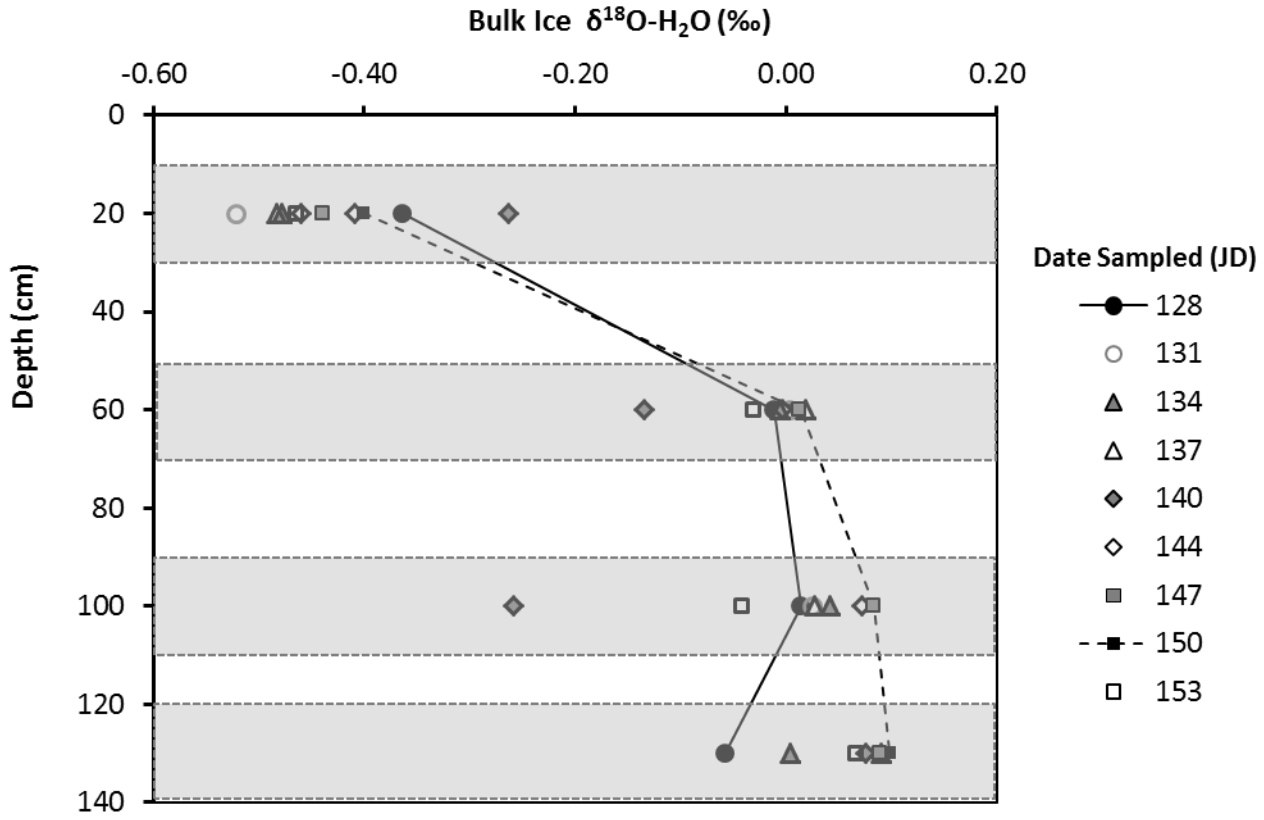

Figure 4-3. Bulk ice melt stable oxygen isotope $\delta^{18}O\text{-}H_2O$ (‰) signatures plotted by depth in the ice column and distinguished by sampling date (Julian Day, JD). Grey shading indicates depth interval of sea ice sample (20 cm). Isotopically light values in the upper ice suggest snow melt ($\delta^{18}O\text{-}H_2O$ = -20.72 ± 1.11 ‰) penetrated only as deep as the upper 30-50 cm of sea ice. Under-ice surface water $\delta^{18}O\text{-}H_2O$ (-1.83 ± 0.06 ‰) was isotopically depleted compared with the sea ice column.

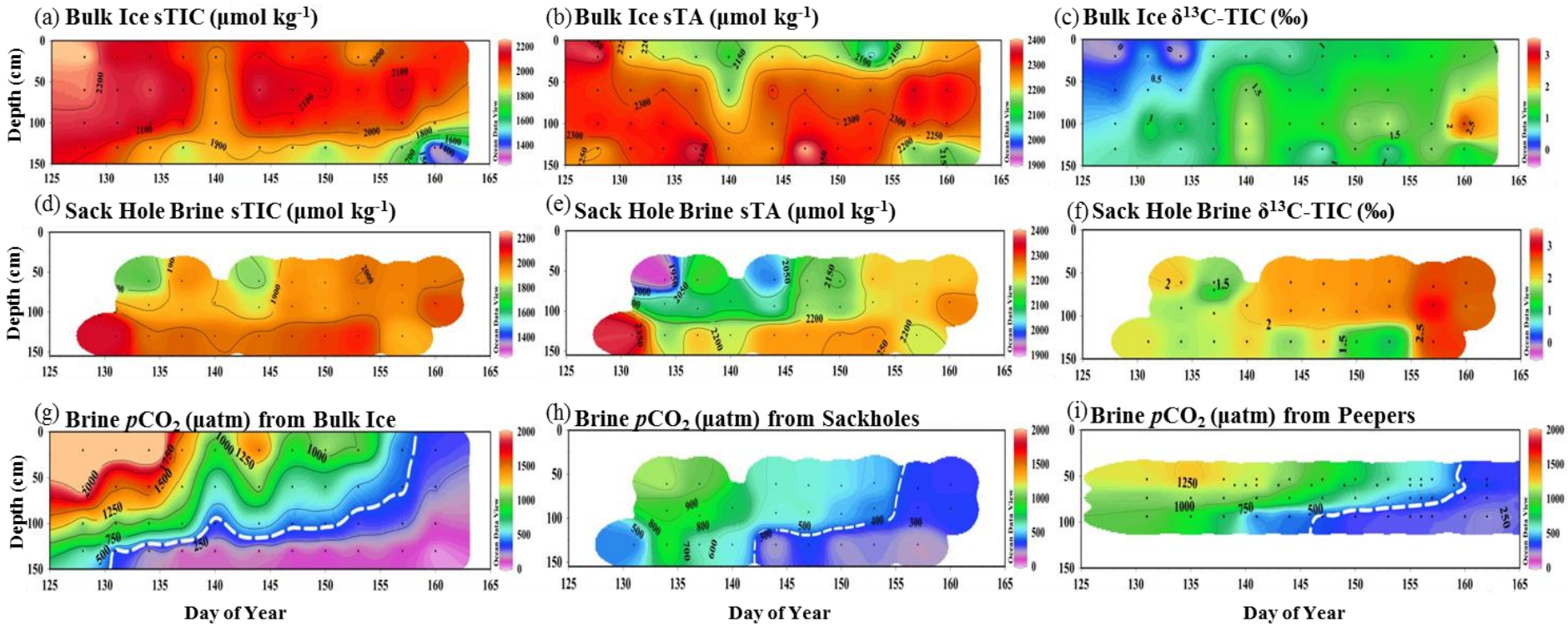

Figure 4-4. Six week time series of carbonate system parameters in sea ice and sackhole brine samples. Prefix "s" denotes TA and TIC data were normalized to a salinity of 32.5, the average S of under-ice surface seawater. (a) Bulk Ice sTIC; (b) Bulk Ice sTA; (c) Bulk Ice δ^{13}C-TIC (‰); (d) Sackhole Brine sTIC; (e) Sackhole Brine sTA; (f) Sackhole Brine δ^{13}C-TIC (‰); (g) Brine pCO_2 (µatm) as calculated from bulk ice TA and TIC; (h) Brine pCO_2 (µatm) as calculated from sackhole brine TA and TIC; (i) Brine pCO_2 (µatm) as measured from in situ peepers. White dashed lines illustrate saturation with respect to atmospheric $pCO_2 \approx 380$ µatm. White space on panels represents no data coverage.

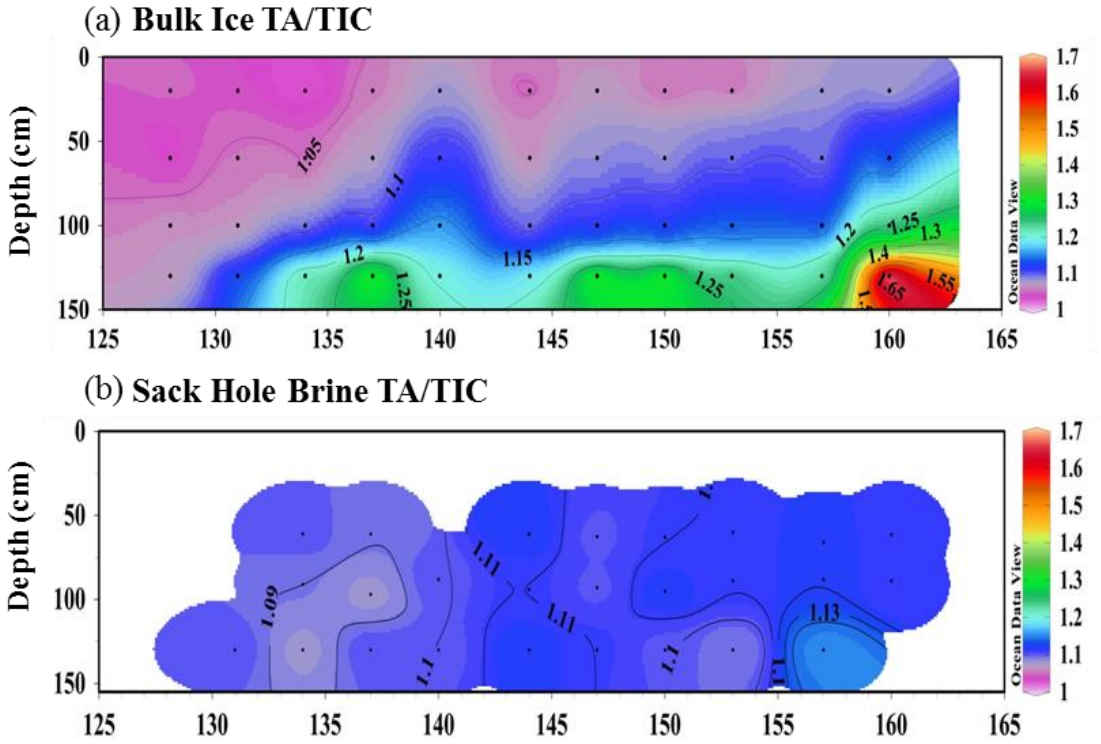

Figure 4-5. Six week time series of TA/TIC within bulk ice (a) and sackhole brine (b) samples.

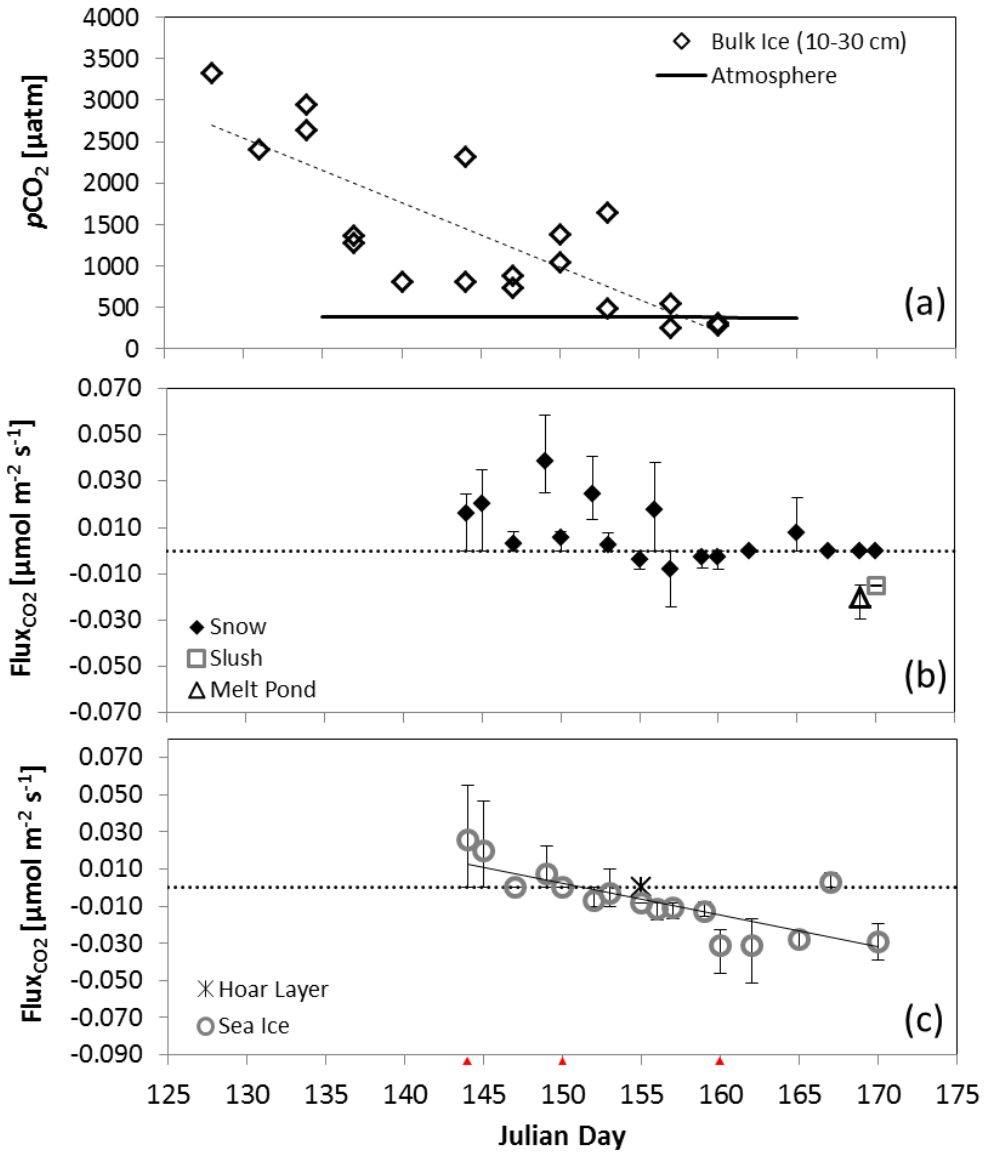

Figure 4-6. (a) Time series of upper ice pCO_2 (µatm) calculated from bulk ice melt TIC and TA (10 - 30 cm). The dashed line represents the linear trend through the data points. Atmospheric pCO_2 measured by the CACS system was ≈ 380 ppm over the study period, indicated by the solid black line; (b) Time series of CO_2 flux measurements on snow (black filled diamonds), slush (open square), and melt pond (open triangle) surfaces. The vertical bars on each data point represent the data range (maximum and minimum measurements from each day); (c) Time series of CO_2 flux measurements on sea ice (snow removed; open circles) and hoar frost layer (snow removed; star) surfaces. The solid black line illustrates the linear trend through the average sea ice data points and the vertical bars on each data point represent the data range (maximum and minimum measurements from each day). Positive fluxes are from the interface toward the atmosphere. Red triangles represent the time points chosen for calculations in Table 4-5.

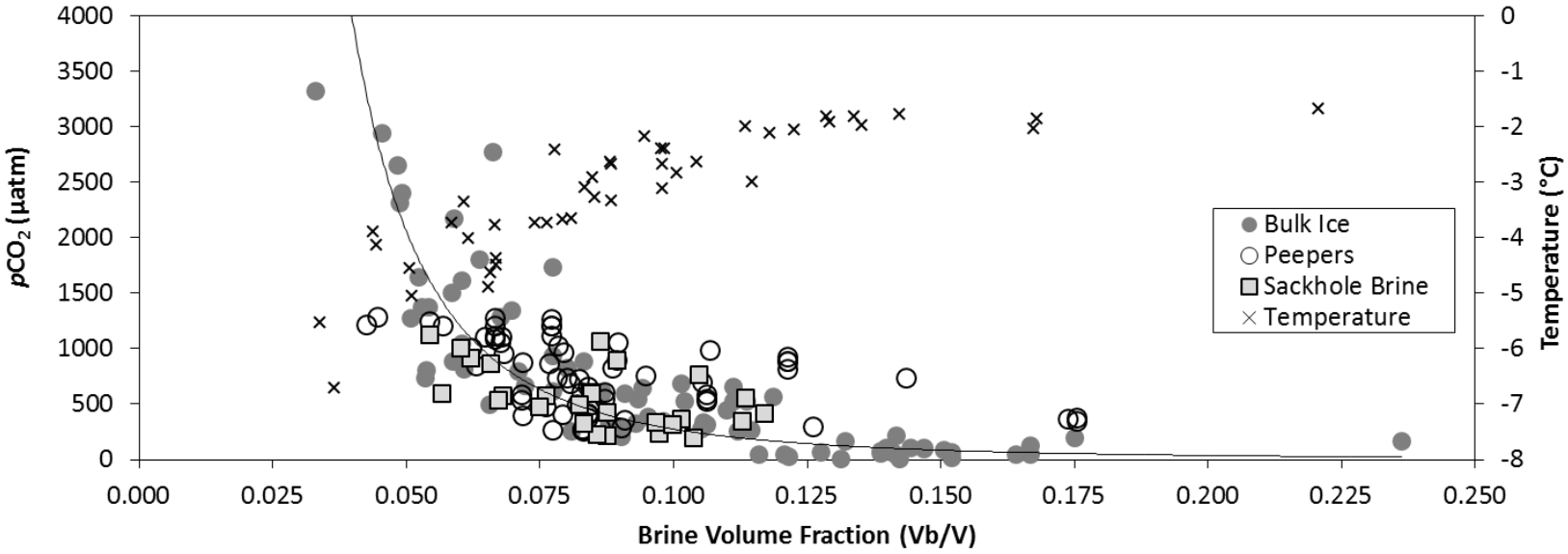

Figure 4-7. Calculated brine volume fraction (V_b/V) plotted against in situ measured pCO_2 (open circles, peepers), calculated brine pCO_2 from bulk ice and sackhole brine measurements of TA and TIC (grey filled circles and squares, respectively), and sea ice temperature (black x's). Brine pCO_2 values can be related to brine volume fraction by an exponential curve, $pCO_2 = 0.339(V_b/V)^{-2.908}$ ($r^2 = 0.65$; black line).

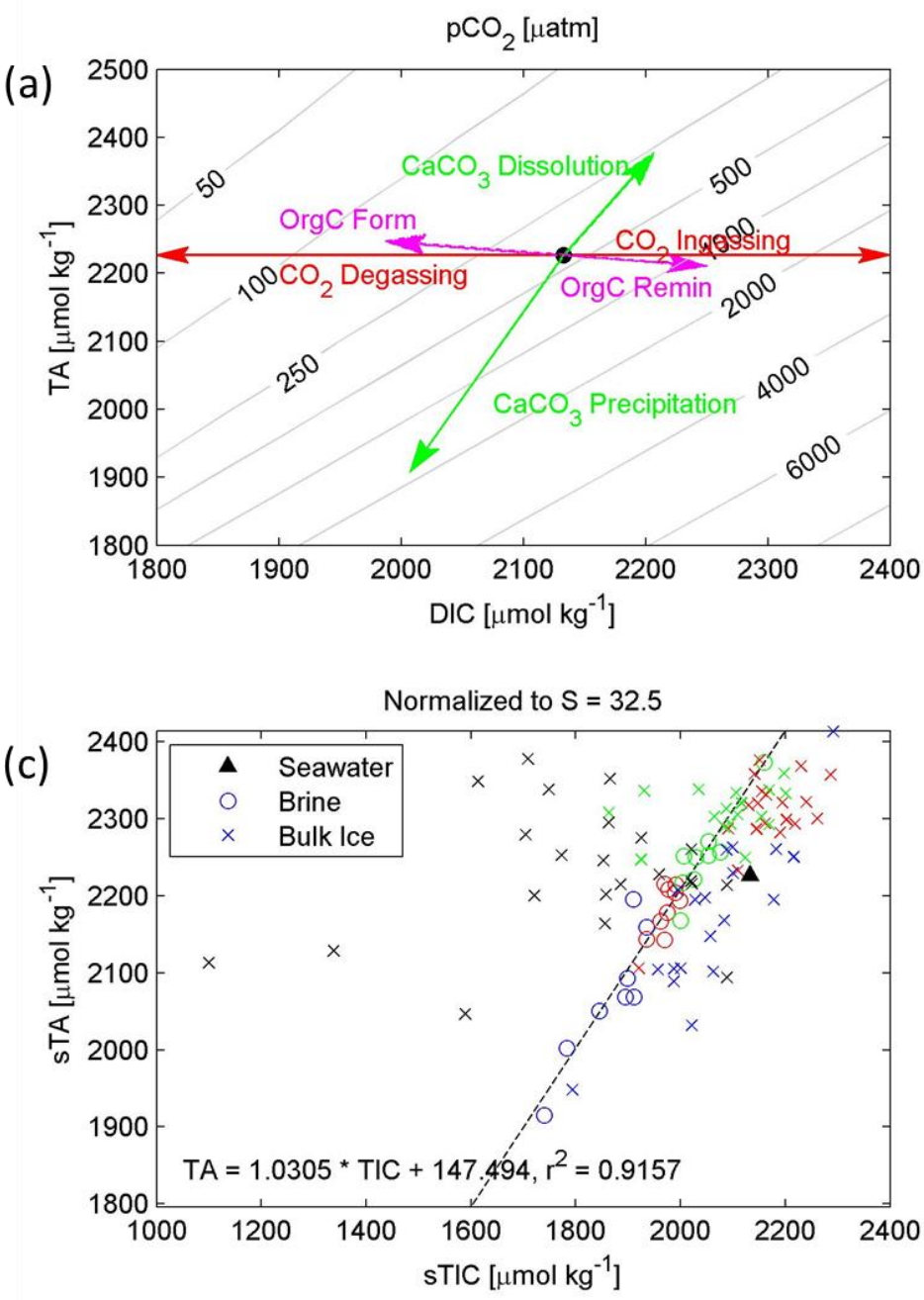

Figure 4-8. (a) Contributions of different biological (organic C formation/remineralization - magenta arrows) and geochemical ($CaCO_3$ dissolution/precipitation - green arrows; CO_2 degassing/absorption - red arrows) processes on the concentration of Dissolved Inorganic Carbon (DIC) and Total Alkalinity (TA) in a typical seawater sample (black filled circle), and their associated impact on seawater pCO_2 (grey lines); (b) Bulk ice measured TA and Total Inorganic Carbon (TIC) from four depth intervals in the ice column. Values from the upper and mid ice column (10 - 110 cm) are linearly related along the line TA = 1.099 * TIC - 7.93 (r^2 = 0.96; black dashed line), with the intercept indistinguishable from the origin (± 10.7)…*continued* →

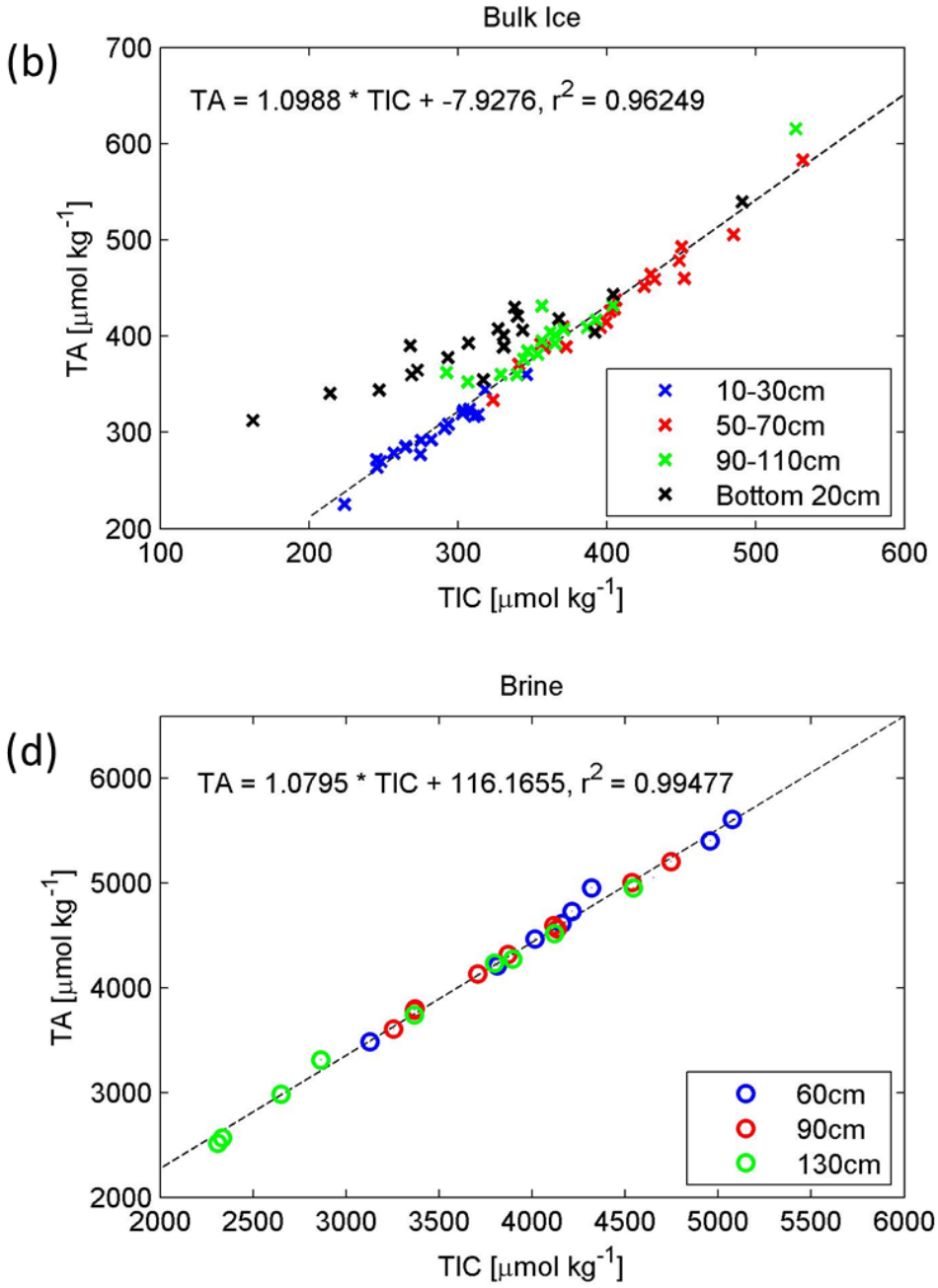

Figure 4-8 continued… Bottom ice samples (black x's) deviate from this general trend, but are also linearly related along the line, TA = 0.615 * TIC + 199.0 (r^2 = 0.85); (c) Salinity normalized TA (sTA, µmol kg^{-1}) plotted against salinity normalized TIC (sTIC, µmol kg^{-1}) for sackhole brine samples (colour coded circles), bulk ice (colour coded x's), and average under-ice surface seawater (black filled triangle). Colour coding in panel (c) follows that in (b) for bulk ice and (d) for brine. Values are normalized to the average under-ice surface seawater salinity of 32.5; (d) Sackhole brine measured TA and TIC. Values fall along a tight regression line (r^2 = 0.995) described by, TA = 1.080 * TIC + 116.17 (black dashed line), with the intercept close to the origin (± 61.0).

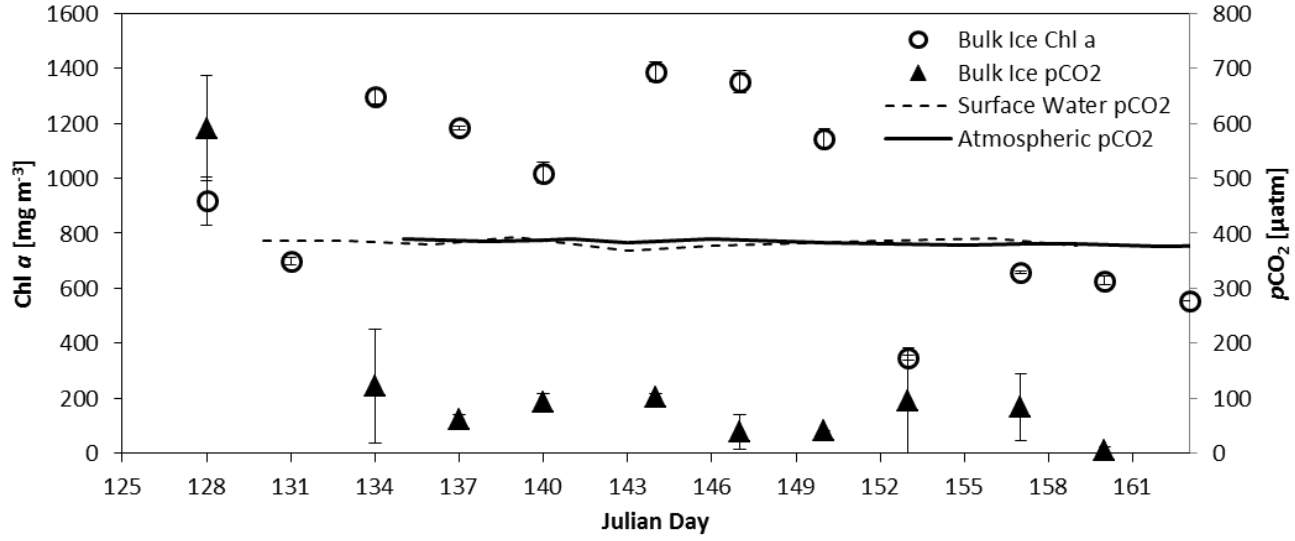

Figure 4-9. Chlorophyll *a* (mg m^{-3}) in the bottom 3 cm of sea ice and pCO_2 (µatm) in the bottom 20 cm of sea ice plotted against date sampled (Julian Day). Chlorophyll *a* from the bottom 3 cm was used because it accounted for > 98 % of the measured chlorophyll *a* throughout the entire ice column (Virginie Galindo, *Personal Communication*). Bottom ice pCO_2 was calculated from measured values of bulk ice TA and TIC. The black solid line indicates CACS measured atmospheric pCO_2 and the black dashed line illustrates pCO_2 values determined from TIC and TA samples collected at the ice-water interface.

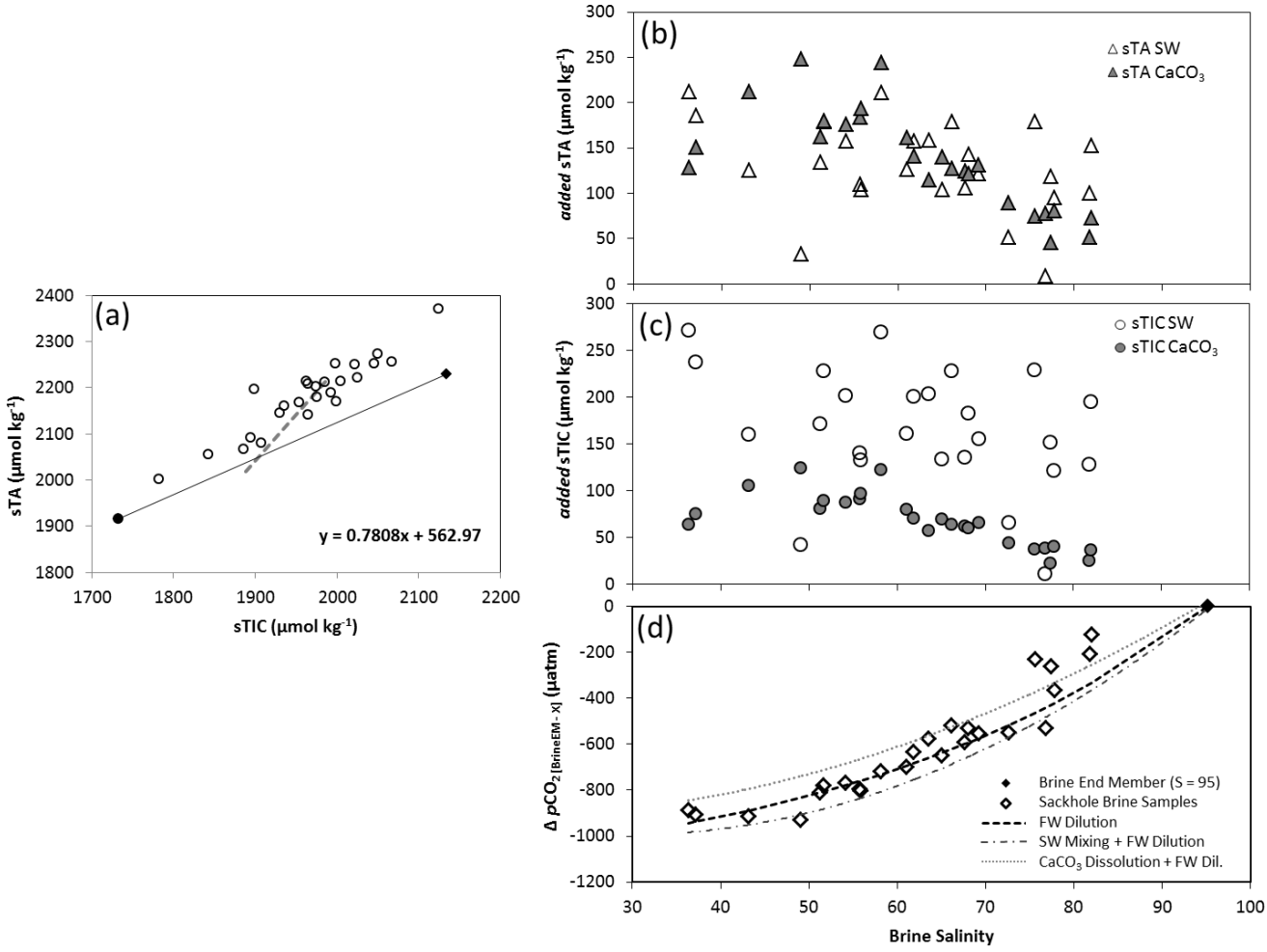

Figure 4-10. Contributions of seawater mixing and $CaCO_3$ dissolution to sackhole brine sTA, sTIC, and pCO_2 change over the time series. Prefix "s" denotes TA and TIC values are normalized to the average under-ice surface seawater salinity of 32.5 (a) Sackhole brine sTA verses sTIC (open circles) compared to the mixing line (black line; slope = 0.780) between the most saline brine value end member (black filled circle) and seawater (black filled diamond), and the 2:1 TA:TIC addition from $CaCO_3$ dissolution (grey dashed line); (b) sTA added by either seawater mixing (open triangles) or $CaCO_3$ dissolution (grey filled triangles) as a function of brine salinity; (c) as in (b), sTIC added from either seawater mixing (open circles, X_1) or $CaCO_3$ dissolution (grey filled circles, X_2), as a function of brine salinity; (d) the calculated difference ($\Delta pCO_{2[\text{Brine End Member - X}]}$) between pCO_2 in the sackhole brine end member (S = 95; black diamond) and that calculated from freshwater Dilution (black dashed line, X_1), seawater mixing + freshwater dilution (grey dashed-dotted line, X_2) or $CaCO_3$ dissolution + freshwater dilution (grey dotted line, X_3), plotted as a function of brine salinity.

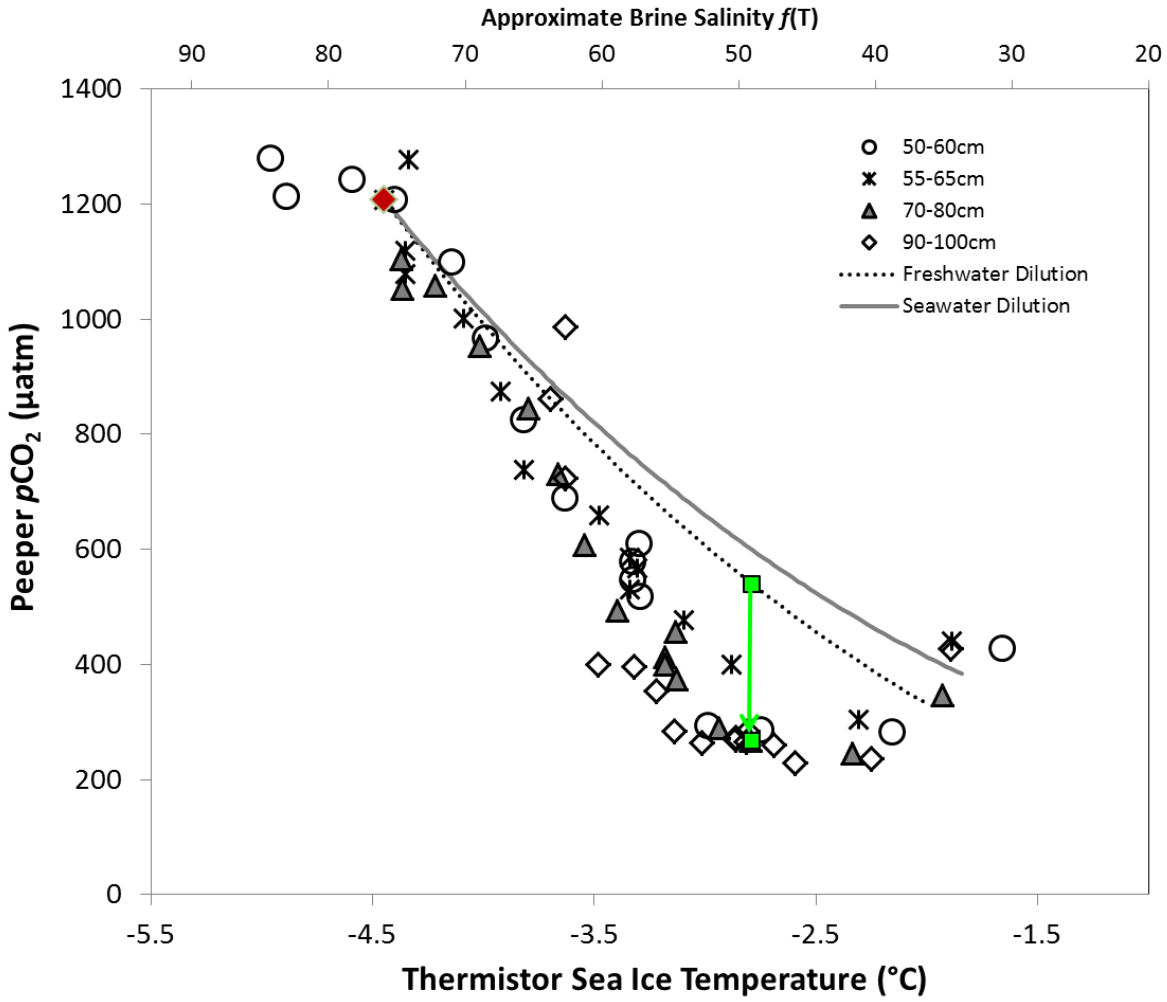

Figure 4-11. Sea ice pCO_2 measured with in situ peeper samplers versus thermistor-recorded, in situ sea ice temperature from various depths in the mid-ice column (50 - 100 cm). Brine salinity, calculated from thermistor temperature (equation 1), is listed as an alternate X axis. The pCO_2 change associated with ice melt (freshwater) dilution alone is approximated by calculating brine TIC from an early season peeper measurement (pCO_2 = 1207 µatm; T = -4.45 °C; Depth = 60 cm) and sackhole brine sample (Depth = 61 cm; TA = 5005 µmol kg^{-1} ; S_b = 75.96) (red diamond). The TA and TIC of this start value (red diamond) was then diluted as a function of S and pCO_2 values recalculated according to the change in brine salinity with increasing T (black dashed line). Seawater dilution was determined by mixing the start value (red diamond) with amounts of average under-ice seawater (S = 32.5; TA = 2230 µmol kg^{-1}; TIC = 2134 µmol kg^{-1}) and recalculating pCO_2 (grey line). Peeper observations that deviate from the expected freshwater-dilution trajectory can be explained by dissolution of $CaCO_3$ depressing brine pCO_2 (green arrow; see text for details).

Chapter 5: Over-Determination of the Carbonate System in Natural Sea Ice Brine and Assessment of Carbonic Acid Dissociation Constants Under Low Temperature, High Salinity Conditions

By over-determining the carbonate system in natural sea ice brine samples, we have confirmed that stoichiometric equilibrium constants for the dissociation of carbonic acid in seawater (K_1^*, K_2^*) derived for general oceanic conditions may not be readily extrapolated to sea ice brine systems. Dissolved inorganic carbon, total alkalinity, pH, and pCO_2 measurements in sea ice brine have allowed us to rigorously examine the validity of K_1^* and K_2^* at salinities as high as 82 and in-situ temperatures as low as - 4.8 °C. The use of seawater-derived constants yields average offsets between calculated and measured values ranging from 10 % to 43 % for brine salinities of 38 to 82. Future high accuracy determination of sea ice brine carbonate system components will require the specific determination of carbonate system equilibrium constants under appropriate temperature and salinity conditions. Furthermore, the community is in need of a means to evaluate the accuracy of carbonate system measurements in natural, high salinity brine samples using the presently available analytical methods.

5.1 Introduction

The polar oceans play a pivotal role in the global carbon cycle as sites of significant deep water formation and atmospheric CO_2 sequestration. Recent reduced summer sea ice extent and polar warming have stimulated increased effort to understand the role of sea ice in the transfer of carbon between the atmosphere and the ocean (e.g., Barber et al., 2012; Loose et al., 2011;

Parmentier et al., 2013; Rysgaard et al., 2011). High-salinity brine contained within the sea ice matrix is of particular interest in the polar carbon cycle, as the brine acts as both a seasonal repository of inorganic carbon (e.g., Delille et al., 2007; Geilfus et al., 2012; Miller et al., 2011a, 2011b; Papadimitriou et al., 2012) and as an important ecological province conducive to high primary productivity (e.g., Arrigo et al., 2010; Boetius et al., 2013; Kirst and Wiench, 1995; Niemi et al., 2011; Welch and Bergmann, 1989). Furthermore, export of high salinity brine into the underlying surface waters can transport dissolved inorganic carbon from sea ice into, and below, the mixed layer (e.g., Miller et al., 2011b; Omar et al., 2005; Rysgaard et al., 2011, 2009, 2007), potentially contributing to the sequestration of carbon on timescales longer than the seasonal cycle of sea ice formation-growth-melt.

Understanding the role of sea ice in the polar ocean carbon cycle depends on an accurate characterization of the thermodynamic equilibria which govern the inorganic carbon system in sea ice. In ice free, open ocean systems, the thermodynamic equations governing inorganic carbon speciation have been studied extensively (see Millero, 1995 and Millero et al., 2006, 2002, for comprehensive reviews), resulting in robust equations to calculate the first and second dissociation constants of carbonic acid (K_1 and K_2, respectively) over the relatively narrow range of oceanographic temperature and salinity conditions. Empirically derived stoichiometric equilibrium constants (K_1*, K_2*) describe the system as a function of oceanic salinity, temperature, and pressure (as in equations 1 and 2, where brackets refer to total stoichiometric concentrations in mol kg^{-1} of seawater). These constants represent the equilibrium concentrations of dissolved CO_2 (CO_2 = CO_2(aq) + H_2CO_3), bicarbonate (HCO_3^-), and carbonate (CO_3^{2-}), according to their equilibrium speciation in the ocean (equation 3).

$$K_1^* = \frac{[HCO_3^-][H^+]}{[CO_2]} \quad (1)$$

$$K_2^* = \frac{[CO_3^{2-}][H^+]}{[HCO_3^-]} \quad (2)$$

$$CO_2 + H_2O \xleftrightarrow{K_1} HCO_3^- + H^+ \xleftrightarrow{K_2} CO_3^{2-} + 2H^+ \quad (3)$$

In contrast to the large body of carbonate system data in seawater, relatively few published studies have successfully collected and analyzed brine carbonate system samples from the field (Delille et al., 2007; Fransson et al., 2011; Geilfus et al., 2012; Gleitz et al., 1995; Miller et al., 2011a; Nomura et al., 2013b, 2010b; Papadimitriou et al., 2012, 2007). Standard operating procedures for carbonate system measurements developed for open ocean and estuarine conditions (such as Dickson et al., 2007) are often impractical in the polar regions, as freezing conditions and difficult access to sampling sites complicate routine sampling and analyses (e.g., Loose et al., 2011; Miller et al., 2011a, 2011b). Moreover, inconsistency between pH measurement methods (e.g., spectrophotometric vs. potentiometric) and scales (e.g., pH_F, Miller et al., 2011a; pH_T, Delille et al., 2007; pH_{SWS}, Gleitz et al., 1995) are particularly problematic in sea ice brine. As a result of these limitations, only a handful of studies have presented field measurements of two or more components of the sea ice brine carbonate system (Table 5-1).

Beyond the difficulty associated with actual measurements of carbonate system parameters in sea ice brine, there is a fundamental lack of information on the thermodynamic constants governing

the equilibrium among different carbonate species in these environments. Rigorous determination of K_1* and K_2* in natural and artificial seawater has only been carried out at temperatures above -1 °C and salinities less than 50 (Table 5-2), conditions at the warm, fresh extreme of sea ice brine systems (Petrich and Eicken, 2010). Straightforward extrapolation to high S, low T conditions found in natural sea ice brine is tenuous given the non-linear nature of the governing equations. Even so, the difficulty in accurately measuring brine carbonate system components in the field (particularly pH and pCO_2) has led investigators in sea ice environments to generously apply these constants outside of their experimental ranges (e.g., see discussions in Delille et al., 2007, and Miller et al., 2011a). Furthermore, validation of these extrapolations has been elusive, as few studies in the literature have reported independent measurement of a third component of the carbonate system in sea ice brine (Delille et al., 2007; Geilfus et al., 2012; Miller et al., 2011a;Table 5-1). With appropriate equilibrium constants, the full carbonate system can be resolved from measurements of any two parameters. As a result, the measurement of a third parameter provides an 'over-determination' which can be used to directly validate computed values against measurements. Such an over-determination is critical to evaluate the robustness of extrapolated carbonate system equilibrium constants to sea ice brine systems.

Our goal with this study was to over-determine the carbonate system in natural sea ice brine samples and address the question of how applicable seawater-derived carbonic acid dissociation constants are to sea ice brine. We collected brine samples from sackholes in spring sea ice during two field campaigns in the Canadian Arctic Archipelago, during the spring seasons of 2010 (Resolute Passage) and 2011 (Allan Bay), and analyzed the samples for DIC, TA, pCO_2, and pH. With these results we determined the utility of seawater carbonic acid dissociation constant

parameterizations for reproducing the measured values using CO2SYS XLS v. 2.1 (Pierrot et al., 2006). Our findings indicate that agreement between measured and calculated parameters can be poor, and that a more rigorous, laboratory-based study to define the carbonic acid dissociation constants (K_1^*, K_2^*) at low T and high S is warranted.

5.2 Methods

Sackhole brine samples were collected over two spring seasons as part of the Arctic-ICE (Arctic - Ice Covered Ecosystem) program, based out of the Polar Continental Shelf Program (PCSP) in Resolute Bay, Nunavut, Canada. The 2010 program was from May 8th to June 19th in land-fast, first year sea ice in Resolute Passage (74.708 N, 95.250 W), whereas the 2011 program was from April 16th to July 9th, under similar land-fast sea ice conditions in Allan Bay (74.716 N, 95.15 W). In both years, brine samples were collected from smooth, land-fast, first-year sea ice with a relatively uniform thickness of 140 ± 2 cm and 144 ± 7 cm in 2010 and 2011, respectively. Sampling was conducted in the early spring season, when warm air temperatures (-7.6 ± 3.1 °C and - 2.5 ± 2.5 °C, for the 2010 and 2011 sampling dates, respectively, listed in Table 5-3; Environment Canada, 2013) had begun to melt the surface snow pack (16 ± 11 cm and 16 ± 4 cm over the 2010 and 2011 sampling dates, respectively).

5.2.1 Brine Sampling and Physical Description

Sea ice brine sampling was conducted at a new, undisturbed site each sampling day, away from generators and foot traffic. Sackholes were drilled with a 10” auger to depths between 60 and 130 cm within the sea ice (Table 5-3) and sealed at the ice/snow interface with a plastic-covered,

high density foam plug to limit gas exchange. Brine was allowed to accumulate in the sackholes over the course of the coring day (~ 5-6 hrs) then collected into 10-L cubitainers (Fisher Scientific) using an aquarium pump (QuietOne 800, Lifeguard Aquatics). This allowed for the collection of a single, homogenized, large volume sample of brine from each sackhole, rather than collecting discrete samples directly into smaller sampling bottles and risking brine heterogeneity over the depth of the sackhole. Cubetainers were filled with a laminar stream to reduce bubble entrainment (any bubbles were removed before sealing) and covered in black plastic bags to limit light exposure. Cubetainers of collected brine were then transported to the PCSP laboratory, inverted gently several times to homogenize, then a spigot fitted with Tygon tubing was used to collect subsamples (see below) of the mixture for measurements of carbonate system parameters. The salinity (S) of the remaining brine was determined using a hand-held conductivity meter (WTW Cond 330i) calibrated to a 0.01 mol L^{-1} KCl standard solution. Brine samples with S values greater than the instrument measurement range (S = 0 to 70) were diluted with equal parts distilled water before measurement. Here we report brine S on the Practical Salinity Scale 1978 (PSS78), but at the precision of our measurements reported values would be the same regardless of the scale used. Although brine temperature (T) was measured within the sackholes using a digital hand-held probe, these temperature readings were influenced by exposure time of brine samples within the sackhole, and we use calculated in-situ T based on brine salinity (T_{Sb}), following Petrich and Eicken (2010). Ionic strength (I) was calculated from measured S after Dickson et al. (2007).

5.2.2 Carbonate System Analyses

5.2.2.1 Total Dissolved Inorganic Carbon (DIC)

Brine subsamples for total dissolved inorganic carbon (DIC) were collected in triplicate into 250 mL borosilicate glass reagent bottles (Pyrex), allowed to overflow 1 full volume, and the headspace was adjusted to 1 % of sample volume. Samples were preserved with 200 μL saturated $HgCl_2$ and sealed with ground-glass stoppers coated with silicon-free high vacuum grease (Apizon-M) and secured with vinyl electrical tape (3M). Samples were stored at room temperature in the PCSP laboratory until shipping south for analysis.

Brine DIC was measured coulometrically (Dickson et al., 2007) using either a VINDTA 3D (Marianda) or SOMMA system (e.g., Johnson et al., 1993). The samples collected in 2010 were analyzed six months after collection at the Institute of Ocean Sciences (IOS), Sidney, B.C., Canada, whereas samples collected in 2011 were analyzed three months following collection aboard the *CCGS Louis S. St. Laurent*. The DIC measurements were calibrated against certified reference materials (CRM 109) provided by Andrew Dickson (Scripps Institute of Oceanography). Analytical precision for our sea ice brine analyses was 2.5 μmol kg^{-1}, based on the pooled standard deviation (*S*p) of k sample sets (triplicates or quadruplicates) analyzed in each sample set (IUPAC, 1997; Table 5-4).

5.2.2.2 Total Alkalinity (TA)

During both field programs, brine Total Alkalinity (TA) was analyzed in samples collected in the same way as the DIC samples, and often the same samples were analyzed for both parameters. During the 2011 program, TA brine samples were collected in quadruplicate, with three samples

saved for analysis at IOS (as in 2010) and one sample analyzed on shore in the PCSP laboratory facility. Brine analyzed at PSCP was collected into pre-rinsed 500 mL glass bottles (Wheaton), without poisoning, and analyzed within 24 hrs of collection. Single replicate samples analyzed at PCSP were within ± 3.6 μmol kg^{-1} of triplicate analyses determined at IOS.

Brine TA was determined using an open-cell titration with an automated Dosimat 665 titrator (Metrohm) and Red Rod pH combination electrode (Radiometer Analytical). Endpoint detection was determined by a non-linear least squares fit (Dickson et al., 2007). All TA analyses were performed on the same instrument, either at PCSP immediately after collection, within three months aboard the *CCGS Louis S. St. Laurent* (2011 samples), or within six months of collection at the Institute of Ocean Sciences, Sidney, B.C., Canada (2010 samples). As with DIC, brine TA measurements were calibrated against certified reference materials (CRM 101, 109) provided by Andrew Dickson (Scripps Institute of Oceanography), with an Sp for sea ice brine samples of 4.4 μmol kg^{-1} (Table 5-4). To test whether the seawater CRMs were appropriate standards for high-salinity brine samples, several brine samples were gravimetrically diluted by a factor of 3 with DMQ water and re-titrated to examine the effects of salt content on measured TA values. The resulting values agreed within ± 2 μmol kg^{-1}, indicating that the high brine salt content did not significantly affect the TA determinations.

To test for the potential influence of Particulate Inorganic Carbon (PIC) on brine TA measurements, large volume brine samples were collected for filtration on three separate occasions in 2010. Sackholes were sampled as outlined above and extracted brines were kept cold (refrigerated at < 4°C) in the dark until sub-sampling within 24 hrs of collection.

Subsamples were collected in triplicate and filtered to remove various particle size classes (0.7 μm nominal GF/F, 0.45 μm Nuclepore cartridge, 0.22 μm durapore filter sandwich). Salinity was measured with the hand-held conductivity meter before and after filtration to confirm no loss of salts to the filtration apparatus. TA measurements were then performed on the filtered and unfiltered brine samples, following the procedure described above.

5.2.2.3 pH_F

During the 2011 field season, pH was measured spectrophotometrically on the free hydrogen ion scale (pH_F ; mol kg-SW^{-1}) using the indicator dye *m*-cresol purple (Clayton and Byrne, 1993). Following Miller et al. (2011a), we used the parameterizations of pK_a for *m*-cresol purple (*m*CP) from Millero et al. (2009) and ionic strength as in Table 5-3. As discussed in Miller et al. (2011a), the Millero et al. (2009) parameterizations result in pH values on the free hydrogen ion scale in mol kg^{-1} of pure water, which we converted to mol kg-SW^{-1} following Clayton and Byrne (1993). We found no clear trend between dye addition and pH perturbation in our samples, so we have chosen not to correct measured pH for the *m*CP added (50 μL *m*CP, pH = 7.873). However, as our method utilized a cell with a 10-cm pathlength (≈ 32 mL volume), the correction for the *m*CP addition should be much smaller than ± 0.001 (Chierici et al., 1999), well within our estimated analytical precision for sea ice brine (Table 5-4).

The majority of spectrophotometric analyses carried out in this study measured absorbance of the acid form of *m*-cresol purple ($[HI^-]$) at 430 nm instead of the standard wavelength of 434 nm. To account for the resulting small absorbance difference we have adjusted measured absorbance values by a correction factor determined from samples where absorbance was measured at both

wavelengths. Although the uncertainty added to pH_F measurements by the use of this correction was an order of magnitude lower than calculated Sp (Table 5-4), it nonetheless contributed to increased uncertainty in our analyses.

Brine pH_F was converted to in-situ values (S, T_{Sb}, P) using the average measured DIC (section 5.2.2.1) for each sample and measured pH_F in CO2Sys. We derived carbonic acid dissociation constants ($K_1^*$and K_2^*) as per Table 5-2 and used the $KHSO_4$ dissociation constants of Dickson (1990). Calculated Sp (Table 5-4) was determined after correcting measured pH_F values to in-situ conditions (S, T_{Sb}, P) using the combined equilibrium constants K_1 and K_2 determined by Hansson (1973) and Mehrbach et al. (1973) as refit by Dickson and Millero (1987).

5.2.2.4 *p*CO_2

Gas samples for *p*CO_2 determination were collected in quadruplicate in 125 mL serum bottles (Wheaton), preserved with 100 µL saturated $HgCl_2$ solution, and sealed without headspace using an aluminum crimped 20 mm chlorobutyl-isoprene stopper (Wheaton). Samples were stored at room temperature in the PCSP laboratory until shipment south, where they were stored at 4°C until analysis ~ 2 years after collection.

Brine *p*CO_2 was determined by gas chromatography-mass spectrometry (GCMS) using a static headspace equilibration (Dickson et al., 2007; Neill et al., 1997). Samples were brought to room temperature (≈ 24°C) overnight and then placed in a constant temperature bath at 25 ± 0.2 °C for 1-2 hrs before creating a 24.5 mL headspace of high purity He gas (99.999%; PRAXAIR). We used a syringe pump (Kloehn) to withdraw water while allowing He to flow into bottles at

≈ 20 ml min^{-1}. Samples equilibrated with the headspace in the shaking temperature bath for at least 1 hr before analysis. Equilibrated headspace pCO_2 was measured using a GCMS (Shimadzu QP-2010) by allowing headspace to flush and then fill a 1 ml sampling loop (Valco Instruments), which was injected onto a CarbonPlot column (Jandell Scientific), for separation by gas chromatography. The elution time of the CO_2 peak was determined using a CO_2 standard tank. We used a mass flow controller (Advanced Specialty Gas Equipment, FM4575A), to generate a series of CO_2 / He dilutions, which were used to calibrate the instrument response and derive the absolute CO_2 content (mol) of the sample loop. This in turn was used to calculate head space pCO_2 following the iterative approach of Neill et al. (1997). To derive sample pCO_2, brine DIC in the sample post-equilibration was calculated from measured headspace pCO_2 (Neill et al., 1997) and then used to determine "calculated" TA (cTA) under analysis conditions (S, T, P) using CO2Sys. Brine pCO_2 in the original sample (pre-equilibration) at in-situ T_{Sb} was then calculated using the average measured DIC (section 5.2.2.1) for each sample and derived cTA, again in CO2Sys. We have chosen to report measured CO_2 values as partial pressure (pCO_2) rather than fugacity (fCO_2), because the determination of pCO_2 relies on fewer assumptions and our results were less precise than those of Neill et al. (1997).

As with pH_F, analytical precision (Sp) for brine pCO_2 was determined with measured pCO_2 values corrected to in-situ T_{Sb}, S, and P in CO2Sys using average measured DIC and the combined equilibrium constants $K_1$and K_2 determined by Hansson (1973) and Mehrbach et al. (1973) as refit by Dickson and Millero (1987).

We evaluated the accuracy of our GCMS pCO_2 measurements with analyses of certified seawater reference material (CRM 101) provided by Andrew Dickson (Scripps Institute of Oceanography) following the same headspace equilibration method, which gave an average pCO_2 for the CRM samples of 572 ± 16 µatm (n = 8), compared with a value of 569 µatm calculated from the certified DIC and TA values using CO2Sys, with equilibrium constants $K_1$and K_2 determined by Mehrbach et al. (1973) and refit by Dickson and Millero (1987). This close agreement validates the accuracy of our measurement approach.

5.2.3 Evaluation of Seawater Derived Carbonic Acid Dissociation Constants (K_1^*, K_2^*) Applied to the Carbonate System in Natural Sea Ice Brine

We chose to compare four of the more commonly used sets of stoichiometric equilibrium constant definitions previously used in sea ice brine studies: Hansson (1973) refit by Dickson and Millero, 1987 (Hansson87); Mehrbach et al. (1973) refit by Dickson and Millero, 1987 (Mehrbach87); Goyet and Poisson, 1989 (G&P89); and Roy et al., 1993 (Roy93), as well as more recent sets reported by Mojica Prieto and Millero, 2002 (MP&M02), and Millero et al., 2006 (M06), as summarized inTable 5-2.

We applied each of these six sets of carbonic acid dissociation constants to calculate each measurable parameter of the brine carbonate system (DIC, TA, pH, pCO_2) from measured values of two parameters. Comparison of the measured and calculated values (measured - calculated) was used to evaluate the applicability of each set of constants outside its empirical S and T range.

5.3 Results

5.3.1 Removal of Particulate Material and the Determination of Brine TA

Brine TA measured in filtered and unfiltered samples is reported in Table 5-5. Brine S ranged from 58 to 79 over the three treatments. None of the filtration treatments were significantly different ($p > 0.1$) from unfiltered samples over this salinity range, and we thus conclude that particulate phases did not appreciably affect alkalinity in these samples. We assume this to be the case for all of our samples.

5.3.2 Measured versus Calculated Carbonate System Parameters in Sea Ice Brine

Table 5-6 and Figure 5-1 compare measured and calculated values for carbonate system parameters using the carbonic acid dissociation constant parameterizations fromTable 5-2. Both measured and calculated values were corrected to in-situ T_{Sb} (Table 5-3).

5.3.2.1 DIC Calculation versus Measurement

Calculated DIC (DIC_C) was generally lower than measured DIC (DIC_M) when determined from measured TA (TA_M) and either pH_F (pH_{FM}) or pCO_2 (pCO_{2M}), whereas the combination of pH_{FM} and pCO_{2M} gave calculated DIC values that were higher than the measurements (Figure 5-1; Table 5-6). Either pH_{FM} or pCO_{2M} combined with TA_M produced DIC_C values closest to DIC_M, likely due to the robustness of the TA_M values (Table 5-4). In general, the constants from Roy93, G&P89, and Hansson87 produced DIC_C values closest to DIC_M (Table 5-6), whereas the values calculated from M06 were furthest from DIC_M values (Figure 5-1). Generally DIC_C values were within 10 % of DIC_M for all combinations of measured values and stoichiometric

constant definitions, except for M06, which differed from DIC_M by an average of 25 % when pH_{FM} and pCO_{2M} were used for the calculation (Table 5-6).

5.3.2.2 TA Calculation versus Measurement

In contrast to DIC_C, calculated TA (TA_C) was generally higher than measured TA (TA_M), with the average offset almost always within 10 % of TA_M (Figure 5-1; Table 5-6). Similarly, TA_C was closest to TA_M when determined from DIC_M and either pH_{FM} or pCO_{2M}, whereas the combination of pH_{FM} and pCO_{2M} produced more widely varied results. This is likely to be at least partially attributable to the better precision of DIC analyses (Table 5-4). The Roy93, G&P89, and Hansson87 constants generally produced TA_C values closet to TA_M, while M06 TA_C values were furthest from TA_M values (Figure 5-1). The M06 constants produced TA_C values that were offset by an average of 31 % from TA_M when pH_{FM} and pCO_{2M} were used in calculations (Table 5-6).

5.3.2.3 pH_F Calculation versus Measurement

Calculated pH_F (pH_{FC}) was lower than pH_{FM} by an average of 0.06, an order of magnitude higher than the Sp of measured values (Figure 5-1; Table 5-6). Despite our relatively high confidence in DIC_M and TA_M, the discrepancy between pH_{FM} and pH_{FC} was found to be even greater when calculated using these measured values than with pCO_{2M} and either DIC_M or TA_M. In this case, the carbonic acid dissociation constant definitions of Roy 93, G&P89, and Hansson87 yielded pH_{FC} values closest to pH_{FM}. The M06 constants deviated from pH_{FC} by as much as 0.31 (Figure 5-1).

5.3.2.4 pCO_2 Calculation versus Measurement

Calculated pCO_2 (pCO_{2C}) was generally lower and within 10 % (on average) of pCO_{2M} when calculated from pH_{FM} and either TA_M or DIC_M (Figure 5-1; Table 5-6). However, when pCO_{2C} was determined using TA_M and DIC_M it deviated from pCO_{2M} to a greater degree with all sets of carbonic acid dissociation constants (Table 5-6), and by as much as 150 % using the M06 K^* parameterizations at high salinities (Figure 5-1). The constant definitions of G&P89 gave the closest agreement between pCO_{2M} and pCO_{2C} across all three combinations of measured parameters (Table 5-6).

5.4 Discussion

The goal of this study was to assess the validity of carbonic acid dissociation constants (K_1^*, K_2^*) derived from oceanic waters in high S, low T sea ice brine samples. We used sample collection techniques and analytical methods previously employed by our group in other Polar studies. Alternative methods could have been used, each with particular strengths and weaknesses, and detailed analytical inter-comparisons are required. Nonetheless, here we endeavour to address some of the questions surrounding the application of oceanic carbonic acid dissociation constants to natural sea ice brine samples. It is important to recognize that some of our specific conclusions, particularly regarding which set of constants give better agreement with specific measurements, may be dependent on the methods we used.

5.4.1 Brine Carbonate System Sampling and Analyses

While measurement precision was good for both DIC and TA, accuracy was more difficult to determine. Only TA measurements could be verified directly against seawater standards by diluting brine samples (section 5.2.2.2). Although our DIC analyses were calibrated against the same standards (section 5.2.2.1), dilution of the brine would have changed the total DIC content, due to alteration of CO_2 solubility, dilution of TA, and exposure to the atmosphere associated with extended handling. Likewise, the GCMS pCO_2 analyses were compared to CRMs, but could not be diluted to a comparable S. We propose that a high S CRM be developed by evaporating natural seawater, as outlined by Millero et al. (2006), to ensure all laboratories are able to produce accurate and precise measurements of carbonate system parameters at high S.

Sackhole brine samples analyzed in this study were collected into large volume plastic containers (8-10 L) and allowed to sit in cool conditions, shielded from light, until they were homogenized and sub-sampled. Although this method was adequate to determine carbonate system components from a homogenized sample, our analysis does not consider disequilibria or heterogeneity (including density gradients within the sea ice sackhole) occurring in situ, nor potential CO_2 losses during sampling and storage. Field studies intending to describe the natural sea ice carbonate system cannot ignore these issues, particularly with samples collected from sackholes. We recommend that sackhole brine samples be collected via syringe (Miller et al., 2011a) or peristaltic pump (Geilfus et al., 2012) and immediately sub-sampled for discrete carbonate system measurements to reduce potential CO_2 loss. Notwithstanding potential CO_2 losses during sampling and storage before sub-sampling, our brine samples can be used to

compare measured and calculated carbonate system components in an internally consistent manner.

5.4.1.1 Spectrophotometric pH_F Determination

Sea ice brine pH_F has been measured spectrophotometrically in only a few studies (Fransson et al., 2011; Hare et al., 2013; Miller et al., 2011a), and questions remain as to the application of this method to high-S brine samples. Although our measurements and those of Miller et al. (2011a) were similarly precise (Table 5-1), measurement accuracy relies heavily on the pK_a* used for the *m*-cresol purple indicator dye. We used the pK_a* determined by Millero et al. (2009) in NaCl brine at ionic strengths up to 5.5 m (S ≈ 216). Minor components of natural seawater have been shown to have little effect on carbonic acid dissociation constants (Goyet and Poisson, 1989), lending confidence to the comparison between *m*-cresol purple in NaCl brine and natural sea ice brine; however, differences between K* values in artificial versus natural seawater suggest that interactions of dissolved constituents, such as boric acid, with HCO_3^- and CO_3^{2-} may be important (Millero et al., 2002; Mojica Prieto and Millero, 2002). The uncertainty in *m*-cresol purple behaviour underscores the importance of archiving raw absorbance data obtained from spectrophotometric pH analyses so that the final pH values can be recalculated as our understanding of the indicator behaviour improves. In this study, the influence of ionic interactions present in seawater and sea-ice brines, but absent in NaCl, may have affected the accuracy of our spectrophotometric pH_F measurements, possibly explaining some of the offset between our measured and calculated values.

5.4.1.2 Determination of pCO_2 by GCMS

We measured brine pCO_2 using a headspace equilibration technique coupled with GCMS (section 5.2.2.4). Calculation of the mass balance needed to derive pCO_2 from this analysis requires knowledge of sample DIC, as well as a reliable set of carbonic acid dissociation constants. Furthermore, the correction of measured brine pCO_2 values to in-situ T also relies on DIC concentrations and carbonic acid dissociation constants. This pCO_2 method is well established for seawater applications (Dickson et al., 2007) but is problematic when determining brine pCO_2 independent of other carbonate system parameters. As discussed below (section 5.4.3), this dependence on the carbonic acid dissociation constants and other measured carbonate system parameters may be partly responsible for the lower precision of our pCO_2 measurements (Table 5-4) and larger relative discrepancy between pCO_{2M} and pCO_{2C} than was observed for DIC and TA (Table 5-6).

Direct measurements of brine pCO_2 using gas exchangers in-line with non-dispersive infrared (NDIR) detectors have been quite successful (Delille et al., 2007; Geilfus et al., 2012), yielding direct pCO_2 determination at in-situ S, T, and P. Delille et al. (2007) found that their pCO_2 values measured by in-line NDIR were within about 25 μatm of values computed from direct measurements of brine pH and TA, for pCO_2 up to nearly 150 μatm. We recommend this in-situ, infrared-based approach as a more independent method for determining sea-ice brine pCO_2.

5.4.2 Removal of Particulate Material from Sea Ice Brine and its Affect on Total Alkalinity

Calcium carbonate salts ($CaCO_3$) can precipitate within the sea ice brine channel network (e.g., Dieckmann et al., 2008; Fischer et al., 2013; Geilfus et al., 2013; Nomura et al., 2013a; Rysgaard et al., 2013). If this solid particulate inorganic carbon is mobile with the brine, its dissolution in samples during storage or titration would introduce a positive bias to measured TA values. Our results suggest that filtering to different degrees (i.e., using various pore size filters) had no consistent effect on brine TA measurements over the S range of our samples (Table 5-5). We interpret this as an indication that no appreciable $CaCO_3$ was present in our sackhole brine samples and that all contributors to TA were in the dissolved form when sampled. Although we would expect $CaCO_3$ precipitates to be present within the brine channel network early in the spring season (Fischer et al., 2013; Nomura et al., 2013a), our samples appear to reflect only the liquid fraction of the brine channel system, and any $CaCO_3$ salts were left in place as the brine drained into the sackholes.

5.4.3 Validity of Oceanic Carbonic Acid Dissociation Constants (K_1^*, K_2^*) under Low Temperature, High Salinity Conditions in Natural Sea Ice Brine

Our brine DIC and TA analyses had the best precision of the four measurable carbonate system parameters, even at brine S as high as 82. Despite high confidence in our DIC and TA measurements, calculated pH_F derived from these parameters was considerably lower than measured values, while pCO_2 was higher (Table 5-6). However when pCO_2 was calculated from pH_F measurements combined with either DIC or TA, the results were closer to GCMS measurements than when pCO_2 was calculated with DIC and TA. This was observed across all

six sets of K_1^* and K_2^* equations and suggests either that pH_F values determined in this study may have been robust enough to compensate for errors in the DIC and TA analyses, or the errors in the pH and pCO_2 analyses coincidentally counteract each other. Although brine pH_F and pCO_2 values were measured with reasonable analytical precision (Table 5-4), our present data set cannot satisfactorily verify either of these possibilities.

Carbonic acid dissociation constant definitions from Roy93 yield higher calculated pH_F than the other constant definitions, whereas M06 yield lower pH_F than the other five sets of constants. In many cases the spread between the results from using different constants increased as a function of brine salinity (for S > 60, Figure 5-1), further underscoring the need for a set of carbonic acid dissociation constants relevant to sea ice brine conditions. Part of the discrepancy between the constants, and the increase in this discrepancy with S, could result from the different ionic composition of media used to determine K_1^* and K_2^*. Measurements of K_2^* in artificial seawater have been shown to be lower than values in natural seawater, likely due to the interactions of boric acid with HCO_3^- and CO_3^{2-} (MP&M02; Millero et al., 2002). Therefore, the derivation of constants by Roy93, G&P89, and Hansson87 have been cited as only reliable for artificial seawater and inappropriate for application to natural seawater (MP&M02). This issue may be further compounded in concentrated sea ice brine, with ionic strengths more than double that of seawater.

Another important consideration within sea ice brine systems is the precipitation of solid salts as brine becomes more concentrated, changing the relative concentrations of the major ions in solution from standard seawater ratios (Assur, 1958). Re-dissolution of precipitated salts back

into the brine solution as the melt season progresses may be gradual (e.g., crystals persist even after ice has fully melted, Dieckmann et al., 2008), likely depending on the rate of temperature change and dilution. Our analysis here and the general use of conditional stability constants determined in seawater to describe sea-ice brine chemistry are predicated on the assumption that the ionic composition of collected brine is proportional to standard seawater. However, calculated in-situ brine temperatures (T_{sb} < -2 °C;Table 5-3) for our samples indicate that some amount of ikaite ($CaCO_3 \cdot 6H_2O$) may have remained within brine channels, as precipitates are expected to form at temperatures < -2.2 °C (Assur, 1958) and have been observed throughout winter sea ice with a temperature profile similar to our measured in-situ values (e.g., Rysgaard et al., 2013). This deviation from standard seawater ionic composition further complicates the application of a seawater derived K^* to sea ice brine, irrespective of its determination in artificial or natural seawater.

Using the analytical instrumentation and methods described in this study, we found that the Roy93 and G&P89 constants generally provided the most consistent calculations of brine carbonate system parameters when compared to our measurements (Table 5-6). We note that G&P89 included F^- and SO_4^{2-} in their artificial seawater media and extended their experimental range to within freezing temperatures (-1 °C), matching most closely the attributes of brine samples used in this study. Therefore, until carbonic acid dissociation constants are explicitly determined for low temperature (< -1 °C) and high salinity (> 50) sea-ice brine conditions, we recommend the use of G&P89 carbonic acid dissociation constant definitions for the calculation of natural sea ice brine carbonate system parameters.

5.5 Conclusions

In this study we over-determined the carbonate system in natural sea ice brine samples and used the CO2SYS program to investigate the application of seawater carbonic acid dissociation constant parameterizations to describing the sea ice brine carbonate system. Notwithstanding the analytical uncertainty of our measurements, our data strongly suggest that more rigorous, laboratory based investigations are warranted to derive conditional carbonic acid dissociation constants that are relevant to sea-ice brine systems. Furthermore, our analyses underscore the need for high salinity certified reference material to evaluate the accuracy of carbonate system measurements in natural sea ice brine samples.

Our investigation illustrates that extrapolating seawater derived carbonic acid dissociation constants (K_1^* and K_2^*) to sea ice conditions allows calculated carbonate system values to be estimated within no better than 10 % of measured values, with deviations possibly as high as 150 %. Until carbonic acid dissociation constants are explicitly determined for low temperature (< -1 °C) and high salinity (> 50) sea-ice brine conditions, the parameterizations of K_1^* and K_2^* determined by Goyet and Poisson (1989) appear to provide the least erroneous estimates of carbonate system parameters in ice brine (at least, when using our analytical methods). We would like to emphasize the importance of archiving raw data so that published results can be revaluated against future methodological advances and derivation of sea ice appropriate carbonic acid dissociation constants.

5.6 Tables

Table 5-1. Field studies measuring two or more carbon system parameters in sea ice brine

Sea Ice Brine Study	S		DIC (µmol kg^{-1})			TA (µmol kg^{-1})			pH_F^{pot}			pCO_2 (µatm)		
	Min	**Max**	**Min**	**Max**	**RU (±)**	**Min**	**Max**	**RU (±)**	**Min**	**Max**	**RU (±)**	**Min**	**Max**	**RU (±)**
Gleitz et al. (1995)	21.0	107.8				1728	7835	*n.r.*	7.830[a]	9.932[a]	*n.r.*			
Papadimitriou et al. (2007)	40	63	2091	3551	± 2%	2690	4620	± 2%	*n.r.*	*n.r.*	± 0.04			
Delille et al. (2007)	~20	90				*n.v.*	*n.v.*	± 4	8.405[b]	9.457[b]	± 0.01	~30[c]	~420[c]	*n.r.*
Nomura et al. (2010b)	23.3	33.2	*n.r.*	*n.r.*	± 0.1%	*n.r.*	*n.r.*	± 0.2%						
									pH_F^{spec}					
Miller et al. (2011a)	68	163	4000	9600	± 3	*n.r.*	*n.r.*	± 3	8.281	8.496	± 0.002			
Fransson et al. (2011)	33	43.3	1451	2191	*n.r.*	2201	2932	*n.r.*	*n.r.*	*n.r.*	*n.r.*			
Gelifus et al. (2012)	0	138	165	8254	± 2	173	8191	± 3				0	1839	*n.r.*
Papadimitriou et al. (2012)	58	134	2839	8405	± 2%	3912	9054	± 2%						
This Study	*38*	*82*	*2491.38*	*4801.30*	*± 2.54*	*2625.57*	*5238.96*	*± 4.36*	*8.216*	*8.389*	*± 0.0064*	*278*	*656*	*± 15*

RU refers to Reported Uncertainty
pH_F^{pot} indicates potentiometric measurement with a glass probe, corrected to in-situ T and S
pH_F^{spec} indicates spectrophotometric pH measurements, corrected to in-situ T and S
n.v. refers to only salinity normalized values reported
n.r. refers to "not reported" values, although methods for collection and determination are listed
[a] Gleitz et al. (1995) pH_{SWS} data were converted to the Free Ion scale for this comparison following Zeebe and Wolf-Gladrow (2001)
[b] Delille et al. (2007) pH_T data were converted to the Free Ion scale for this comparison following Zeebe and Wolfe-Gladrow (2001)
[c] It is unclear whether only low pCO_2 (< 150 µatm) brine samples were independently measured using the modified equilibrator method of Delille (2006) (Fig. 2 in Delille et al., 2007), meaning the high end of this range might include pCO_2 values calculated from pH_T and TA measurements.

Table 5-2. Summary of measurements to determine the 1st and 2nd carbonic acid dissociation constants in seawater

Reference	S	T (°C)	Seawater Composition (in addition to $NaHCO_3$ and Na_2CO_3)	pH Scale	σ pK_1^*	σ pK_2^*	Electrochemical Cell
Hansson (1973) (refit by Dickson and Millero, 1987)	20 to 40	5 to 30	*Artificial seawater* ($NaCl$, Na_2SO_4, $MgCl_2$, $CaCl_2$)	SWS[b]	0.007[c]	0.009[c]	Glass electrode + AgCl|AgCl, Ag reference
Mehrbach et al. (1973) (refit by Dickson and Millero, 1987)	19 to 43	2 to 35	*Real seawater* ($NaCl$, Na_2SO_4, KCl, KBr, NaF, Na_2CO_3, $NaHCO_3$, $B(OH)_3$, $MgCl_2$, $CaCl_2$, $SrCl_2$)[a]	SWS[b]	0.006[c]	0.010[c]	Glass electrode + calomel reference
Goyet and Poisson (1989)	10 to 50	-1 to 40	*Artificial seawater* ($NaCl$, Na_2SO_4, KCl, KBr, H_8BrO_3, NaF, $MgCl_2$, $CaCl_2$, $SrCl_2$)	SWS	0.007[c]	0.011[c]	Glass electrode + calomel reference
Roy et al. (1993)	5 to 45	0 to 45	*Artificial seawater* ($NaCl$, Na_2SO_4, KCl, $MgCl_2$, $CaCl_2$)	Total	0.002[c]	0.006[c]	Pt, H_2|AgCl, Ag
Mojica Prieto and Millero (2002)	5 to 42	0 to 45	*Real seawater stripped of CO_2* ($NaCl$, Na_2SO_4, KCl, KBr, NaF, Na_2CO_3, $NaHCO_3$, $B(OH)_3$, $MgCl_2$, $CaCl_2$, $SrCl_2$)[a] *Artificial seawater* ($NaCl$, Na_2SO_4, KCl, KBr, H_8BrO_3, NaF, $MgCl_2$, $CaCl_2$, $SrCl_2$)	SWS	0.0040[e]	0.008[e]	Glass electrode + Ag, AgCl reference (as well as a spectrophotometer)
Millero et al. (2006)	1 to 50	0 to 50	*Filtered Natural Gulf Stream Seawater* ($NaCl$, Na_2SO_4, KCl, KBr, NaF, $NaHCO_3$, $B(OH)_3$, $MgCl_2$, $CaCl_2$, $SrCl_2$)[d]	SWS	0.0054[e]	0.011[e]	Glass electrode + Ag, AgCl reference

[a] After Mojica Prieto and Millero (2002) and Dickson et al. (2007)
[b] Dickson and Millero (1987) corrected initial measurements to the pH(SWS) scale, correcting Mehrbach et al.'s results with a more appropriate *f*H and Hansson's data for solution composition (no fluoride and different sulphate ion content compared to natural seawater)
[c] As summarized in Millero et al. (2002) from their Table 1, where standard errors are 1σ from fits of pK_1 and pK_2 as a function of temperature and salinity.
[d] After Millero (1996)
[e] As summarized in Millero et al. (2006) from their Table 1, where standard errors are based upon fitting the measurements by various workers to the same function form.

Table 5-3. Sackhole brine samples collected during the Arctic-ICE program

Year	Date	Sackhole Depth (cm)	Salinity	In-situ T_{Sb} [a]	Ionic Strength [b]
2010	May 13	130	51.7	-2.95	1.09
2010	May 16	70	38.1	-2.14	0.79
2010	May 17	75	79.8	-4.69	1.73
2010	May 20	70	81.8	-4.82	1.78
2011	May 30	90	66.4	-3.85	1.42
2011	May 30	130	63.4	-3.66	1.35
2011	June 4	60	61	-3.52	1.29
2011	June 4	90	61.3	-3.53	1.30
2011	June 4	130	60.2	-3.47	1.28
2011	June 8	130	52.8	-3.02	1.11
2011	June 8	60	56.1	-3.22	1.18
2011	June 8	90	54.3	-3.11	1.14

[a] In-situ Temperature determined from brine salinity, Petrich and Eicken (2010)
[b] Ionic Strength determined after Dickson et al. (2007)

Table 5-4. Analytical precision (Pooled Standard Deviation, Sp) of carbonate system

Parameter	Units	*Sp* (%)[a]	k[c]
DIC	µmol kg^{-1}	2.5 (< 1)	12
TA	µmol kg^{-1}	4.4 (< 1)	12
pH_F	@ in-situ T, S, Ct_{AVG}, P = 1	0.006[b] (< 1)	8
pCO_2	µatm @ in-situ T, S, cTA, Ct_{AVG}, P = 1	15[b] (3)	12

[a] Sp as a percentage of the average measured value).
[b] Measured values corrected to in-situ conditions using average measured DIC for each sample and the combined equilibrium constants $K_1$and K_2 determined by Hansson (1973) and Mehrbach et al. (1973) as refit by Dickson and Millero (1987) and dissociation constants for $KHSO_4$ determined by Dickson (1990) in CO2Sys (Pierrot et al., 2006).
[c] k is the number of sample sets analyzed (in triplicate or quadruplicate)

Table 5-5. Average ($\bar{x}$) measured brine Total Alkalinity (TA, µmol kg^{-1}) after filtration to remove particulate matter. P-values (T-test) in parentheses indicate difference between filtration treatment and unfiltered sample

Filtration	S = 58		S = 69		S = 79	
	TA (µmol kg^{-1})		TA (µmol kg^{-1})		TA (µmol kg^{-1})	
	$\bar{x}$ (n = 3)	σ (n=3)	$\bar{x}$ (n = 3)	σ (n=3)	$\bar{x}$ (n = 3)	σ (n=3)
unfiltered	3931	5	4526	4	5361	4
0.7 µm	3930 (0.7)	5	4524 (0.5)	7	5360 (0.7)	3
0.45 µm	3932 (0.8)	3	4526 (1.0)	8	5367 (0.1)	1
0.22 µm	3923 (0.1)	5	4514 (0.3)	10	5355 (0.4)	9

Table 5-6. Average differences between calculated and measured carbonate system parameters in sea ice brine using different parameterizations of the carbonic acid dissociation constants

Measured Brine Input Parameters	$\bar{x}$ [Measured Brine - Calculated Brine] (%)[a]								Seawater K_1*, K_2*
	Δ DIC (μmol kg^{-1})		Δ TA (μmol kg^{-1})		Δ pH_F		Δ pCO_2 (μatm)		
pH, TA	67.2	(1.9)	--	--	--	--	27.6	(6.2)	Hansson87
	68.4	(1.9)	--	--	--	--	43.6	(10.1)	Mehrbach87
	46.6	(1.3)	--	--	--	--	31.6	(8.0)	G&P89
	55.3	(1.5)	--	--	--	--	46.4	(11.2)	ROY93
	89.8	(2.5)	--	--	--	--	30.3	(7.1)	MP&M02
	190.5	(5.1)	--	--	--	--	135.5	(27.3)	M06
	2.7	(0.1)					-3.7	(1.1)	Seawater [b]
pH, DIC	--	--	-73.1	(1.8)	--	--	20.2	(4.5)	Hansson87
	--	--	-74.3	(1.9)	--	--	36.5	(8.5)	Mehrbach87
	--	--	-50.4	(1.3)	--	--	27.4	(6.9)	G&P89
	--	--	-59.9	(1.5)	--	--	41.2	(9.9)	ROY93
	--	--	-98.1	(2.4)	--	--	20.3	(4.8)	MP&M02
	--	--	-215.1	(5.3)	--	--	116.6	(23.5)	M06
			-3.1	(0.1)			-4.1	(1.2)	Seawater [b]
pH, pCO_2	-190.8	(5.3)	-281.5	(7.1)	--	--	--	--	Hansson87
	-356.4	(9.8)	-461.6	(11.6)	--	--	--	--	Mehrbach87
	-288.9	(7.9)	-362.1	(9.1)	--	--	--	--	G&P89
	-95.6	(2.7)	-164.5	(4.3)	--	--	--	--	ROY93
	-203.3	(5.7)	-321.2	(8.2)	--	--	--	--	MP&M02
	-916.6	(24.7)	-1250.8	(30.7)	--	--	--	--	M06
	34.1	(1.7)	35.1	(1.5)					Seawater [b]
pCO_2, DIC	--	--	-74.5	(1.8)	0.019	(4.8)	--	--	Hansson87
	--	--	-64.0	(1.5)	0.036	(9.0)	--	--	Mehrbach87
	--	--	-29.3	(0.8)	0.030	(7.3)	--	--	G&P89
	--	--	-67.3	(1.6)	-0.023	(4.9)	--	--	ROY93
	--	--	-120.6	(2.7)	0.021	(5.1)	--	--	MP&M02
	--	--	-205.8	(4.5)	0.084	(21.7)	--	--	M06
			-7.9	(0.3)	-0.007	(1.5)			Seawater [b]
pCO_2, TA	62.1	(1.6)	--	--	0.024	(6.0)	--	--	Hansson87
	53.4	(1.4)	--	--	0.040	(9.9)	--	--	Mehrbach87
	25.1	(0.7)	--	--	0.032	(7.9)	--	--	G&P89
	56.8	(1.5)	--	--	-0.018	(3.8)	--	--	ROY93
	97.7	(2.4)	--	--	0.028	(6.9)	--	--	MP&M02
	155.5	(3.8)	--	--	0.094	(24.6)	--	--	M06
	6.2	(0.3)			-0.005	(1.2)			Seawater [b]
TA, DIC	--	--	--	--	0.077	(20.1)	-101.2	(20.7)	Hansson87
	--	--	--	--	0.079	(20.7)	-84.5	(17.4)	Mehrbach87
	--	--	--	--	0.056	(14.8)	-36.6	(9.9)	G&P89
	--	--	--	--	0.033	(8.8)	-46.6	(10.4)	ROY93
	--	--	--	--	0.100	(26.6)	-155.7	(32.3)	MP&M02
	--	--	--	--	0.193	(57.4)	-259.2	(42.9)	M06
					0.004	(1.0)	-7.6	(2.2)	Seawater [b]

[a] Average difference [Measured - Calculated] as a percentage of the measured sea ice brine value.
[b] Typical seawater values calculated from Gulf Stream seawater reported in Millero et al. (2006), Table 7: TA = 2400 μmol kg^{-1}, TCO_2 = 2052.3 μmol kg^{-1}, pH_F = 8.209, pCO_2 = 351.1 μatm, S = 35 and T = 25 °C. Here pH_F was calculated from pH_{SWS} following Zeebe and Wolf-Gladrow (2001), and pCO_2 was calculated from fCO_2 = 350 μatm. Seawater values reported in this table represent the average difference [Measured - Calculated] over all six sets of constants, $\bar{x}$, and as a percentage of measured seawater values (%).

5.7 Figures

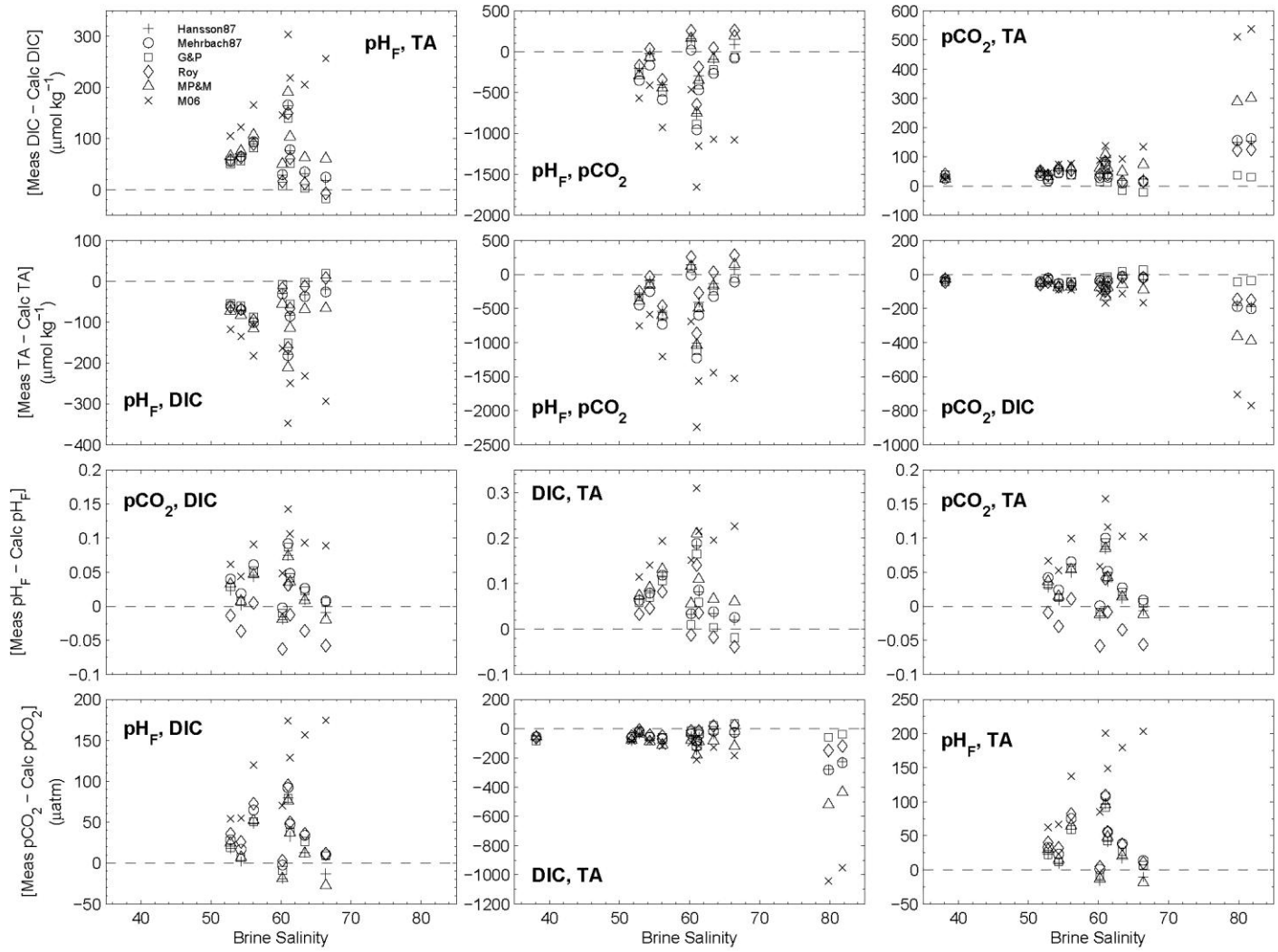

Figure 5-1. Differences between measured and calculated carbonate system parameters for each sample, plotted against brine salinity. Input values (measurements) used to determine calculated values are indicated in bold-faced type within each subplot (e.g., DIC, TA). Zero differences (Measured Values = Calculated Values) are indicated by a grey dashed lines. Note the different y-axes scales for each parameter (DIC, TA, pH_F, and pCO_2) and for each combination of input parameters (e.g., DIC, TA; pH_F, pCO_2; etc.). Carbonic acid dissociation constants parameterizations applied in each comparison are listed in the legend, as in Table 5-2 and Table 5-6.

Chapter 6: Conclusion

The primary goal of this thesis was to investigate carbon transfer across the atmosphere-sea ice-ocean interface using a suite of biogeochemical tracers measured in a range of Arctic marine environments. The main question addressed by each chapter can be summarized as: (1) what are the carbon sources to the perennially ice-covered interior Canada Basin?; (2) what is the relative importance of different sources of inorganic carbon to the dissolved inorganic carbon maximum in the Canada Basin halocline?; (3) how do sea ice biogeochemical processes over the winter-spring transition govern the switch between late-winter CO_2 efflux to the atmosphere and late-spring CO_2 uptake?; and (4) how accurately do thermodynamic equilibrium constants derived from seawater conditions describe the carbonate system in sea ice?

These questions are critical to advancing our understanding of the role of sea ice in the polar ocean carbon cycle, in both the contemporary ocean and in a warmer future climate. This thesis presents the first stable carbon isotope data for dissolved inorganic carbon in Arctic Sea Ice, as well as the first assessment of surface mixed layer particulate organic carbon stable isotope signature distributions across the deep Canada Basin. It also provides the first attempt to evaluate the thermodynamic equilibria governing the inorganic carbon system in sea ice brines. As such, the data presented in this thesis provide important new insights into Arctic carbon dynamics, and a foundation for much needed future studies.

6.1 Summary of Major Findings and Contributions

Chapter 2 presents stable carbon isotope data to evaluate the sources of particulate organic material (POC) in the surface mixed layer of the central Canada Basin. As the first basin-wide assessment of δ^{13}C-POC in the Canada Basin surface mixed layer, this work provides a new perspective on the spatial variability of POC in the Arctic Ocean, and the potential sources of C to surface waters. In addition, the results provide baseline data against which future studies can be compared. This basin-wide data set illuminates a persistent dichotomy between the highly productive Beaufort Shelf and the low productivity central Canada Basin. I found isotopic enrichment of ^{13}C in POC to be tightly correlated to carbon uptake rates along the highly productive continental shelf, indicating that in situ processes dominated carbon isotopic distributions in this region. In the low productivity deep basin, however, δ^{13}C-POC distributions reflected external POC sources, in particular the advective transport of riverine organic matter. Contrary to expectation, multi-year sea ice within the central basin appeared to contribute negligibly to δ^{13}C-POC distributions. This work illustrates that alkalinity and meteoric water content can be used as geochemical tracers to distinguish POC inputs from North American and Russian rivers. Our analysis suggests that Russian river inputs are the predominant source of ^{13}C-depleted organic matter to the mixed layer of the central Canada Basin.

In chapter 3, I applied nutrient and stable isotope tracers to investigate the sources of the Canada Basin halocline dissolved inorganic carbon (DIC) maximum. This is the first study to use stable carbon isotopes in DIC to investigate the halocline DIC maximum and to quantitatively examine the contribution of sea ice formation to this feature. Non-conservative sources of DIC, including air-sea gas exchange and sea ice brine rejection, were found to negligibly influence DIC

concentrations in the winter shelf waters feeding the halocline. Instead, the maxima in both nutrient and DIC concentrations within the halocline were explained by the remineralization of organic material within the sediments of the highly productive Bering and Chukchi Sea shelves. Furthermore, mixing between Pacific and Atlantic layer waters in the lower halocline was responsible for the greater salinity range of the DIC maximum, compared to that of the nutrient maximum in the south-western Canada Basin.

Chapter 4 summarizes observations carried out during a six-week time series study of land-fast sea ice during the winter-spring transition in the Canadian Arctic Archipelago. This work represents the first application of stable isotope signatures to investigate the inorganic carbon system in Arctic sea ice brine during a period where abiotic processes generally dominated the ice column. The main findings of this chapter include the first quantification of seawater brine dilution and $CaCO_3$ dissolution on CO_2 concentrations in spring sea ice. As has been observed in other studies, our time series observations illustrated an overwhelming thermodynamic control of freshwater brine dilution on pCO_2, leading to a dramatic reduction of pCO_2 within the ice. This CO_2 reduction occurred during a period when CO_2 flux across the ice-atmosphere and ice-water interfaces was impeded. Our results also reveal a minor role for $CaCO_3$ dissolution in the uptake of CO_2 as sea ice brine warms and dilutes. The results of geochemical mass-balance calculations used in this study were reinforced by the qualitative application of stable isotope tracers ($\delta^{13}C$-DIC), which showed a measurable isotopic enrichment of brine solutions resulting from $CaCO_3$ dissolution within sea ice brine channels.

In the last data chapter, chapter 5, I examined the accuracy of thermodynamic carbonate equilibrium constants for use in sea ice brines. This was accomplished by over determining the carbonate system through discrete measurement of DIC, Total Alkalinity, pH, and CO_2 partial pressure. This study represents the first attempt to determine the applicability of seawater carbonic acid dissociation constant parameterizations to sea ice brine systems. The results show that seawater derived carbonic acid dissociation constants may not be readily extrapolated to high salinity, low temperature sea ice brine systems. I show that extrapolation of seawater-derived carbonic acid dissociation constants leads to calculation errors ranging from 10 % to 150% of measured values, and I identified the particular set of published thermodynamic constants that are likely to lead to the least erroneous results. This work illustrates a large uncertainty in our interpretation of calculated sea ice carbonate system parameters and underscores a fundamental need for the specific determination of carbonate system equilibrium constants under appropriate sea ice temperature and salinity conditions.

6.2 Future Directions

It is hoped that this thesis will not be a stand-alone document, but that questions raised or left un-answered within its pages will provide a starting point for future questions. Moreover, I hope that the results I have generated and presented in the thesis can be used as baseline data against which to compare future studies. This section highlights some future research questions that have been raised throughout this thesis and suggests some next steps.

(1) *what are the carbon sources to the perennially ice-covered interior Canada Basin?*

Chapter 2 carried out the first basin-wide survey of δ^{13}C-POC and δ^{13}C-DIC within the surface mixed layer of the Canada Basin. Although this work illustrated the dominance of terrestrial (i.e., riverine) sources of POC to the central basin, changing patterns of freshwater diversion and continued sea ice retreat have the potential to significantly influence this signal. Stable carbon isotopes represent a tool that is both useful and easy to collect from a ship's underway system. It is hoped that future basin-wide studies will include δ^{13}C-POC sampling to compare with data presented here from 2008 and 2009. With a longer term time series, δ^{13}C-POC may become a valuable tool to monitor future changes to the Arctic Ocean carbon cycle associated with climate change. For example, a long-term time series of surface mixed layer δ^{13}C-POC data would help to evaluate whether the dominant terrestrial POC signal in the interior Canada Basin is a persistent feature, or if marine POC production would dominate this signal under a relaxed Beaufort Gyre circulation, when freshwater storage in the basin is diminished (e.g., McLaughlin et al., 2011 and references therein).

(2) *what is the relative importance of different sources of inorganic carbon to the dissolved inorganic carbon maximum in the Canada Basin halocline?*

A main goal of chapter 3 was to use stable isotope tracers to investigate the sources of the Canada Basin halocline dissolved inorganic carbon (DIC) maximum. One of the components investigated was the non-conservative contribution of DIC (relative to total alkalinity) associated with $CaCO_3$ formation within sea ice and the subsequent rejection of high-DIC brines. Our

results showed that DIC within winter modified Pacific waters was overwhelmingly dominated by organic matter remineralization in the sediments, such that a sea ice brine signal was not apparent in our data set. Other studies have demonstrated a direct contribution of sea ice derived DIC to the water column in other polar coastal regions (e.g., Anderson et al., 2004; Omar et al., 2005; Rysgaard et al., 2007). Such coastal regions may prove better locations to apply stable carbon isotope tracers to distinguish brine contributions of "excess" DIC (over total alkalinity) to the water column. Future research questions include quantifying the impact of exported high-DIC brines to carbon sequestration below the mixed layer and determining the sensitivity of this DIC sink to the freshening of Arctic Ocean surface waters with increased sea ice melt and riverine inputs.

(3) *how do sea ice biogeochemical processes over the winter-spring transition govern the switch between late-winter CO_2 efflux to the atmosphere and late-spring CO_2 uptake?*

Chapter 4 captured an important window in the winter-spring transition in Arctic land-fast sea ice. This time series illustrated that pCO_2 within the ice is strongly controlled by physical processes associated with warming, with an additional contribution from biological processes in bottom ice layers. To date, much of the work in sea ice biogeochemistry has been carried out as warming advances over spring and into summer, as sea ice melts and biological assemblages dominate. This has left a gap in our knowledge of the deep winter period, both from a biological and chemical perspective. Stable isotope samples from sea ice brines collected over the deep winter period would be particularly interesting, and may shed light on the importance of CO_2 degassing from $CaCO_3$ supersaturated brines. The salting out effect on CO_2 solubility indicates

that winter-time brines will be a huge reservoir for CO_2, suggesting that any brine rejection and seawater flushing in the lower portions of cold winter time sea ice could transfer some of this CO_2 into the water below. Carbonate system and stable isotope measurements from sea ice brines during this period would further aid in the investigation of "excess" DIC contributed to the water column as a result of $CaCO_3$ precipitation.

(4) *can we apply a general ocean description of the carbonate system to characterize the thermodynamic equilibria governing the inorganic carbon system in sea ice?*

Chapter 5 indicated that there is a fundamental need for the specific determination of carbonate system equilibrium constants under appropriate sea ice temperature and salinity conditions. Until the sea ice biogeochemistry community has parameterized equilibrium constants for natural sea ice brine conditions, over-determining the carbonate system should become a standard practice. Additionally, the work in this chapter highlighted the shortcomings of our present pH and pCO_2 analyses and the difficulty determining analytical accuracy in carbonate system measurements at high salinity. The uncertainty in the behaviour of pH indicator dyes (*m*-cresol purple) within natural sea ice brine samples is just one of the unknowns surrounding pH determination at high salinity, and more work needs to be done in this field before we have confidence in brine pH data produced by the spectrophotometric method. For carbonate system analyses to be comparable between laboratories and research groups there is an urgent need for the development of a high salinity marine certified reference material to evaluate the accuracy of carbonate system measurements in natural sea ice brine samples.

The Arctic Ocean is undergoing a period of rapid change. The next decade promises the transition to a seasonally-ice free, highly stratified surface ocean, with dramatic summer warming and an increased contribution of freshwater and carbon from river inputs (e.g., Bates and Mathis, 2009; Maslowski et al., 2012; McGuire et al., 2009; McLaughlin et al., 2011; Prowse et al., 2006). Changes to physical ocean properties (temperature and salinity) alone will dramatically influence CO_2 solubility in the surface Arctic Ocean, reducing the atmospheric CO_2 sink potential of the deep basins (e.g., Cai et al., 2010; Else et al., 2013; Steiner et al., 2013). On the other hand, the increased transport of terrestrial carbon to the shelves may act as a source of CO_2 to the atmosphere (e.g., McGuire et al., 2009), while upwelling of Pacific nutrients onto the shelves may increase the shelf CO_2 sink by promoting primary production (e.g., Carmack and Chapman, 2003; McLaughlin et al., 2011). It is clear that the Arctic Ocean's role in the global balance of CO_2 sources and sinks will undoubtedly change over the next decade, raising the urgency for increased investigation in the transfer of CO_2 across the atmosphere-sea ice-ocean interface and for a more quantitative understanding of the role of sea ice in polar carbon cycling (e.g., Barber et al., 2012; Loose et al., 2011; Parmentier et al., 2013; Rysgaard et al., 2011).

References

Aagaard, K., Carmack, E., 1989. The role of sea ice and other fresh water in the Arctic circulation. J. Geophys. Res. 94, 14,485–14,498.

Aagaard, K., Carmack, E.C., 1994. The Arctic Ocean and climate: A Perspective. Geophys. Monogr. 85, 5–20.

Aagaard, K., Coachman, L.K., Carmack, E., 1981. On the halocline of the Arctic Ocean. Deep Sea Res. Part A. Oceanogr. Res. Pap. 28, 529–545.

Anderson, L.G., Dyrssen, D., Jones, E.P., 1990. An Assessment of the Transport of Atmospheric CO_2 Into the Arctic Ocean 95, 1703–1711.

Anderson, L.G., Falck, E., Jones, E.P., Jutterström, S., Swift, J.H., 2004. Enhanced uptake of atmospheric CO_2 during freezing of seawater: A field study in Storfjorden, Svalbard. J. Geophys. Res. 109, 4–11.

Anderson, L.G., Peter Jones, E., Lindegren, R., Rudels, B., Sehlstedt, P.-I., 1988. Nutrient regeneration in cold, high salinity bottom water of the Arctic shelves. Cont. Shelf Res. 8, 1345–1355.

Anderson, L.G., Tanhua, T., Björk, G., Hjalmarsson, S., Jones, E.P., Jutterström, S., Rudels, B., Swift, J.H., Wåhlstöm, I., 2010. Arctic ocean shelf–basin interaction: An active continental shelf CO_2 pump and its impact on the degree of calcium carbonate solubility. Deep Sea Res. Part I Oceanogr. Res. Pap. 57, 869–879.

Arrigo, K.R., Mock, T., Lizotte, M.P., 2010. Primary Producers and Sea Ice, in: Thomas, D.N., Dieckmann, G.S. (Eds.), Sea Ice. Wiley-Blackwell, pp. 283–325.

Arrigo, K.R., Robinson, D.H., Dunbar, R.B., Leventer, A.R., Lizotte, M.P., 2003. Physical control of chlorophyll a , POC, and TPN distributions in the pack ice of the Ross Sea, Antarctica. J. Geophys. Res. 108, 1–23.

Arrigo, K.R., Sullivan, C.W., 1992. The influence of salinity and temperature covariation on the photophysiological characteristics of Antarctic sea ice microalgae. J. Phycol. 28, 746–756.

Arrigo, K.R., van Dijken, G., Pabi, S., 2008. Impact of a shrinking Arctic ice cover on marine primary production. Geophys. Res. Lett. 35, L19603.

Assur, A., 1958. Composition of sea ice and its tensile strength, in: Thurston, W. (Ed.), Arctic Sea Ice. US National Academy of Sciences, National Research Council, pp. 106–138.

Barber, D.G., Asplin, M.G., Papakyriakou, T.N., Miller, L., Else, B.G.T., Iacozza, J., Mundy, C.J., Gosslin, M., Asselin, N.C., Ferguson, S., Lukovich, J. V., Stern, G. A., Gaden, A., Pućko, M., Geilfus, N.-X., Wang, F., 2012. Consequences of change and variability in sea ice on marine ecosystem and biogeochemical processes during the 2007–2008 Canadian International Polar Year program. Clim. Change 115, 135–159.

Bates, N.R., Best, M., Hansell, D., 2005. Spatio-temporal distribution of dissolved inorganic carbon and net community production in the Chukchi and Beaufort Seas. Deep Sea Res. Part II Top. Stud. Oceanogr. 52, 3303–3323.

Bates, N.R., Mathis, J.T., 2009. The Arctic Ocean marine carbon cycle: evaluation of air-sea CO_2 exchanges , ocean acidification impacts and potential feedbacks. Biogeosciences 6, 2433–2459.

Boetius, A., Albrecht, S., Bakker, K., Bienhold, C., Felden, J., Fernández-Méndez, M., Hendricks, S., Katlein, C., Lalande, C., Krumpen, T., Nicolaus, M., Peeken, I., Rabe, B., Rogacheva, A., Rybakova, E., Somavilla, R., Wenzhöfer, F., 2013. Export of algal biomass from the melting Arctic sea ice. Science 339, 1430–2.

Broecker, W.S., Maier-Reimer, E., 1992. The influence of air and sea exchange on the carbon isotope distribution in the sea. Global Biogeochem. Cycles 6, 315–320.

Broecker, W.S., Peng, T.-H., 1982. Tracers in the Sea. Eldigio Press, Palisades. p. 690.

Broecker, W.S., Peng, T.-H., 1992. Interhemispheric transport of carbon dioxide by ocean circulation. Nature 356, 587–589.

Brown, K. A., McLaughlin, F., Tortell, P.D., Varela, D., Yamamoto-Kawai, M., Hunt. B., François, R. 2014. Determination of Particulate Organic Carbon Sources to the Surface Mixed Layer of the Central Canada Basin, Arctic Ocean. J. Geophys. Res. Oceans 119, doi:10.1002/2013JC009197.

Burkhardt, S., Riebesell, U., Zondervan, I., 1999. Stable carbon isotope fractionation by marine phytoplankton in response to daylength, growth rate, and CO_2 availability, Marine Ecology Progress Series, 184, 31–41, doi:10.3354/meps184031.

Cai, P., Rutgers van der Loeff, M., Stimac, I., Nöthig, E.-M., Lepore, K., Moran, S.B., 2010. Low export flux of particulate organic carbon in the central Arctic Ocean as revealed by 234 Th: 238 U disequilibrium. J. Geophys. Res. 115, C10037.

Cai, W. -J., Bates, N.R., Guo, L., Anderson, L.G., Mathis, J.T., Wanninkhof, R., Hansell, D.A., Chen, L., Semiletov, *in press*. Carbon Fluxes Across Boundaries in the Pacific Sector of the Arctic Ocean in a Changing Environment, in: The Pacific Arctic Sector: Status and Trends. Springer.

Cai, W.-J., Chen, L., Chen, B., Gao, Z., Lee, S.H., Chen, J., Pierrot, D., Sullivan, K., Wang, Y., Hu, X., Huang, W.-J., Zhang, Y., Xu, S., Murata, A., Grebmeier, J.M., Jones, E.P., Zhang, H., 2010. Decrease in the CO_2 uptake capacity in an ice-free Arctic Ocean basin. Science 329, 556–9.

Carmack, E., Barber, D., Christensen, J., Macdonald, R.W., Rudels, B., Sakshaug, E., 2006. Climate variability and physical forcing of the food webs and the carbon budget on panarctic shelves. Prog. Oceanogr. 71, 145–181.

Carmack, E., Chapman, D.C., 2003. Wind-driven shelf/basin exchange on an Arctic shelf: The joint roles of ice cover extent and shelf-break bathymetry. Geophys. Res. Lett. 30, 1778.

Carmack, E.C., McLaughlin, F., Yamamoto-Kawai, M., Itoh, M., Shimada, K., Krishfield, R., Proshutinsky, A., 2008. Freshwater Storage in the Northern Ocean and the Special Role of the Beaufort Gyre, in: Dickson, R., Meincke, J., Rhines, P. (Eds.), Arctic-Subarctic Ocean Fluxes. Springer, pp. 145–169.

Chang, B.X., Devol, A.H., 2009. Seasonal and spatial patterns of sedimentary denitrification rates in the Chukchi sea. Deep Sea Res. Part II Top. Stud. Oceanogr. 56, 1339–1350.

Charles, C.D., Fairbanks, R.G., 1990. Glacial to interglacial changes in the isotopic gradients of Southern Ocean surface waters, in: Bleil, U., Thiede, J. (Eds.), Geological History of the Polar Oceans: Arctic Versus Antarctic. Kluwer Academic Publishers, pp. 519–538.

Chierici, M., Fransson, A., Anderson, L.G., 1999. Influence of m-cresol purple indicator additions on the pH of seawater samples: correction factors evaluated from a chemical speciation model. Mar. Chem. 65, 281–290.

Chierici, M., Fransson, A., Lansard, B., Miller, L. A., Mucci, A., Shadwick, E., Thomas, H., Tremblay, J.-E., Papakyriakou, T.N., 2011. Impact of biogeochemical processes and environmental factors on the calcium carbonate saturation state in the Circumpolar Flaw Lead in the Amundsen Gulf, Arctic Ocean. J. Geophys. Res. 116, C00G09.

Clayton, T.D., Byrne, R.H., 1993. Spectrophotometric seawater pH measurements: total hydrogen ion concentration scale calibration of *m*-cresol purple and at-sea results 40, 2115–2129.

Cooper, L.W., Benner, R., McClelland, J.W., Peterson, B.J., Holmes, R.M., Raymond, P. A., Hansell, D., Grebmeier, J.M., Codispoti, L., 2005. Linkages among runoff, dissolved organic carbon, and the stable oxygen isotope composition of seawater and other water mass indicators in the Arctic Ocean. J. Geophys. Res. 110, 1–14.

Cooper, L.W., Cota, F., Pomeroy, R., Grebmeier, M., Whitledge, T.E., 1999. Modification of NO, PO, and NO/PO during flow across the Bering and Chukchi shelves: Implications for use as Arctic water mass tracers. J. Geophys. Res. 104, 7827–7836.

Cooper, L.W., McClelland, J.W., Holmes, R.M., Raymond, P. A., Gibson, J.J., Guay, C.K., Peterson, B.J., 2008. Flow-weighted values of runoff tracers ($\delta^{18}O$, DOC, Ba, alkalinity) from the six largest Arctic rivers. Geophys. Res. Lett. 35, L18606.

Cooper, L.W., Whitledge, T.E., Grebmeier, M., Weingartner, T., 1997. The nutrient, salinity , and stable oxygen isotope composition of Bering and Chukchi Seas waters in and near the Bering Strait. J. Geophys. Res. 102, 12,563-12,573.

Cox, G.F.N., Weeks, W.F., 1983. Equations for determining the gas and brine volumes in sea ice samples. J. Glaciol. 29, 306–316.

Delille, B., 2006. Inorganic carbon dynamics and air-ice-sea CO_2 fluxes in the open and coastal waters of the Southern Ocean. PhD Thesis, p. 296., Univ. de Liège, Liège, France.

Delille, B., Jourdain, B., Borges, A. V, Tison, J.-L., Delille, D., 2007. Biogas (CO_2, O_2, dimethylsulfide) dynamics in spring Antarctic fast ice. Limnol. Oceanogr. 52(4), 1367–1379.

Deming, J.W., 2010. Sea Ice Bacteria and Viruses, in: Thomas, D.N., Dieckmann, G.S. (Eds.), Sea Ice. Wiley-Blackwell, pp. 247–282.

Devol, A.H., Codispotit, L.A., Christensen, J., P., 1997. Summer and winter denitrification rates in western Arctic shelf sediments. Continent. Shelf Res. 17(9), 1029–1050.

Dickson, A.G., 1990. Standard potential of the reaction : AgCl (s) + $1/2H_2$ (g) = Ag (s) + HCl (aq), and and the standard acidity constant of the ion HSO_4^- in synthetic sea water from 273.15 to 318.15 K. J. Chem. Thermodyn. 22, 113–127.

Dickson, A.G., Millero, F.J., 1987. A comparison of the equilibrium constants for the dissociation of carbonic acid in seawater media. Deep Sea Res. 34, 1733–1743.

Dickson, A.G., Sabine, C.L., Christian, J.R. (Eds.), 2007. Guide to best practices for ocean CO_2 measurements. PICES Special Publication 3, p.191.

Dieckmann, G.S., Nehrke, G., Papadimitriou, S., Göttlicher, J., Steininger, R., Kennedy, H., Wolf-Gladrow, D., Thomas, D.N., 2008. Calcium carbonate as ikaite crystals in Antarctic sea ice. Geophys. Res. Lett. 35, L08501, doi: 10.1029/2008GL033540.

Dieckmann, G.S., Nehrke, G., Uhlig, C., Göttlicher, J., Gerland, S., Granskog, M. A., Thomas, D.N., 2010. Brief Communication: Ikaite ($CaCO_3 \cdot 6H_2O$) discovered in Arctic sea ice. Cryosph. 4, 227–230.

Drenzek, N., Montlucon, D., Yunker, M., Macdonald, R.W., Eglinton, T.I., 2007. Constraints on the origin of sedimentary organic carbon in the Beaufort Sea from coupled molecular ^{13}C and ^{14}C measurements. Mar. Chem. 103, 146–162.

Else, B.G.T., Galley, R.J., Lansard, B., Barber, D.G., Brown, K., Miller, L. A., Mucci, A., Papakyriakou, T.N., Tremblay, J.-É., Rysgaard, S., 2013. Further observations of a decreasing atmospheric CO_2 uptake capacity in the Canada Basin (Arctic Ocean) due to sea ice loss. Geophys. Res. Lett. 40, 1-6. doi:10.1002/grl.50268.

Environment Canada, 2013. Daily Weather Data Report: Resolute Bay. URL http://climate.weather.gc.ca/climateData/dailydata_e.html?timeframe=2&Prov=NU&StationID=32150&dlyRange=2002-10-01|2013-12-03&Year=2010&Month=5&Day=01 (accessed 11.9.13).

Epstein, S., Mayeda, T., 1953. Variation of O18 content of waters from natural sources. Geochim. Cosmochim. Acta 4, 213–224.

Fischer, M., Thomas, D.N., Krell, A., Nehrke, G., Göttlicher, J., Norman, L., Meiners, K.M., Riaux-Gobin, C., Dieckmann, G.S., 2013. Quantification of ikaite in Antarctic sea ice. Antarct. Sci. 25, 421–432.

Forest, A., Galindo, V., Darnis, G., Pineault, S., Lalande, C., Tremblay, J.-É., Fortier, L., 2011. Carbon biomass, elemental ratios (C:N) and stable isotopic composition (^{13}C, ^{15}N) of dominant calanoid copepods during the winter-to-summer transition in the Amundsen Gulf (Arctic Ocean). J. Plankton Res. 33, 161–178.

François, R., Altabet, M.A., Goericke, R., McCorkle, D.C., Brunet, C., Poisson, A., 1993. Changes in the ^{13}C of surface water particulate organice matter across the subtropical convergence in the SW Indian Ocean. Global Biogeochem. Cycles 7, 627–644.

Fransson, A., Chierici, M., Yager, P.L., Smith, W.O., 2011. Antarctic sea ice carbon dioxide system and controls. J. Geophys. Res. 116, C12035, doi:10.1029/2010JC006844.

Friis, K., Kortzinger, A., Wallace, D.W.R., 2003. The salinity normalization of marine inorganic carbon chemistry data. Geophys. Res. Lett. 30, 1085.

Gawarkiewicz, G., Weingartner, T., Chapman, D.C., 1998. Sea-Ice Processes and Water Mass Modification and Transport over Arctic Shelves, in: Brink, K.H., Robinson, A.R. (Eds.), The Sea. John Wiley & Sons, p. 595.

Geilfus, N.-X., Carnat, G., Dieckmann, G.S., Halden, N., Nehrke, G., Papakyriakou, T., Tison, J.-L., Delille, B., 2013. First estimates of the contribution of $CaCO_3$ precipitation to the release of CO_2 to the atmosphere during young sea ice growth. J. Geophys. Res. Ocean. 118, 244–255.

Geilfus, N.-X., Carnat, G., Papakyriakou, T., Tison, J.-L., Else, B., Thomas, H., Shadwick, E.H., Delille, B., 2012. Dynamics of pCO_2 and related air-ice CO_2 fluxes in the Arctic coastal zone (Amundsen Gulf, Beaufort Sea). J. Geophys. Res. 117, C00G10. doi:10.1029/2011JC007118.

Gibson, J.A.E., Trull, T., Nichols, P.D., Summons, R.E., McMinn, A., 1999. Sedimentation of ^{13}C-rich organic matter from Antarctic sea-ice algae: A potential indicator of past sea-ice extent. Geology 27, 331–334.

Gleitz, M., Rutgers v.d. Leoff, M., Thomas, D.N., Dieckmann, G.S., Millero, F.J., 1995. Comparison of summer and winter inorganic carbon, oxygen and nutrient concentrations in Antarctic sea ice brine. Mar. Chem. 51, 81–91.

Glud, R., Rysgaard, S., Kühl, M., 2002. A laboratory study on O_2 dynamics and photosynthesis in ice algal communities : quantification by microsensors, O_2 exchange rates, C incubations and a PAM fluorometer. Aquat. Microb. Ecol. 27, 301–311.

Gosink, T., Pearson, J., Kelley, J., 1976. Gas movement through sea ice. Nature 263, 41-42.

Goyet, C., Poisson, A., 1989. New determination of carbonic acid dissociation constants in seawater as a function of temperature and salinity. Deep Sea Res. 36, 1635–1654.

Granger, J., Prokopenko, M.G., Mordy, C.W., Sigman, D.M., 2013. The proportion of remineralized nitrate on the ice-covered eastern Bering Sea shelf evidenced from the oxygen isotope ratio of nitrate. Global Biogeochem. Cycles 27, 962–971.

Griffith, D.R., McNichol, A.P., Xu, L., McLaughlin, F.A., Macdonald, R.W., Brown, K.A., Eglinton, T.I., 2012. Carbon dynamics in the western Arctic Ocean: insights from full-depth carbon isotope profiles of DIC, DOC, and POC. Biogeosciences 9, 1217–1224.

Gruber, N., Sarmiento, J.L., 1997. Global patterns of marine nitrogen fixation and denitrification. Global Biogeochem. Cycles 11, 235–266.

Guay, C.K.H., McLaughlin, F.A., Yamamoto-Kawai, M., 2009. Differentiating fluvial components of upper Canada Basin waters on the basis of measurements of dissolved barium combined with other physical and chemical tracers. J. Geophys. Res. 114, C00A09.

Guo, L., Cai, Y., Belzile, C., Macdonald, R.W., 2012. Sources and export fluxes of inorganic and organic carbon and nutrient species from the seasonally ice-covered Yukon River. Biogeochemistry 107, 187–206.

Hama, T., Miyazaki, T., Ogawa, Y., Iwakuma, T., Takahashi, M., Otsuki, A., Ichimura, S., 1983. Measurement of photosynthetic production of a marine phytoplankton population using a stable ^{13}C isotope. Mar. Biol. 36, 31–36.

Hansson, I., 1973. A new set of acidity constants for carbonic acid and boric acid in sea water. Deep Sea Res. 20, 461–478.

Hare, A.A., Wang, F., Barber, D., Geilfus, N.-X., Galley, R.J., Rysgaard, S., 2013. pH evolution in sea ice grown at an outdoor experimental facility. Mar. Chem. 154, 46–54.

Henley, S.F., Annett, A. L., Ganeshram, R.S., Carson, D.S., Weston, K., Crosta, X., Tait, A., Dougans, J., Fallick, A. E., Clarke, A., 2012. Factors influencing the stable carbon isotopic composition of suspended and sinking organic matter in the coastal Antarctic sea ice environment. Biogeosciences 9, 1137–1157.

Hobson, K.A., Fisk, A., Karnovsky, N., Holst, M., Gagnon, J., Fortier, M., 2002. A stable isotope ($\delta^{13}C$, $\delta^{15}N$) model for the North Water food web: implications for evaluating trophodynamics and the flow of energy and contaminants. Deep. Res. 49, 5131–5150.

Honjo, S., Krishfield, R. A., Eglinton, T.I., Manganini, S.J., Kemp, J.N., Doherty, K., Hwang, J., McKee, T.K., Takizawa, T., 2010. Biological pump processes in the cryopelagic and hemipelagic Arctic Ocean: Canada Basin and Chukchi Rise. Prog. Oceanogr. 85, 137–170.

IUPAC, 1997. Compendium of Chemical Terminology, 2nd ed. Blackwell Scientific Publications, Oxford. XML on-line corrected version: http://goldbook.iupac.org (2006-) created by M. Nic, J. Jirat, B. Kosata; updates compiled by A. Jenkins. doi:10.1351/goldbook.

Jackson, J.M., Allen, S.E., Carmack, E.C., McLaughlin, F.A., 2010a. Suspended particles in the Canada Basin from optical and bottle data, 2003–2008. Ocean Sci. 6, 799–813.

Jackson, J.M., Carmack, E.C., McLaughlin, F.A., Allen, S.E., Ingram, R.G., 2010b. Identification, characterization, and change of the near-surface temperature maximum in the Canada Basin, 1993–2008. J. Geophys. Res. 115, C05021.

Johnson, K.M., Kortzinger, A., Mintrop, L., Duinker, J.C., Wallace, D.W.R., 1999. Coulometric total carbon dioxide analysis for marine studies : measurement and internal consistency of underway TCO_2 concentrations. Mar. Chem. 67, 123–144.

Johnson, K.M., Wills, K.D., Butler, D.B., Johnson, W.K., Wong, C.S., 1993. Coulometric total carbon dioxide analysis for marine studies: maximizing the performance of an automated gas extraction system and coulometric detector. Mar. Chem. 44, 167–187.

Jones, E., Anderson, L., 1986. On the origin of the chemical properties of the Arctic Ocean halocline. J. Geophys. Res. 91, 10,759–10,767.

Jones, E.P., Anderson, L.G., Swift, J.H., 1998. Distribution of Atlantic and Pacific waters in the upper Arctic Ocean: Implications for circulation distinguish between oceanic waters of Pacific. Geophys. Res. Lett. 25(6), 765–768.

Jones, E.P., Coote, A.R., 1981. Oceanic CO_2 Produced by the Precipitation of $CaCO_3$ From Brines in Sea Ice. J. Geophys. Res. 86, 11041–11043.

Juranek, L.W., Hamme, R.C., Kaiser, J., Wanninkhof, R., Quay, P.D., 2010. Evidence of O_2 consumption in underway seawater lines: Implications for air-sea O_2 and CO_2 fluxes. Geophys. Res. Lett. L01601, doi:10.1029/2009GL040423.

Kaltin, S., Anderson, L.G., 2005. Uptake of atmospheric carbon dioxide in Arctic shelf seas: evaluation of the relative importance of processes that influence pCO_2 in water transported over the Bering–Chukchi Sea shelf. Mar. Chem. 94, 67–79.

Keeling, R.F., Peng, T.-H., 1995. Transport of heat, CO_2 and O_2 by the Atlantic's thermohaline circulation. Philosphoical Trans. R. Soc. London 348, 133–142.

Kennedy, H., Thomas, D.N., Kattner, G., Haas, C., Dieckmann, G.S., 2002. Particulate organic matter in Antarctic summer sea ice : concentration and stable isotopic composition. Mar. Ecol. Prog. Ser. 238, 1–13.

Kirst, G., Wiench, C., 1995. Ecophysiology of Polar Algae. J. Phycol. 31, 181–199.

Kroopnick, P.M., 1985. The distribution of ^{13}C of $\sum CO_2$ in the world oceans. Deep Sea Res. 32, 57–84.

Kwok, R., Cunningham, G.F., Wensnahan, M., Rigor, I., Zwally, H.J., Yi, D., 2009. Thinning and volume loss of the Arctic Ocean sea ice cover: 2003–2008. J. Geophys. Res. 114, C07005.

Lalande, C., Forest, A., Barber, D.G., Gratton, Y., Fortier, L., 2009. Variability in the annual cycle of vertical particulate organic carbon export on Arctic shelves: Contrasting the Laptev Sea, Northern Baffin Bay and the Beaufort Sea. Cont. Shelf Res. 29, 2157–2165.

Lee, K., Millero, F.J., Byrne, R.H., Feely, A., Wanninkhof, R., 2000. the recommended dissociation constant for carbonic acid in seawater. Geophys. Res. Lett. 27, 229–232.

Lee, S.H., McRoy, C.P., Joo, H.M., Gradinger, R., 2011. Holes in progressively thinning Arctic sea ice lead to new ice algae habitat. Oceanography 24, 302–308.

Lee, S.H., Whitledge, T.E., 2005. Primary and new production in the deep Canada Basin during summer 2002. Polar Biol. 28, 190–197.

Leppäranta, M., Manninen, T., 1988. The Brine and Gas Content of Sea ice with Attention to Low Salinities and High Temperatures. Helsinki, Finland.

Loose, B., Miller, L., Elliot, S., Papakyriakou, T., 2011. Sea Ice Biogeochemistry and Material Transport Across the Frozen Interface. Oceanography 24, 202–218.

Lueker, T.J., Dickson, A.G., Keeling, C.D., 2000. Ocean pCO_2 calculated from dissolved inorganic carbon, alkalinity, and equations for K_1 and K_2: validation based on laboratory measurements of CO_2 in gas and seawater at equilibrium. Mar. Chem. 70, 105–119.

Lynch-Stieglitz, J., Stocker, T.F., Broecker, W.S., Fairbanks, R.G., 1995. The influence of air-sea exchange on the isotopic composition of oceanic carbon: Observations and modeling. Global Biogeochem. Cycles 9, 653–665.

Macdonald, R., Carmack, E.C., McLaughlin, F.A., Iseki, K., Macdonald, D.M., O'Brien, M.C., 1989. Composition and modification of water masses in the Mackenzie Shelf Estuary. J. Geophys. Res. 94, 18,057–18,070.

Macdonald, R.W., Anderson, L.G., Christensen, J.P., Miller, L.A., Semiletov, I.P., Stein, R., 2010. The Arctic Oceans, in: Lui, K.K., Atkinson, L., Quinones, R., Talaue-McManus, L. (Eds.), Polar Margins. Springer, pp. 291–303.

Macdonald, R.W., Naidu, A.S., Yunker, M.B., Gobeil, C., 2004a. The Beaufort Sea: Distribution, Sources, Fluxes, and Burial of Organic Carbon, in: Stein, R., Macdonald, R.W. (Eds.), The Organic Carbon Cycle in the Arctic Ocean. Springer, Berlin., pp. 177–193.

Macdonald, R.W., Sakshaug, E., Stein, R., 2004b. The Arctic Ocean: Modern Status and Recent Climate Change, in: Stein, R., Macdonald, R.W. (Eds.), The Organic Carbon Cycle in the Arctic Ocean. Springer, Berlin., pp. 6–21.

Macdonald, R.W., Solomon, S., Cranston, R., Welch, H.E., Yunker, M.B., Gobeil, C., 1998. A sediment and organic carbon budget for the Canadian Beaufort Shelf. Mar. Geol. 144, 255–273.

Marion, G., 2001. Carbonate mineral solubility at low temperatures in the Na-K-Mg-Ca-H-Cl-SO_4-OH-HCO_3-CO_3-CO_2-H_2O system. Geochim. Cosmochim. Acta 65, 1883–1896.

Maslowski, W., Clement Kinney, J., Higgins, M., Roberts, A., 2012. The Future of Arctic Sea Ice. Annu. Rev. Earth Planet. Sci. 40, 625–654.

Mathis, J.T., Bates, N.R., Hansell, D. A., Babila, T., 2009. Net community production in the northeastern Chukchi Sea. Deep Sea Res. Part II Top. Stud. Oceanogr. 56, 1213–1222.

Mathis, J.T., Pickart, R.S., Hansell, D. A., Kadko, D., Bates, N.R., 2007. Eddy transport of organic carbon and nutrients from the Chukchi Shelf: Impact on the upper halocline of the western Arctic Ocean. J. Geophys. Res. 112, C05011.

McClelland, J., Holmes, R.M., Peterson, B.J., Amon, R., Brabets, T., Cooper, L., Gibson, J., Gordeev, V.V., Guay, C., Milburn, D., Staples, R., Raymond, P.A., Shiklomanov, I., Striegel, R., Zhulidov, A., Gurtovaya, T., Zimov, S., 2008. Development of a pan-Arctic database for river chemistry. Eos, Trans. Am. Geophys. Union 89, 217–218.

McGuire, A.D., Anderson, L.G., Christensen, T.R., Dallimore, S., Guo, L., Hayes, D.J., Heimann, M., Lorenson, T.D., Macdonald, R.W., Roulet, N., 2009. Sensitivity of the carbon cycle in the Arctic to climate change. Ecol. Monogr. 79, 523–555.

McLaughlin, F.A., Carmack, E.C., 2010. Deepening of the nutricline and chlorophyll maximum in the Canada Basin interior, 2003-2009. Geophys. Res. Lett. L01601, doi:10.1029/2009GL040423

McLaughlin, F.A., Carmack, E.C., Macdonald, R.W., Melling, H., Swift, J.H., Wheeler, P., Sherr, B., Sherr, E., 2004. The joint roles of Pacific and Atlantic-origin waters in the Canada Basin, 1997–1998. Deep Sea Res. Part I Oceanogr. Res. Pap. 51, 107–128.

McLaughlin, F.A., Carmack, E.C., Proshutinsky, A., Krishfield, R.A., Guay, C., Yamamoto-Kawai, M., Jackson, J.M., Williams, B., 2011. The rapid response of the Canada Basin to climate forcing: From bellwether to alarm bells. Oceanography 24, 146–159.

McLaughlin, F.A., Proshutinsky, A., Carmack, E.C., Shimada, K., Brown, K., Corkum, M., Dempsey, M., Drost, H., Eert, J., Green, I., Guay, C., Hutchings, J., Illasiak, J., Jackson, J., Krishfield, R., Li, W.K.W., Maclean, H., Nelson, J., Newhall, K., Nishino, S., Ostrom, W., Smith, J., Steel, M., Sutherland, N., White, L., Zhao, J., Zimmermann, S., 2012. Physical , Chemical and Zooplankton Data from the Canada Basin and Canadian Arctic Archipelago , July 20 to September 14 , 2006 Canadian Data Report of Hydrography and Ocean Sciences 186. Sidney.

Mehrbach, C., Culberson, C.H., Hawley, J.E., Pytkowicz, R.M., 1973. Measurement of the apparent dissociation constants of carbonic acid in seawater at atmospheric pressure. Limnol. Oceanogr. 18, 897–907.

Melling, H., Agnew, T.A., Falkner, K.K., Greenberg, D.A., Lee, C.M., Munchow, A., Petrie, B., Prinsenberg, S.J., Samelson, R.M., Woodgate, R.A., 2008. Fresh-Water Fluxes via Pacific and Arctic Outflows Across the Canadian Polar Shelf, in: Dickson, R.R., Meincke, J., Rhines, P. (Eds.), Arctic-Subarctic Ocean Fluxes. Springer, pp. 193–247.

Melling, H., Lewis, E.L., 1982. Shelf drainage flows in the Beaufort Sea and their effect on the Arctic Ocean pycnocline. Deep Sea Res. Part A. Oceanogr. Res. Pap. 29, 967–985.

Melling, H., Moore, R.M., 1995. Modification of halocline source waters during freezing on the Beaufort Sea shelf: evidence from oxygen isotopes and dissolved nutrients. Cont. Shelf Res. 15, 89–113.

Michener, R.H., Schell, D.M., 1994. Stable isotope ratios as tracers in marine aquatic food webs, in: Lajtha, K., Michener, R. (Eds.), Stable Isotopes in Ecology and Environmental Science. Blackwell Scientific Publications, pp. 138–157.

Mikaloff Fletcher, S.E., Gruber, N., Jacobson, A.R., Gloor, M., Doney, S.C., Dutkiewicz, S., Gerber, M., Follows, M., Joos, F., Lindsay, K., Menemenlis, D., Mouchet, A., Müller, S.A., Sarmiento, J.L., 2007. Inverse estimates of the oceanic sources and sinks of natural CO_2 and the implied oceanic carbon transport. Global Biogeochem. Cycles 21, 19.

Miller, L.A., Carnat, G., Else, B.G.T., Sutherland, N., Papakyriakou, T.N., 2011a. Carbonate system evolution at the Arctic Ocean surface during autumn freeze-up. J. Geophys. Res. 116, C00G04, doi: 10.1029/2011JC007143.

Miller, L.A., DiTullio, G.R., 2007. Gas fluxes and dynamics in polynyas, in: Smith, W.O.J., Barber, D.G. (Eds.), Polynyas: Windows to the World. Elsevier Oceanography Series 74, p. 474.

Miller, L.A., Papakyriakou, T.N., Collins, R.E., Deming, J.W., Ehn, J.K., Macdonald, R.W., Mucci, A., Owens, O., Raudsepp, M., Sutherland, N., 2011b. Carbon dynamics in sea ice: A winter flux time series. J. Geophys. Res. 116, C02028, doi: 10.1029/2009JC006058.

Millero, F. J., 1995. Thermodynamics of the carbon dioxide system in the oceans. Geochim. Cosmochim. Acta 59, 661–677.

Millero, F.J., 1996. Chemical Oceanography, 2nd ed. CRC Press, Boca Raton. p.496.

Millero, F.J., DiTrolio, B., Suarez, A.F., Lando, G., 2009. Spectroscopic measurements of the pH in NaCl brines. Geochim. Cosmochim. Acta 73, 3109–3114.

Millero, F.J., Graham, T.B., Huang, F., Bustos-Serrano, H., Pierrot, D., 2006. Dissociation constants of carbonic acid in seawater as a function of salinity and temperature. Mar. Chem. 100, 80–94.

Millero, F.J., Pierrot, D., Lee, K., Wanninkhof, R., Feely, R., Sabine, C.L., Key, R.M., Takahashi, T., 2002. Dissociation constants for carbonic acid determined from field measurements. Deep Sea Res. Part I Oceanogr. Res. Pap. 49, 1705–1723.

Mojica Prieto, F.J., Millero, F.J., 2002. The values of $pK_1 + pK_2$ for the dissociation of carbonic acid in seawater. Geochim. Cosmochim. Acta 66, 2529–2540.

Mook, W., Bommerson, J., Staverman, W., 1974. Carbon isotope fractionation between dissolved bicarbonate and gaseous carbon dioxide. Earth Planet. Sci. Lett. 22, 169–176.

Mook, W.G., 1986. ^{13}C in Atmospheric CO_2. Netherlands J. Sea Res. 20, 211–223.

Moore, R., Lowings, M., Tan, F., 1983. Geochemical profiles in the central Arctic Ocean: Their relation to freezing and shallow circulation. J. Geophys. Res. 88, 2667–2674.

Morel, F.M.M., Hering, J.G., 1993. Principals and Applications of Aquatic Chemistry. John Wiley & Sons, Toronto. p.588.

Morison, J., Kwok, R., Peralta-Ferriz, C., Alkire, M., Rigor, I., Andersen, R., Steele, M., 2012. Changing Arctic Ocean freshwater pathways. Nature 481, 66–70.

Mundy, C.J., Gosselin, M., Gratton, Y., Brown, K.A., Galindo, V., Campbell, K., Levasseur, M., Barber, D., Papakyriakou, T. 2014. The role of environmental factors on under-ice phytoplankton bloom initiation: A case study on landfast sea ice in Resolute Passage, Canada. Mar. Eco. Prog. Ser. 497: 39–49, doi: 10.3354/meps10587

Munro, D.R., Dunbar, R.B., Mucciarone, D. A., Arrigo, K.R., Long, M.C., 2010. Stable isotope composition of dissolved inorganic carbon and particulate organic carbon in sea ice from the Ross Sea, Antarctica. J. Geophys. Res. 115, C09005.

Murata, A., Takizawa, T., 2003. Summertime CO_2 sinks in shelf and slope waters of the western Arctic Ocean. Cont. Shelf Res. 23, 753–776.

Naidu, A.S., Cooper, L.W., Finney, B.P., Macdonald, R.W., Alexander, C., Semiletov, I.P., 2000. Organic carbon isotope ratios ($\delta^{13}C$) of Arctic Amerasian Continental shelf sediments. Int. J. Earth Sci. 89, 522–532.

Najjar, R.G., Keeling, R.F., 1997. Analysis of the mean annual cycle of the dissolved oxygen anomaly in the World Ocean. J. Mar. Res. 55, 117–151.

National Snow and Ice Data Center, 2010. Weather and feedbacks lead to third-lowest extent [WWW Document]. Boulder, Colorado. URL http://nsidc.org/arcticseaicenews/2010/10/weather-and-feedbacks-lead-to-third-lowest-extent/ (accessed 10.4.10).

Neill, C., Johnson, K.M., Lewis, E., Wallace, D.W.R., 1997. Accurate headspace analysis of fCO_2 in discrete water samples using batch equilibration. Limnol. Oceanogr. 42, 1774–1783.

Newton, R., Schlosser, P., Mortlock, R., Swift, J., MacDonald, R., 2013. Canadian Basin freshwater sources and changes: Results from the 2005 Arctic Ocean Section. J. Geophys. Res. Ocean. 118, 2133–2154.

Niemi, A., Michel, C., Hille, K., Poulin, M., 2011. Protist assemblages in winter sea ice: setting the stage for the spring ice algal bloom. Polar Biol. 34, 1803–1817.

Nishino, S., Kikuchi, T., Yamamoto-Kawai, M., Kawaguchi, Y., Hirawake, T., Itoh, M., 2011. Enhancement/reduction of biological pump depends on ocean circulation in the sea-ice reduction regions of the Arctic Ocean. J. Oceanogr. 67, 305–314.

Nishino, S., Shimada, K., Itoh, M., 2005. Use of ammonium and other nitrogen tracers to investigate the spreading of shelf waters in the western Arctic halocline. J. Geophys. Res. 110, 1–6.

NOAA, 2010. NOAA Earth System Research Laboratory: Trends in Atmospheric Carbon Dioxide [WWW Document]. URL http://www.esrl.noaa.gov/gmd/ccgg/trends/ (accessed 7.1.10).

Nomura, D., Assmy, P., Nehrke, G., Granskog, M. A., Fischer, M., Dieckmann, G.S., Fransson, A., Hu, Y., Schnetger, B., 2013a. Characterization of ikaite ($CaCO_3$ •$6H_2O$) crystals in first-year Arctic sea ice north of Svalbard. Ann. Glaciol. 54, 125–131.

Nomura, D., Eicken, H., Gradinger, R., Shirasawa, K., 2010a. Rapid physically driven inversion of the air–sea ice CO_2 flux in the seasonal landfast ice off Barrow, Alaska after onset of surface melt. Cont. Shelf Res. 30, 1998–2004.

Nomura, D., Granskog, M. A., Assmy, P., Simizu, D., Hashida, G., 2013b. Arctic and Antarctic sea ice acts as a sink for atmospheric CO_2 during periods of snow melt and surface flooding. J. Geophys. Res. Ocean. 118, 1–14, doi:10.1002/2013JC009048.

Nomura, D., Yoshikawa-Inoue, H., Toyota, T., 2006. The effect of sea-ice growth on air-sea CO_2 flux in a tank experiment. Tellus B 58, 418–426.

Nomura, D., Yoshikawa-Inoue, H., Toyota, T., Shirasawa, K., 2010b. Effects of snow, snowmelting and refreezing processes on air–sea-ice CO_2 flux. J. Glaciol. 56, 262–270.

O'Brien, M.C., Melling, H., Pedersen, T.F., Macdonald, R.W., 2011. The role of eddies and energetic ocean phenomena in the transport of sediment from shelf to basin in the Arctic. J. Geophys. Res. 116, C08001.

Omar, A., Johannessen, T., Bellerby, R.G.J., Olsen, A., Anderson, L.G., Kivimae, C., 2005. Sea-ice and brine formation in Storjgorden: Implications for the Arctic wintertime air-sea CO_2 flux, in: H. Drange, T. Dokken, T. Furevik, R. Gerdes, and W.B. (Ed.), The Nordic Seas: An Integrated Perspective. American Geophysical Union, pp. 177–187.

Östlund, H.G., Hut, G., 1984. Arctic Ocean water mass balance from isotope data. J. Geophys. Res. 89, 6373.

Papadimitriou, S., Kennedy, H., Kattner, G., Dieckmann, G.S., Thomas, D.N., 2004. Experimental evidence for carbonate precipitation and CO_2 degassing during sea ice formation. Geochim. Cosmochim. Acta 68, 1749–1761.

Papadimitriou, S., Kennedy, H., Norman, L., Kennedy, D.P., Dieckmann, G.S., Thomas, D.N., 2012. The effect of biological activity, $CaCO_3$ mineral dynamics, and CO_2 degassing in the

inorganic carbon cycle in sea ice in late winter-early spring in the Weddell Sea, Antarctica. J. Geophys. Res. 117, C08011, doi:10.1029/2012JC008058.

Papadimitriou, S., Thomas, D., Kennedy, H., Kuosa, H., Dieckmann, G., 2009. Inorganic carbon removal and isotopic enrichment in Antarctic sea ice gap layers during early austral summer. Mar. Ecol. Prog. Ser. 386, 15–27.

Papadimitriou, S., Thomas, D.N., Kennedy, H., Haas, C., Kuosa, H., Krell, A., Dieckmann, G.S. 2007. Biogeochemical composition of natural sea ice brines from the Weddell Sea during early austral summer. Limnol. Oceanog. 52(5), 1809–1823.

Papakyriakou, T., Miller, L.A., 2011. Springtime CO_2 exchange over seasonal sea ice in the Canadian Arctic Archipelago. Ann. Glaciol. 52, 215–224.

Parmentier, F.-J.W., Christensen, T.R., Sørensen, L.L., Rysgaard, S., McGuire, A. D., Miller, P. A., Walker, D. A., 2013. The impact of lower sea-ice extent on Arctic greenhouse-gas exchange. Nat. Clim. Chang. 3, 195–202.

Parsons, T., Webb, D., Rokeby, B., Lawrence, M., Hopky, G.E., Chiperzak, D.B., 1989. Autotrophic and heterotrophic production in the Mackenzie River/Beaufort Sea estuary. Polar Biol. 9, 261–266.

Perovich, D.K., Grenfell, T., Richter-Menge, J.A., Light, B., Tucker, W.B.I., Eicken, H., 2003. Thin and thinner: Sea ice mass balance measurements during SHEBA. J. Geophys. Res. 108, 8050.

Petrich, C., Eicken, H., 2010. Growth, Structure and Properties of Sea ice, in: Thomas, D.N., Dieckmann, G.S. (Eds.), Sea Ice. Wiley-Blackwell, pp. 23–78.

Pierrot, D., Lewis, E., Wallace, D.W.R., 2006. MS Excel program developed for CO_2 system calculations. ORNL/CDIAC-105. Carbon Dioxide Information Analysis Center, Oak Ridge National Laboratory, U.S. Department of Energy, Oak Ridge, Tennessee.

Pineault, S., Tremblay, J.-É., Gosselin, M., Thomas, H., Shadwick, E.H., 2013. The isotopic signature of particulate organic C and N in bottom ice: key influencing factors and applications for tracing the fate of ice-algae in the Arctic Ocean. J. Geophys. Res. 118, 1–14.

Proshutinsky, A., 2002. The role of the Beaufort Gyre in Arctic climate variability: Seasonal to decadal climate scales. Geophys. Res. Lett. 29, 2100.

Prowse, T.D., Wrona, F.J., Reist, J.D., Gibson, J.J., Hobbie, J.E., Lévesque, L.M.J., Vincent, W.F., 2006. Climate change effects on hydroecology of arctic freshwater ecosystems. Ambio A J. Hum. Environ. 35, 347–58.

Rachold, V., Eicken, H., Gordeev, V.V., Grigoriev, M.N., Hubberten, H.-W., Lisitzin, A.P., Shevchenko, V.P., Schirrmeister, L., 2004. Modern Terrigenous Organic Carbon Input to the Arctic Ocean, in: Stein, R., Macdonald, R.W. (Eds.), The Organic Carbon Cycle in the Arctic Ocean. Springer, Berlin., pp. 33–55.

Rau, G.H., Froelich, P.N., Takahashi, T., Des Marais, D.J., 1991. Does Sedimentary Organic ^{13}C Record Variations in Quaternary Ocean [CO_2(aq)] ? Paleoceanography 6, 335–347.

Rau, G.H., Takahashi, T., Des Marais, D.J., 1989. Latitudinal variations in plankton $\delta^{13}C$: implications for CO_2 and productivity in past oceans. Nature 341, 516–518.

Rau, G.H., Takahashi, T., Des Marais, D.J., Repeta, D.J., Martin, J.H., 1992. The relationship between $\delta^{13}C$ of organic material and [CO_2(aq)] in ocean surface water: Data from a JGOFS site in the northeast Atlantic Ocean and a model. Geochim. Cosmochim. Acta 56, 1413–1419.

Romanek, C.S., Grossman, E.L., Morse, J.W., 1992. Carbon isotopic fractionation in synthetic aragonite and calcite: Effects of temperature and precipitation rate. Geochim. Cosmochim. Acta 56, 419–430.

Roy, R., Roy, L., Vogel, K., Porter-Moore, C., Pearson, T., Good, C., Millero, F.J., Campbell, D., 1993. The dissociation constants of carbonic acid in seawater at salinities 5 to 45 and temperatures 0 to 45°C. Mar. Chem. 44, 249–267.

Rysgaard, S., Bendtsen, J., Delille, B., Dieckmann, G.S., Glud, R.N., Kennedy, H., Mortensen, J., Papadimitriou, S., Thomas, D.N., Tison, J.-L., 2011. Sea ice contribution to the air-sea CO_2 exchange in the Arctic and Southern Oceans. Tellus B 63, 823–830.

Rysgaard, S., Bendtsen, J., Pedersen, L.T., Ramløv, H., Glud, R.N., 2009. Increased CO_2 uptake due to sea ice growth and decay in the Nordic Seas. J. Geophys. Res. 114, 1–9.

Rysgaard, S., Glud, R.N., Sejr, M.K., Bendtsen, J., Christensen, P.B., 2007. Inorganic carbon transport during sea ice growth and decay: A carbon pump in polar seas. J. Geophys. Res. 112, 1–8.

Rysgaard, S., Søgaard, D.H., Cooper, M., Pucko, M., Lennert, K., Papakyriakou, T.N., Wang, F., Geilfus, N.X., Glud, R.N., Ehn, J., McGinnis, D.F., Attard, K., Sievers, J., Deming, J.W., Barber, D., 2013. Ikaite crystal distribution in winter sea ice and implications for CO_2 system dynamics. Cryosph. 7, 707–718.

Sallon, A., Michel, C., Gosselin, M., 2011. Summertime primary production and carbon export in the southeastern Beaufort Sea during the low ice year of 2008. Polar Biol. 34, 1989–2005.

Sánchez-García, L., Alling, V., Pugach, S., Vonk, J., van Dongen, B., Humborg, C., Dudarev, O., Semiletov, I., Gustafsson, Ö., 2011. Inventories and behavior of particulate organic carbon in the Laptev and East Siberian seas. Global Biogeochem. Cycles 25, GB2007, doi:10.1029/2010GB003862.

Sarmiento, J.L., Gruber, N., 2006. Ocean Biogeochemical Dynamics. Princeton University Press, Princeton. p.503.

Schmittner, A., Gruber, N., Mix, A.C., Key, R.M., Tagliabue, A., Westberry, T.K., 2013. Biology and air–sea gas exchange controls on the distribution of carbon isotope ratios ($\delta^{13}C$) in the ocean. Biogeosciences 10, 5793–5816.

Schubert, C., Calvert, S., 2001. Nitrogen and carbon isotopic composition of marine and terrestrial organic matter in Arctic Ocean sediments: implications for nutrient utilization and organic matter composition. Deep Sea Res. Part I Oceanogr. 48, 789–810.

Semiletov, I.P., Makshtas, A., Akasofu, S.-I., 2004. Atmospheric CO_2 balance: The role of Arctic sea ice. Geophys. Res. Lett. 31, 2–5.

Serreze, M.C., Barrett, A.P., Slater, A.G., Woodgate, R. A., Aagaard, K., Lammers, R.B., Steele, M., Moritz, R., Meredith, M., Lee, C.M., 2006. The large-scale freshwater cycle of the Arctic. J. Geophys. Res. 111, C11010.

Shadwick, E.H., Thomas, H., Gratton, Y., Leong, D., Moore, S.A., Papakyriakou, T., Prowe, A.E.F., 2011. Export of Pacific carbon through the Arctic Archipelago to the North Atlantic. Cont. Shelf Res. 31, 806–816.

Shcherbina, A.Y., 2004. Dense water formation on the northwestern shelf of the Okhotsk Sea: 1. Direct observations of brine rejection. J. Geophys. Res. 109, 1–14.

Shimada, K., 2005. Halocline structure in the Canada Basin of the Arctic Ocean. Geophys. Res. Lett. 32, 1–5.

Shimada, K., Carmack, E.C., Hatakeyama, K., Takizawa, T., 2001. Variets of Shallow Temperature Maximum Waters in the Western Canadian Basin of the Arctic Ocean. Geophys. Res. Lett. 28, 3441–3444.

Shirasawa, K., Ingram, R.G., 1997. Currents and turbulent fluxes under the first-year sea ice in Resolute Passage, Northwest Territories, Canada. J. Mar. Syst. 11, 21–32.

Spreen, G., Kaleschke, L., Heygster, G., 2008. Sea ice remote sensing using AMSR-E 89-GHz channels. J. Geophys. Res. 113, C02S03.

Stein, R., Macdonald, R.W., 2004. Geochemical Proxies used for Organic Carbon Source Identification in Arctic Ocean Sediments, in: Stein, R., Macdonald, R.W. (Eds.), The Organic Carbon Cycle in the Arctic Ocean. Springer, Berlin., pp. 24–32.

Steiner, N.S., Lee, W.G., Christian, J.R., 2013. Enhanced gas fluxes in small sea ice leads and cracks: Effects on CO_2 exchange and ocean acidification. J. Geophys. Res. Ocean. 118, 1195–1205.

Stroeve, J., Kattsov, V., Barrett, A., Serreze, M., Pavlova, T., Holland, M., Meier, W.N., 2012. Trends in Arctic sea ice extent from CMIP5, CMIP3 and observations. Geophys. Res. Lett. 39, L16502, doi:10.1029/2012GL052676.

Stroeve, J., Serreze, M., Drobot, S., Gearheard, S., Holland, M., Maslanik, J., Meier, W., Scambos, T., 2008. Arctic sea ice extent plummets in 2007. Eos, Trans., 89, 13–14.

Stumm, M., Morgan, J.J., 1996. Aquatic Chemistry: Chemical Equilibria and Rates in Natural Waters, 3rd ed. John Wiley & Sons, New York. p.1022.

Takahashi, T., Sutherland, S.C., Wanninkhof, R., Sweeney, C., Feely, R. A., Chipman, D.W., Hales, B., Friederich, G., Chavez, F., Sabine, C., Watson, A., Bakker, D.C.E., Schuster, U., Metzl, N., Yoshikawa-Inoue, H., Ishii, M., Midorikawa, T., Nojiri, Y., Körtzinger, A., Steinhoff, T., Hoppema, M., Olafsson, J., Arnarson, T.S., Tilbrook, B., Johannessen, T., Olsen, A., Bellerby, R., Wong, C.S., Delille, B., Bates, N.R., de Baar, H.J.W., 2009. Climatological mean and decadal change in surface ocean pCO2, and net sea–air CO_2 flux over the global oceans. Deep Sea Res. Part II Top. Stud. Oceanogr. 56, 554–577.

Tanaka, T., Watanabe, Y.W., Watanabe, S., Noriki, S., Tsurushima, N., Nojiri, Y., 2003. Oceanic Suess effect of $\delta^{13}C$ in subpolar region: The North Pacific. Geophys. Res. Lett. 30, 2159.

Taylor, R.L., Semeniuk, D.M., Payne, C.D., Zhou, J., Tremblay, J.-É., Cullen, J.T., Maldonado, M.T., 2013. Co-limitation by light, nitrate and iron in the Beaufort sea in late summer. J. Geophys. Res. Ocean. 3260–3277.

Thomas, D.N., Papadimitriou, S., Michel, C., 2010. Biogeochemistry of Sea Ice, in: Thomas, D. N., Dieckmann, G.S. (Eds.), Sea Ice. Wiley-Blackwell, pp. 425–467.

Toole, J.M., Timmermans, M.-L., Perovich, D.K., Krishfield, R. A., Proshutinsky, A., Richter-Menge, J. A., 2010. Influences of the ocean surface mixed layer and thermohaline stratification on Arctic Sea ice in the central Canada Basin. J. Geophys. Res. 115, C10018.

Toyota, T., Smith, I.J., Gough, A.J., Langhorne, P.J., Leonard, G.H., Van Hale, R.J., Mahoney, A.R., Haskell, T.G., 2013. Oxygen isotope fractionation during the freezing of sea water. J. Glaciol. 59, 697–710. doi:10.3189/2013JoG12J163

Tremblay, J.-É., Bélanger, S., Barber, D.G., Asplin, M., Martin, J., Darnis, G., Fortier, L., Gratton, Y., Link, H., Archambault, P., Sallon, A., Michel, C., Williams, W.J., Philippe, B., Gosselin, M., 2011. Climate forcing multiplies biological productivity in the coastal Arctic Ocean. Geophys. Res. Lett. 38, L18604, doi:10.1029/2011GL048825.

Tremblay, J.-É., Michel, C., Hobson, K.A., Gosselin, M., Price, N.M., 2006. Bloom dynamics in early opening waters of the Arctic Ocean. Limnol. Oceanogr. 51, 900–912.

Turner, J. V., 1982. Kinetic fractionation of carbon-13 during calcium carbonate precipitation. Geochim. Cosmochim. Acta 46, 1183–1191.

Vancoppenolle, M., Goosse, H., Montety, A. De, Fichefet, T., Tremblay, B., Tison, J.-L., 2010. Modeling brine and nutrient dynamics in Antarctic sea ice : The case of dissolved silica. J. Geophys. Res. 115:C02005, doi:10.1029/2009JC005369.

Wang, M., Overland, J.E., 2009. A sea ice free summer Arctic within 30 years? Geophys. Res. Lett. 36, L07502.

Wanninkhof, R., Lewis, E., Feely, R.A., Millero, F.J., 1999. The optimal carbonate dissociation constants for determining surface water pCO_2 from alkalinity and total inorganic carbon. Mar. Chem. 65, 291–301.

Weingartner, T., Cavalieri, D.J., Aagaard, K., Sasaki, Y., 1998. Circulation , dense water formation , and outflow on shelf. Arctic 103, 7647–7661.

Weiss, R., 1970. The solubility of nitrogen, oxygen and argon in water and seawater. Deep Sea Res. 17, 721–735.

Weiss, R.F., 1974. Carbon Dioxide in Water and Seawater: The Solubility of a Non-Ideal Gas. Mar. Chem. 2, 203–215.

Weiss, R.F., Price, B.A., 1980. Nitrous oxide solubility in water and seawater. Mar. Chem. 8, 347–359.

Welch, H.E., Bergmann, M.A., 1989. Seasonal development of ice algae and its prediction from envrionmental factors near Resolute, N.W.T., Canada. Can. J. Fish Aquat. Sci. 46, 1793–1804.

Winsor, P., Chapman, D.C., 2002. Distribution and interannual variability of dense water production from coastal polynyas on the Chukchi Shelf. J. Geophys. Res. 107. C7, 3079, doi: 10.1029/2001JC000984.

Wong, W.W., Sackett, W.M., 1978. Fractionation of stable carbon isotopes by marine phytoplankton. Geochem. Cosmo. Acta. 42, 1809-1815.

Woodgate, R., Aagaard, K., 2005. Revising the Bering Strait freshwater flux into the Arctic Ocean. Geophys. Res. Lett. 32, 3–6.

Woodgate, R., Aagaard, K., Swift, J.H., Falkner, K.K., Smethie, W.M.J., 2005. Pacific ventilation of the Arctic Ocean's lower halocline by upwelling and diapycnal mixing over the continental margin. Geophys. Res. Lett. 32, 2–6.

Yamamoto-Kawai, M., Carmack, E.C., McLaughlin, F.A., 2006. Nitrogen balance and Arctic throughflow. Nature 443, 43.

Yamamoto-Kawai, M., McLaughlin, F.A., Carmack, E.C., 2011. Effects of ocean acidification, warming and melting of sea ice on aragonite saturation of the Canada Basin surface water. Geophys. Res. Lett. 38, L03601, doi:10.1029/2010GL045501.

Yamamoto-Kawai, M., McLaughlin, F.A., Carmack, E.C., Nishino, S., Shimada, K., 2008. Freshwater budget of the Canada Basin, Arctic Ocean, from salinity, $\delta^{18}O$, and nutrients. J. Geophys. Res. 113, 1–12.

Yamamoto-Kawai, M., McLaughlin, F.A., Carmack, E.C., Nishino, S., Shimada, K., Kurita, N., 2009. Surface freshening of the Canada Basin, 2003–2007: River runoff versus sea ice meltwater. J. Geophys. Res. Ocean. 114, C00A05.

Yamamoto-Kawai, M., Tanaka, N., Pivovarov, S., 2005. Freshwater and brine behaviors in the Arctic Ocean deduced from historical data of $\delta^{18}O$ and alkalinity (1929–2002 A.D.). J. Geophys. Res. 110, C10003.

Yang, J., 2009. Seasonal and interannual variability of downwelling in the Beaufort Sea. J. Geophys. Res. 114, 1–13.

Yun, M.S., Chung, K.H., Zimmermann, S., Zhao, J., Joo, H.M., Lee, S.H., 2012. Phytoplankton productivity and its response to higher light levels in the Canada Basin. Polar Biol. 35, 257–268.

Zeebe, R.E., Wolf-Gladrow, D., 2001. CO_2 in Seawater: Equilibrium, Kinetics, Isotopes. Elsevier Oceanography Series 65, San Diego. p.346.

Zemmelink, H.J., Delille, B., Tison, J.-L.L., Hintsa, E.J., Houghton, L., Dacey, J.W.H., 2006. CO_2 deposition over the multi-year ice of the western Weddell Sea. Geophys. Res. Lett. 33, 2–5.

Zhang, J., Quay, P.D., Wilbur, D., 1995. Carbon isotope fractionation during gas-water exchange and dissolution of CO_2. Geochim. Cosmochim. Acta 59, 107–114.

Zhang, R., Chen, M., Guo, L., Gao, Z., Ma, Q., Cao, J., Qiu, Y., Li, Y., 2012. Variations in the isotopic composition of particulate organic carbon and their relation with carbon dynamics in the western Arctic Ocean. Deep Sea Res. Part II Top. Stud. Oceanogr. 81-84, 72–78.

Zhou, J., Delille, B., Eicken, H., Vancoppenolle, M., Brabant, F., Carnat, G., Geilfus, N.-X., Papakyriakou, T., Heinesch, B., Tison, J.-L., 2013. Physical and biogeochemical properties in landfast sea ice (Barrow, Alaska): Insights on brine and gas dynamics across seasons. J. Geophys. Res. Ocean. 118, 3172–3189.